

DESIGN AND ENGINEERING OF STARCH-BASED POLYMER MATERIALS AS SUBSTITUTES
FOR PERSISTENT NON-BIODEGRADABLE PLASTICS

By

Apoorva Chandrakant Kulkarni

A DISSERTATION

Submitted to
Michigan State University
in partial fulfillment of the requirements
for the degree of

Chemical Engineering – Doctor of Philosophy

2022

ABSTRACT

DESIGN AND ENGINEERING OF STARCH-BASED POLYMER MATERIALS AS SUBSTITUTES FOR PERSISTENT NON-BIODEGRADABLE PLASTICS

By

Apoorva Chandrakant Kulkarni

Replacing carbon-carbon backbone persistent hydrocarbon plastics with biobased and biodegradable plastics offers value proposition of reduced carbon footprint and an environmentally responsible end-of-life. This work focuses on design and engineering of starch based polymeric materials as substitutes for non-biodegradable plastics.

Starch foams are being used as replacement for petroleum-based foams in insulation and cushion protection applications. However, moisture sensitivity remains a problem resulting in collapse of cell structure and loss of mechanical integrity. First section of the thesis focuses on engineering high-performance starch foams with enhanced moisture resistance using reactive extrusion processing technology. Chitosan, polyvinyl butyral (PVB) and sodium trimetaphosphate (STMP) were used with water as a plasticizer and a blowing agent to make foams with desired physico-mechanical properties. The resulting foams were hydrophobic, insoluble in water, and showed improved moisture resistance. The foams were completely biodegradable as established by ASTM/ISO standards. Crosslinking of starch with STMP increased the compressive strength of the foams by three times compared to control foams. Optimization of process parameters ensured an efficient, cost-effective route towards commercialization.

In the second section, our group's chemically modified thermoplastic starch (MTPS) prepared by reactive extrusion technology was explored in three different applications. First, MTPS, was melt blended with glycol modified polyethylene terephthalate (PETG) using

transesterification chemistry to synthesize MTPS-g-PETG in situ graft copolymer with 33% grafting. Second, the use of MTPS as a biobased and biodegradable nucleating agent and barrier property enhancer in polylactide (PLA) was explored. MTPS accelerated the rate of crystallization of PLA by up to 98 times at 100°C, reducing the half time for crystallization from 20 mins to less than 1 minute. Oxygen barrier properties of PLA was improved 127% without causing detrimental impact on mechanical properties or biodegradability.

Third application focused on using MTPS as a carrier for iodine, which is a very effective and strong antimicrobial agent. The new MTPS-iodine complex was incorporated in various proportions to commercial fully biodegradable-compostable polyester films. The morphological, mechanical, and antibacterial properties of these films were evaluated and compared with current commercial additives used to obtain antibacterial properties.

The last section focuses on the end-of-life evaluations for biobased and biodegradable plastics using kinetics approach. The effect of temperature on biodegradation of cellulose and Poly(3-hydroxybutyrate-co-3-hydroxyvalerate) (PHBV) in an aqueous environment seeded with a biologically aggressive microbial inoculum was studied. A global equation was derived from the reparametrized Arrhenius equation and the kinetic rate law to estimate the time required for 90% removal of polymer from the low temperature ocean environment. The t_{90} (time required to remove 90% of the polymer carbon from the environment) for PHBV at 10°C ranged from 6.2-6.9 years. The t_{90} of cellulose at 10 C was found to be 1.1-1.2 years. ASTM/ISO standards for measuring and reporting ocean biodegradability is static and conducted at one temperature (30°C), whereas ocean temperatures can vary from -1.8 °C to 33.4 °C. The kinetic analysis and model developed can provide a method to estimate time for complete removal of the biodegradable polymer carbon in ocean environments.

Copyright by
APOORVA CHANDRAKANT KULKARNI
2022

Dedicated to my family

ACKNOWLEDGMENTS

First, I would like to thank my advisor Dr. Ramani Narayan for his constant support and guidance throughout my journey in graduate school. His unique style of promoting independent research, giving students all the freedom to explore the field of their research own their own made me very confident and independent researcher. Because of his insistence on always exploring new areas and not getting stuck with just your narrow research project, I got to work on a variety of projects throughout my time here at MSU. This truly enabled me to think out of the box and look at the big picture of any project that I worked on. These qualities have proved to be of utmost importance for me in securing a job in the industry and I am sure will help me in the rest of my career as well.

I would also like to thank all my committee members Dr. Robert Ofoli, Dr. Shiwang Cheng and Dr. Rafael Auras for their invaluable feedback during the course of my work. I would especially like to thank Dr. Auras and his students who were always there to help me in using their instruments. Special thanks to Aaron Walworth and Pooja Mayekar who trained me in various instruments at School of Packaging. I am also grateful to all my professors here at MSU who helped in learning the ins and outs of chemical engineering and polymers.

I am also very grateful to all the collaborators – Dr. Jeffrey Catchmark, Dr. Teresa Bergholz, Dr. Shilpa Manjure, and everyone else who supported our work and provided the required facility to conduct the experiments. I would also like to thank Abby Vanderberg at the Center of Advanced Microscopy who helped me in sample preparation and microscopy imaging of all my samples. Thanks to all the members from CMSC center who helped in preparation and testing of various samples.

I am very grateful to all the members of Biobased Materials Research Group (BMRG) including my seniors Dr. Sayli Bote, Dr. Preetam Giri and Manas Nigam who helped me in learning and understanding my group's work and culture. I would also like to thank Dr.(very recent) Moh Alhaj for being there when additional help was required. Moh joined BMRG with me and was always there throughout my journey at MSU. Doing assignments and studies together along with some gossiping made the time at BMRG more enjoyable. I owe a big thank you to all the undergrads – especially Melissa Joslyn, Jakob Emrich and Nicole Mancina who were passionate about their research, constantly gave valuable inputs for improving the experiments and never complained about cleaning up the starch clogged extruder or doing endless amounts of titrations. It was their contribution that allowed me to finish the work in much less time. I would also like to thank and wish all the best to Shrirang, Shehla and Badal for their future work at BMRG.

I would also like to take this opportunity to thank my second family away from home – Aditya (Adi), with whom I always used to pick a fight for no reason. Thank you for tolerating me. And for being there with me throughout my journey. Gouree (Gourabai) my so called 'roommate' who never lived with me but was always there for doing all the shopping trips, cooking, gossips and everything. Thanks to Affan (Wise man) for all your advice and for always bringing me food and trying to make me fat. Thank you Sneha (oo we don't have a nickname for you) for making pakodas with me every day and tormenting Gouree. Thank you to Renu and Sushant for being the wise people amongst this group of jokers and keeping this crazy family together. And thank you for bringing Chintu in our life 😊. We all love him a lot. Finally, thank you to Shalin, who gave me this amazing idea to write such acknowledgements and enjoy the writing and for always doing 'all the work'. My Spartan life

wouldn't be the same without all of you. Last but not the least, I would like to thank my parents and my brother Rushi for their support through each step of my life. It was their motivation and love that helped me in pursuing this dream of PhD. Special thanks to all my grandparents (Aaji and Ajoba), some of whom are unfortunately not with me today. I know you all were always proud of me and will bless me for a great future.

Thank you and apologies to everyone else whom I might have missed in this acknowledgment.

TABLE OF CONTENTS

LIST OF TABLES.....	xiii
LIST OF FIGURES.....	xv
KEY TO ABBREVIATIONS	xxii
1. INTRODUCTION.....	1
1.1 INTRODUCTION.....	1
1.1.1 Starch based bioplastics.....	2
1.2 OVERALL GOALS AND OBJECTIVES.....	7
1.3 ORGANIZATION OF THE THESIS.....	9
REFERENCES	13
2. DESIGN AND ENGINEERING OF INSOLUBLE, HIGH-PERFORMANCE STARCH FOAMS VIA EXTRUSION TECHNOLOGY.....	15
2.1 ABSTRACT.....	15
2.2 INTRODUCTION AND BACKGROUND.....	17
2.2.1 Polyvinyl butyraldehyde (PVB).....	18
2.2.2 Chitosan.....	19
2.2.3 Sodium trimetaphosphate (STMP).....	21
2.3 MATERIALS.....	24
2.4 EXPERIMENTAL.....	25
2.5 FOAM EXTRUSION PROCESS DEVELOPMENT.....	29
2.5.1 Screw Configuration.....	29
2.5.2 Temperature profile.....	32
2.5.3 Die type and diameter.....	33
2.6 CHARACTERIZATION AND ANALYSIS.....	36
2.7 RESULTS AND DISCUSSION.....	42
2.7.1 Effects of various additives on density and expansion ratio.....	42
2.7.2 Water solubility tests.....	46
2.7.3 Water penetration test.....	51
2.7.4 Solution uptake measurements for foams.....	54
2.7.5 Moisture sensitivity.....	56
2.7.6 Contact angle measurements.....	63
2.7.7 Scanning electron microscopy.....	67
2.7.8 Confocal microscopy.....	73
2.7.9 Compressive strength.....	75
2.7.10 Aqueous biodegradability studies.....	77
2.8 DESIGNING AN ANNULAR DIE.....	79
2.9 FUTURE RECOMMENDATIONS.....	83
2.10 CONCLUSIONS.....	84
REFERENCES	86

3. BIOBASED MALEATED THERMOPLASTIC STARCH (MTPS) AND MTPS-G-PETG (GLYCOL MODIFIED PET) GRAFT COPOLYMER VIA REACTIVE EXTRUSION: EVALUATIONS.....	92
3.1 ABSTRACT.....	92
3.2 INTRODUCTION.....	93
3.3 EXPERIMENTAL.....	96
3.3.1 Materials.....	96
3.3.2 Preparation of maleated thermoplastic starch (MTPS).....	96
3.3.3 Preparation of MTPS-PETG graft copolymers.....	97
3.4 CHARACTERIZATION AND ANALYSIS.....	98
3.4.1 Soxhlet extractions using acetone and dichloromethane.....	98
3.4.2 Thermal analysis.....	99
3.4.3 Tensile testing.....	99
3.4.4 Impact Testing.....	100
3.4.5 Fourier Transform Infrared Spectroscopy (FT-IR).....	100
3.4.6 Scanning Electron microscopy.....	101
3.4.7 Aqueous biodegradation.....	101
3.5 RESULTS AND DISCUSSIONS.....	102
3.5.1 MTPS analysis: Soxhlet extraction.....	102
3.5.2 PETG-MTPS analysis: Soxhlet extraction.....	103
3.5.3 PETG-MTPS analysis: FTIR.....	105
3.5.4 PETG-MTPS analysis: Mechanical properties.....	106
3.5.5 MTPS-PETG analysis: Morphology.....	108
3.5.6 MTPS-PETG analysis: Biodegradability testing.....	109
3.6 CONCLUSIONS AND FUTURE STUDY.....	112
REFERENCES.....	113
4. EFFECTS OF MODIFIED THERMOPLASTIC STARCH ON CRYSTALLIZATION KINETICS AND BARRIER PROPERTIES OF PLA.....	116
4.1 ABSTRACT.....	116
4.2 INTRODUCTION.....	117
4.3 MATERIALS AND METHODS.....	121
4.3.1 Materials.....	121
4.3.2 Preparation of and Polylactide (PLA)/MTPS Blends.....	121
4.3.3 Soxhlet extraction.....	122
4.3.4 Thermal analysis.....	123
4.3.5 Isothermal Crystallization Analysis.....	124
4.3.6 Polarized Optical Microscopy (POM).....	124
4.3.7 Mechanical Properties.....	124
4.3.8 Scanning electron microscopy.....	125
4.3.9 Barrier properties.....	125
4.3.10 Aqueous biodegradability Testing.....	126
4.4 RESULTS AND DISCUSSION.....	127
4.4.1 Percent Grafting for MTPS-PLA blends.....	127
4.4.2 Mechanical Testing and Phase Morphology.....	127
4.4.3 Thermal analysis.....	131
4.4.4 Isothermal Crystallization Kinetics.....	135

4.4.5	Permeability Studies.....	142
4.4.6	Biodegradability Studies.....	143
4.5	CONCLUSIONS.....	146
	REFERENCES.....	148
5.	ANTIMICROBIAL SOLID STARCH-IODINE COMPLEX VIA REACTIVE EXTRUSION AND ITS APPLICATION IN PLA-PBAT BLOWN FILMS.....	154
5.1	ABSTRACT.....	154
5.2	INTRODUCTION.....	155
5.3	STARCH IODINE COMPLEX.....	157
5.4	EXPERIMENTAL SECTION.....	159
5.4.1	Materials.....	159
5.4.2	Preparation of MTPS-Iodine pellets.....	159
5.4.3	Preparation of PLA-PBAT-Starch-Iodine films.....	160
5.5	CHARACTERIZATION AND ANALYSIS.....	162
5.5.1	Thermogravimetric analysis (TGA).....	162
5.5.2	Antimicrobial Properties: Antifungal test.....	162
5.5.3	Visual decay and weight loss of strawberries.....	163
5.5.4	Antimicrobial properties.....	163
5.5.5	Mechanical Properties.....	164
5.5.6	Scanning Electron Microscopy.....	165
5.6	Results and discussion.....	166
5.6.1	Iodine content evaluation.....	166
5.6.2	Antifungal properties: Changes in weight loss and visual decay.....	168
5.6.3	Antimicrobial activity studies on the pellets and films.....	169
5.6.4	Mechanical Properties and morphology of the films.....	172
5.7	CONCLUSIONS AND FUTURE WORK.....	176
	APPENDIX.....	178
	REFERENCES.....	181
6.	UNDERSTANDING BIODEGRADABILITY OF BIOBASED POLYMERS IN MARINE ENVIRONMENT.....	184
6.1	ABSTRACT.....	184
6.2	INTRODUCTION AND BACKGROUND.....	185
6.2.1	Need for lifetime prediction and end of life analysis.....	185
6.3	BIODEGRADATION PROCESS.....	189
6.4	MECHANISMS OF BIODEGRADATION.....	191
6.5	FACTORS AFFECTING AQUEOUS BIODEGRADATION.....	193
6.5.1	Shape and surface area.....	193
6.5.2	Crystallinity.....	193
6.5.3	Static vs dynamic water conditions.....	193
6.5.4	Temperature.....	194
6.6	POLYHYDROXY ALKANOATES (PHAS).....	196
6.7	EXPERIMENTAL SECTION.....	198
6.7.1	Materials.....	198
6.8	MATERIAL PROCESSING AND CHARACTERIZATION.....	199
6.8.1	Elemental analysis.....	199

6.8.2	Thermal analysis.....	200
6.8.3	Determination of particle size of pellets.....	201
6.8.4	Scanning electron microscopy.....	201
6.8.5	Molecular weight analysis.....	201
6.8.6	Microbial inoculum.....	202
6.9	EXPERIMENTAL BIODEGRADATION SETUP.....	203
6.10	RESULTS AND DISCUSSION.....	208
6.10.1	Initial characterization of polymer pellets.....	208
6.10.2	Biodegradation: CO ₂ evolution and mineralization.....	210
6.10.3	Biodegradation kinetics: Parameter estimation and order of reaction.....	213
6.10.4	Biodegradation as a first order reaction.....	215
6.10.5	Parameter estimation: Arrhenius equation.....	216
6.10.6	Biodegradation data compilation.....	222
6.10.7	Accumulation of plastics in ocean.....	226
6.11	MECHANISM OF PHBV BIODEGRADATION.....	228
6.12	CONCLUSION AND FUTURE WORK.....	232
	APPENDICES.....	235
	Appendix 1: NMR analysis of PHBV.....	236
	Appendix 2: Carbon removal against time curves.....	238
	Appendix 3: Metagenomic analysis.....	239
	Appendix 4: Order of reaction and rate constant determination using n th order kinetic equation.....	241
	Appendix 5: Using global equation for estimating E _a and A' values.....	247
	Appendix 6: lifetime prediction.....	251
	Appendix 7: Table for obtaining %C remaining vs time graphs.....	252
	Appendix 8: Literature summary.....	253
	Appendix 9: Method 1 calculations.....	259
	Appendix 10: Ocean plastic accumulation model.....	262
	REFERENCES.....	263

LIST OF TABLES

Table 2.1: Extrusion runs with various additives.....	27
Table 2.2: Screw configurations for starch foam extrusion.....	30
Table 2.3: General temperature profile for extrusion	32
Table 2.4: Different salt solutions for relative humidity.....	38
Table 2.5: Mineral solution composition for the test.....	40
Table 2.6: Parameters of Peleg model for kinetics of moisture absorption of starch foams.....	60
Table 2.7: Physico-mechanical properties of extruded starch foams.....	77
Table 3.1: Results for percent grafting of glycerol on MTPS.....	102
Table 3.2: Tensile properties of PETG and MTPS-g-PETG blend.....	107
Table 4.1: Summary of physico-mechanical properties of packaging polymers.....	118
Table 4.2: Sample name and composition.....	122
Table 4.3: Effect of MTPS content on tensile properties of PLA	128
Table 4.4: Thermogravimetric analysis (TGA) of PLA and blends.....	131
Table 4.5: Thermal transition temperatures and percent crystallinity of modified PLA samples.....	133
Table 4.6: Crystallization half times and Avrami constants for PLA samples at different temperatures	142
Table 5.1: Temperature and processing conditions for making blown films.....	161
Table 5.2: Sample name and composition.....	161
Table 6.1: Aqueous biodegradation test setup. Test carried out at 10°C.....	199
Table 6.2: Aqueous biodegradation test setup. Test carried out at 30°C.....	200
Table 6.3: Aqueous biodegradation test setup. Test carried out at 40°C.....	200
Table 6.4: Buffer solutions used for aqueous biodegradation.....	205
Table 6.5: Order of reaction for cellulose and PHBV biodegradation.....	214

Table 6.6: Parameter estimates for activation energy and pre-exponential factor using method 1, 2 and 3	218
Table 6.7: Final estimated parameter values for the global equation for cellulose and PHBV.....	219
Table 6.8: Evolution of number-average molecular weight (M_n), weight-average molecular weight (M_w), polydispersity index (M_n/M_w) and melting point (T_m) of PHBV samples during the course of biodegradation	229
Table 6.9: Lifetime estimation for PHBV and cellulose at 30, 10 and 4° C.....	251
Table 6.10: Percent carbon remaining vs time.....	252
Table 6.11: Literature summary	253
Table 6.12: Ocean plastics accumulation model	262

LIST OF FIGURES

Figure 1.1: Various biobased and fossil-based plastics and their relation to biodegradability (all the polymers below the horizontal line are fully biodegradable or compostable)[3].....	2
Figure 1.2: Global production capacities of bioplastics 2021[1].....	3
Figure 1.3: Structure of starch units - a) Amylose b) Amylopectin	4
Figure 1.4: SEM images for showing structure, size and shape of various starch granules depending on the source.....	4
Figure 1.5: Some applications of bioplastics	5
Figure 1.6: Schematic for overall summary of the work in this thesis.....	8
Figure 1.7: Schematic for the summary of chapter 2	9
Figure 1.8: Schematic for summary of chapter 4.....	10
Figure 1.9: Schematic for summary of chapter 5.....	11
Figure 1.10: Schematic for summary of chapter 6.....	12
Figure 2.1: Structure of polyvinyl butyraldehyde(PVB)	19
Figure 2.2: Schematic for polyelectrolyte complex formation	20
Figure 2.3: Scheme for formation of polyelectrolyte complex between chitosan and starch	20
Figure 2.4: Phosphorylation of starch with STMP	21
Figure 2.5: Experimental setup for foam extrusion.....	26
Figure 2.6: Foams obtained from a) Screw configuration #1 b) Screw configuration #2.....	30
Figure 2.7: Second Screw configuration used for foam extrusion	32
Figure 2.8: Three strand dies used for extrusion and their corresponding expansion ratios	34
Figure 2.9: Process development with slit die.....	35
Figure 2.10: Effect of talc and PVOH addition on density and expansion ratio of foams.....	43
Figure 2.11: Effect of chitosan on density and expansion ratio of foams.....	44

Figure 2.12: Effect of STMP addition on density and expansion ratio of starch foams	45
Figure 2.13: Water solubility for foams with different additives.....	47
Figure 2.14: Solubility of corn starch foams with glycerol	48
Figure 2.15: Solubility studies for potato starch foams	49
Figure 2.16: Water solubility studies for foams containing PVB.....	50
Figure 2.17: Water penetration test for foams with various additives.....	51
Figure 2.18: water penetration test for foams containing PVB, chitosan and STMP.....	52
Figure 2.19: Water penetration test for foams with and without glycerol.....	53
Figure 2.20: Swelling characteristics of starch-chitosan-STMP foams	55
Figure 2.21: Moisture absorption curves for starch foams in different RH conditions a)control foams (starch+water) b)Control foam(PVOH +water), c)corn starch +PVB + chitosan ,d)corn starch+STMP+chitosan	56
Figure 2.22: Sorption isotherms for different types of starch foams	58
Figure 2.23: Shrinkage in foams with high RH of 95% a) control starch foam, b) PVOH foam, c) PVB foam d) chitosan +STMP (1.5%)	59
Figure 2.24: Peleg model constants k1 and k2 for the starch foam samples.....	61
Figure 2.25: Moisture content at equilibrium for different foam formulations at 95% RH	62
Figure 2.26: Effect of different additives on surface hydrophobicity of foams.....	63
Figure 2.27: Effect of increasing percentage of chitosan and addition of STMP on surface hydrophobicity.....	65
Figure 2.28: Effect of glycerol addition on surface hydrophobicity of starch foams.....	66
Figure 2.29: SEM images for various additives used in foam formulations – a) talc, b) chitosan, c)STMP, d) PVB at 200x magnification; e)talc, f)chitosan, g)STMP; h) PVB at 5000x magnification	68
Figure 2.30: SEM images of starch foams containing a)0% talc b) 0.7% talc c)2% talc d)4% chitosan e)7% chitosan f)10% chitosan g) 1% STMP h) 1.5% STMP i) 3% STMP	69
Figure 2.31: Cell size distribution for foams containing different percentages of talc.....	70

Figure 2.32: Cell size distributions for starch foams with PVB at different STMP levels a) 0% b) 1% c)1.5 % d)3%.....	71
Figure 2.33: Cell size distribution of starch foams with increasing percentages of chitosan.....	72
Figure 2.34: Confocal laser scanning microscope (CLSM) 3D MIP images for 0%, 4%, 7% and 10% chitosan foam formulations from the bulk of the sample (a,b,c,d) and from the surface (e,f,g,h)	75
Figure 2.35: Compressive strength of starch foams 1)Control foams (starch+water), 2)Control foams (PVOH), 3)10% PVB,4% chitosan, 4) 10% PVB,7% chitosan, 5) 10% PVB,10% chitosan, 6) 10% PVB,4% chitosan, 1% STMP, 7) 10% PVB,4% chitosan, 1.5 STMP, 8) 10% PVB,4% chitosan, 3% STMP	76
Figure 2.36: Aqueous biodegradation curves for control starch foam, PVB containing foam and STMP containing foam	78
Figure 2.37: Annular die design parts.....	79
Figure 2.38: AUTOCAD design for the die	80
Figure 2.39: 3D printed die	81
Figure 2.40: CNC machined die.....	81
Figure 2.41: a), b) Some annular die foams produced from the trial runs c) flat sheets formed after cutting the foam tubes	82
Figure 3.1: Structure of maleated thermoplastic starch	94
Figure 3.2: Structure of PETG.....	96
Figure 3.3: Preparation of maleated thermoplastic starch.....	97
Figure 3.4: DTG curves of MTPS, glycerol and residue showing only MTPS after Soxhlet extraction	103
Figure 3.5: TGA graphs for MTPS, PETG and MTPS-g-PETG	104
Figure 3.6: DTG curve of residue remaining after Soxhlet extraction	105
Figure 3.7: Comparative FT-IR spectra of PETG, MTPS and MTPS-PETG residue.....	106
Figure 3.8: The average stress-strain curves of PETG and MTPS-g-PETG.....	107
Figure 3.9: Notched Izod impact strength of PETG and MTPS-g-PETG reactive blend.....	108

Figure 3.10: SEM images of a) MTPS-PETG blend after leaching of MTPS phase with HCL; b) Tensile fracture surface of PETG c) Tensile fracture surface of MTPS-g-PETG.....	109
Figure 3.11: Experimental aqueous biodegradation setup	110
Figure 3.12: Biodegradation curve for MTPS-PETG for a) Initial 80 days b) Total 150 days.....	111
Figure 4.1: Modulus, tensile stress, and tensile strain graphs for PLA and blends	128
Figure 4.2: Scanning electron microscopy (SEM) images of fractured tensile surfaces of (a) PLA, (b) PLA + 1% MTPS, (c) PLA + 2% MTPS, (d) PLA + 5% MTPS	129
Figure 4.3: SEM images of the blends after selective extraction of MTPS phase (a) PLA, (b) PLA + 1% MTPS, (c) PLA + 2% MTPS, (d) PLA + 5% MTPS.....	129
Figure 4.4: a) TGA and b) DTG curves for PLA and PLA/MTPS blends.....	132
Figure 4.5: Differential scanning calorimetry (DSC) thermograms of PLA and the blends.....	134
Figure 4.6: Melting curves for PLA blends after annealing.....	135
Figure 4.7: DSC melting thermograms of a) PLA and blends (b) PLA+1%MTPS, c) PLA+2%MTPS, d) PLA+5% MTPS)at various temperatures	136
Figure 4.8: Fractional crystallinity vs. time of a) PLA and blends (b) PLA+1%MTPS, c) PLA+2%MTPS, d) PLA+5% MTPS)at various temperatures	138
Figure 4.9: Plots of $\ln(\ln(1-X(t)))$ vs $\ln t$ of a) PLA and blends (b) PLA+1%MTPS, c) PLA+2%MTPS, d) PLA+5% MTPS)at various temperatures	139
Figure 4.10: Half time for crystallization vs isothermal crystallization temperatures for PLA and blends	139
Figure 4.11: Comparing the $t_{1/2}$ values of PLA/MTPS blends with other nucleating agents	140
Figure 4.12: Polarized optical microscopy (POM) images of PLA/MTPS blends with MTPS content of 0%: (a–c); 1%: (d–f); 2%: (g–i); 5%: (j–l)	141
Figure 4.13: Effect of MTPS content on moisture permeability (WVP) and oxygen permeability (OP) of PLA films	143
Figure 4.14: Experimental aqueous biodegradation setup	144
Figure 4.15: Aqueous biodegradation curves for PLA and PLA + 5% MTPS.....	144

Figure 5.1: Amylose coil structure - due to acetal linkages	157
Figure 5.2: Structure of amylose-iodine complex	158
Figure 5.3: Production of MTPS-iodine pellets via reactive extrusion.....	160
Figure 5.4: DTG curves for MTPS, MTPS-iodine and iodine	167
Figure 5.5: Isothermal TGA for MTPS and MTPS-iodine.....	167
Figure 5.6: Weight loss and visual decay analysis for coated and uncoated strawberries .	168
Figure 5.7: Photographs of the petri plates from disk diffusion and direct inoculation test with E. coli. a) Kirby Bauer test on starch-iodine pellets showing antibacterial zone of inhibition b)-f) bacterial colonies growth on the petri plates after 24 hours b) control PLA films c) AM: Silver antimicrobial films d) SI1: starch-iodine-PLA films with 0.7% iodine and 1 mil thickness e) SI2: starch-iodine-PLA films with 0.7% iodine and 2 mil thickness f) SI3: starch-iodine-PLA films with 1.3% iodine and 2 mil thickness.....	170
Figure 5.8: Average change in Log CFU/ml of the Escherichia coli (E. coli) strains after 24 h incubation on five different PLA film configurations (control PLA;AM film and SI1, SI2 and SI3)	171
Figure 5.9: Mechanical properties for the different PLA blown film formulations in machine and transverse direction a) tensile strength b) Elongation at break c)Tear strength	174
Figure 5.10: Visual and SEM images of the fractured surface of the films after selective extraction of MTPS-iodine phase a), b) and c) : SI1- 0.7% iodine, 1 mil; d), e) and f) : SI2 – 0.7 % iodine, 2 mil; g),h) and i) : 1.3% iodine, 2 mil.....	175
Figure 6.1: Temperature-depth Ocean water profile[11]	187
Figure 6.2: The different steps involved in the biodegradation process.....	189
Figure 6.3: Degradation mechanisms for biodegradable polymers A) Bulk erosion, B) Surface erosion[15]	192
Figure 6.4: Chemical structures of cellulose and PHBV	198
Figure 6.5: A typical biodegradation curve for %biodegradation vs time.....	203
Figure 6.6: Experimental biodegradation setup	206
Figure 6.7: TGA and DTG curves for a) cellulose, b) PHBV; DSC curves for c) cellulose d)PHBV.....	209

Figure 6.8: Average biodegradation curves of Cellulose tested at different temperature (10, 30, 40°C). Each curve represents average of 2 replicates.....	211
Figure 6.9: Average biodegradation curves of PHBV tested at different temperature (10, 30, 40°C). Each curve represents average of 2 replicates.....	211
Figure 6.10: C/C ₀ as a function of time for aqueous biodegradation of a) Cellulose and b) PHBV at 10, 30 and 40°C. Points represent experimental data whereas dotted lines indicate fitting of 1st order equation	212
Figure 6.11: Schematic for showing the comparison between standard linear regression analysis, reparametrized Arrhenius equation analysis and the one step global equation approach	217
Figure 6.12: Precision differences for biodegradation time estimations for the three methods	220
Figure 6.13: percent carbon remaining as a function of time for cellulose and PHBV at 30, 10 and 4 °C.....	221
Figure 6.14: Comparing the experimental rate constants to literature values for Cellulose and PHBV	223
Figure 6.15: Statistical analysis of rate constants for a) cellulose and b) PHBV at 25 and 30 C	224
Figure 6.16: Model for plastics accumulation in ocean – impact of replacing a fraction of non-biodegradable plastics with biodegradable plastics.....	227
Figure 6.17: PHBV SEM and optical microscopy images at various stages of biodegradation.....	228
Figure 6.18: a) DSC melting peaks and b) TGA degradation curves of PHBV pellets as a function of biodegradation percentage in laboratory scale aqueous biodegradation	230
Figure 6.19: NMR curve for PHBV	237
Figure 6.20: Comparing the microbial populations from wastewater and seawaters from various places	240
Figure 6.21: ln(-dC/dt) vs lnC plot for cellulose at A)10 C, B) 30 C, C) 40 C	242
Figure 6.22: ln(-dC/dt) vs ln C plots for PHBV at A)10 C, B) 30 C, C)40 C	243
Figure 6.23: mmoles of carbon remaining vs time plots for cellulose at A)10C, B)30C, C) 40 C	245

Figure 6.24: Mmoles of carbon remaining vs time plots for PHBV at A)10C, B)30C, C) 40C	246
Figure 6.25: minitab methodology for global equation-1	248
Figure 6.26: minitab methodology for global equation-2	248
Figure 6.27: minitab methodology for global equation-3	249
Figure 6.28: Percent carbon remaining vs time graphs (lifetime prediction) for cellulose at various temperatures	250
Figure 6.29: $\ln(C_0/C_t)$ vs time for PHBV and cellulose at 10, 30 and 40°C	260
Figure 6.30: Arrhenius plots for PHBV and cellulose.....	261

KEY TO ABBREVIATIONS

PLA – Polylactide

PE – Polyethylene

LDPE – Low density polyethylene

PCL – Polycaprolactone

MTPS – Maleated thermoplastic starch

PETG – Polyethylene terephthalate glycol

PHBV - Poly(3-hydroxybutyrate-co-3-hydroxyvalerate)

PVB – Polyvinyl butyral

STMP – Sodium trimetaphosphate

PHAE – Polyhydroxylamino ether

PBAT - Polybutylene adipate terephthalate

BPA – Bisphenol A

PEC – Polyelectrolyte complex

PVOH - Polyvinyl alcohol

MCC – Microcrystalline cellulose

FITC - fluorescein isothiocyanate

ISO - International Organization for Standardization

SEM – Scanning electron microscopy

CLSM - Confocal laser scanning microscopy

TGA – Thermogravimetric analysis

DSC – Differential scanning calorimetry

MIP – Maximum intensity projection

REX – Reactive extrusion

DCM – Dichloromethane

FT-IR - Fourier Transform Infrared Spectroscopy

ThCO₂ – Theoretical CO₂

PS – Polystyrene

MA – Maleic anhydride

WVP – water vapor permeability

POM – Polarized optical microscopy

OTR – Oxygen transmission rate

WVTR – Water vapor transmission rate

CSI – Crosslinked starch iodine

TPS – Thermoplastic starch

DTG – Derivative thermogravimetric graphs

MD – Machine direction

TD – Transverse direction

PGA – poly (glycolic acid)

BD – Biodegradation

CI – Confidence intervals

SD – Standard deviation

MT – Million tones

PDI – Polydispersity index

1. INTRODUCTION

1.1 INTRODUCTION

Plastics and polymers have emerged as a vast market for a wide range of applications including electronics, packaging, automotive, medical etc. According to European bioplastics, the global market for plastics was about 367 million tonnes. Amongst those plastics, biobased and biodegradable plastics share is still less than one percent. But rising awareness about environmental pollution due to fossil fuel-based plastics is fueling the research and use of biobased and biodegradable plastics in various fields. The demand for bioplastics is surging. Global bioplastics production capacities are set to increase from around 2.42 million tonnes in 2021 to approximately 7.59 million tonnes in 2026[1].

European bioplastics defines bioplastics as biobased, biodegradable, or both. They have the same or similar properties as conventional plastics but offer additional benefits, such as a reduced carbon footprint, better functionalities, or additional waste management options, such as organic recycling[1]. Biodegradability is an end-of-life option that harnesses the power of microorganisms present in the selected disposal environment, to completely remove plastic products, designed to be biodegradable, from the environmental compartment via the microbial food chain in a timely, safe, and efficacious manner[2]. The property of biodegradation does not depend on the resource basis of a material but is rather linked to its chemical structure. In other words, 100 percent biobased plastics may be non-biodegradable, and 100 percent fossil-based plastics can biodegrade. Figure 1.1 shows the schematic for various biobased and fossil-based plastics and their relation with biodegradability based on their chemical structure[3].

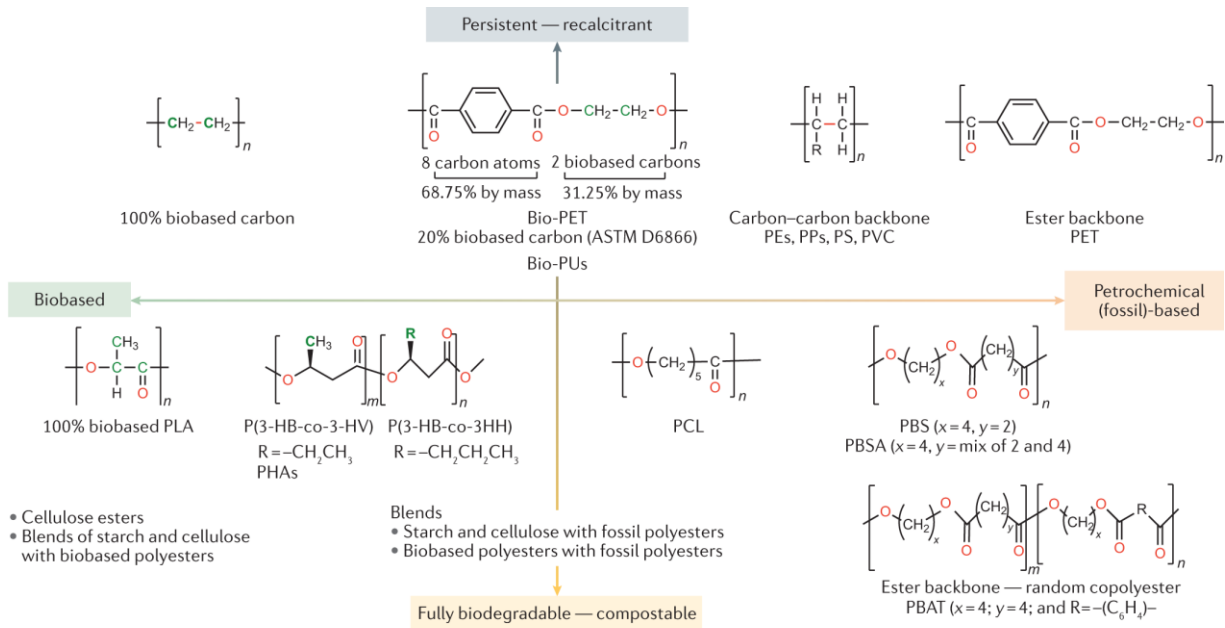


Figure 1.1: Various biobased and fossil-based plastics and their relation to biodegradability (all the polymers below the horizontal line are fully biodegradable or compostable)[3]

Replacing the petro/fossil carbon with biobased carbon derived from plant/biomass resources offers the value proposition of a zero-material carbon footprint[2]. Target markets for biodegradable polymers include packaging materials like trash bags, loose-fill foam, food containers, film wrapping, laminated paper, hygiene products like diaper back sheets and cotton swabs, consumer goods like fast-food tableware and containers, egg cartons, and toys, and agricultural tools like mulch films and planters etc.

1.1.1 Starch based bioplastics

Biobased plastics are derived from various biomass sources. The most widely used resource is starch. Starch based plastics are often incorporated in various petroleum-based polymers or biobased polymers to create unique composite materials. The main advantage of using starch based polymeric materials is the ability of starch to biodegrade in almost all different environments: soil, compost and water. Hence, starch-based products are particularly ideal

for products when the risk of leakage in the environment after its use is high. Starch based bioplastics are not generally thought as a direct replacement for traditional plastics. Because of their peculiar properties, they present an opportunity to redesign the systems to enable the use of starch products[4, 5]. Out of the 2.42 million tons of bioplastics produced in 2021, 16.4% were starch-based plastics[6]. Figure 1.2 shows the global production capacities of bioplastics in 2021 by their material types.

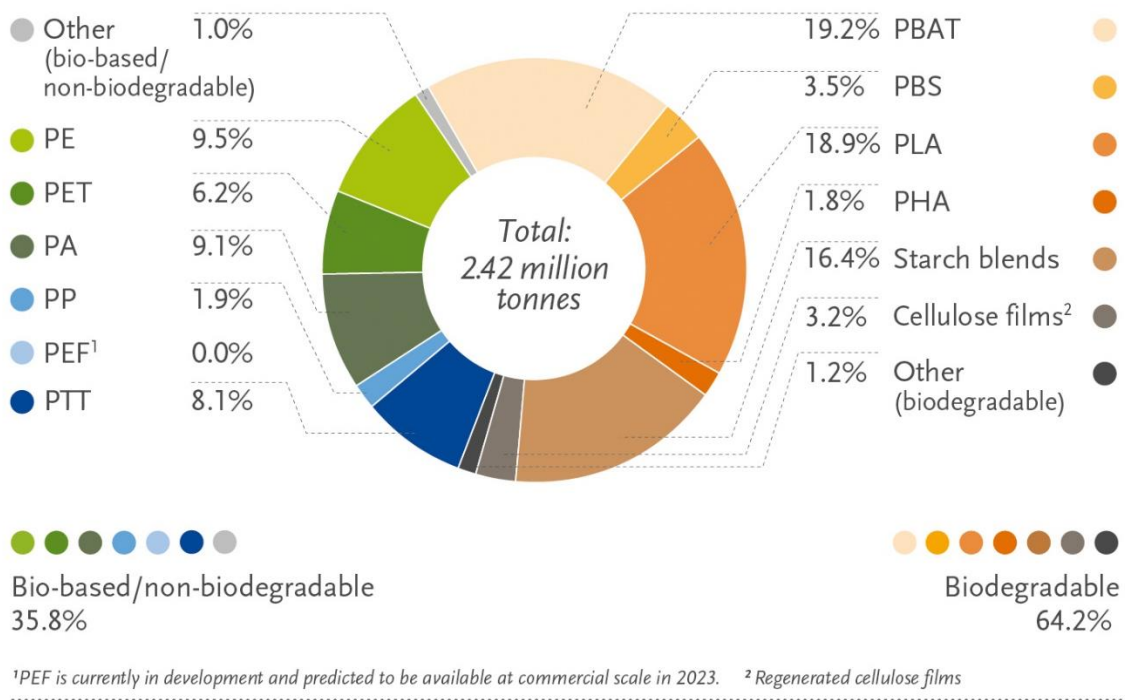


Figure 1.2: Global production capacities of bioplastics 2021[1]

Starch is used as a starting material for a wide range of green materials. 75% of all organic material on earth is present in the form of polysaccharides. Most important industrial starch sources are crops such as corn (82%), wheat (8%), potato (5%) and cassava (5%). US is the 2nd largest producer of corn with 15.1 billion bushels produced in 2021[7]. Starch consists of two polymers – 1) amylose which is a linear polymer containing chains of α -1,4-anhydroglucose units which are mainly responsible for film-forming abilities and 2)

amylopectin which is a highly branched polymer containing α -1,4-anhydroglucose units and α -1,6-glycosidic branched chains [8, 9, 10]. Figure 1.3 shows the structures of the two units.

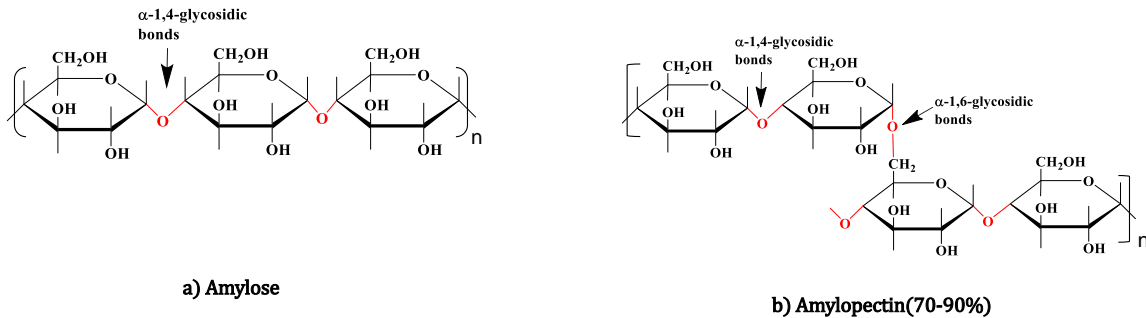


Figure 1.3: Structure of starch units - a) Amylose b) Amylopectin

The ratio of amylose and amylopectin is different in different starches [11]. The properties of the products like films, foams depend on the type of starch being used. Waxy starches contain less than 15% amylose, normal starches contain about 30% amylose whereas high amylose starches contain more than 40-50% amylose. Starch granules occur in all shapes and sizes and their dimensions range from 2-200 μ m depending on the source of the starch. Figure 1.4 shows two such examples of different granule shapes and sizes for potato and corn starch.

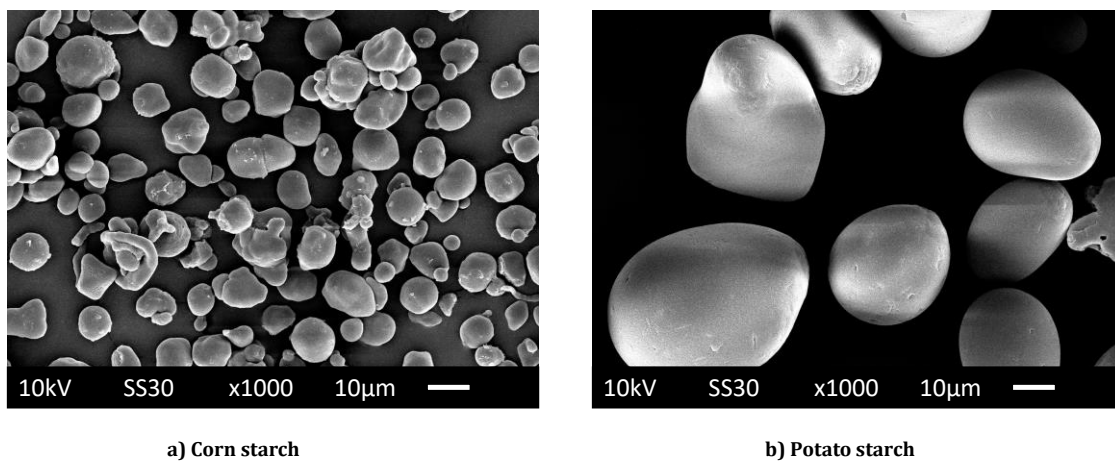


Figure 1.4: SEM images for showing structure, size and shape of various starch granules depending on the source

Starch in its native state is not thermoplastic. Various plasticizers such as water, glycerol, sorbitol etc. are added during processing to make the starch pseudo thermoplastic and processable. Starch is commonly blended with other biodegradable or non-biodegradable polymers such as polylactide (PLA), polyethylene (PE), Low density polyethylene (LDPE), polycaprolactone (PCL) etc. Other common applications are in loose fill packaging foams, cups, plates, films and trays. Figure 1.5 shows some of the common products available commercially which make use of bioplastics.



Figure 1.5: Some applications of bioplastics

In the current work we have focused on design and engineering of various starch based polymeric materials including starch foams, maleated thermoplastic starch (MTPS) and its applications as – a blend with a non-biodegradable polymer (PETG), as a nucleating agent and barrier property enhancer in PLA and as a vector for safe delivery of antimicrobial iodine in an environment without the usual hazards associated with handling solid iodine. Next part of the thesis focuses on the end-of-life assessments for such bioplastics. Biodegradation of the polymers in aqueous environment was studied in detail, impact of temperature on the

rate of biodegradation was analyzed, and a global kinetic analysis model was proposed for predicting the persistence of microplastics in oceans.

1.2 OVERALL GOALS AND OBJECTIVES

This study focuses on using starch as a backbone to design various polymeric products – starch foams, thermoplastic starch, blends of thermoplastic starch with polyesters such as PLA and PETG for improving their performance properties, thermoplastic starch as a vehicle to deliver antimicrobial iodine into other polymers, plastic films, foams etc. and evaluating the biodegradability of these bioplastics at their end of life for their lifetime prediction in natural environments like ocean.

This study targeted the design and engineering of high performance, water insoluble and moisture resistant starch foams. One part of the study was focused on the scale up of a starch-chitosan polyelectrolyte complex foam product prepared via microwave expansion. The target applications were use in medical field as hemostatic pads and in packaging where long-term moisture resistance and mechanical properties are required. Polyvinyl butyral (PVB) was also investigated as an additive along with chitosan and sodium trimetaphosphate (STMP) and their synergistic effects on the performance properties of foams were studied.

Next part of the thesis was development and application of another value-added product from starch– Maleated thermoplastic starch (MTPS). Covalently grafted glycerol containing MTPS was prepared in a twin-screw extruder and its reactive blends to form graft copolymers with glycol modified polyethylene terephthalate (PETG) achieving in-situ grafting using transesterification chemistry were evaluated. It also targets on studying the effect of MTPS in a PLA- another biobased polymer, as nucleating agent, and barrier property enhancer. Further, A solid starch-iodine complex resin was also developed in this study as an antibacterial additive for application in active packaging, films, and foams using reactive extrusion.

Finally, this thesis also covers the aqueous biodegradation studies for various polymers and their kinetic analysis. The models developed here are useful for predicting the lifetime of these polymers in low temperature marine environment. Figure 1.6 shows the schematic for overall summary of the work in this thesis.

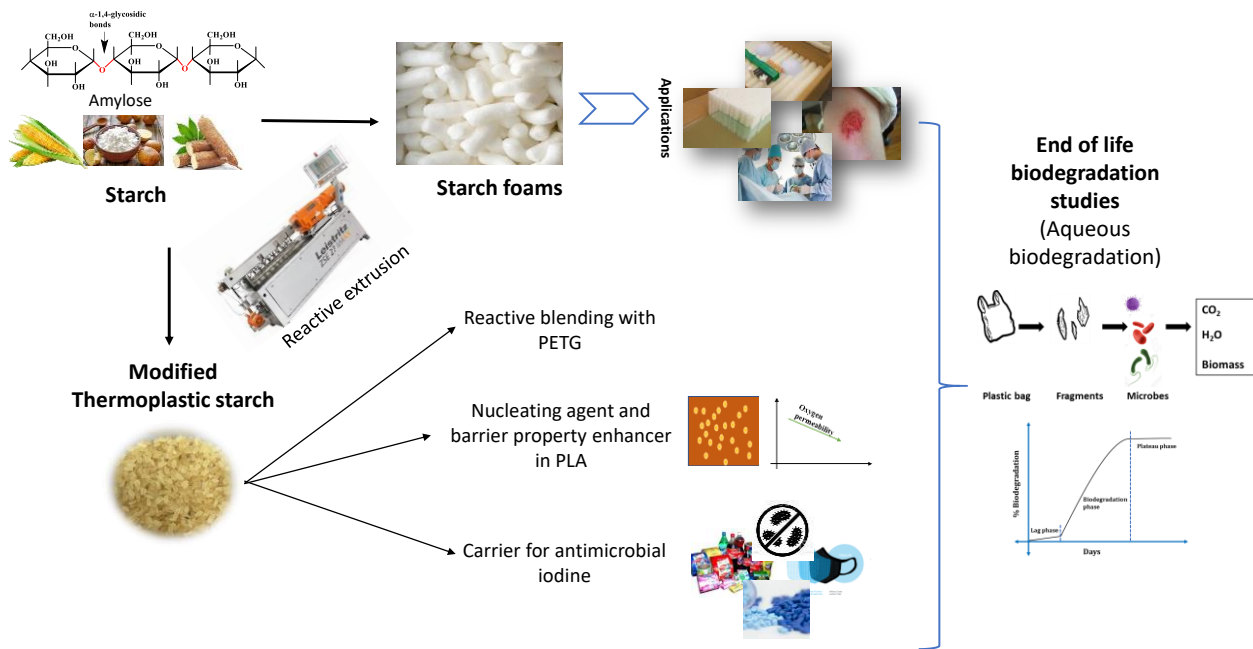


Figure 1.6: Schematic for overall summary of the work in this thesis

1.3 ORGANIZATION OF THE THESIS

This thesis is divided into six chapters, each of which individually addresses the work that has been done in relation to the objectives outlined above.

Chapter 2 deals with the existing starch foams technology and the optimization of the process variables such as screw configuration, temperature profile, die type and diameter, water content etc. It also covers the procedures for all characterization techniques used for all the foam formulations developed. It includes the different formulations developed using additives and reactive modifiers such as PVOH, PVB, chitosan, STMP, glycerol and talc. The impact of each of these on various properties of foam such as density, expansion ratio, contact angle, water sensitivity, TGA, cell size, water absorption, mechanical properties, biodegradation etc. is studied in detail. This chapter also includes the design of a new annular die and some preliminary trials done with that which form the basis for future work in this area. Figure 1.7 shows the summary of chapter 2.

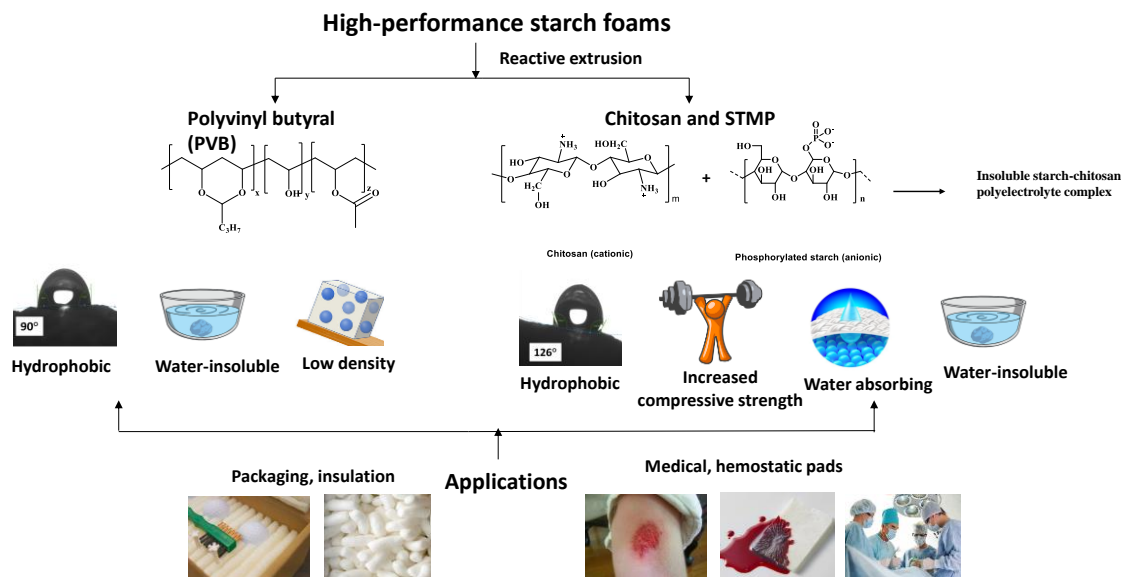


Figure 1.7: Schematic for the summary of chapter 2

Chapter 3 covers the synthesis and characterization of maleated thermoplastic starch (MTPS) and its use for making reactive blends with PETG. Present grafting calculations for both MTPS and MTPS/PETG blends are performed. The changes in mechanical and thermal properties of PETG and the effect on biodegradation due to addition of MTPS for are compared and contrasted with neat PETG.

Chapter 4 studies the effect of addition of MTPS in PLA as a nucleating agent and barrier property enhancer. The changes in crystallinity, crystallization kinetics and barrier properties of PLA due to addition of MTPS is studied. Additional properties such as thermal degradation temperatures, tensile modulus and strength and aqueous biodegradation of the blends is also evaluated. Figure 1.8 shows the summary for chapter 4.

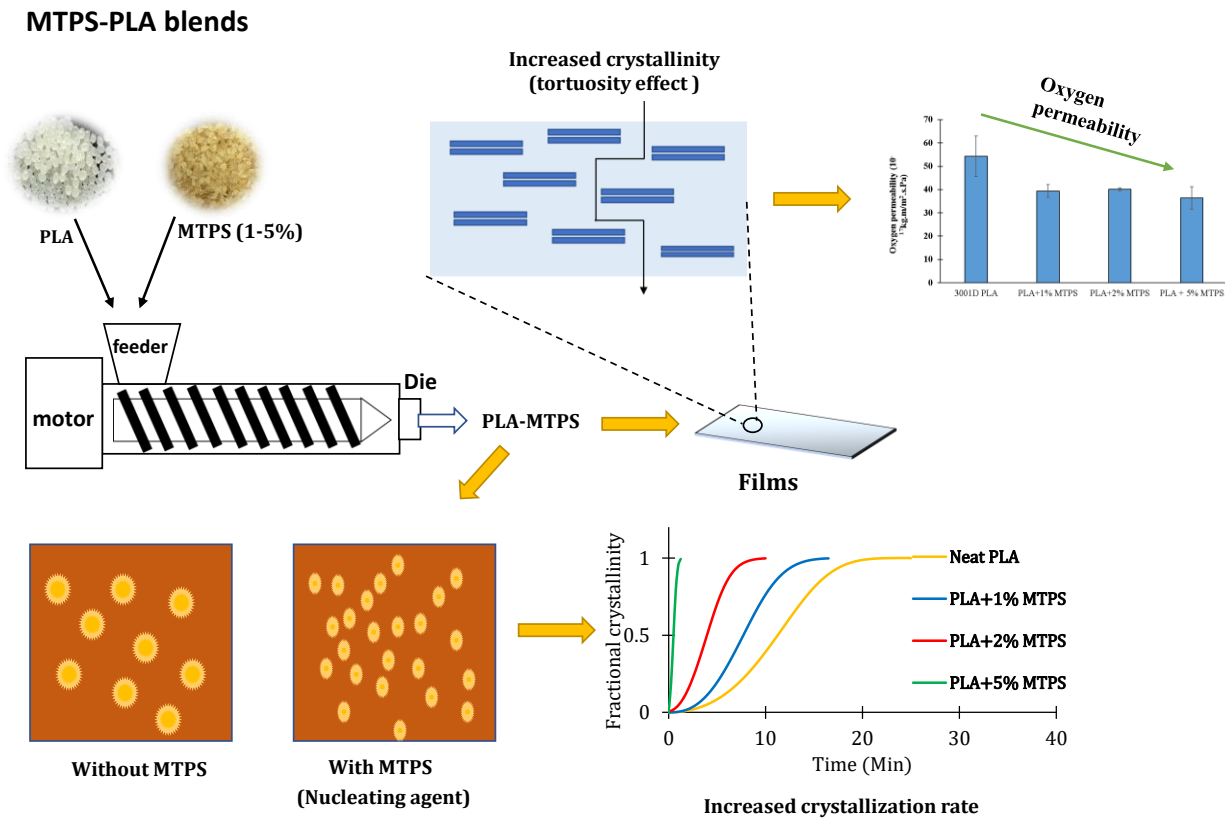


Figure 1.8: Schematic for summary of chapter 4

Chapter 5 deals with the synthesis of a solid MTPS-iodine resin as an antibacterial and antiviral additive. The iodine release and antibacterial properties of these pellets were studied. Further, they were used as an additive for making blown films with PLA and PBAT. The mechanical properties, morphology and antimicrobial properties of these films were compared with other commercial PLA films with and without other antimicrobial additives. Figure 1.9 shows the schematic for summary of chapter 5.

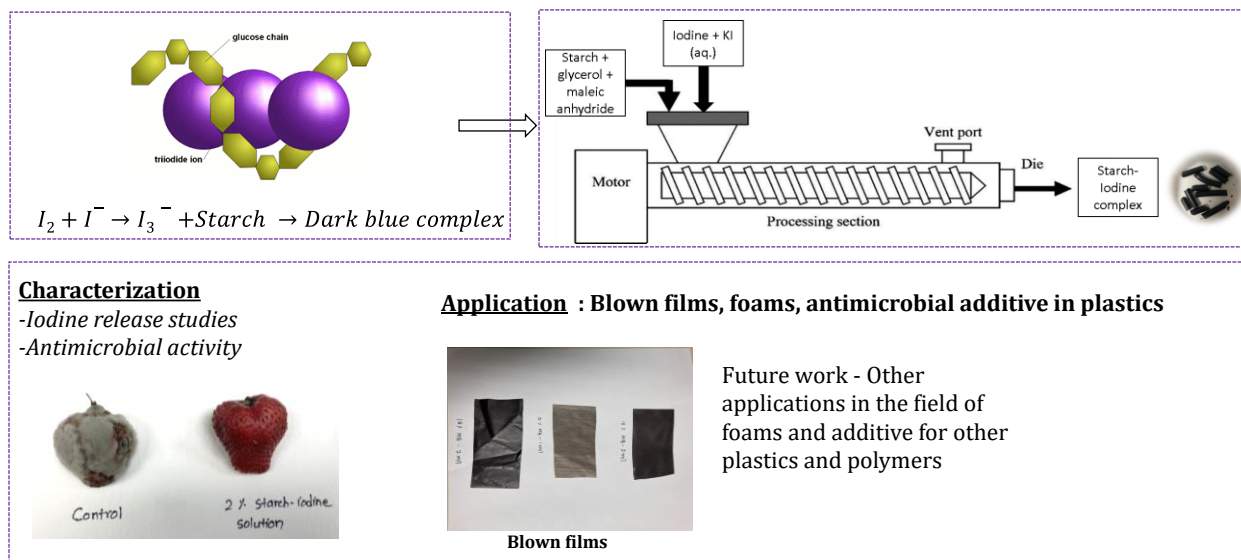
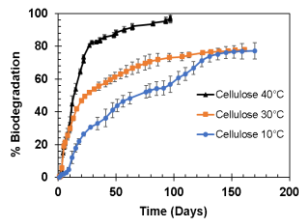
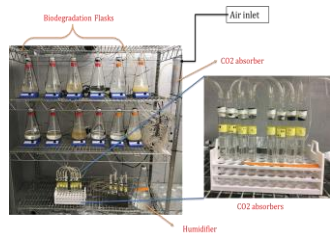


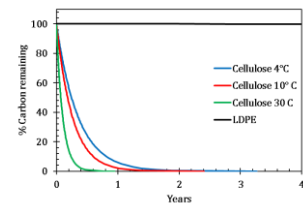
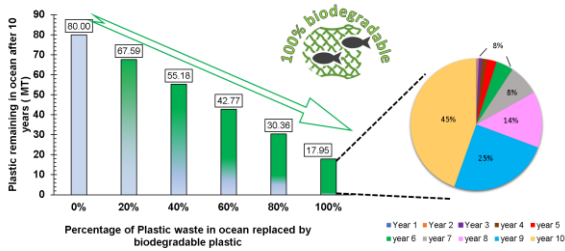
Figure 1.9: Schematic for summary of chapter 5

Final chapter 6 covers various studies related to aqueous biodegradation of biobased polymers cellulose and Poly(3-hydroxybutyrate-co-3-hydroxyvalerate) (PHBV). Mechanisms of biodegradation for these polymers and various factors affecting the rate of biodegradation are evaluated. Then detailed studies on the effect of temperature on the rate of biodegradation are performed at three different temperatures. A global equation using the reparametrized Arrhenius equation is developed and lifetime predictions for these polymers in low temperature ocean environments are made. Figure 1.10 shows the summary for chapter 6.



Biodegradation Kinetics and persistence of microplastics in the oceans

$$\frac{C}{C_0} = \exp \left(-A' \exp \left(-\frac{E_a}{R} \left(\frac{1}{T} - \frac{1}{T_{ref}} \right) \right) t \right)$$



Model for accumulation of plastics in ocean

To be used as basis for developing new ASTM D7081 standard.

Figure 1.10: Schematic for summary of chapter 6

REFERENCES

REFERENCES

- [1] "Materials – European Bioplastics e.V." <https://www.european-bioplastics.org/bioplastics/materials/> (accessed May 07, 2022).
- [2] R. Narayan, "Principles, drivers, and analysis of biodegradable and biobased plastics," *Handbook of Biodegradable Polymers*, pp. 455–473, Jan. 2020, doi: 10.1515/9781501511967-016/PDF.
- [3] K. L. Law and R. Narayan, "Reducing environmental plastic pollution by designing polymer materials for managed end-of-life," *Nature Reviews Materials*, 2021, doi: 10.1038/S41578-021-00382-0.
- [4] R. v. Gadhave *et al.*, "Starch Based Bio-Plastics: The Future of Sustainable Packaging," *Open Journal of Polymer Chemistry*, vol. 8, no. 2, pp. 21–33, May 2018, doi: 10.4236/OJPCHEM.2018.82003.
- [5] C. Bastioli, P. Magistrali, and S. G. Garcia, "Starch-based technology," *Handbook of Biodegradable Polymers*, pp. 217–243, Jan. 2020, doi: 10.1515/9781501511967-008/PDF.
- [6] "The utility of starch-based plastics - Green Dot Bioplastics." <https://www.greendotbioplastics.com/starch-based-plastics/> (accessed Apr. 21, 2022).
- [7] "Corn and soybean production up in 2021, USDA Reports Corn and soybean stocks up from year earlier, Winter Wheat Seedings up for 2022." <https://www.nass.usda.gov/Newsroom/2022/01-12-2022.php> (accessed Apr. 15, 2022).
- [8] G. Colomines, V. Ducruet, C. Courgneau, A. Guinault, and S. Domenek, "Barrier properties of poly(lactic acid) and its morphological changes induced by aroma compound sorption," *Polymer International*, vol. 59, no. 6, p. n/a-n/a, Jun. 2010, doi: 10.1002/pi.2793.
- [9] "Starch," *Britannica*. Encyclopædia Britannica, inc. Accessed: Mar. 01, 2020. [Online]. Available: <https://www.britannica.com/science/starch>.
- [10] F. Carosio *et al.*, "Efficient gas and water vapor barrier properties of thin poly(lactic acid) packaging films: Functionalization with moisture resistant Nafion and clay multilayers," *Chemistry of Materials*, vol. 26, no. 19, pp. 5459–5466, Oct. 2014, doi: 10.1021/cm501359e.
- [11] J. Muller, C. González-Martínez, and A. Chiralt, "Combination Of Poly(lactic) acid and starch for biodegradable food packaging," *Materials*, vol. 10, no. 8, pp. 1–22, Aug. 2017, doi: 10.3390/ma10080952.

2. DESIGN AND ENGINEERING OF INSOLUBLE, HIGH-PERFORMANCE STARCH FOAMS VIA EXTRUSION TECHNOLOGY

2.1 ABSTRACT

Insoluble, high-performance starch foams with high resistance to moisture were prepared by ZSK-30 twin-screw extruder using additives and reactive modifiers such as chitosan, polyvinyl butyral (PVB) and sodium trimetaphosphate (STMP). Under the optimized extrusion conditions, water acted as a plasticizer and a blowing agent breaking up the hydrogen bonds within the starch granules and releasing the starch polymer chains without significantly reducing their molecular weight. The pressure drop at the die led to expansion, and formation of closed cell foams. A screw configuration made up of 3 kneading sections was found to be the most effective for better mixing and foaming. It was found that properties like density, expansion ratio, compressive strength, resiliency, and cell size distribution of foams can be controlled by adjusting feed rates of starch, chitosan, and the crosslinking agent. The use of PVB and STMP was extremely effective in minimizing moisture sensitivity and made the foams hydrophobic and insoluble in water. Crosslinking of starch with STMP gave anionic mono and di-starch phosphates which formed an insoluble polyelectrolyte complex with cationic chitosan in presence of formic acid in the extruder due to electrostatic attraction. This made the foams water insoluble and water absorbing. These insoluble composite foams absorbed over 600% by weight water and formed a gel kind structure; a property which could be useful in hemostatic applications. It also increased the compressive strength of the foams by 3 times compared to the control foams. STMP, chitosan, and talc acted as nucleating agents with varying efficiencies. They reduced the cell size and gave more uniform cell size distribution. Densities of foams were found to vary from

21 to 51 kg/m³ for different compositions studied. A maximum expansion ratio of 38.7 was obtained for the formulation containing 10% PVB and 4% chitosan. Increased stability of the foams had no negative impact on the biodegradability and end of life for these products. With increasing drive to eliminate the carbon-carbon backbone persistent polymers, these biobased and biodegradable foams will provide a great value.

2.2 INTRODUCTION AND BACKGROUND

Biodegradable and biobased plastics have received increased attention in recent years for replacing petroleum-based counterparts. Traditional polystyrene, polyethylene, polyvinyl chloride and polyurethane foams are not biodegradable or require a long time, even hundreds of years, to degrade completely. They also impact the soil, water or other environments negatively during this time. Therefore, the exploration of degradable plastics that can replace traditional plastics holds great practical significance. Currently, the foam packaging market is facing growing pressure from environmental and disposal regulations that call for better carbon management and new end-of-life initiatives. There is an urgent need to reduce the carbon footprint of the package and provide environmentally responsible end-of-life disposal alternatives. Biobased and biodegradable starch foams are well-known alternatives for polystyrene foams in packaging, insulation, and medical applications[1–4]. Starch based foams are prepared by various processes such as extrusion, baking, microwave expansion, freeze drying etc. Reactive extrusion has allowed for mass production of starch foams. It offers several advantages over other methods like fast reaction time, enhanced heat and mass transfer, better mixing and it does not require any solvents[1]

Food industry has been using the extrusion process for making various modified starch products including expanded snack products for several years. Starch is not thermoplastic. It does not soften or flow. The thermal degradation temperature of starch is higher than its melting temperature. Various plasticizers such as water, glycerol, sorbitol etc. are added to make the starch processable and flow like a thermoplastic. The plasticizers such as water disrupt the intermolecular hydrogen bonding between the starch molecules and destroy its crystalline structure. Starch foam extrusion is a 2-step process. In the first step- starch,

additives and water are added to the extruder. In presence of high temperature, shear and pressure, water gets mixed with the starch and the starch granular structure is destroyed. Then as the mixture exits the die, a sudden drop in pressure causes water to evaporate and form the cellular structure of the foam. The foam formation can be divided into 3 steps- nucleation, bubble growth and stabilization. The nature of foam and cellular structure depends on various extrusion conditions such as screw configuration, starch type, temperature, water content, other additives like blowing or nucleating agents etc.

Starch is an abundantly available polysaccharide which is nontoxic, easily biodegradable in almost any environment, inexpensive and also possesses many superior properties. However, starch foams have some shortcomings such as very low mechanical strength[5], poor moisture resistance, immediate solubility in water etc.[6]. They are sensitive to moisture, and they tend to shrink and lose their cell structure in presence of high moisture environments. Condensation of water on the surface of the foams tends to dissolve them and they lose their mechanical integrity in humid and wet conditions which also causes loss in mechanical properties. This limits the use of starch foams in certain applications involving packaging and insulation. Hence, significant research is being conducted on using various additives for overcoming these problems. This chapter focuses on the design and engineering of high-performance starch foams for addressing these issues.

Three types of additives were used in this study either alone or in combination with each other and their impact on the properties of foams was studied.

2.2.1 Polyvinyl butyraldehyde (PVB)

Hydrophobic polymers like polyhydroxylamino-ether (PHAE), PLA, polybutylene adipate terephthalate (PBAT) and crosslinkers like glyoxal, glutaraldehyde, citric acid have been

investigated as an additive and were found to greatly improve humidity resistance of the foam[7]–[11]. However, production of PHAE was discontinued in 2002 and currently it is not available commercially. Also, one of the building blocks of PHAE is Bisphenol A (BPA), which is a suspected endocrine disrupter [12] and its use in “green” material negates the “green” nature of the product. Crosslinking agents like glyoxal are toxic and hazardous and hence cannot be used for making foams for medical and food contact purposes[13]. One approach that was used in the past to solve the moisture sensitivity was to employ starch esters instead of native starch [14, 15]. This approach, however, was proven to be economically unattractive because of cost constraints. In this work we have investigated the use of readily available polyvinyl butyral (PVB) as an environmentally friendly additive to improve the moisture resistance of starch foams. PVB is a thermoplastic obtained by condensation reaction between polyvinyl alcohol and butyraldehyde. Figure 2.1 shows the structure of PVB. It is hydrophobic, non-toxic and could be used in applications involving direct food contact.[16]

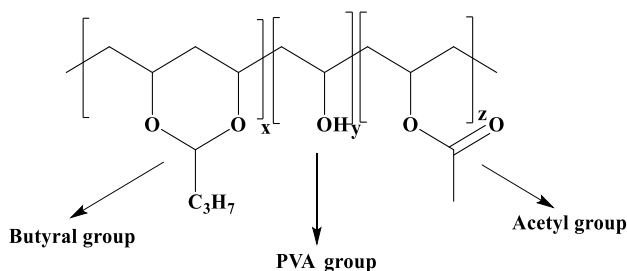


Figure 2.1: Structure of polyvinyl butyraldehyde(PVB)

2.2.2 Chitosan

Another area where low density foams are widely being used is in biomedical applications[17]. Chitosan, a derivative of second most abundant polymer chitin, has unique physicochemical and biomedical properties which make it useful for hydrogels, films and

sponges which could be used in biomedical domain. Chitin when heated in alkaline media, the acetamide groups present on C-2 position get transformed to primary amino groups to get chitosan. This chitosan can become positively charged in weakly acidic aqueous solutions via protonation of the amine group.[18] When two oppositely charged polyelectrolytes are mixed, a polyelectrolyte complex (PEC) can form due to electrostatic attraction.[19] Figure 2.2 shows the schematic for polyelectrolyte formation. Since chitosan cationic polyelectrolyte, it can form crosslinking with anionic starch to form an insoluble polyelectrolyte complex.[17, 20] Figure 2.3 shows the possible scheme for formation of polyelectrolyte complex between starch and chitosan.

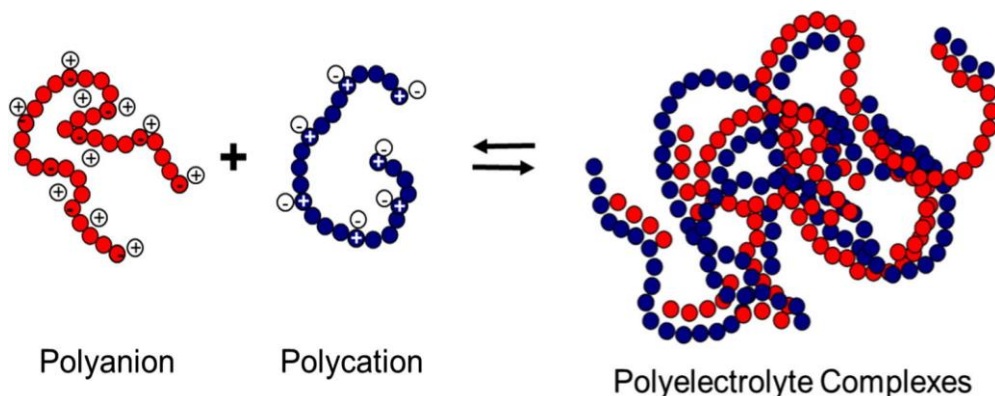


Figure 2.2: Schematic for polyelectrolyte complex formation

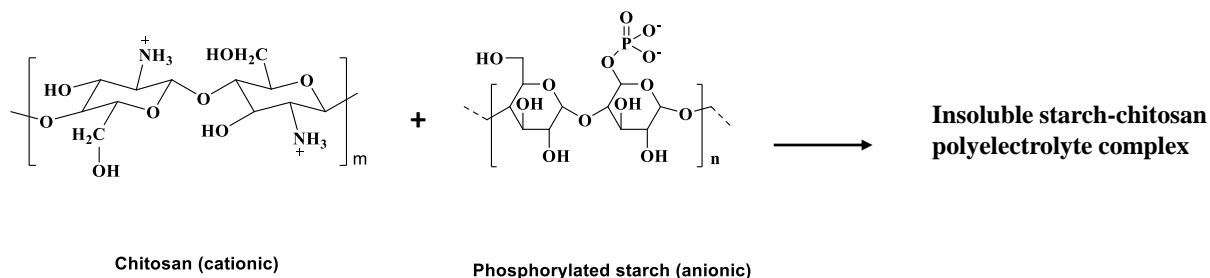


Figure 2.3: Scheme for formation of polyelectrolyte complex between chitosan and starch

Chitosan in foam is expected to promote the blood coagulation and thrombosis, inhibit the growth of bacteria and fungi and promote repair of damaged tissues[21]. Therefore, this foam is expected to have good hemostatic properties and find applications in medical field in the form of surgical pads. Studies have reported such polyelectrolyte foams made using microwave expansion.[17,22]. Dang et al. also reported that, when blended with starch, chitosan migrates to the surface of the films and decreases the hydrophilicity of the materials[23]. This could be an additional advantage for improving the moisture sensitivity of starch foams.

2.2.3 Sodium trimetaphosphate (STMP)

One approach for improving the mechanical and performance properties of starch foams is crosslinking. Starch has abundant hydrophilic hydroxyl groups, and therefore composites made from it have poor moisture barrier properties[24]. The hydrophilicity of starch can be substantially decreased by blocking some of its hydroxyl groups by crosslinking. Citric acid[25], glutaraldehyde[26], and malonic acid [27] have been investigated for the crosslinking of hydroxyl groups of starch and cellulose. STMP is widely used as phosphorylating agent in food and construction industries[28]–[30]. Starch reacts with sodium trimetaphosphate to give mono and distarch phosphates as shown in Figure 2.4 –

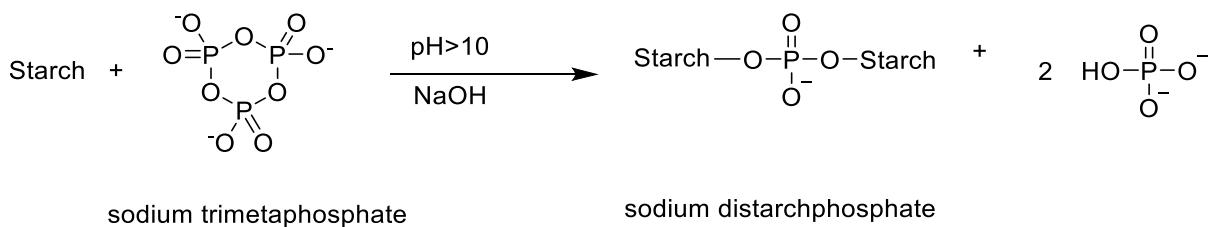


Figure 2.4: Phosphorylation of starch with STMP

Phosphate crosslinked starches improve the starch stability against high temperature, pH and shear. It also improves the firmness of swollen starch granule and its textural

characteristics. Plus, phosphorylated anionic starch has a better tendency to form polyelectrolyte complex with cationic chitosan compared to native starch.

To our best knowledge, no studies have reported the synergistic use of PVB and STMP for making high performance starch foams with chitosan by formation of polyelectrolyte complexes.

Another approach for making the insoluble polyelectrolyte complexes used in this project was using potato starch instead of High amylose corn starch. Potato starch has high amylopectin content (~70%) and it also has a high amount of phosphates present naturally[31] (0.01-0.6% by wt.) compared to corn starch[32] (0.016%). Hence, these foams do not need an external addition of STMP to form polyelectrolyte complexes with chitosan. Such foams have been prepared using microwave expansion technique by Deng et al.[17] Efforts were also done to scale up those foams using extrusion technology as a part of a collaboration work between MSU and Penn State University.

Extrusion technique has allowed mass production of starch foams.[9, 11, 33, 34] It offers several advantages over other methods like fast reaction time, enhanced heat and mass transfer, better mixing and it does not require any solvents [35]. In this study, water insoluble starch-chitosan polyelectrolyte complexes with and without crosslinking agent were prepared in the form of foams using the extrusion technology. Use of PVB as an additive for making the foams hydrophobic and water insoluble was also investigated. Extrusion parameters like screw configuration, temperature profile, rpm and feed ratios were optimized. Two types of starches – high amylose corn starch and potato starch, were used for making foams with different properties. Physico-mechanical properties of the foams including density, expansion ratio and compressive strength were investigated and

compared with the commercial starch foams. Properties like moisture sensitivity, contact angle and water absorption were also reported for the various formulations studied. Finally, the end of life of these foams in aqueous environment was investigated. These foams could find potential applications in various fields such as in making hemostatic pads in the field of wound care, in packaging or insulation require long term moisture resistance and mechanical properties.

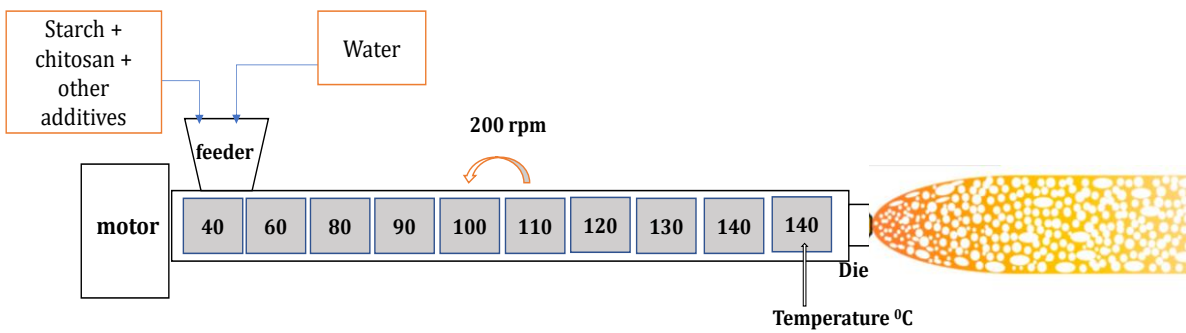
2.3 MATERIALS

High amylose corn starch was obtained from National starch and chemicals (Indianapolis, IN) with equilibrium moisture content of 12% (w/w). Native potato starch was obtained from Ingredion (NJ, USA) under the commercial name of PenPure®10 with equilibrium moisture content of about 12% (w/w). Water was used as both plasticizer and blowing agent. Chitosan was obtained from Primex EHF, Iceland under the trade name ChitoClear® 42010-cg110 75cp. It was obtained from Fresh North Atlantic Shrimp Shells, *Pandalus borealis* as raw material source. Chitosan was used to make insoluble polyelectrolyte complex foams with starch. The degree of deacetylation for chitosan was >75%. Sodium trimetaphosphate (STMP) was used for phosphorylation and light crosslinking of starch for its efficient reaction with chitosan. It was purchased from Fischer scientific (Pittsburgh, PA) and was used as it is. Polyvinyl alcohol (PVOH) was used as an additive to make control foams and was supplied from Kuraray America, Inc. under the trade name Mowiol 40-88. Polyvinyl butyral (PVB) was supplied by Kuraray America, Inc. (Houston, TX) under the trade name PVB 60HH. Other additives like polyvinyl alcohol (PVOH) (Kuraray America, Inc. (Houston, TX) and talc (magnesium silicate) used as nucleating agent was obtained from Luzenac (Ontario, Canada). These additives were used to prepare the control foams. Formic acid was used in some formulations to make chitosan cationic and increase the efficiency of polyelectrolyte formation. It was obtained from Fisher scientific (Pittsburgh, PA).

2.4 EXPERIMENTAL

The laboratory starch foam extrusion was done with a co-rotating twin screw extruder (Century ZSK-30)(MI, USA) with an L/D of 42:1 (Figure 2.5) . A peristaltic pump (model C.P. 78017-10, Ismatec) was used for injecting water into the extruder and accurate single-screw feeders were used for feeding starch and additives. A screw speed of 180-200 rpm was used for laboratory experiments for foam noodle extrusion. Three different types of dies were used for various formulations. The strand dies used were 3.5, 4.3 and 8 mm in diameter. A Slit die and annular die were also used for making the foams in form of sheets as explained in later sections of this chapter. Both peristaltic pump and single screw feeders were calibrated for different feed rates of water and starch. Initially during start-up, the starch feed rate was kept lower (50-60%) than the final feed rate and water feed rate was kept at a higher level than the final water feed rate (about 20-25% of starch feed rate). Once the mixture starts coming out from the die, starch feed rate is increased, and water feed rate is decreased gradually till a point where the product starts foaming. Starch feed rate used for most of the runs was 9 kg/ h and it was observed that water flow rate of 6-8% of starch was optimum for consistent foam production. The starch used was not dried and hence it had 12% of equilibrium moisture content. Thus, the total water content was 18-20% on dry basis. A 1% v/v formic acid aqueous solution was used in some formulations instead of distilled water. Formic acid was added for protonation of amino groups on the backbone of chitosan in acidic medium which could form PEC with anionic starch molecules. Table 2.1 shows all the runs with various additives used for foam extrusion and their contents.

Typical Processing conditions



Co-rotating twin screw CENTURY ZSK-30 extruder.

Figure 2.5: Experimental setup for foam extrusion

Table 2.1: Extrusion runs with various additives

<i>Formulation #</i>	<i>Starch type</i>	<i>Water or formic acid</i>	<i>talc (%)</i>	<i>chitosan (%)</i>	<i>PVOH (%)</i>	<i>PVB (%)</i>	<i>STMP (%)</i>	<i>Glycerol</i>	<i>Other</i>	<i>die type</i>	<i>die diameter (mm)</i>
<i>Variation in talc content</i>											
1	High amylose corn starch	Water	0	-	-	-	-	-	-	Strand	4.3
2	High amylose corn starch	Water	0.5	-	-	-	-	-	-	Strand	4.3
3	High amylose corn starch	Water	0.7	-	-	-	-	-	-	Strand	4.3
4	High amylose corn starch	water	2	-	-	-	-	-	-	Strand	4.3
<i>Using PVOH and chitosan</i>											
5	High amylose corn starch	Water	-	-	10	-	-	-	-	Strand	4.3
6	High amylose corn starch	Water	-	4	-	-	-	-	-	Strand	4.3
<i>Variation in die diameter</i>											
7	High amylose corn starch	Water	-	4	10	-	-	-	-	Strand	4.3
<i>Variation in die diameter</i>											
8	High amylose corn starch	Water	-	4	10	-	-	-	-	Strand	3.5
<i>Variation in die diameter</i>											
9	High amylose corn starch	Water	-	4	10	-	-	-	-	Strand	8
<i>Using PVB and Variation in chitosan content</i>											
11	High amylose corn starch	Water	-	0	-	10	-	-	-	Strand	4.3

Table 2.1cont'd

12	High amylose corn starch	Water	-	4	-	10	-	-	-	Strand	4.3
13	High amylose corn starch	Water	-	7	-	10	-	-	-	Strand	4.3
14	High amylose corn starch	Water	-	10	-	10	-	-	-	Strand	4.3
<i>Variation in STMP content</i>											
15	High amylose corn starch	Water	-	4	-	10	1	-	-	Strand	4.3
16	High amylose corn starch	Water	-	4	-	10	1.5	-	-	Strand	4.3
17	High amylose corn starch	Water	-	4	-	10	3	-	-	Strand	4.3
<i>Use of formic acid and glycerol</i>											
18	High amylose corn starch	Formic acid	-	4	-	-	1.5	-	-	Slit	25*1.5
19	High amylose corn starch	Formic acid	-	4	-	-	1.5	5	-	Slit	25*1.5
20	High amylose corn starch	Formic acid	-	4	-	-	1.5	10	-	Slit	25*1.5
<i>Use of annular die</i>											
1	High amylose corn starch	Water	-	4	-	10	1.5	-	-	Annular die	
<i>Potato starch foams</i>											
22	Potato starch (Ingredient)	Formic acid	-	4	-	-	-	-	-	Slit	25*1.5
23	Potato starch (Ingredient)	Formic acid	-	4	-	-	-	10	-	slit	25*1.5
24	Potato starch (Ingredient)	Formic acid	-	4	-	-	-	10	MCC 2%	Slit	25*1.5

2.5 FOAM EXTRUSION PROCESS DEVELOPMENT

First step was optimizing the various parameters for extrusion process to achieve a consistent, uniform process for foam production. The main parameters varied in this study include – screw configuration, temperature, water content, feeding ratios, screw speed, and die type and diameter.

2.5.1 Screw Configuration

Screw configuration plays an important role in the foaming process. During foaming, the crystalline structure of starch granule is disrupted using water as plasticizer. Water and additives also need to be mixed together properly to form a single phase for production of consistent quality foams. Hence the screw configuration was designed specifically to achieve these objectives. Two different screw configurations were used for production of starch foams as shown in the Table 2.2. The first configuration was mostly conveying elements and thus had less shear. It did not mix the starch, additives and water efficiently and hence the foams produced were not consistent. They also showed presence of some solid blocks in between the foam strands which indicated inadequate mixing as shown in Figure 2.6-a. Thus, the first screw configuration was not much of a success. However, it did help in forming a baseline for different parameters of extrusion. In the second screw configuration, more kneading elements were added to the screw to improve mixing and increase the torque. The feed zone contained the largest single pitch screw elements to convey the starch rapidly and avoid buildup of material in the feed zone. The pitch of the screw was then reduced to force the materials downstream. Kneading elements were introduced after regular intervals to provide efficient mixing of raw materials. This second screw configuration with more kneading elements proved to be more efficient in terms of mixing and torque and was used

for all further experiments. The foams produced by second configuration were much more consistent in production and had uniform structure and surface properties (Figure 2.6-b).

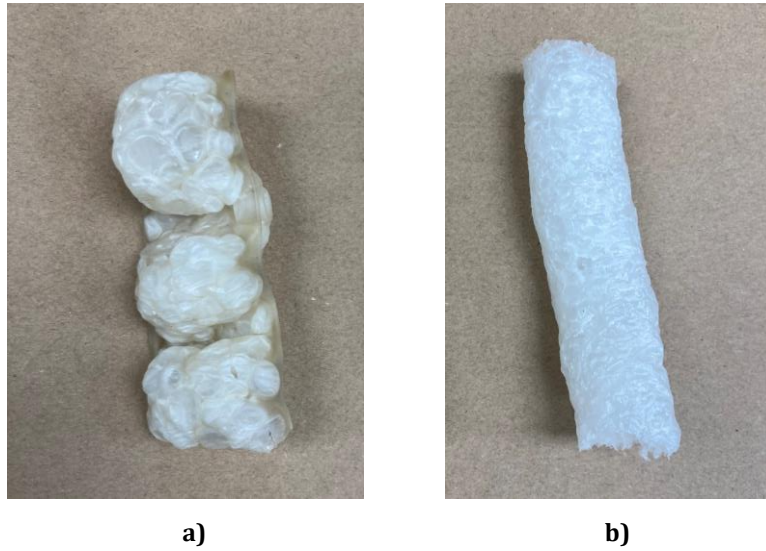


Figure 2.6: Foams obtained from a) Screw configuration #1 b) Screw configuration #2

Table 2.2: Screw configurations for starch foam extrusion

#	Screw config #1	Screw config #2
1	28/14	28/14
2	60/60	60/60
3	60/60	60/60
4	60/60	60/60
5	42/42	42/42
6	42/42	28/28
7	28/28	28/28
8	20/20	20/20
9	20/20	20/20
10	20/20	KB 45/5/14
11	20/20	KB 45/5/14
12	KB 45/5/28	KB 45/5/14
13	KB 90/5/28	KB 45/5/20
14	KB 90/5/28	KB 45/5/20

Table 2.2 cont'd

15	KB 45/5/14	60/60
16	KB 45/5/14	42/42
17	28/28	28/28
18	28/28	28/28
19	28/28	20/20
20	20/20	KB 45/5/42
21	20/20	KB 45/5/42
22	20/20	KB 45/5/42
23	20/20	KB 45/5/42
24	20/20	60/60
25	20/20	42/42
26	20/20	28/28
27	KB 45/5/14	28/28
28	KB 45/5/14	20/20
29	KB 90/5/28	KB 45/5/14
30	KB 90/5/28	KB 45/5/14
31	28/28	KB 90/5/28
32	28/28	KB 90/5/28
33	20/20	60/60
34	42/42	42/42
35	42/42	42/42
36	42/42	28/28
37	42/42	28/28
38	42/42	28/14
39	28/28	20/20
40	28/28	KB 90/5/28
41	20/20	20/20
42		20/20
43		20/20

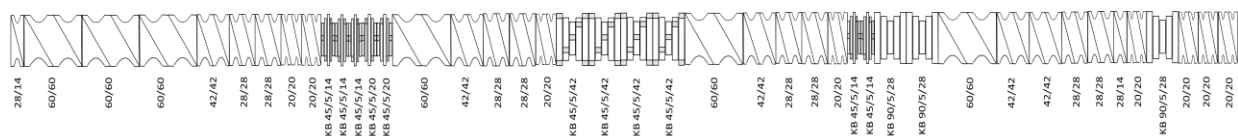


Figure 2.7: Second Screw configuration used for foam extrusion

2.5.2 Temperature profile

Gelatinization is a process of breaking down the intermolecular bonds of starch molecules in presence of water and heat. High amylose corn starch gelatinizes at higher temperatures above 90-100°C. Hence, efforts were done to keep the initial zones at lower temperatures and the last 4 or 5 zones at temperatures higher than the gelatinization temperatures of starch. This allowed the gelatinization and cross-linking with chitosan to occur in the end zones just before foaming. For other additives like PVOH and PVB, the temperatures were adjusted according to their melting temperatures. But most of the times the temperature profile given in Table 2.3 worked well for all the formulations with minor adjustments. Table 2.3 shows the optimized temperature profile used for extrusion. Sometimes, the initial 2 heat zone temperatures were increased to 80°C to get the screws moving properly. This was due to the LDPE purge material used in the extruder. A higher temperature was required to soften the LDPE present in the extruder and get the screws moving. Efforts were made to keep the temperature of the initial zones below 90°C to avoid the evaporation and loss of water from the feeding zone.

Table 2.3: General temperature profile for extrusion

Zone	1	2	3	4	5	6	7	8	9	die
Temperature (°C)	40	60	80	90	100	110	120	130	140	140

2.5.3 Die type and diameter

Strand die

The density and expansion ratio of the foams depends on the pressure developed the end of the extruder. Apart from the screw configuration and screw speed, one more factor that affects the pressure at the end of the extruder is die type and diameter. Smaller the die diameter, larger is the pressure developed at the die face. This causes more extreme drop in the pressure and the expansion ratio increases. Hence, the effect of die diameter on density and expansion ratio of the foams was studied with 3 strand dies of 3.5 mm, 4.3 mm and 8 mm diameter. The foam formulation contained high amylose corn starch, 10 wt% PVOH and 4 wt % chitosan. The figure below shows the dies, the foams produced form them and their respective expansion ratios. Expansion ratios for strand die foams are calculated as the ratio of cross section area of the foam vs cross section area of the die. As expected, it was observed that the smallest die yielded foams with lowest density and highest expansion ratio. Density increased and ER decreased on increasing the die diameter. But the smallest strand die with 3.5 mm diameter was also prone to causing more blockages at the die face. The small opening of the die was causing it to get plugged with starch more often making the runs done more unstable. The runs with 4.3 mm die were more consistent and yielded a uniform product. Hence, 4.3 mm die was used on most of the runs after that. The largest strand die yielded foams with highest density and lowest ER. So, it was not used further.



Die diameter :	3.5 mm	4.3 mm	8 mm
Expansion ratio:	11.4 ± 1.1	15.1 ± 1.2	6.5 ± 0.2

Figure 2.8: Three strand dies used for extrusion and their corresponding expansion ratios

Slit Die

The shape of the foams is also determined from the type of the die used. Second part of this work was to develop starch foam sheets for using as hemostatic pads. For this purpose, slit die and annular die were used for those formulations. The foams obtained from slit die were not completely flat. They showed presence of a ridge in the middle due to the rheology of the flow material coming out from the die. Efforts were done to flatten these foams by immediately passing them through a roller press when they were hot. Figure 2.9 shows the slit die foams with ridges and after they were flattened with the press. The details for design and use of annular die are covered in chapter 3.



a) Slit die



b) Foam sheets with ridges



c) Roll press for pressing foam noodles and sheets



d) Pressed foam sheets

Figure 2.9: Process development with slit die

Optimized water content of 6-8%, starch feeding rate of 150g/min and screw speed of 180-200 rpm was used for all the experiments. These values were based on the previous research done in our group on starch foams [8, 9, 11]. These parameters were qualitatively adjusted to give optimum properties, but detailed quantitative studies were not done.

2.6 CHARACTERIZATION AND ANALYSIS

All the samples were conditioned for at least 72 hours at 50% relative humidity and 23°C as per ASTM D4332 before performing any testing.

Density: The density of the foams was calculated from the mass to volume ratio of the samples according to ASTM D3575. The dimensions of the sample were measured using a Vernier caliper graduated to an accuracy of ± 0.01 mm. For the cylindrical foams (noodle), samples were collected at various time intervals from each run and 10 measurements were taken for each sample to determine an average diameter and density.

Expansion ratio: The expansion ratio of the cylindrical foam was calculated by dividing the cross-sectional area of the foam by the cross-sectional area of the die in mm^2 . The result was the mean of ten samples of each formulation.

Water solubility test: 0.5 g of starch foam was kept in water and stirred. Pictures were taken at various times like 1min, 5 min, 30 min, 3 hours and after 2 days to see whether the foams dissolved in water or not.

Surface wetting test: Foam sheets or noodles were dipped into water, removed and left undisturbed for five hours. After five hours, photographs were taken of the foam sheets to determine the degree of disintegration.

Solution uptake measurements: For the samples which did not dissolve readily in water, solution uptake measurements were performed. Swelling experiments were performed using the method described by Deng et al. (2014). Swelling ratio (S) was calculated for the samples in DI water at 25°C. Approximately 0.5 g of samples were cut and immersed in DI water for predefined time intervals. After that, the swollen samples were taken out and

weighed after excess liquid on the sample surfaces was absorbed by paper towels. This was continued till a set time interval of 120 h was reached. Swelling ratio is calculated as:

Equation 2.1

$$S\% = \frac{M_s - M_d}{M_d} \times 100$$

Where M_s is the weight of swollen sample and M_d is the weight of dry sample before immersing in water.

Moisture sorption analysis: 3 samples of each foam formulation were kept in 95% relative humidity chamber at 25°C. Weight and dimensions of the samples were monitored and measured at regular intervals until a steady state value was achieved.

Scanning electron microscopy (SEM): A JOEL 6610 LV scanning electron microscope (JEOL Ltd., Tokyo, Japan) was used examine cell size distributions and surface morphology of all the samples. Foam samples were sectioned with a razor blade, mounted on aluminum stubs, and coated with sputter coater before observing in scanning electron microscope. ImageJ software was used to determine the average cell size and cell size distribution for the foams.

Absorption isotherms: For studying moisture adsorption isotherms of starch foams under different relative humidity conditions, 6 different saturated salt solutions were prepared and placed at the bottom of desiccators to obtain the relative humidity ranging from 11 to 95 %. The starch foams were dried in an oven at 90 C for 2 days, weighed and then placed in the closed desiccators for a definite amount of time. Change in the moisture content of the starch foams as a function of time for different foam samples were reported to create the adsorption isotherms. Table 2.4 shows the salt solutions used for creating different humidity environments.

Table 2.4: Different salt solutions for relative humidity

Salt	RH
Lithium chloride	11 %
Magnesium chloride	33 %
Magnesium nitrate	52 %
Sodium chloride	75 %
Potassium Nitrate	95 %

Confocal microscopy: The chitosan containing foam samples were visualized using Fluoview FV1000 CLSM inverted type microscope (Olympus, Japan). A fluorescein isothiocyanate (FITC)/water solution (50mg/ml) was prepared and the starch foam samples were soaked in it for about 1 minute. Then the samples were taken out, washed with distilled water to remove any excess dye and were plated on glass slides for observation. A UPLFLN objective with 10X magnification and numerical aperture of 0.3 was used for capturing the images. The chitosan was labelled with FTIC for getting green fluorescence [23]. Excitation at 488 nm was provided using argon lasers. Emission filter SDM560 and BF505-525 were used for collecting green fluorescence in channel 1. Then a Z series was collected over the thickness of 388 um with z step size of 6.93 microns. Maximum intensity projection image (MIP) was generated and saved using Olympus FLUOVIEW 4.2 software. Kalman average of 4 images was used for reducing the background noise in the image. The foam samples were analyzed for 2 positions in the sample – surface and middle part of the foam.

Contact angle measurements: Contact angle measurements were carried out using a contact angle goniometer DSA30S (Krüss GmbH, Germany) at 25°C. Water droplets were dropped carefully on the surface of the foams with a micro syringe and contact angles were measured with the help of Advance software (Krüss GmBH, Germany). An average of 4 to 5 different measurements were taken for a single sample at different positions. The measured values

were reported 30 sec after the deposition of water droplets. Change in the contact angle after 1 min of deposition was also observed.

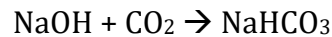
Compressive strength and resiliency: Compressive strength of the foam noodle specimens was measured according to the test method described by Tatarka et al.[36]. using an Instron testing machine. The cylindrical foam samples were placed between the compression plates and an initial load of 0.5 N was applied. Then the samples were pressed at a rate of 19 mm/min for a deformation of 13% or yield point, whichever occurs first. The maximum compression load was recorded. Compressive strength was recorded by dividing the maximum compression load by cross section area. Then the plate was returned to its original position and a second relaxation load was measured after 60 sec. Percent resilience was calculated as the force required for the second compression divided by the first. All the readings were obtained as an average of 5-7 samples for each formulation.

Biodegradability: The biodegradability of 3 foam samples (formulation 7, 12 and 16) was tested in an aqueous environment. These foams contained 1. PVOH and chitosan, 2. PVB and chitosan 3. PVB, STMP and chitosan. All the tests were performed in an aerobic environment at 30 °C. A respirometric mineralization test system for calculating CO₂ evolution was set up based on International Standard ISO 14852. The system comprised blank, positive reference (cellulose) and the test materials for all the runs. All the samples, blanks, and references were run in duplicates. An optimized test medium containing all the nutrients and buffers was prepared according to the ISO standard. Table 2.5 gives the detailed composition of the mineral solution prepared for all the tests.

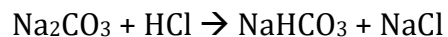
Table 2.5: Mineral solution composition for the test

1 L Mineral Solution	g
Solution A	
KH ₂ PO ₄ (anhydrous)	3.75
Na ₂ HPO ₄ ·2H ₂ O	8.73
NH ₄ Cl	0.2
Solution B	
MgSO ₄ ·7H ₂ O	2.25
Solution C	
CaCl ₂ ·2H ₂ O	3.64
Solution D	
FeCl ₃ ·6H ₂ O	0.025 g
Wastewater inoculum (ml)	50
Distilled water (ml)	Remaining

Wastewater inoculum obtained from a local waste water treatment plant was added to all the flasks to obtain the concentration of 5% v/v in the test medium as described in ISO 14852. Then the foam samples were added to these flasks, and they were subjected to the test conditions. A solution of 1 N NaOH was used for trapping the CO₂ generated from test flasks. CO₂ trapping is a two-step process as shown below:



1 g of sample was taken from each of the 50 mL NaOH trapping solution and titrated with 0.1 N standardized hydrochloric acid (HCl) solution to find the amount of CO₂ trapped. The reactions are as follows:



The titrations were done with the help of an auto titrator to get the volumes of HCl, V_1 , and V_2 required for reactions 1 and 2 respectively. The amount of HCl consumed can be used to calculate the *mmoles of CO₂* evolved using the following Equation:

Equation 2.2

$$\text{Mmoles of } CO_2 = \frac{(V_2 - V_1) * N_{HCl} * V_{NaOH}}{Wt \text{ of sample}}$$

The percentage biodegradation (% B) was further calculated by the following Equation:

Equation 2.3

$$\% B = \frac{\sum(CO_2)_{sample} - \sum(CO_2)_{blank}}{ThCO_2} \times 100$$

$\sum(CO_2)_{sample}$ is the amount of carbon dioxide that evolved in a test flask between the start of the test and time t ; $\sum(CO_2)_{blank}$ is the amount of carbon dioxide that evolved in a blank flask between the start of the test and time t ; $ThCO_2$ is the theoretical amount of carbon dioxide that evolved from the test material. All the values were expressed as *mmoles of CO₂*. The samples were replaced every 2–3 days in the starting phase when the rate of biodegradation was expected to be maximum and weekly or biweekly in the end [43,44]. Plots of cumulative CO₂ evolution for all the samples and blanks and % biodegradation vs. time were made for all the samples and compared for any differences between the foam samples.

2.7 RESULTS AND DISCUSSION

2.7.1 *Effects of various additives on density and expansion ratio*

Talc

Figure 2.10 shows the effects of talc and PVOH on density and expansion ratios of starch foams. While optimizing the processing conditions of extrusion for making starch foams talc was used as an additive. It was observed that the density of starch foams increased, and the expansion ratio reduced with increasing talc content from 0-2%. The control foams containing only starch and water showed density of $40.7 \pm 8.9 \text{ kg/m}^3$ and expansion ratio of 24.2 ± 4.2 . This was higher as compared to the values reported by Nabar et. al[9]. Control starch foams without any other additives were highly inconsistent in nature and very brittle which could explain the higher standard deviation in the measurements. Increasing talc content to 0.7 and 2% yielded increased densities of $42.3 \pm 7.3 \text{ kg/m}^3$ and $49.7 \pm 5.4 \text{ kg/m}^3$ and expansion ratios of 17 and 17.4 respectively. Similar nucleating effect of talc on density and ER has been observed in many studies[39][8]. Besides increasing density and expansion ratio, talc addition also helped in increasing the formation of large number of smaller cells. And the diameter of the cells reduced. These results were quantified further in the SEM studies as explained in section 2.7.7.

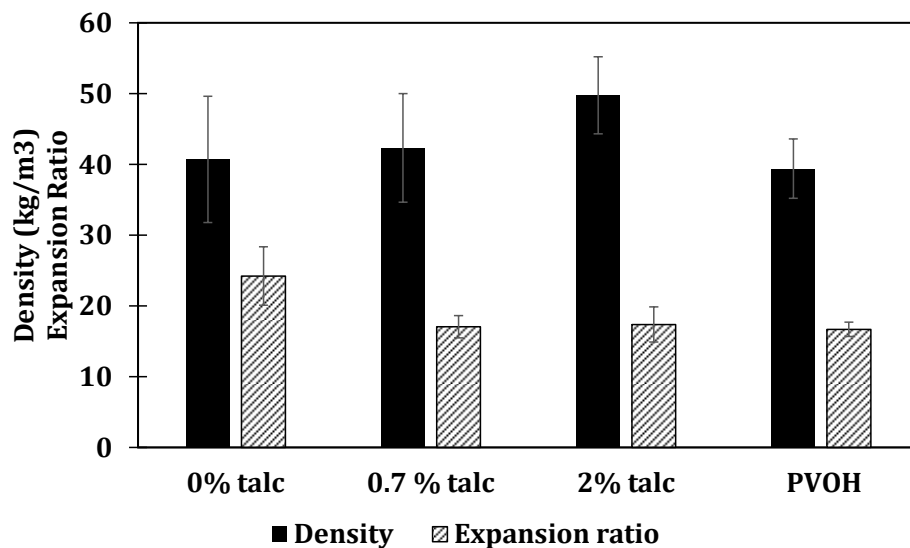


Figure 2.10: Effect of talc and PVOH addition on density and expansion ratio of foams
Polyvinyl alcohol

It was found that by adding PVOH and chitosan to the formulation, the density was reduced ($39.4 \pm 4.7 \text{ kg/m}^3$) but the expansion ratio remained almost the same (16.7 ± 1.0). Addition of PVOH made the foams much more consistent, less brittle and made the surface smoother. This could be attributed to the fact that polyvinyl alcohol is a high molecular weight molecule and highly soluble in water. So, addition of PVOH reduced the diffusivity of water and led to a more controlled expansion and hence lower expansion ratios [8].

Polyvinyl butaral (PVB)

Next additive used was PVB. Polyvinyl butyraldehyde is a resin used in automotive applications for safety shields, in adhesives, for increasing flexibility and toughness. It is prepared by reaction between polyvinyl alcohol and butyraldehyde. Studies have reported that use of polyvinyl butyraldehyde (PVB) increased the water barrier properties of paper boards and starch films [40, 41]. Hence it was added to the starch foams to study its effect on water solubility and moisture resistance. It was observed that PVB also acted as a blowing

agent and increased the expansion ratio and decreased the density of starch foams significantly to 38.7 ± 2.1 and 21.1 ± 1.7 kg/m³ respectively. This might be due to the hydrolysis of PVB in presence of water to yield butaraldehyde which evaporates to form gas and causes more expansion of foams[42].

Chitosan

The effect of chitosan % on density and expansion ration of foams was also studied. Density of foams was found to increase from 21.1 to 36.2 kg/m³ by increasing the chitosan content from 4 to 10 % whereas expansion ratio reduced from 38.75 to 26.05 as shown in Figure 2.11. Addition of chitosan showed a similar nucleating effect as talc. The detailed studies on cell size and cell size distribution are covered in in the SEM section 2.7.7.

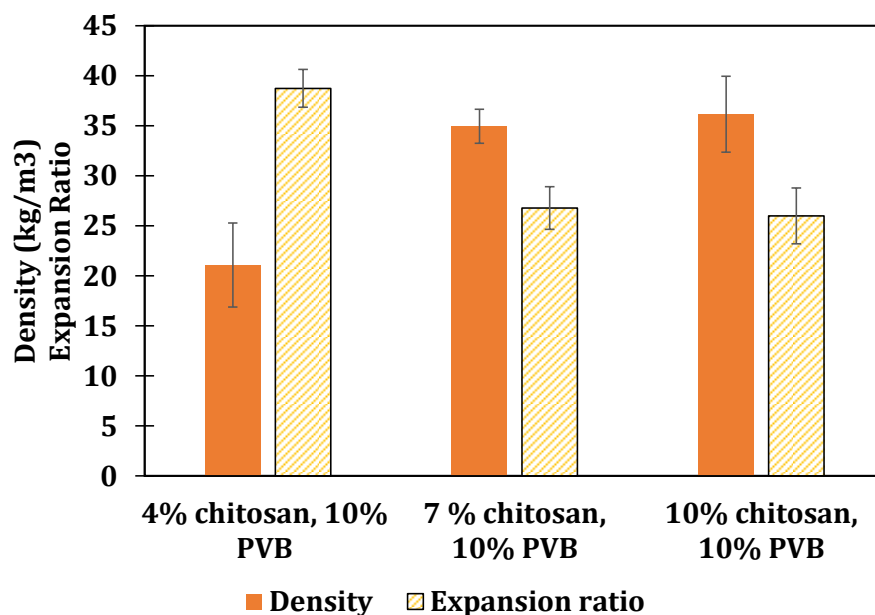


Figure 2.11: Effect of chitosan on density and expansion ratio of foams

Sodium trimetaphosphate

STMP was added to the foams as a crosslinking agent to form mono and di-starch phosphates which can then form a polyelectrolyte complex with cationic chitosan as shown in Figure

2.3[17]. Crosslinking of starch is also known to improve the mechanical properties and water resistance of the starch which are important characteristics for some applications like packaging and high humidity applications. 1, 1.5 and 3 % of STMP was added to the formulations and it was found that the density increased, and expansion ratio decreased steadily with increasing degree of crosslinking as expected (Figure 2.12). STMP acted as a crosslinker for starch increasing its molecular weight and making it stiffer restricting the expansion due to loss of flexibility.

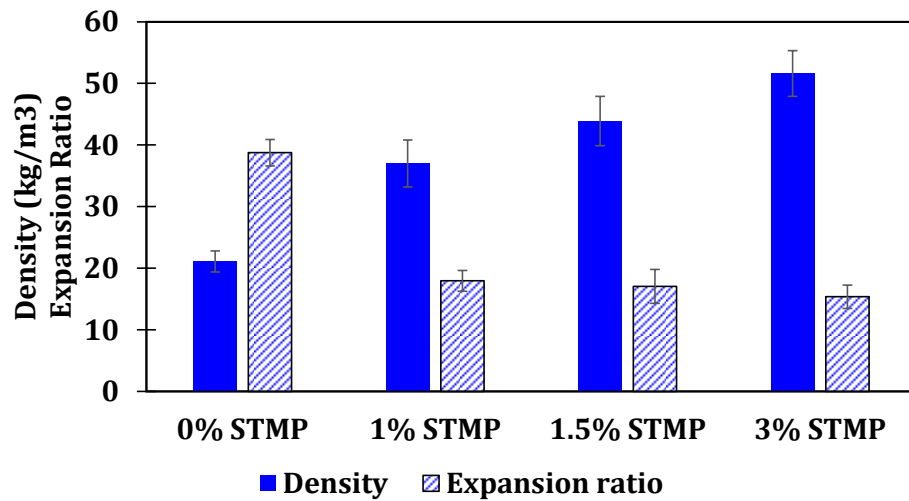


Figure 2.12: Effect of STMP addition on density and expansion ratio of starch foams

2.7.2 Water solubility tests

Corn starch foams, potato starch foams and control foams with PVOH and talc additives were tested for their water solubility. Control foams and PVOH containing foams dissolved almost immediately in water within a few minutes. When chitosan was added to the foams, a gelling effect was observed. For 4% chitosan containing foams with corn starch, they did not dissolve completely even after a day. Instead, they formed a gel kind of structure as shown in Figure 2.13. This suggested that a polyelectrolyte complex was starting to form. However, for efficient formation of polyelectrolyte complex, it is necessary that chitosan should be positively charged, and starch should have a greater number of anionic phosphate groups which can electrostatically get attracted to the positive chitosan. Formic acid and STMP are necessary for this to happen. These were not added in corn starch + chitosan 4% formulation (#6 form Table 2.1). Hence, the polyelectrolyte formation was not complete and efficient, and these foams did not hold their shape well. When formic acid solution was used for making the foams along with addition of 1.5 % STMP (formulation #18 Table 2.1) it was in fact seen that the foams did not dissolve in water even after 5 days, they held their shape in water and absorbed water as shown in Figure 2.13. This confirmed that addition of formic acid and STMP resulted in better electrolyte complex formation. However, these foams started to lose their shape after day 5 and were completely dissolved in water by day 30 (images not included). This demonstrated that the interaction between starch and chitosan and formic acid can keep the morphological structure of foams intact for a few days making them more stable as compared to control foams. But this interaction is reversible and effective only for limited time. Similar results were observed by Zhang et. al 2020[43], when they studied starch chitosan foams for solubility in water and other pH solutions.

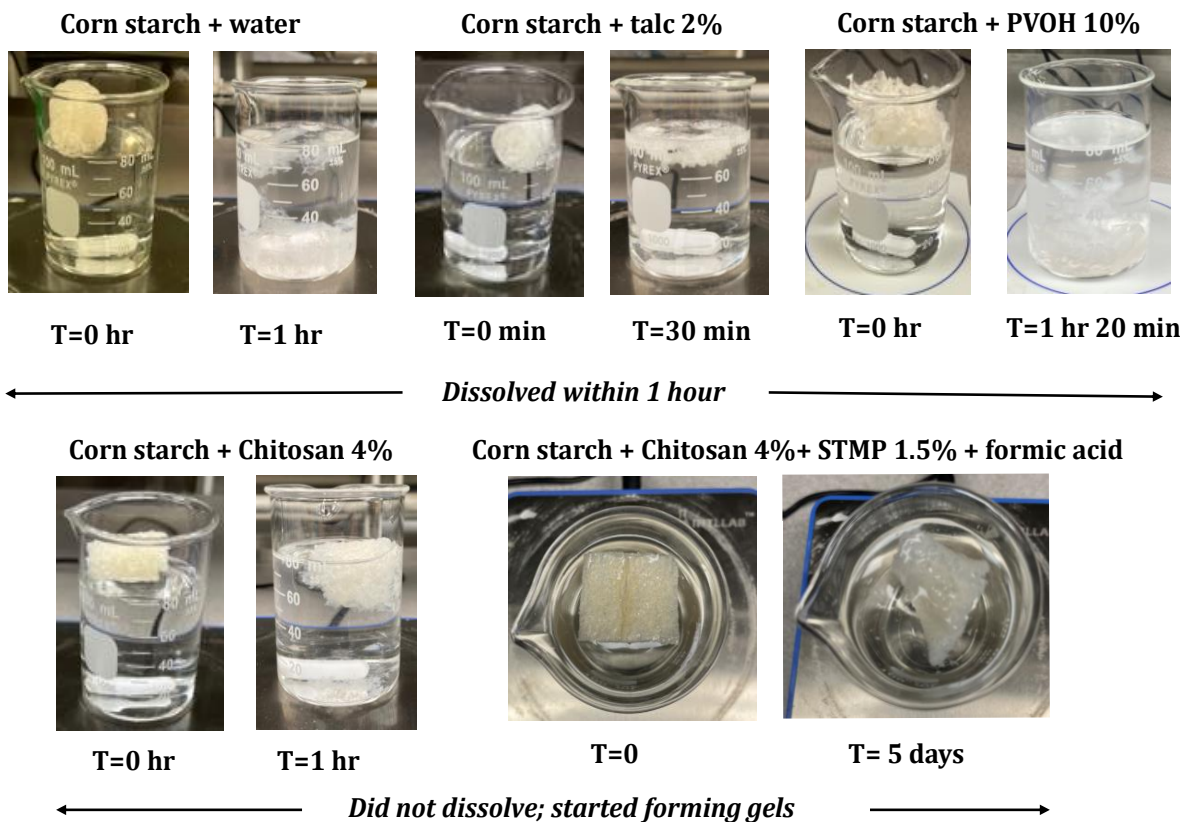


Figure 2.13: Water solubility for foams with different additives

Once the parameters for insoluble foams were optimized, the effect of glycerol addition on the water solubility was also studied (Figure 2.14). The foams containing 5 and 10% of glycerol were more flexible compared to the foams with no glycerol. These foams also contained 1.5% wt./wt. STMP. So, it was expected that they should form electrolyte complexes. This was confirmed when they did not dissolve in water for a day. But it was observed that the glycerol containing foams did start to break a little after a day in water. And finally, they dissolved after 5 days. Addition of glycerol made the corn starch foams more flexible but more soluble in water. This could be attributed to the hydrophilic nature of glycerol.

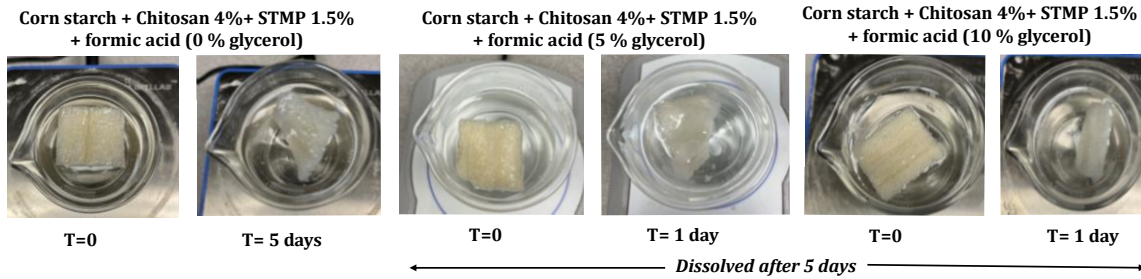


Figure 2.14: Solubility of corn starch foams with glycerol

Similar studies were also done with potato starch foams. It was observed that all the potato starch foams were insoluble in water even without the addition of STMP. This might be due to the fact that native potato starch contains more number phosphates groups naturally compared to corn starch[32]. Hence, addition of STMP was not necessary for formation of polyelectrolyte complex with chitosan. Surprisingly, opposite results were observed in case of these foams with glycerol addition. Both the 0% and 10 % glycerol foams were insoluble in water. But the 10% glycerol foams (formulation 23-Table 2.1) maintained the structure better as compared to 0% glycerol foams (formulation 22). The reason for this observation was not clear. It might be that there was some processing issue encountered during production of these foams due to which the polyelectrolyte complex was not formed properly in the 0% glycerol foams. In case of potato starch foams one more formulation was also made with addition of microcrystalline cellulose (MCC)(formulation #24-Table 2.1). This was done to see if cellulose acts as a biobased nucleating agent in foams as well and make the cell size smaller and more uniform. MCC has been used in polymers like PLA as a nucleating agent[44]. However, in case of water solubility studies, it was found that the MCC containing foams were much more brittle compared to other potato starch foams and the foams could not hold their shape. These foams dissolved in water completely after a few hours.

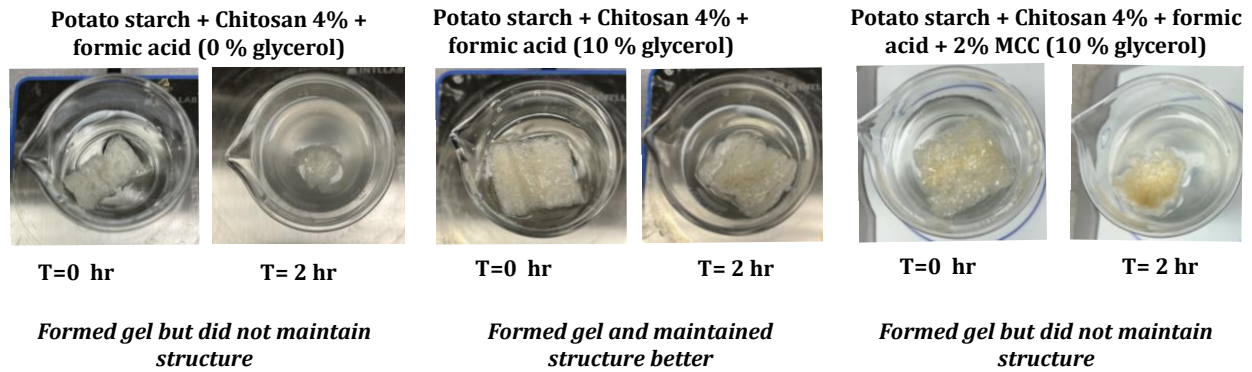


Figure 2.15: Solubility studies for potato starch foams

Another additive which had a significant impact on foam solubility in water was PVB. It was observed that the foams containing only PVB or chitosan and PVB or chitosan and PVB and STMP did not dissolve in water as shown in Figure 2.16 . This could be due to the hydrophobic nature and film forming and binding properties of PVB. PVB helped in binding the foam structure together and hence foams did not dissolve in water. However, without STMP crosslinking, the foams containing only PVB could not maintain their cell structure for long after immersing in water. Crosslinking of starch with STMP and its polyelectrolyte complex with chitosan, made the foams more rigid and cell structure strong. So, these foams did not lose their cell structure in water (formulation 15-17 -Table 2.1). Instead, they absorbed water and formed a gel kind of structure without getting dissolved in the water. This could be an important property for making the use of these foams in making absorbent, hemostatic pads.

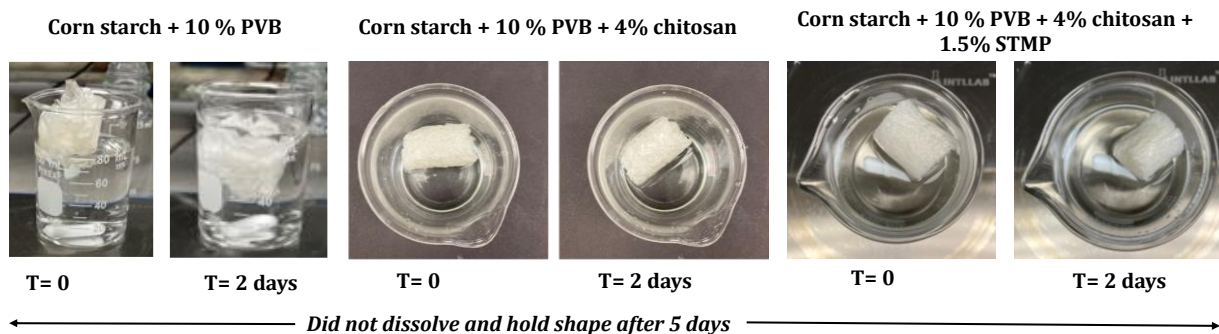


Figure 2.16: Water solubility studies for foams containing PVB

In summary – the formulations containing chitosan, PVB and STMP showed a synergistic effect (formulation 15 to 17-Table 2.1) and the best water insolubility characteristics while maintaining their shape.

2.7.3 Water penetration test

As a qualitative test for water penetration, starch foam sheets or noodles were dipped in water, taken out and kept undisturbed for 5 hrs. Photographs were taken before and after to see the effect of water on the sheets and noodles. It was found that the control foams with no additives and foams with talc and PVOH as additive were affected the most by dipping in water. They disintegrated and shrunk the most. Whereas, addition of chitosan, PVB and STMP seemed to increase the water penetration time for the sheets and noodles. There was not much disintegration or shrinkage observed in these foams (Figure 2.17)

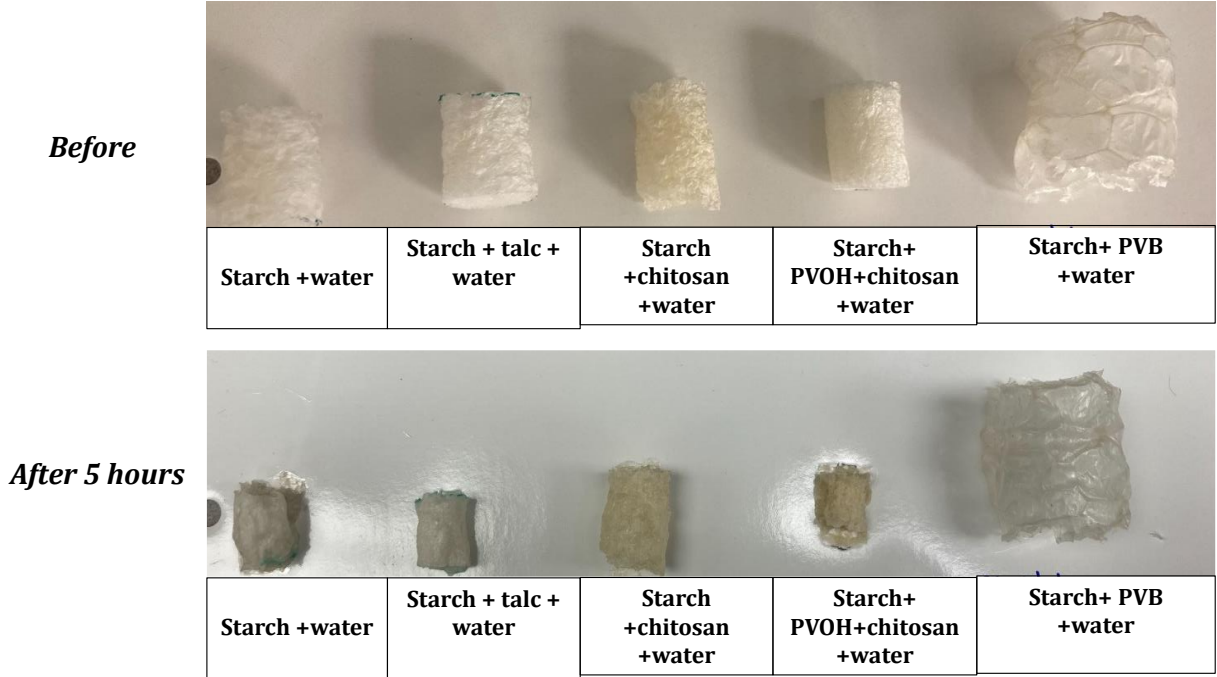


Figure 2.17: Water penetration test for foams with various additives

Figure 2.18 shows all the foams with varying content of PVB and/or chitosan with or without STMP. All of these foams showed minimum surface disintegration upon contact with water. This was in agreement with the previous studies of water solubility discussed in section 2.8.

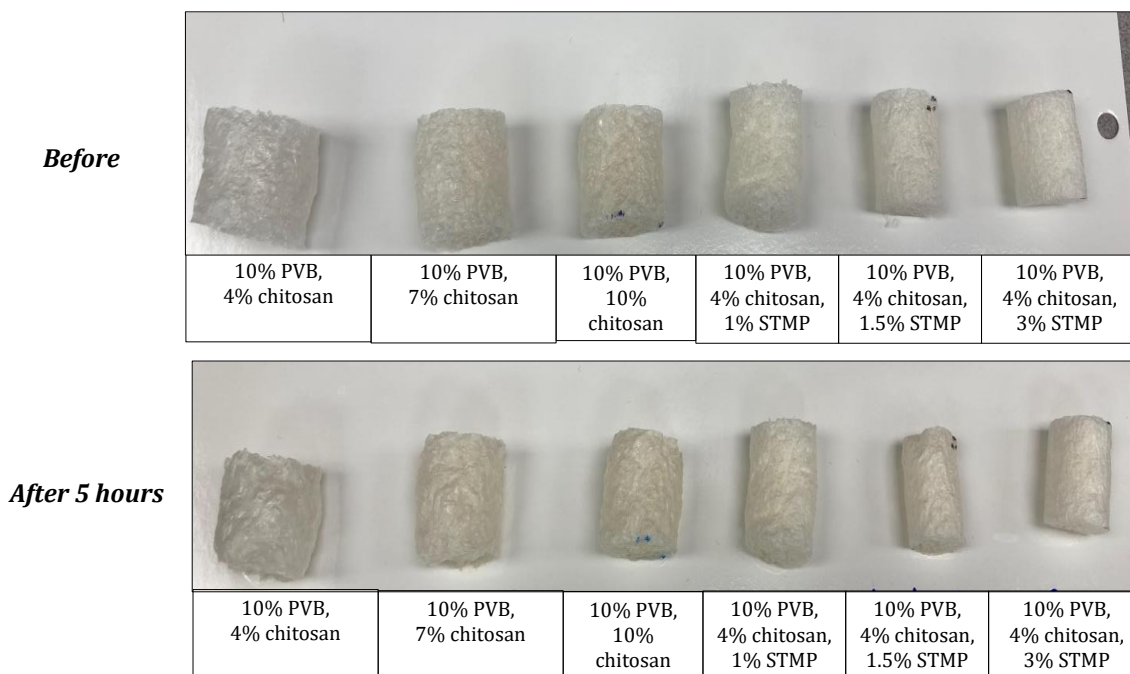


Figure 2.18: water penetration test for foams containing PVB, chitosan and STMP

Similar studies were also done with corn and potato starch foams with varying content of glycerol (Figure 2.19). It was observed that the foams with 0% glycerol showed least surface disintegration after contact with water. The foam surface became much more hydrophilic and sensitive to water after addition of hydrophilic glycerol. It was also interesting to note that addition of MCC which made the potato starch foams brittle and more soluble in water, also made the foam surface more sensitive to water. These foams were almost disintegrated completely after 5 hours. This made them a poor candidate for use in the intended application of moisture resistant foams.

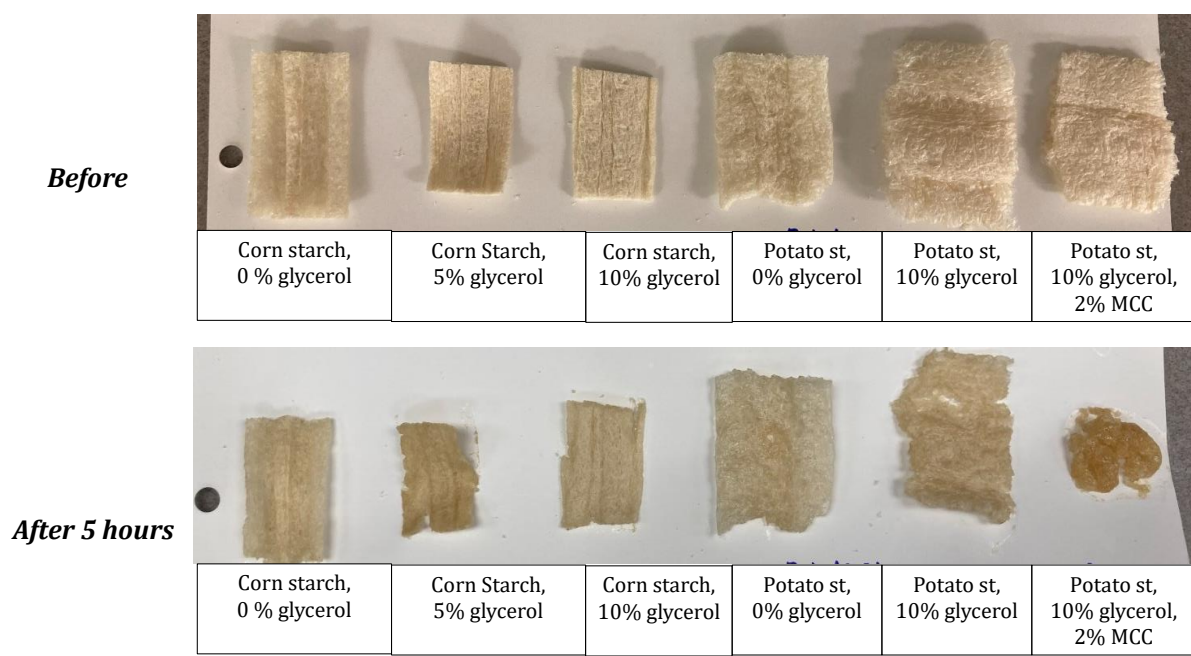


Figure 2.19: Water penetration test for foams with and without glycerol

2.7.4 Solution uptake measurements for foams

The foams which did not dissolve in water for more than 1 day and formed insoluble polyelectrolyte complexes, were tested for solution uptake measurements. These included the corn starch formulations containing STMP and PVB and STMP (formulation #15-20) and foams containing glycerol. Figure 2.20 shows the swelling ratios for all the corn starch formulations.

The solution uptake by all the corn starch foams with PVB and STMP was similar regardless of STMP content. Equilibrium solution uptake ratio of about 600% was reached in 80-100 hours. These foams maintained the structure well and formed gels after absorbing water. There was little to no disintegration observed for these foams even after 120 hours.

For foams containing glycerol (0, 5 and 10%) and 1.5 % STMP, it was observed that the addition of glycerol made these foams more hydrophilic and soluble in water. Their initial solution uptake was faster than the PVB containing foams to reach between 450-500% by weight. After that they started disintegrating in water and that caused mass loss for the foams and reduction in the swelling ratios. This testing was not continued after 72 hours due to continued mass loss in these foams. Hence, it could be concluded that the binding abilities of PVB were helping these foams in 1st case to retain their shape and structure together properly. In absence of PVB, the polyelectrolyte complex between starch and chitosan was more unstable and lead to loss of structure in water more easily. These studies were only performed in distilled water in this project. As a part of the collaboration project with Penn state university, these foams were further tested in different buffer solutions for their solution uptake characteristics. That data also showed that the STMP and PVB containing

foams were performing better compared to other foams in different pH solutions. That data is not shown here.

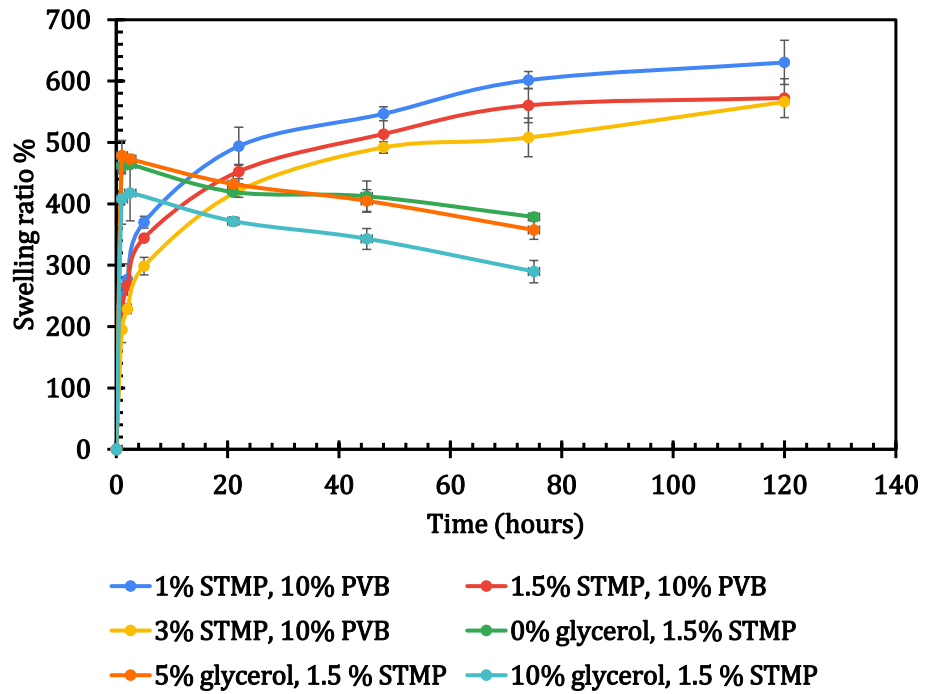


Figure 2.20: Swelling characteristics of starch-chitosan-STMP foams

2.7.5 Moisture sensitivity

The moisture absorption curves of different starch foams prepared using various additives are as shown in Figure 2.21 at room temperatures under different relative humidity conditions.

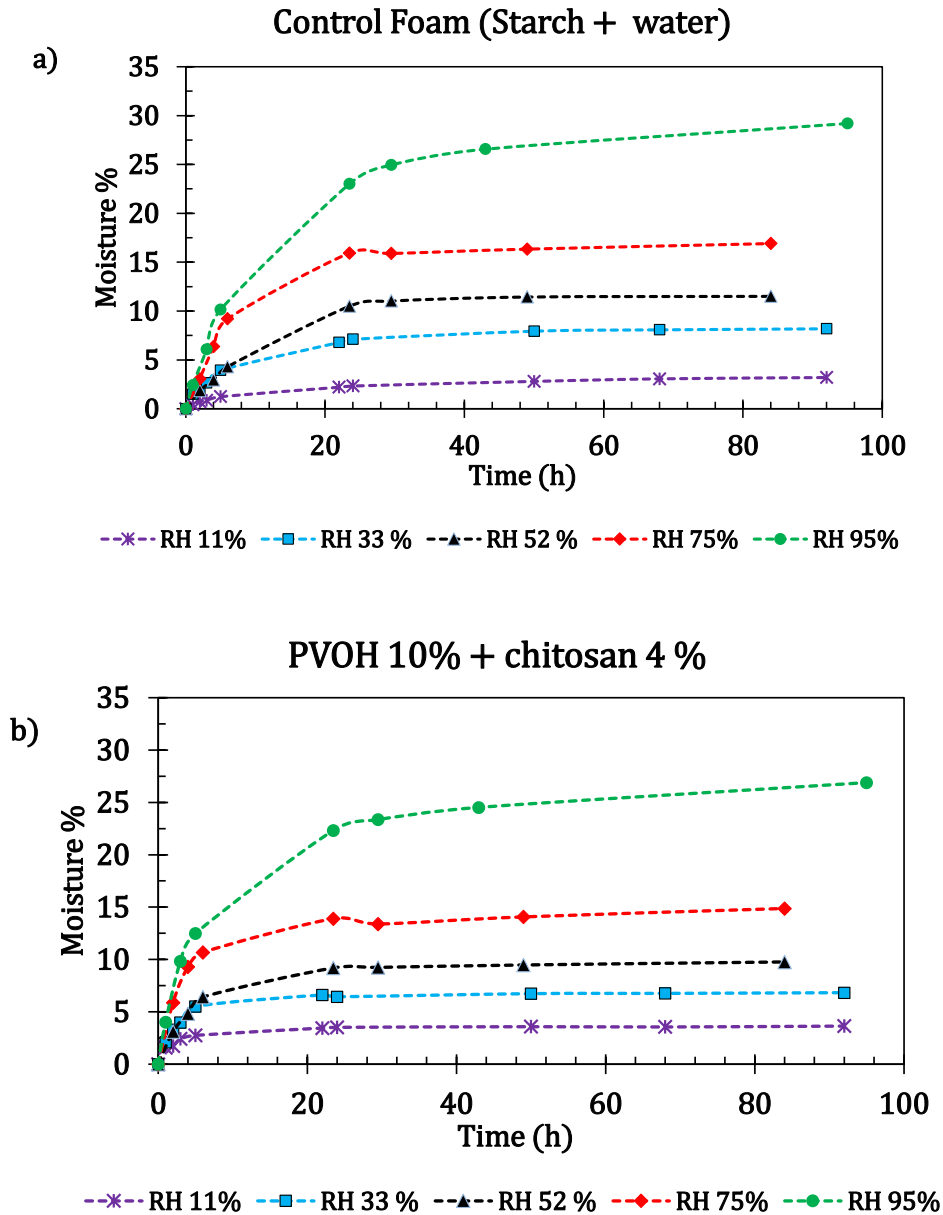
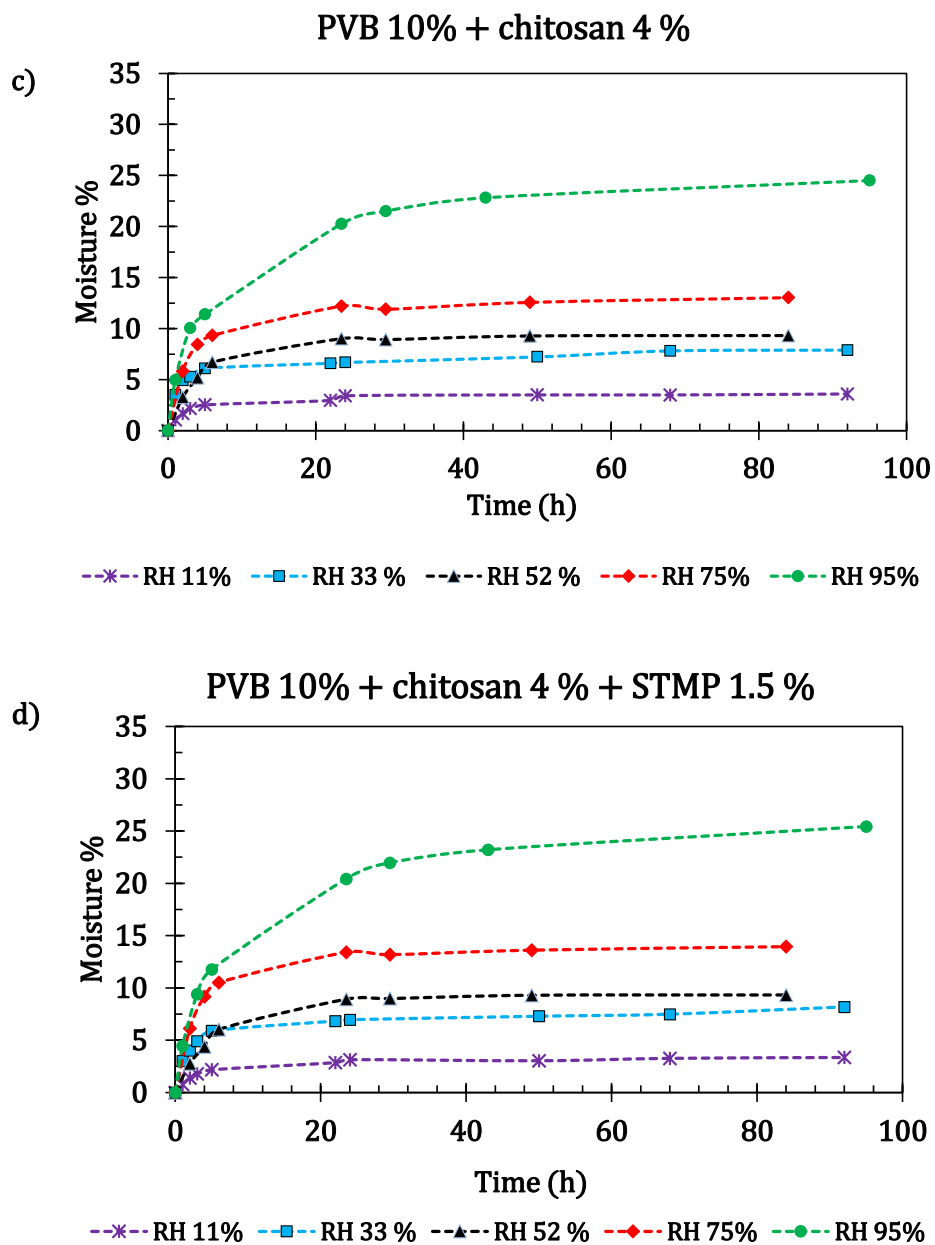


Figure 2.21: Moisture absorption curves for starch foams in different RH conditions a)control foams (starch+water) b)Control foam(PVOH +water), c)corn starch +PVB + chitosan ,d)corn starch+STMP+chitosan

Figure 2.21 cont'd



For all the samples, the foams exhibited typical adsorption behavior. Figure 2.22 shows the adsorption isotherms for the different foam samples. All sorption isotherms were of sigmoidal shape therefore can be classified as a type II according to Branauer classification. This type of isotherms is common for starch-rich products.

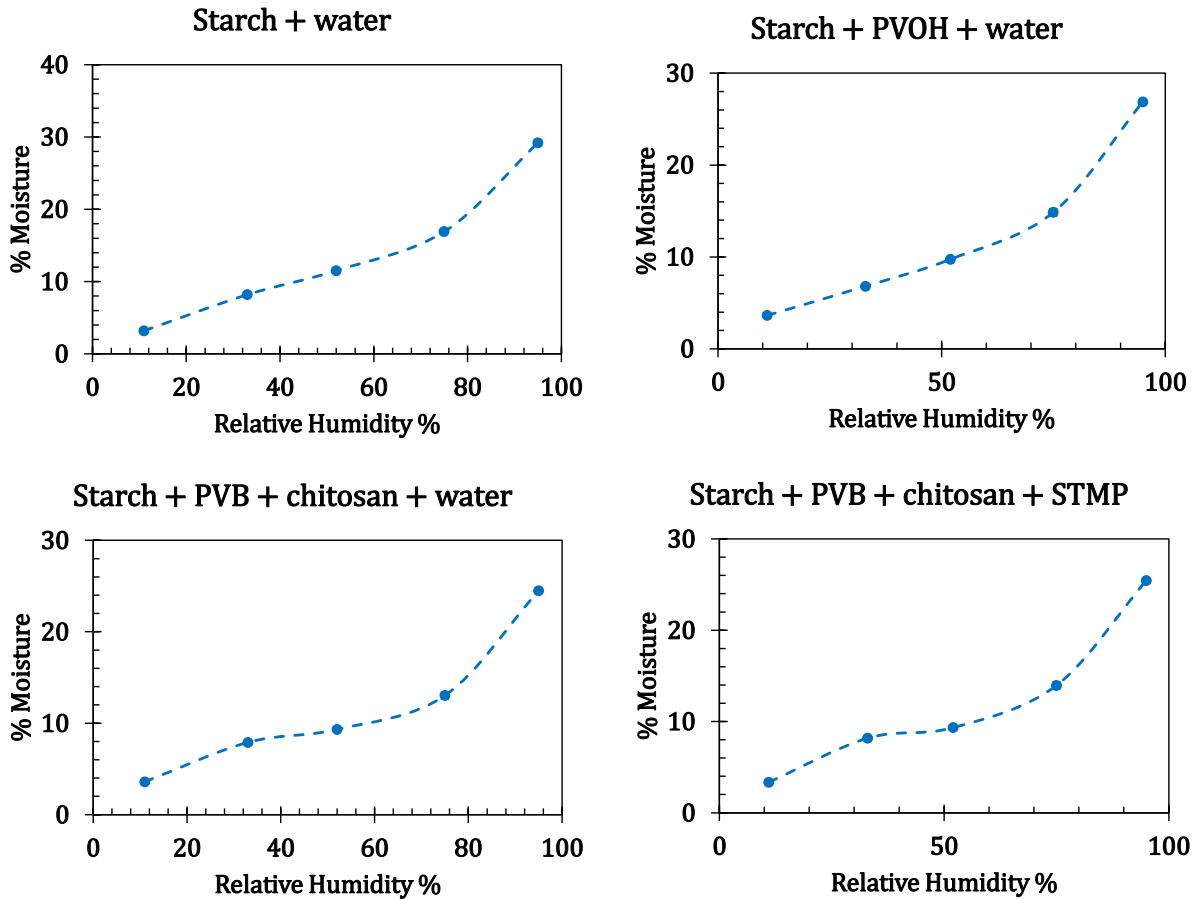


Figure 2.22: Sorption isotherms for different types of starch foams

It was observed that the rate of moisture absorption was fast initially, but it decreased gradually with time and an equilibrium was achieved after about 40 hours. The foams became brittle when placed in low RH environments like 11 and 33 %. When kept in high RH environment of 95%, a noticeable shrinkage occurred in control foams without additives and foams with PVOH (40 and 45 % of their original dimensions) as shown in Figure 2.23- a and b. Foams with PVB and STMP showed much better dimensional stability (15 and 10% loss in dimensions respectively) and did not shrink as much (Figure 2.23- c and d). Further quantitative analysis of the adsorption isotherms can be done using models such as GAB (Guggenheim-Anderson-de Boer). However, that was not focused on in this study.

Loss in the original dimensions

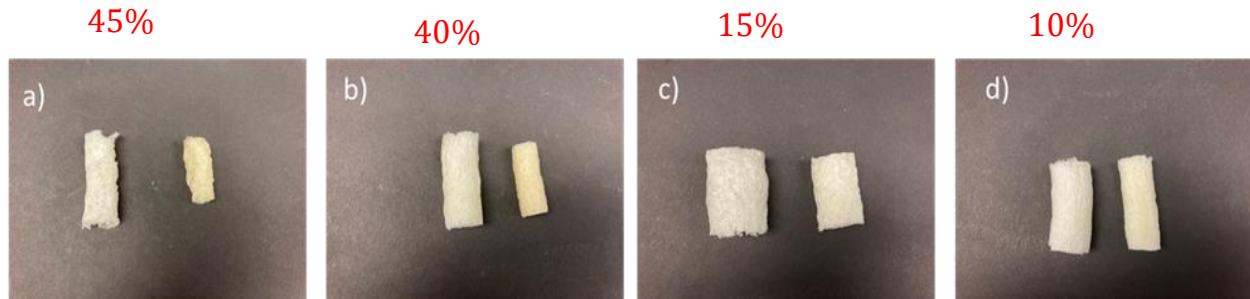


Figure 2.23: Shrinkage in foams with high RH of 95% a) control starch foam, b) PVOH foam, c) PVB foam d) chitosan +STMP (1.5%)

From the shape of the moisture absorption curves, it was apparent that the moisture absorption was directly proportional to the RH. The moisture sorption kinetics was described using the well-known Peleg model [45],[46] given as:

Equation 2.4

$$M(t) = M_0 + \frac{t}{k_1 + k_2 t}$$

Where $M(t)$ is the moisture content at any time t and M_0 is the initial moisture content of the sample. The major advantage of Peleg model is it helps in saving time by predicting the moisture sorption kinetics for samples containing equilibrium moisture content using short time experimental data. Here, k_1 is the constant related to mass transfer rate. The lower the k_1 , the higher the initial water absorption rate. k_2 is the constant related to maximum water absorption capacity i.e. the lower the k_2 , the higher the maximum water absorption capacity [45]. The parameters for Peleg model and the goodness of fit (R^2) were estimated using MATLAB and are shown in Table 2.6.

Table 2.6: Parameters of Peleg model for kinetics of moisture absorption of starch foams

Sample	RH	k ₁	k ₂	R ²
Control foam	LiCl= 11%	0.444	0.249	0.984
PVOH 10%, chitosan 4%		0.460	0.270	0.988
PVB 10%, chitosan 4%		0.615	0.279	0.987
PVB 10%, chitosan 4%, STMP 1.5 %		0.842	0.299	0.993
Control foam	MgCl ₂ = 33%	0.114	0.131	0.998
PVOH 10%, chitosan 4%		0.302	0.141	0.991
PVB 10%, chitosan 4%		0.147	0.136	0.994
PVB 10%, chitosan 4%, STMP 1.5 %		0.212	0.133	0.997
Control foam	MgNO ₃ = 52%	0.100	0.093	0.997
PVOH 10%, chitosan 4%		0.410	0.095	0.996
PVB 10%, chitosan 4%		0.352	0.100	0.994
PVB 10%, chitosan 4%, STMP 1.5 %		0.466	0.097	0.994
Control foam	NaCl = 75 %	0.129	0.050	0.994
PVOH 10%, chitosan 4%		0.181	0.066	0.884
PVB 10%, chitosan 4%		0.185	0.075	0.998
PVB 10%, chitosan 4%, STMP 1.5 %		0.168	0.069	0.998
Control foam	KNO ₃ = 95%	0.070	0.037	2.662
PVOH 10%, chitosan 4%		0.215	0.035	0.999
PVB 10%, chitosan 4%		0.206	0.039	0.995
PVB 10%, chitosan 4%, STMP 1.5 %		0.223	0.038	0.998

The data from table 5 indicates that the k_1 and k_2 values were smallest for the control starch foams indicating their fast water absorption and high-water absorbing capacity. Figure 2.24 shows the change in k_1 and k_2 values for the different foam samples. It was observed that the k_1 values increased for foams containing PVB, chitosan and STMP, which indicated that the rate of moisture absorption was less for these foams compared to the control foams. On the contrary, k_2 values for all the samples remained almost the same. This showed that the maximum water absorption capacity for the foams remained the same. Thus, even though these foams showed a delayed moisture absorption, after some time a breakthrough will be

achieved and the foams will absorb water. This was a very important property for the end of life of the foams.

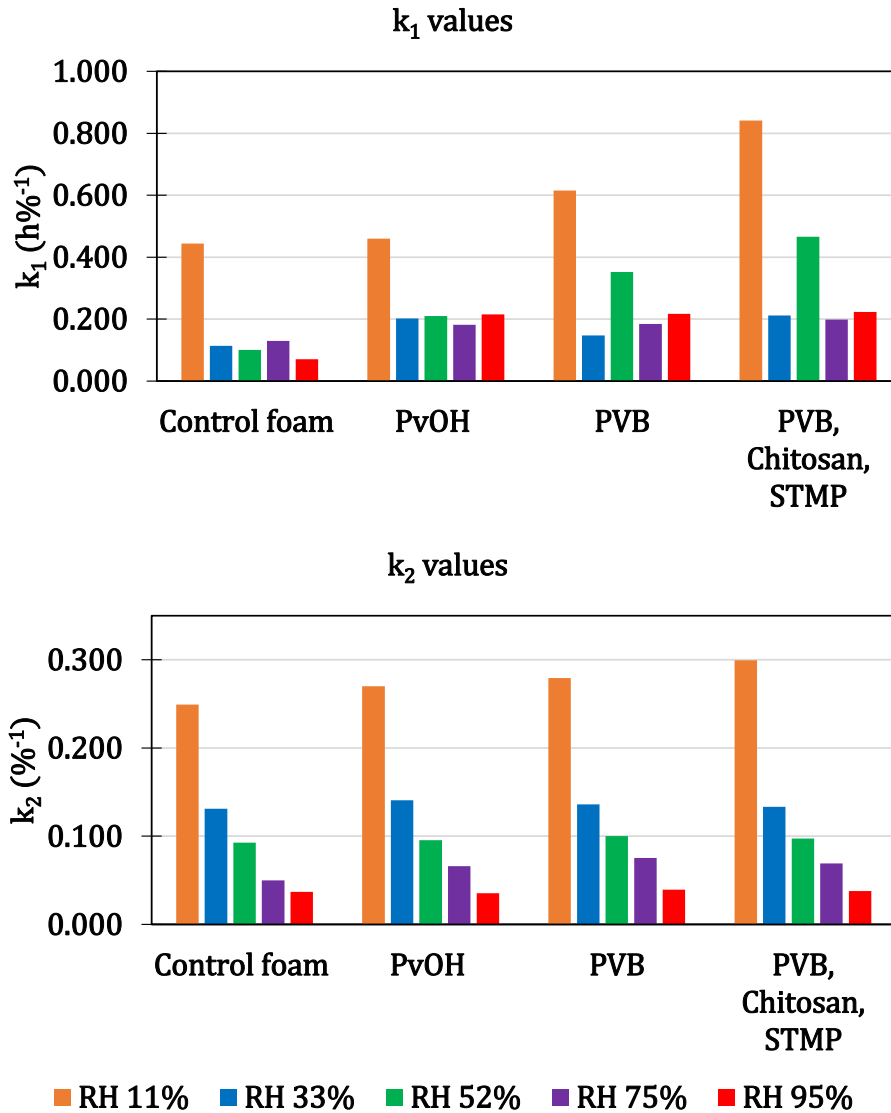


Figure 2.24: Peleg model constants k₁ and k₂ for the starch foam samples

Addition of PVOH and chitosan increased k₁ and k₂ values by small amounts which is probably due to the hydrophobic effect of chitosan [47, 48]. Addition of PVB to minimize the water sensitivity was found to be extremely effective. It also made the foams insoluble in water as opposed to the control foams and the foams made with starch and PVOH. This was

also observed in the water penetration tests (2.7.3 Water penetration test) done on the foams where it was observed that control foams and PVOH containing foams disintegrated in 5 hours whereas similar foams extruded with PVB remained intact. It was also observed that addition of STMP as crosslinking agent made the foams even more hydrophobic in most of the cases. Both rate of water absorption and maximum moisture absorption capacity (k_1 and k_2) were found to reduce. Figure 2.25 shows the equilibrium moisture content achieved by these foams after 80 hours when kept in a 95% RH environment. It was found to reduce from 29% by weight to 24% and 25% for PVB and STMP foams.

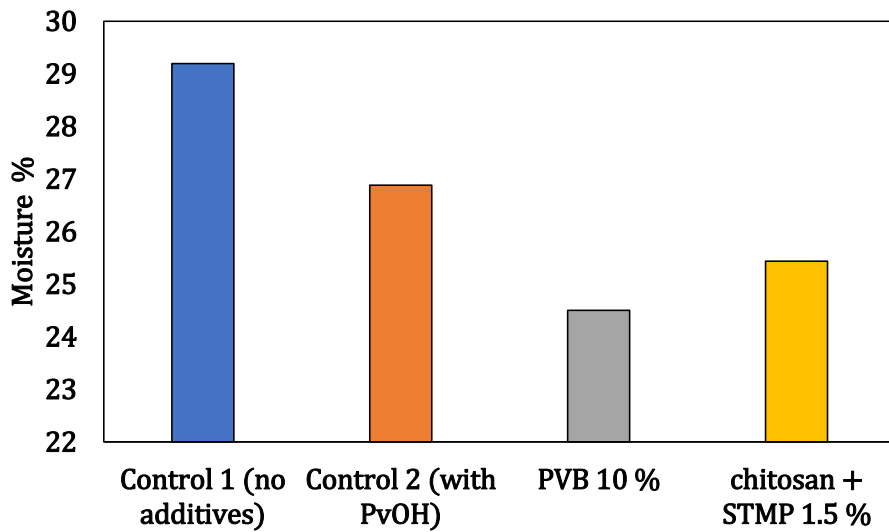


Figure 2.25: Moisture content at equilibrium for different foam formulations at 95% RH

2.7.6 Contact angle measurements

Starch foam's surface hydrophobicity water was studied with contact angle measurements. Figure 2.26 shows the contact angles of water droplets on different starch foam surfaces with various additives after 30 sec and after 1 min.

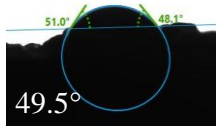
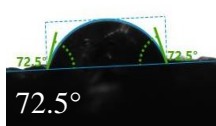
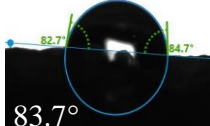
Formulation	Contact angle after 30 sec	Contact angle after 60 sec
Corn Starch + water (no additives)		
Corn Starch + water + talc (2%)		
Corn Starch + water + PVOH (10%)		
Corn Starch + water + Chitosan (4%)		
Corn Starch + water + Chitosan (4%) + PVB (10%)		

Figure 2.26: Effect of different additives on surface hydrophobicity of foams

For the control corn starch foams with just starch and water, it was observed that the water droplet did not stay on the surface. It was absorbed inside the foam almost immediately due to hydrophilic starch surface (Figure 2.26). Addition of talc increased the hydrophobicity of the foam surface. This might be attributed to the hydrophobic nature of talc[49]. However, previous tests of water solubility and moisture absorption showed that it was not sufficient

to make the foams moisture resistant. Addition of PVOH made the surface of foams smoother as compared to control foams. So, it was observed that the water droplet did stay for longer time on PVOH containing foams starting with a contact angle of 80° . However, the contact angle did decrease rapidly with time and the droplet was absorbed inside after ~ 3 mins.

With addition of chitosan, similar, slightly higher contact angle was observed (82.4°). But with chitosan, the water droplet did stay for much longer time on the surface of foam and did not get absorbed. With addition of chitosan the contact angle and the surface hydrophobicity increased. Interaction between the amino groups of chitosan and OH groups of starch may have resulted in stabilization of hydrophilic starch matrix and reduced the number of polar groups available to bond with water[50]. With increasing chitosan content from 4 to 10 %, a steady increase in contact angle to 101° was observed (Figure 2.27). This might be due to the same reason of hydrogen bonding between polar groups of chitosan and starch which reduced the polar groups available on the surface of foam for contacting with water.

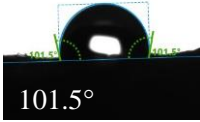
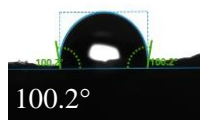
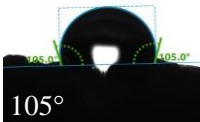
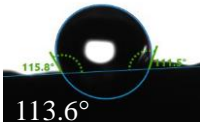
Formulation	Contact angle after 30 sec	Contact angle after 60 sec
Corn Starch + water+ chitosan (7%) + PVB (10%)	 98°	 94°
Corn Starch + water + chitosan 10% + PVB (10%)	 101.5°	 100.2°
Corn Starch + water+ chitosan (7%) + PVB (10%)+ STMP 1%	 105°	 107°
Corn Starch + water+ chitosan (7%) + PVB (10%)+ STMP 1.5%	 102°	 100.8°
Corn Starch + water+ chitosan (7%) + PVB (10%)+ STMP 3%	 113.6°	 112.2°

Figure 2.27: Effect of increasing percentage of chitosan and addition of STMP on surface hydrophobicity

Interestingly, starch-PVB-chitosan-STMP foams demonstrated much better hydrophobicity. Increase in hydrophobicity of starch due to cross linking has been observed by some authors including Shuzhen et. al. (2018) [51] and Shah et al. (2016)[52]. The contact angles were found to increase to almost 123° for 1.5 % STMP containing foams. Chitosan, PVB and STMP had a synergistic effect on making the foams dense and foam surface smoother which might have caused the highest contact angles for these foams.

Corn and potato starch foams with and without glycerol were also compared for the contact angle measurement. Addition of glycerol made both potato and corn starch foams more

hydrophilic. The contact angle reduced from Potato starch foams were found to be less hydrophilic in general than corn starch foams (71.3° for potato starch foam vs 65.7° for corn starch foam).

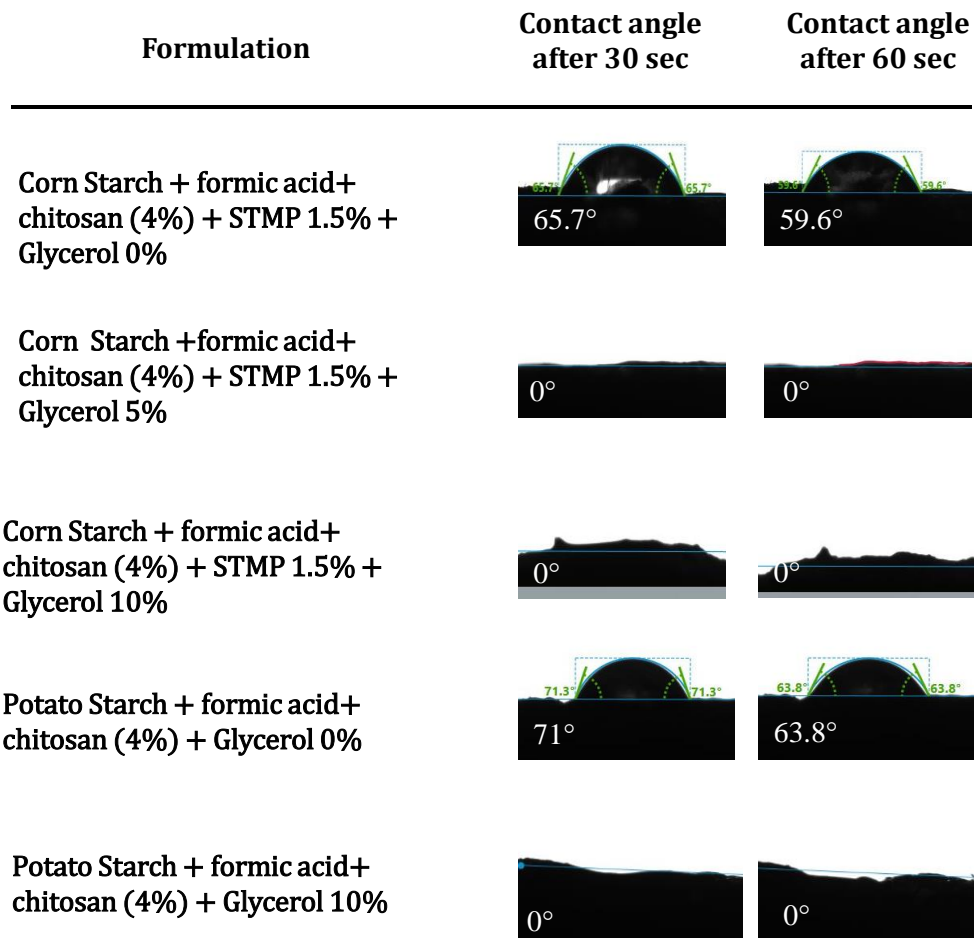


Figure 2.28: Effect of glycerol addition on surface hydrophobicity of starch foams

Also, they absorbed the water droplet slowly compared to similar formulations with corn starch. We suspect that this contact angle variation is due to differences in amylose and amylopectin contents and the size of the starch molecules and the degree of polymerization, of the two starches. Potato starch had higher amount of amylopectin compared to corn starch and its particle size was also much higher than the corn starch which was observed in the SEM studies as explained in chapter 1. [53].

2.7.7 Scanning electron microscopy

Cell size and cell size distribution are important parameters which affect the physico-mechanical properties of the foams. SEM images were taken for all the different foam formulations to study the effect of different additives and processing conditions on the cell size and morphology of the foams.

Effect of various additives

Without any additives, the starch foams produced were non uniform in nature. The cell sizes were very large, and the foams were brittle. Different additives used in the foams for improving various performance properties included – talc, PVOH, chitosan, STMP and glycerol

Additives such as talc, chitosan and STMP, acted as nucleating agents and helped to reduce the cell size of the foams and made them more uniform. According to the qualitative guidelines by McClurg [54], ideal nucleating agents have uniform size, geometries and surface properties and they are easily dispersible. Different additives used here showed different efficiencies in reducing the cell sizes of the foams. As studied by Leung et al[55] the geometry the nucleating agent affects the efficiency of nucleation. Hence the shapes of various nucleating agents were examined using SEM. Figure 2.29 shows the SEM images for talc, chitosan and STMP at 200 and 5000x magnifications. Talc particles were the smallest in size and had a scaly structure compared to all the other nucleating agents which might be a reason that makes them one of the most efficient nucleating agents (Figure 2.29-a and e). Figure 2.30 shows the SEM image for different foams with various additives. It can be observed that increasing the talc content from 0-2% reduced the cell size of the foams and made the cell size distribution more uniform (Figure 2.30-a-c). The cell size distributions

were also quantified using image analysis and plotted as normalized graphs as shown in Figure 2.31. It was clearly observed that with increasing percentage of talc, the number of smaller cells increased, and the cell distribution became more and more narrow.

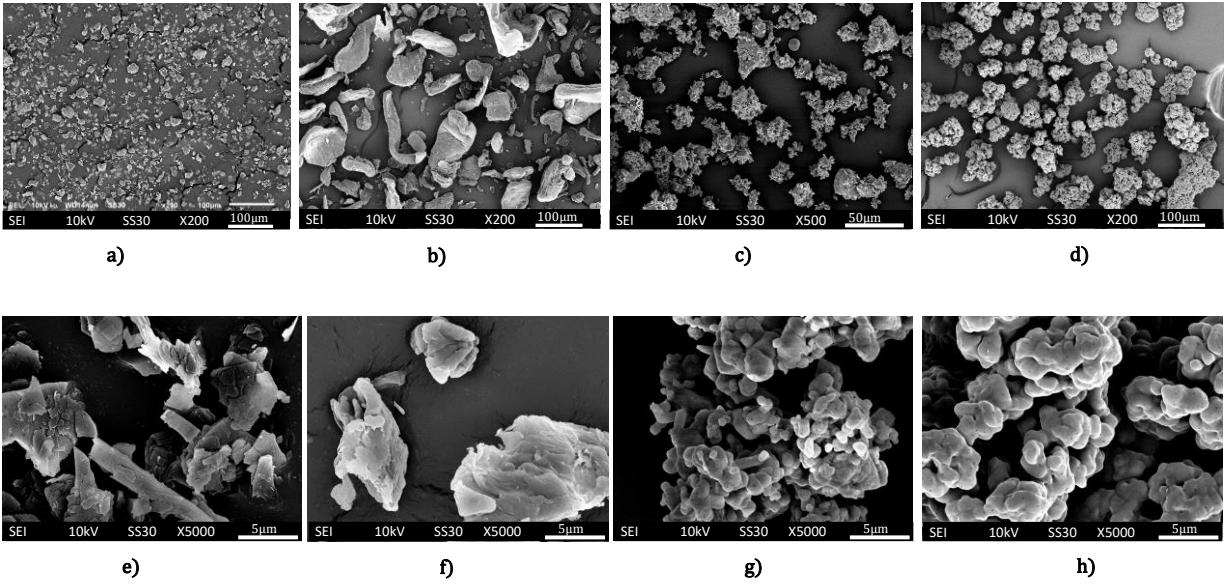


Figure 2.29: SEM images for various additives used in foam formulations – a) talc, b) chitosan, c) STMP, d) PVB at 200x magnification; e) talc, f) chitosan, g) STMP; h) PVB at 5000x magnification

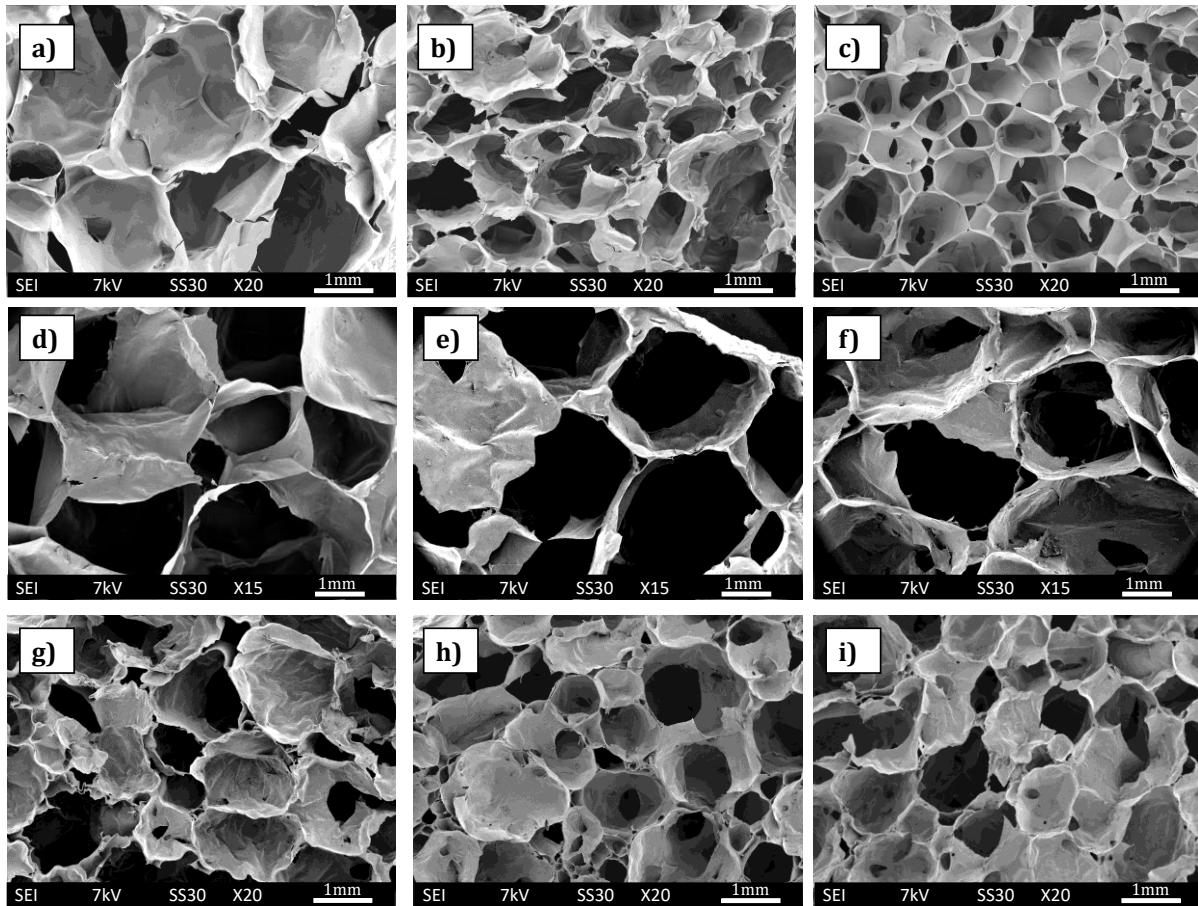


Figure 2.30: SEM images of starch foams containing a)0% talc b) 0.7% talc c)2% talc d)4% chitosan e)7% chitosan f)10% chitosan g) 1% STMP h) 1.5% STMP i) 3% STMP

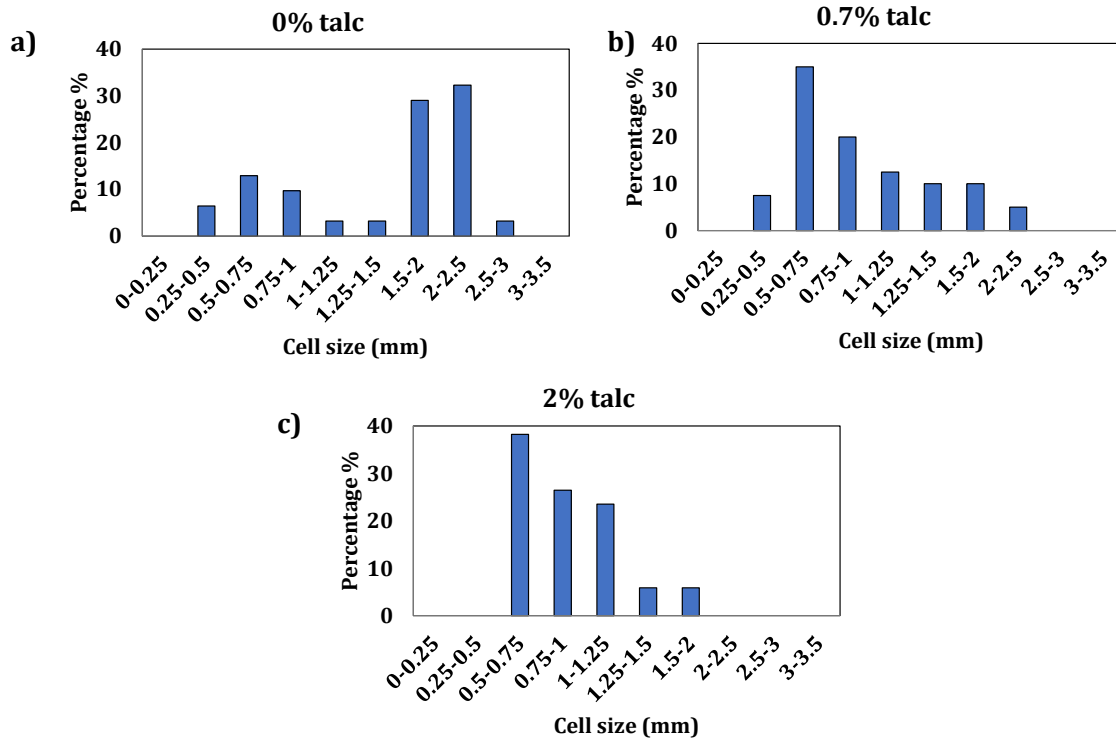


Figure 2.31: Cell size distribution for foams containing different percentages of talc

Even with SMTP, the shapes of the particles were very uniform and small (Figure 2.29- c and g). Hence, a greater number of nucleation sites were available in the foams and STMP proved to be efficient as a nucleating agent. One more theory that can be used for explaining the impact of STMP is the crosslinking of starch by sodium trimetaphosphate. Starch reacts with sodium trimetaphosphate to give mono and distarch phosphates as shown in Figure 2.4. Studies have reported the effects of crosslinking on the growth of cells[56, 57]. Foaming and crosslinking reactions compete with each other and the foamed structure can be controlled by adjusting the process conditions[56]. The cell sizes of foams with increasing percentages of STMP were monitored and plotted as a function of % of cells (Figure 2.32). It was observed that the cell sizes became narrower and the distribution became more uniform as the percentage of STMP increased from 0 to 3%. Due to increasing crosslinking of starch with

STMP, the cell sizes go on reducing giving a narrower cellular size distribution as shown in Figure 2.29-g, h,i. Furthermore, strain hardening is a necessary requirement for the foaming process. A lower extensional viscosity is necessary for expansion of the bubbles whereas a high extensional viscosity is needed to stabilize the bubbles. Crosslinking of starch with STMP increases the melt viscosity of the mixture making the bubbles more stable and cell distribution more uniform, thus giving the nucleating effect.

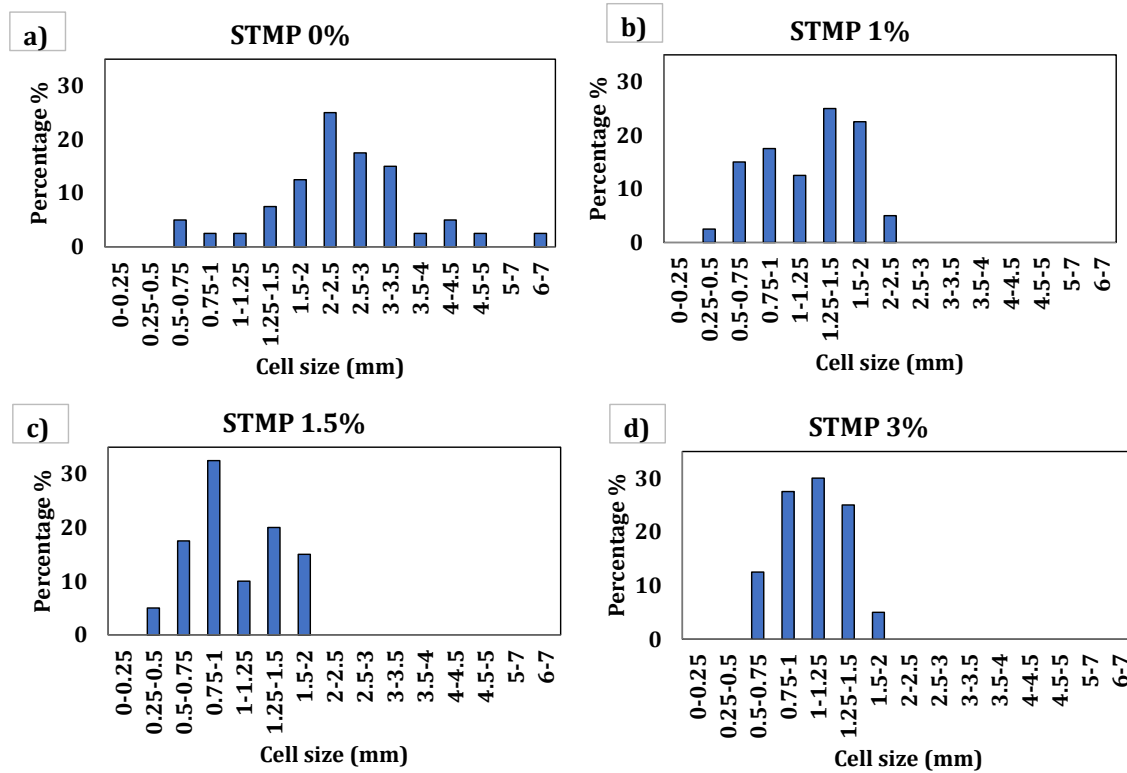


Figure 2.32: Cell size distributions for starch foams with PVB at different STMP levels a) 0% b) 1% c) 1.5 % d) 3%

Addition of increasing amounts of chitosan showed a similar nucleating effect as talc although the effect was not as drastic (d, e, f). This might be due to the fact that chitosan particles were much larger and more non uniform compared to talc or STMP as observed from their SEM (Figure 2.29-b and f). Va'zquez et al. studied chitosan as nucleating agent for thermoplastics foams and they found that, for every nucleating agent there is a 'critical

concentration' at which the cell size and distribution is most uniform. And the critical concentration depends on the size of the particles. Larger the particle size, higher the percentage required for nucleating effect[58]. So, it might be possible that higher concentrations of chitosan were needed in the formulation to have more impact on the nucleation and cell size which were not tried in this study. Figure 2.33 shows the cell size distribution of starch foams containing 4, 7 and 10% chitosan respectively. Higher amounts of chitosan were required for achieving similar nucleating effect as talc.

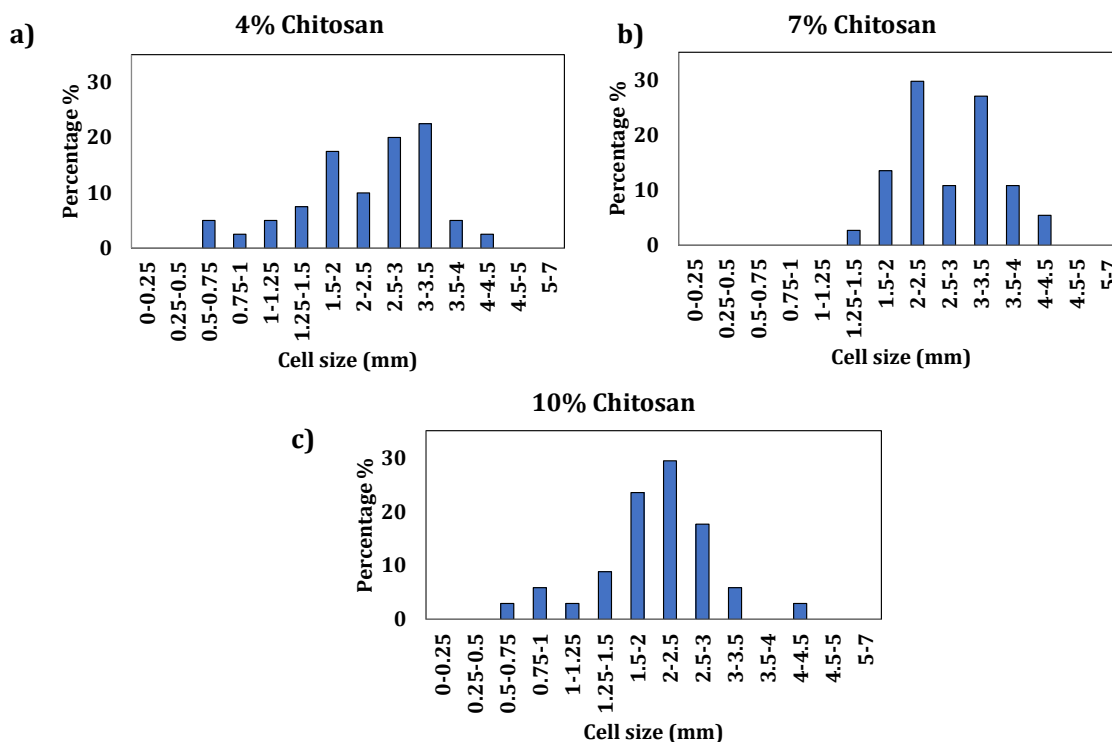


Figure 2.33: Cell size distribution of starch foams with increasing percentages of chitosan

PVB acted as a foaming agent and increased the cell size and expansion ratios of the foams considerably as compared to control foams and foams with PVOH. The reason for that could be the hydrophobic nature of PVB. It is very sensitive to hydrolysis in presence of water[42] to form polyvinyl alcohol and butyraldehyde. The boiling point of butyraldehyde (74.8°C) is

lower than the extrusion processing temperatures. Hence it might be generating extra vapor apart from the steam generated from evaporation of water and act as a chemical blowing agent to increase the cell size and reduce the density of resulting foams.

2.7.8 Confocal microscopy

Confocal laser scanning microscopy (CLSM) was applied to determine the distribution of chitosan in starch foams. Several studies have reported on the characterization of chitosan stained with different types of fluorescent labels, such as fluorescein isothiocyanate (FITC) (Onishi & Machida, 1999) and rhodamine B isothiocyanate (RBITC) (Ma et al., 2008) using CLSM technique (Ma et al., 2003, Ma et al., 2008, Onishi and Machida, 1999). Here FITC was used for green fluorescent staining of chitosan. Some studies have reported the migration of chitosan from the bulk of the material to the surface[23]. The migration of chitosan to the surface of the foams can be one of the reasons for increased hydrophobicity of the foams. Hence the difference between the chitosan distribution in the bulk of the foam (middle part) and the surface of the foams was observed using CLSM. The foams were cut in thin slices from two parts- the inner bulk and the surface. Then they were stained and mounted on the slides as per the method explained in section 2.4 and compared for amount of chitosan present in the bulk vs the surface of the foam. Figure 2.34 shows the 3D MIP images for 0%, 4%, 7% and 10% chitosan foam formulations from the surface of the sample and from the bulk. Dang et. al 2016, have confirmed that chitosan gets distributed on the surface of the films, forms hydrogen bonds with the starch molecules and reduces the surface hydrophobicity of the films[23]. Similar results were observed with the foams as well. It was clearly observed for all the samples that more chitosan was present on the surface of the foams as compared to the bulk. Chitosan chains might have oriented towards the surface of

the foams during cooling of the foams after coming out from the die or during the storage of the foams. This also explains the increased hydrophobicity of the foam surface as observed from contact angle measurements. One more possible explanation for this hydrophobicity is - during gradual drying of a polyelectrolyte it is possible for relatively non-polar polymers or their segments to migrate to the air-water interface (Khavet and Essalhi 2015). Such orientation achieves an arrangement that is thermodynamically favorable – providing a relatively low-energy surface facing the air. In this case, most of the polar groups, including both the amine and hydroxyl groups, will face inwards or parallel to the surface. The formation of hydrogen bonds might be expected to drive such a reorientation during drying. The presence of non-polar groups on the surface of the foams could account, at least in part, for the often-observed relatively hydrophobic nature of chitosan containing foams. To confirm this, the foam surfaces can be scratched and the contact angles can be measured again to see if more hydrophilic groups, then get exposed and change the hydrophobicity of the surface.

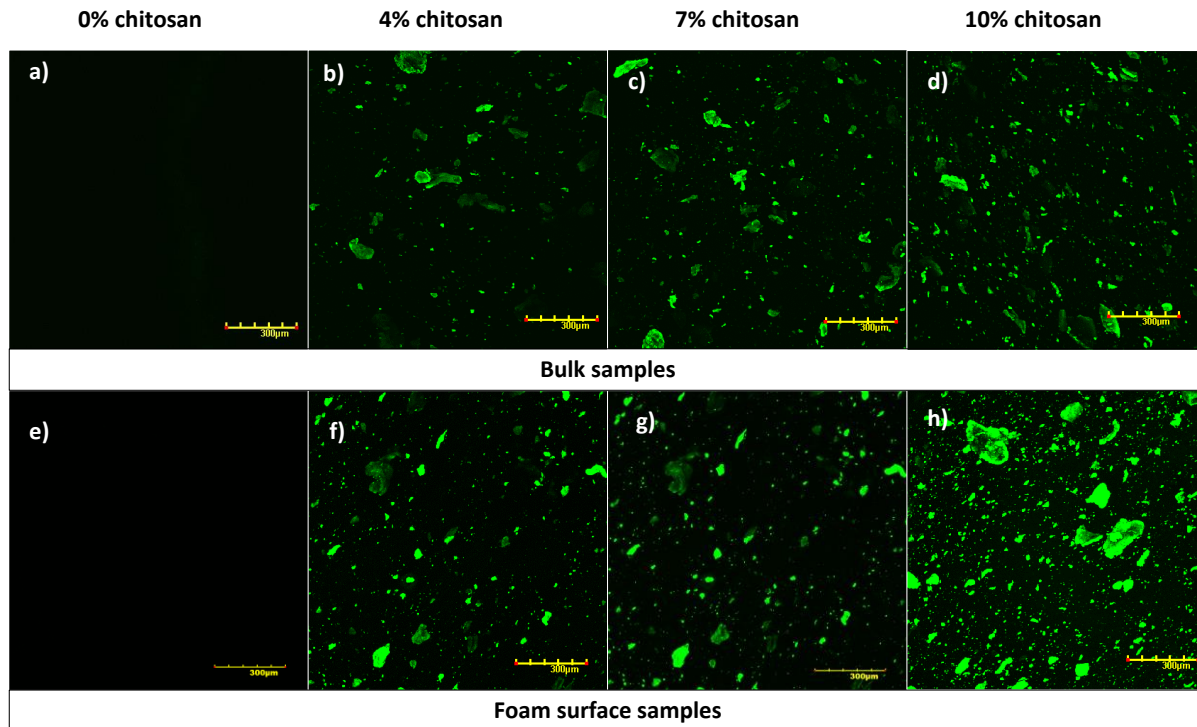


Figure 2.34: Confocal laser scanning microscope (CLSM) 3D MIP images for 0%, 4%, 7% and 10% chitosan foam formulations from the bulk of the sample (a,b,c,d) and from the surface (e,f,g,h)

2.7.9 Compressive strength

Compressive strength is the measure of ability of foam to deform under load. Figure 2.35 shows the effect of various additives on the compressive strength. The detailed results for compressive testing of starch foam samples are listed in Table 2.7. Denser foams tend to have thicker walls and hence resist the deformation better and thus have a higher compressive strength. Since addition of PVB reduced the density of foams considerably as explained previously, the compressive strength was also found to be less for these foams. (0.04 MPa vs 0.08 MPa for control foams). However, addition of STMP as crosslinking agent made the foams stronger, less resilient and increased the compressive strength to 0.215 MPa; 3 times that of the control foams. Similar results were observed by Hassan et al. 2020[25] where crosslinking of starch by citric acid increased the compressive strength to double the value.

The compressive strain at maximum stress is also an indicator of sample's resilience and elastic limit. It was found to increase from 8% for control foams to 12% for foams with PVB which indicated increase in resilience. Crosslinking of starch with STMP reduced this strain to around 9% which was still higher compared to control foams.

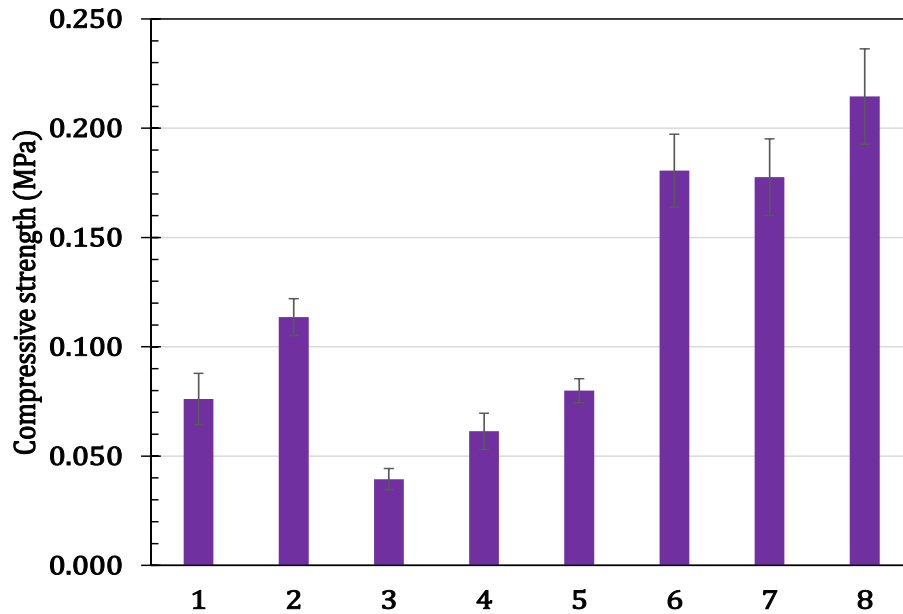


Figure 2.35: Compressive strength of starch foams 1)Control foams (starch+water), 2)Control foams (PVOH), 3)10% PVB,4% chitosan, 4) 10% PVB,7% chitosan, 5) 10% PVB,10% chitosan, 6) 10% PVB,4% chitosan, 1% STMP, 7) 10% PVB,4% chitosan, 1.5 STMP, 8) 10% PVB,4% chitosan, 3% STMP

Table 2.7: Physico-mechanical properties of extruded starch foams

Sample	Density (kg/m ³)	Expansion ratio	Compressive strength (MPa)	Compressive strain at maximum compressive load (%)
Control foam	40.7 ± 8.9 ^a	46.6 ± 7.9 ^a	0.076 ± 0.01 ^a	7.95
PVOH 10%, chitosan 4%	45.7 ± 2.3 ^a	27.5 ± 0.9 ^b	0.114 ± 0.01 ^b	7.15
PVB 10%, chitosan 4%	21.1 ± 1.7 ^b	74.5 ± 3.9 ^c	0.040 ± 0.005 ^c	12.08
PVB 10%, chitosan 7%	35.0 ± 3.8 ^c	51.1 ± 5.5 ^d	0.0614 ± 0.008 ^d	11.14
PVB 10%, chitosan 10%	35.7 ± 3.0 ^c	50.1 ± 5.7 ^d	0.0800 ± 0.005 ^a	10.63
PVB 10%, chitosan 4%, STMP 1 %	37.0 ± 3.8 ^c	50.3 ± 5.3 ^d	0.181 ± 0.017 ^e	9.82
PVB 10%, chitosan 4%, STMP 1.5 %	43.9 ± 4.0 ^a	43.9 ± 4.0 ^e	0.178 ± 0.017 ^e	9.54
PVB 10%, chitosan 4%, STMP 3 %	51.6 ± 3.7 ^e	51.6 ± 3.7 ^d	0.215 ± 0.022 ^f	12.12

Different superscript letters within the same column indicate significant differences among formulations ($p < 0.05$).

2.7.10 Aqueous biodegradability studies

Various moisture resistant and water insoluble starch foams were prepared in this project. It was important to check the impact of these additives and modifiers on the end of life of foams. Hence 3 foam samples – 1. control foam containing PVOH, 2. Foam with 4% chitosan, and 10% PVB and 3. Foams with 4% chitosan, 10% PVB and 1.5% STMP, were studied for their aqueous biodegradation according to ISO 14852 at 30°C. The CO₂ evolved from all the samples was subtracted from the cumulative CO₂ of the blanks to calculate % biodegradation as explained in section 2.4. Figure 2.36 shows the graphs of percent biodegradation vs time for the 3 foams.

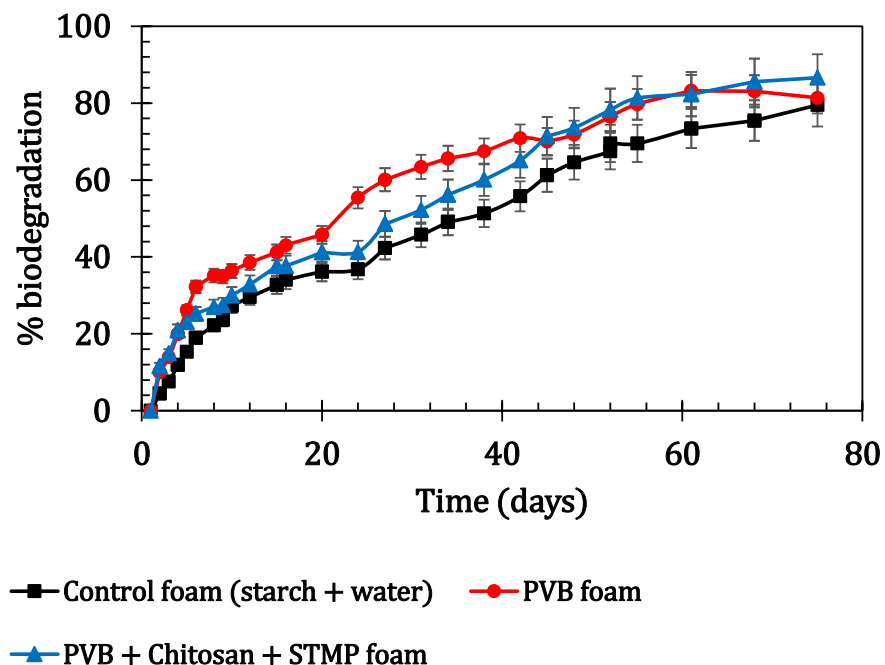


Figure 2.36: Aqueous biodegradation curves for control starch foam, PVB containing foam and STMP containing foam

It was observed that there was not much difference in the rates of biodegradation of the 3 foams. Even in presence of PVB and STMP, the foams reached ~90% biodegradation in 80 days which was a positive result. Similar results were obtained by Merino et. al 2019 [59] where they observed that neither crosslinking of starch by phosphorylation nor chitosan addition has any significant impact on the soil biodegradation of the starch films. Thus, even if the starch foams were made more resistant to moisture using PVB, chitosan and STMP, their end of life was not impacted much due to these modifications and these foams still remained readily biodegradable in aqueous environment. Thus, in case of inadvertent leakage of these products in the marine environment, they will be completely removed within a reasonable timeframe and may cause minimum impact to the environment.

2.8 DESIGNING AN ANNULAR DIE

In order to get rid of the ridges occurring in the foams made with slit die, another approach of using an annular die is being studied. The idea is to make the foams in the form of hollow tubes from this annular die which can be then cut to open up the tubes and get flat sheets. The first step was making a preliminary die design using AUTOCAD with all the measurements suitable for our extruder.

Die design

A preliminary design for an annular die was developed to fit the Century ZSK-30 twin screw extruder. The die was designed in 2 parts. The outer part included the die plate and a tube-like structure and a cylindrical mandrel was designed to fit inside this part so as to produce the foams in the form of tubes/cylinders. These cylinders can then be cut using blades to open up the tubes and yield flat sheet foams. The 2 parts are as shown in Figure 2.37.

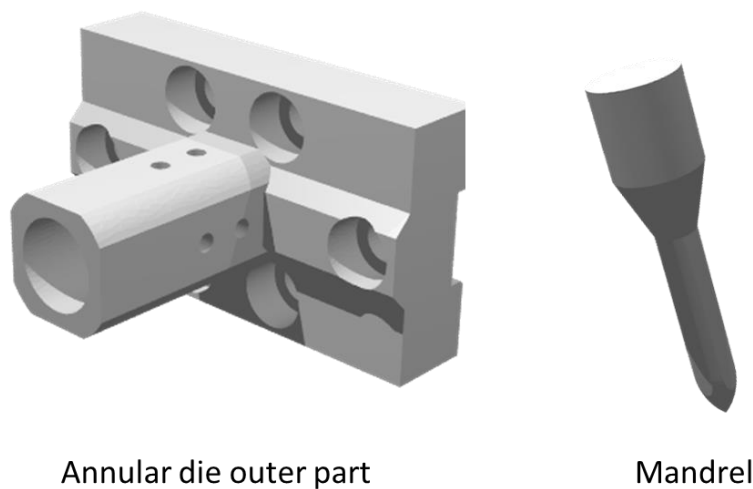


Figure 2.37: Annular die design parts

The detailed design using AUTOCAD is shown in Figure 2.38.

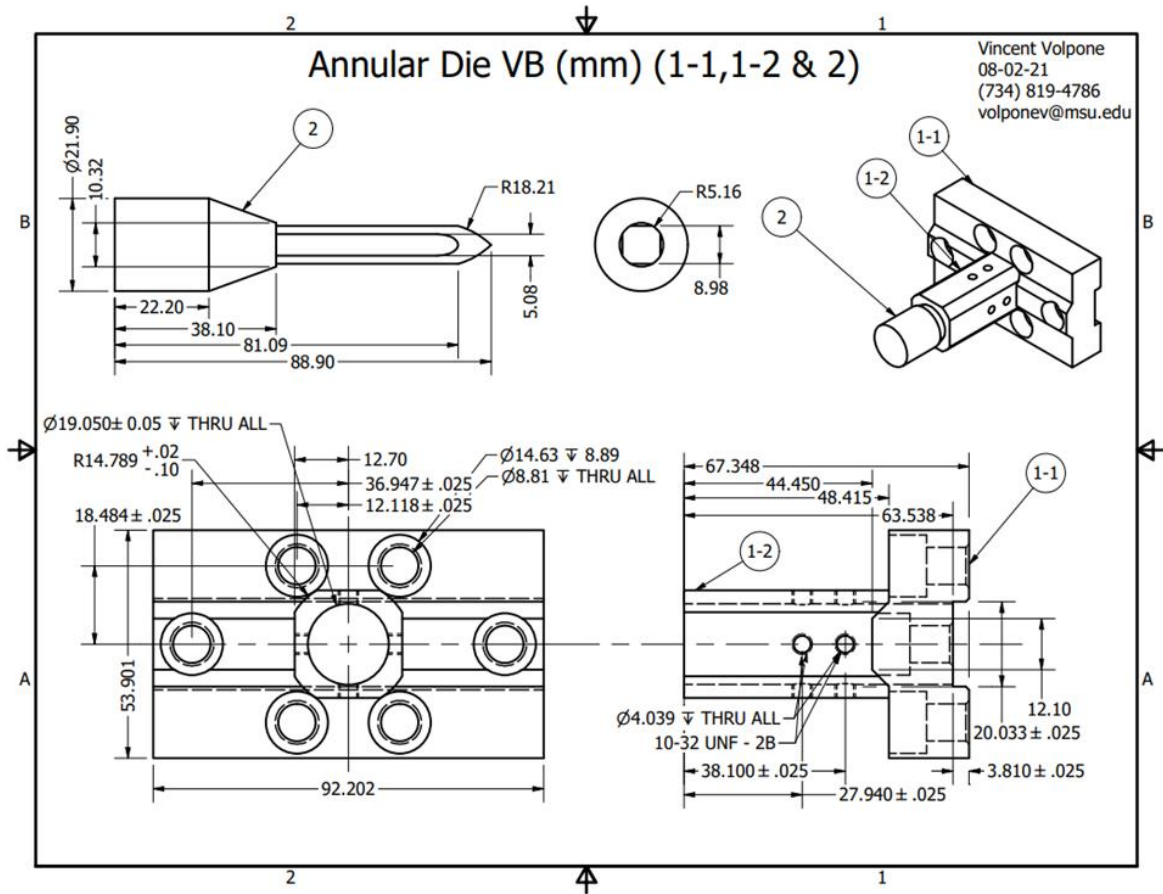


Figure 2.38: AUTOCAD design for the die

Next, this die design was 3D printed using polymer composite to check for all the measurements and also perform a few trial runs before getting the die CNC machined. Figure 3 shows the composite 3D printed die. It did match with all the measurements for extruder die plate. However, the polymer composite could not withstand the high temperatures of 140-150°C which were used for the extruder and the die started to melt. Hence, it could be used for the trial runs. However, this step was useful to ensure the dimensions of the die were appropriate and the die was fitting perfectly on the extruder die head.

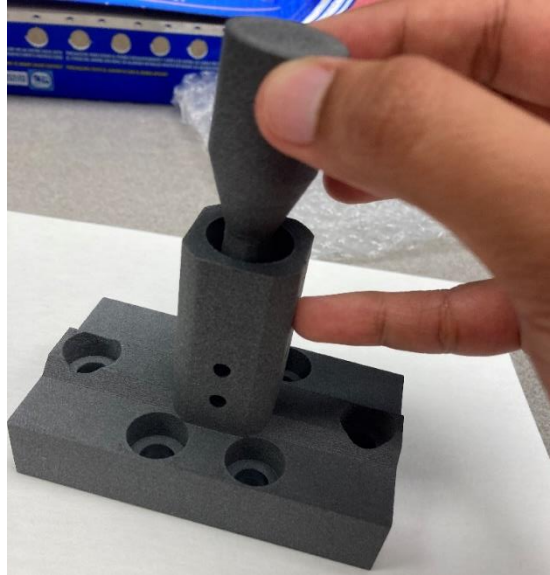


Figure 2.39: 3D printed die

The next step was getting the die CNC machined. We have recently acquired the metal die from a manufacturer, and we are in the process of testing the die for trial runs to make the sheets. Figure 2.40 shows the CNC machined die.

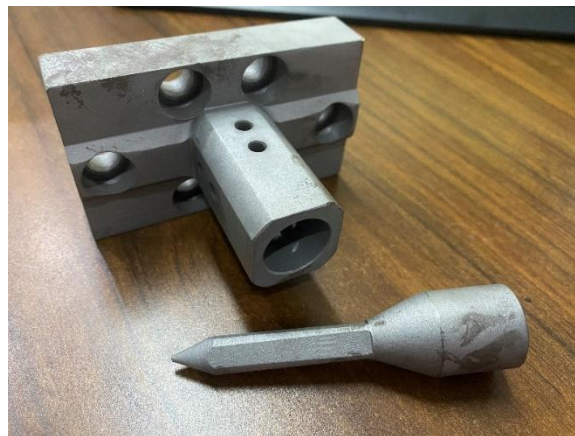


Figure 2.40: CNC machined die

Trial runs

A couple of trial runs were carried out using this die for making the foams. Processing conditions similar to strand and slit die were also used for this die as a starting point. Figure 2.41- a and b show the foams produced from this die. These foam tubes were cut and

flattened to make the sheets as shown in Figure 2.41-c. The formation of ridges was very less using this kind of die. There are still some problems with making the runs smoother and optimizing the processing conditions and design for this die.

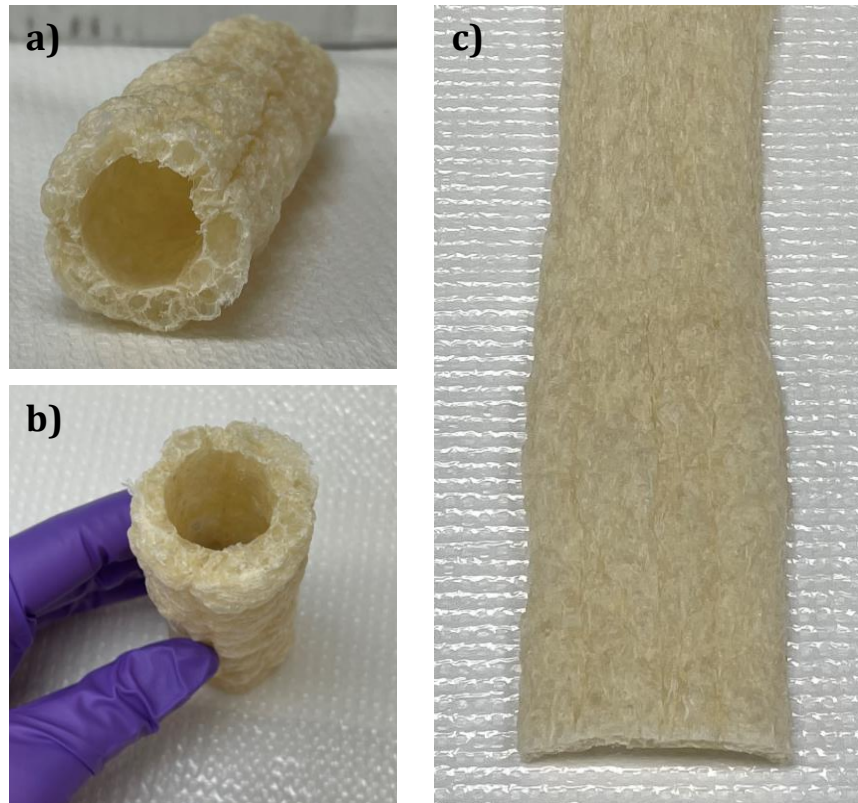


Figure 2.41: a), b) Some annular die foams produced from the trial runs c) flat sheets formed after cutting the foam tubes

2.9 **FUTURE RECOMMENDATIONS**

- The cell size for the foams prepared was in the range of mm in this study. Efforts should be made to make this cell size smaller and more uniform. That might affect the moisture sensitivity as well.
- The chemistry of chitosan-starch polyelectrolyte complex and STMP-starch crosslinking and degree of substitution etc. was not studied in detail in this project. The formation of insoluble foams itself was taken as an indication that polyelectrolyte complex was forming, or crosslinking was taking place. Further quantitative NMR or other studies can be done to get a better idea of these mechanisms.
- The stability of PEC could be affected by many factors, including density of charges, degree of ionization, pH of reaction medium, concentration of polyelectrolytes, distribution of ionic groups, molecular weight, mixing ratio, order of reacting polyelectrolytes, and drying process, etc. these factors could be studied in detail to make these foams more or less stable as required.
- A design of experiments approach can be used to study the effect of multiple factors on the properties of the foams.
- The foams sheets need to be completely flat and of uniform thickness to make their use in hemostatic pads. First steps in this direction have been taken by design of the annular die and the trial runs as a proof of concept. Further optimization in die design and processing conditions is required to calibrate this process.

2.10 CONCLUSIONS

Cylindrical and sheet starch foams were prepared in ZSK-30 twin screw extruder using various reactive modifiers and additives such as PVB, chitosan, STMP and glycerol. Water and formic acid aqueous solutions were used as a plasticizer as well as blowing agent. The extrusion conditions were optimized for each formulation to obtain lowest density consistent foams with controlled expansion. Various extrusion parameters such as temperature, screw configuration, water content and feeding rates were optimized for process development of foam extrusion. Both slit and strand dies were used for making foams in different shapes. A roller press was used for making foams as flat sheets.

Talc, chitosan and STMP acted as nucleating agents and reduced the cell size of the foams and made the cell size distribution more uniform. With addition of increasing percentage of talc, chitosan and/or STMP, the density increased, and expansion ratio reduced steadily. PVB seemed to act as a blowing agent and resulted in foams with the lowest density and highest expansion ratio of 21 kg/m³ and 38.7 respectively. Solubility testing of starch foams showed that the control starch foams without any additives and with PVOH as additive dissolved immediately in water. When chitosan was added to the foams, a polyelectrolyte complex was formed, and the foams formed gel structures in water. Addition of formic acid for protonation of amino groups and addition of STMP for making anionic starch increased the efficiency and stability of polyelectrolyte complex in water. Addition of PVB proved to be extremely efficient in improving the moisture resistance of starch foams. PVB and STMP together made the cell structure strong and improved the humidity resistance of the foams. These foams showed the best performance in terms of water insolubility, dimensional stability and surface hydrophobicity. Addition of glycerol made the foams more flexible but also more

hydrophilic and susceptible to moisture. Starch foams were kept in different relative humidity environments to study the rate and moisture absorption capacity using Peleg model. CLSM imaging showed that chitosan from the foams was preferentially migrating to the surface of the foams making the surface hydrophobic. Crosslinking of starch with STMP and forming its polyelectrolyte complex with chitosan also improved the mechanical properties of the foams upto 3 times compared to control foams. Efforts were also done to design an annular die to make the foams as flat sheets. Further optimization is required to fine tune the design and runs for the annular die.

Finally, the aqueous biodegradability studies of the foams showed that even though PVB and STMP made the foams insoluble and resistant to moisture, they were still readily biodegradable. These foams could find applications in various fields including packaging, insulation requiring long term humidity resistance, and in medical fields such as disposable hemostatic pads to be used by 1st responders in the field. This will translate to a significant reduction in the carbon footprint associated with conventional PE or polystyrene foams and will also provide an environmentally responsible end-of-life.

REFERENCES

REFERENCES

- [1] G. Abinader, C. Lacoste, M. Le Baillif, D. Erre, and A. Copinet, "Effect of the formulation of starch-based foam cushions on the morphology and mechanical properties," *J. Cell. Plast.*, vol. 51, no. 1, pp. 31–44, Jan. 2015.
- [2] "Starch Medical | Starch Medical Launches Novel Plant Sourced Surgical Hemostatic Pad," 2009. [Online]. Available: <https://starchmedical.com/starch-medical-launches-novel-plant-sourced-surgical-hemostatic-pad/>. [Accessed: 10-Nov-2020].
- [3] N. H. P. Rodrigues, J. T. de Souza, R. L. Rodrigues, M. H. G. Canteri, S. M. K. Tramontin, and A. C. de Francisco, "Starch-Based Foam Packaging Developed from a By-Product of Potato Industrialization (*Solanum tuberosum* L.)," *Appl. Sci.*, vol. 10, no. 7, p. 2235, Mar. 2020.
- [4] F. Debiagi, S. Mali, M. V. E. Grossmann, and F. Yamashita, "Biodegradable foams based on starch, polyvinyl alcohol, chitosan and sugarcane fibers obtained by extrusion," *Brazilian Arch. Biol. Technol.*, vol. 54, no. 5, pp. 1043–1052, Sep. 2011.
- [5] Q. Fang and M. A. Hanna, "Mechanical properties of starch based foams as affected by ingredient formulations and foam physical characteristics," *Am. Soc. Agric. Eng.*, vol. 43, no. 6, pp. 1715–1723, 2000.
- [6] Y. Nabar, R. Narayan, and M. Schindler, "Twin-screw extrusion production and characterization of starch foam products for use in cushioning and insulation applications," *Polym. Eng. Sci.*, vol. 46, no. 4, pp. 438–451, Apr. 2006.
- [7] Q. Fang and M. A. Hanna, "Functional properties of polylactic acid starch-based loose-fill packaging foams," *Cereal Chem.*, vol. 77, no. 6, pp. 779–783, 2000.
- [8] Y. U. Nabar, D. Draybuck, and R. Narayan, "Physicomechanical and hydrophobic properties of starch foams extruded with different biodegradable polymers," vol. 102, no. 1. John Wiley & Sons, Ltd, 2006, pp. 58–68.
- [9] Y. Nabar, J. M. Raquez, P. Dubois, and R. Narayan, "Production of starch foams by twin-screw extrusion: Effect of maleated poly(butylene adipate-co-terephthalate) as a compatibilizer," *Biomacromolecules*, vol. 6, no. 2, pp. 807–817, Mar. 2005.
- [10] J. Stagner and R. Narayan, "Preparation and Properties of Biodegradable Foams," *J. Polym. Environ.*, vol. 19, no. 3, pp. 598–606, Sep. 2011.
- [11] Z. Yang, D. Graiver, and R. Narayan, "Extrusion of humidity-resistant starch foam sheets," *Polym. Eng. Sci.*, vol. 53, no. 4, pp. 857–867, Apr. 2013.
- [12] B. S. Rubin, "Bisphenol A: An endocrine disruptor with widespread exposure and multiple effects," *J. Steroid Biochem. Mol. Biol.*, vol. 127, no. 1–2, pp. 27–34, Oct. 2011.

- [13] "Scientific committee on consumer products : Opinion on Glyoxal," 2005.
- [14] Y. Xu and M. A. Hanna, "Physical, mechanical, and morphological characteristics of extruded starch acetate foams," *J. Polym. Environ.*, vol. 13, no. 3, pp. 221–230, Jul. 2005.
- [15] J. Guan and M. A. Hanna, "Extruding foams from corn starch acetate and native corn starch," *Biomacromolecules*, vol. 5, no. 6, pp. 2329–2339, Nov. 2004.
- [16] "PVB Films," *Polymer Properties Database*, 2015. [Online]. Available: [http://polymerdatabase.com/Films/PVB Films.html](http://polymerdatabase.com/Films/PVB%20Films.html). [Accessed: 10-Nov-2020].
- [17] Y. Deng and J. M. Catchmark, "Insoluble starch composite foams produced through microwave expansion," *Carbohydr. Polym.*, vol. 111, pp. 864–869, 2014.
- [18] I. A.V. and V. P. Varlamov, "Chitosan-Based Polyelectrolyte Complexes: A Review.: EBSCOhost," *Appl. Biochem. Microbiol.*, vol. 41, pp. 5–11, 2005.
- [19] T. Sakiyama, C. -H Chu, T. Fujii, and T. Yano, "Preparation of a polyelectrolyte complex gel from chitosan and κ -carrageenan and its pH-sensitive swelling," *J. Appl. Polym. Sci.*, vol. 50, no. 11, pp. 2021–2025, Dec. 1993.
- [20] "Chitosan-based polyelectrolyte complexes as pharmaceutical excipients," in *Controlled Drug Delivery*, Elsevier, 2015, pp. 127–161.
- [21] P. Makvandi *et al.*, "Biofabricated Nanostructures and Their Composites in Regenerative Medicine," *ACS Appl. Nano Mater.*, vol. 3, no. 7, pp. 6210–6238, Jul. 2020.
- [22] G. E. Risser, B. L. Banik, J. L. Brown, and J. M. Catchmark, "Structural properties of starch-chitosan-gelatin foams and the impact of gelatin on MC3T3 mouse osteoblast cell viability," *J. Biol. Eng.*, vol. 11, no. 1, Nov. 2017.
- [23] K. M. Dang and R. Yoksan, "Morphological characteristics and barrier properties of thermoplastic starch/chitosan blown film," *Carbohydr. Polym.*, vol. 150, pp. 40–47, Oct. 2016.
- [24] T. Jiang, Q. Duan, J. Zhu, H. Liu, and L. Yu, "Starch-based biodegradable materials: Challenges and opportunities," *Adv. Ind. Eng. Polym. Res.*, vol. 3, no. 1, pp. 8–18, Jan. 2020.
- [25] M. M. Hassan, N. Tucker, and M. J. Le Guen, "Thermal, mechanical and viscoelastic properties of citric acid-crosslinked starch/cellulose composite foams," *Carbohydr. Polym.*, vol. 230, no. November 2019, p. 115675, Feb. 2020.
- [26] I. Gonenc and F. Us, "Effect of Glutaraldehyde Crosslinking on Degree of Substitution, Thermal, Structural, and Physicochemical Properties of Corn Starch," *Starch/Staerke*, vol. 71, no. 3–4, Mar. 2019.

- [27] T. Ghosh Dastidar and A. N. Netravali, "'Green' crosslinking of native starches with malonic acid and their properties," *Carbohydr. Polym.*, vol. 90, no. 4, pp. 1620–1628, Nov. 2012.
- [28] M. Gui-Jie, W. Peng, M. Xiang-Sheng, Z. Xing, and Z. Tong, "Crosslinking of corn starch with sodium trimetaphosphate in solid state by microwave irradiation," *J. Appl. Polym. Sci.*, vol. 102, no. 6, pp. 5854–5860, Dec. 2006.
- [29] N. Da Silva, M. Sechi, and P. T. Marques, "Preparation and Physicochemical, Structural and Morphological Characterization of Phosphorylated Starch," *Mater. Res.*, vol. 20, pp. 174–180, 2017.
- [30] F. Gao, D. Li, C. H. Bi, Z. H. Mao, and B. Adhikari, "Preparation and characterization of starch crosslinked with sodium trimetaphosphate and hydrolyzed by enzymes," *Carbohydr. Polym.*, vol. 103, no. 1, pp. 310–318, Mar. 2014.
- [31] H. E. Grommers and D. A. Van Der Krogt, *Potato Starch* :, Third Edit. Elsevier Inc., 2009.
- [32] S.-T. Lim, T. Kasemsuwan, and J.-L. Jane, "Characterization of Phosphorus in Starch by ³¹P-Nuclear Magnetic Resonance Spectroscopy.," *Cereal Chemistry*, vol. 71, no. 5, pp. 488–493, 1994.
- [33] J. F. Zhang and X. Sun, "Biodegradable foams of poly(lactic acid)/starch. I. Extrusion condition and cellular size distribution," *J. Appl. Polym. Sci.*, vol. 106, no. 2, pp. 857–862, Oct. 2007.
- [34] H. A. Pushpadass, G. S. Babu, R. W. Weber, and M. A. Hanna, "Extrusion of starch-based loose-fill packaging foams#: Effects of temperature, moisture and talc on physical properties," *Packag. Technol. Sci.*, vol. 21, no. 3, pp. 171–183, Apr. 2008.
- [35] L. P. B. M. Janssen, *Reactive extrusion systems*. Marcel Dekker, 2004.
- [36] P. D. Tatarka and R. L. Cunnincham, "Properties of protective loose-fill foams," *J. Appl. Polym. Sci.*, vol. 67, no. 7, pp. 1157–1176, 1998.
- [37] A. Hoshino *et al.*, "Study of the Aerobic Biodegradability of Plastic Materials under Controlled Compost," in *Biodegradable Polymers and Plastics*, Springer US, 2003, pp. 47–54.
- [38] A. Hoshino, H. Sawada, M. Yokota, M. Tsuji, K. Fukuda, and M. Kimura, "Influence of weather conditions and soil properties on degradation of biodegradable plastics in soil," *Soil Sci. Plant Nutr.*, vol. 47, no. 1, pp. 35–43, 2001.
- [39] H. A. Pushpadass, G. S. Babu, R. W. Weber, and M. A. Hanna, "Extrusion of starch-based loose-fill packaging foams#: Effects of temperature, moisture and talc on physical properties," *Packag. Technol. Sci.*, vol. 21, no. 3, pp. 171–183, Apr. 2008.

- [40] C. Sita, M. Burns, R. Häßler, and W. W. Focke, "Tensile properties of thermoplastic starch-PVB blends," *J. Appl. Polym. Sci.*, vol. 101, no. 3, pp. 1751–1755, Aug. 2006.
- [41] J. Han, S. Salmieri, C. Le Tien, and M. Lacroix, "Improvement of water barrier property of paperboard by coating application with biodegradable polymers," *J. Agric. Food Chem.*, vol. 58, no. 5, pp. 3125–3131, Mar. 2010.
- [42] W. Luan, C. Wang, Z. Zeng, W. Xue, X. He, and Y. Bai, "Kinetics of polyvinyl butyral hydrolysis in ethanol/water solutions," vol. 38, no. 9, pp. 1810–1817, Aug. 2021.
- [43] X. Zhang, Z. Teng, and R. Huang, "Biodegradable Starch/Chitosan Foam via Microwave Assisted Preparation: Morphology and Performance Properties," *Polym. 2020, Vol. 12, Page 2612*, vol. 12, no. 11, p. 2612, Nov. 2020.
- [44] S. Mohan Bhasney, A. Kumar, and V. Katiyar, "Microcrystalline cellulose, polylactic acid and polypropylene biocomposites and its morphological, mechanical, thermal and rheological properties," *Compos. Part B Eng.*, vol. 184, p. 107717, Mar. 2020.
- [45] M. Turhan, S. Sayar, and S. Gunasekaran, "Application of Peleg model to study water absorption in chickpea during soaking," *J. Food Eng.*, vol. 53, no. 2, pp. 153–159, 2002.
- [46] M. Combrzyński *et al.*, "Moisture sorption characteristics of extrusion-cooked starch protective loose-fill cushioning foams," *Int. agrophysics*, vol. 31, pp. 457–463, 2017.
- [47] A. G. Cunha, S. Fernandes, C. S. R. Freire, and A. J. D. Silvestre, "Why, After All, Are Chitosan Films Hydrophobic?," *Biomacromolecules*, vol. 9, pp. 610–614, 2008.
- [48] S. Santacruz, C. Rivadeneira, and M. Castro, "Edible films based on starch and chitosan. Effect of starch source and concentration, plasticizer, surfactant's hydrophobic tail and mechanical treatment," *Food Hydrocoll.*, vol. 49, pp. 89–94, Jul. 2015.
- [49] I. Fabi, "Talc filled PLA," vol. 9, pp. 24–26.
- [50] C. M. Machado, P. Benelli, and I. C. Tessaro, "Study of interactions between cassava starch and peanut skin on biodegradable foams," *Int. J. Biol. Macromol.*, vol. 147, pp. 1343–1353, Mar. 2020.
- [51] N. Shuzhen *et al.*, "Enhancing hydrophobicity, strength and UV shielding capacity of starch film via novel co-cross-linking in neutral conditions," *R. Soc. Open Sci.*, vol. 5, no. 11, p. 181206, Nov. 2018.
- [52] N. Shah, R. K. Mewada, and T. Mehta, "Crosslinking of starch and its effect on viscosity behaviour," *Rev. Chem. Eng.*, vol. 32, no. 2, pp. 265–270, Apr. 2016.
- [53] Z. Żołek-Tryznowska and A. Kałuża, "The influence of starch origin on the properties of starch films: Packaging performance," *Materials (Basel)*, vol. 14, no. 5, pp. 1–11, Mar. 2021.

- [54] R. B. McClurg, "Design criteria for ideal foam nucleating agents," *Chem. Eng. Sci.*, vol. 59, no. 24, pp. 5779–5786, Dec. 2004.
- [55] S. N. Leung, A. Wong, C. B. Park, and J. H. Zong, "Ideal surface geometries of nucleating agents to enhance cell nucleation in polymeric foaming processes," *J. Appl. Polym. Sci.*, vol. 108, no. 6, pp. 3997–4003, Jun. 2008.
- [56] B. Xia and W. Dong, "Study on Cellular Structure and Mechanical Property of Foaming/Cross-linking Polyethylene System."
- [57] I. Chodák, "Properties of crosslinked polyolefin-based materials," *Prog. Polym. Sci.*, vol. 20, no. 6, pp. 1165–1199, Jan. 1995.
- [58] R. González-Núñez *et al.*, "Using chitosan as a nucleation agent in thermoplastic foams for heavy metal adsorption," *Macromol. Symp.*, vol. 283–284, no. 1, pp. 152–158, Sep. 2009.
- [59] D. Merino and V. A. Alvarez, "In-soil Biodegradation Behavior of Chitosan-Coated Phosphorylated Starch Films," *Res. Artic.*, vol. 2019, no. 12, pp. 907–912.

3. BIOBASED MALEATED THERMOPLASTIC STARCH (MTPS) AND MTPS-G-PETG (GLYCOL MODIFIED PET) GRAFT COPOLYMER VIA REACTIVE EXTRUSION: EVALUATIONS

3.1 ABSTRACT

This study reports on using reactive extrusion (REX) modified thermoplastic starch for making in situ MTPS-PETG (glycol modified Polyethylene terephthalate) graft copolymers. Reactive blends of maleated thermoplastic starch (MTPS) and PETG in 30:70 ratio (wt/wt) were prepared using a ZSK-30 twin-screw extruder. 80% glycerol was grafted on the starch during the preparation of MTPS as determined by soxhlet extraction with acetone. 30% of added PETG was grafted on MTPS backbone was obtained by soxhlet extraction with dichloromethane (DCM). The results were confirmed by TGA and FT-IR analysis of residue and extracts. The tensile and impact properties of graft copolymer were analyzed and compared with the properties of PETG. Scanning electron microscopy (SEM) images showed a uniform, microdispersion of MTPS in PETG matrix. Aqueous biodegradation for these blends did not show any improvement in the biodegradability of PETG.

3.2 INTRODUCTION

Replacing petro-fossil carbon with bio-based carbon in polymers offers a reduced material carbon footprint and managed end of life [1–3]. This has given rise to the area of biopolymers i.e. synthesis of polymers from renewable resources.

Starch is an abundant, inexpensive, 100% bio-based, and completely biodegradable polymer. As explained in chapter 1, the ratio of amylose and amylopectin is different in different starches [4]. The properties of the products like films and foams depend on the type of starch being used. When amylose content is more, the film is stronger and more flexible whereas when amylopectin content is more it leads to poor mechanical properties like brittleness. Another application of starch-based bioplastics is in the form of thermoplastic starch. The melting temperature of pure starch is above its decomposition temperature. Therefore, it does not flow on thermal processing [5]. To make starch processable, plasticizers such as water, glycerol, sorbitol are used[6] . This thermoplastic starch can then be blended with other biodegradable or non-biodegradable polymers for use in several applications such as food packaging, films, disposable utensils, pharmaceutical etc. The cost reduction due to use of starch and increased biobased content are additional benefits. However, such thermoplastic starches (TPS) have poor dimensional stability and reduced mechanical properties with time. More problematic is the leaching of the plasticizer (glycerol for example) over time contributing to brittleness and making the film surface tacky and unusable[7]. In our group, we have synthesized a maleated thermoplastic starch (MTPS) using reactive extrusion (REX) in which the glycerol plasticizer is covalently bonded to the starch, thereby eliminating glycerol migration and maintaining good processability[8–11].

The structure of the glycerylated starch polymer is shown below in Figure 3.3 and described in our earlier papers.

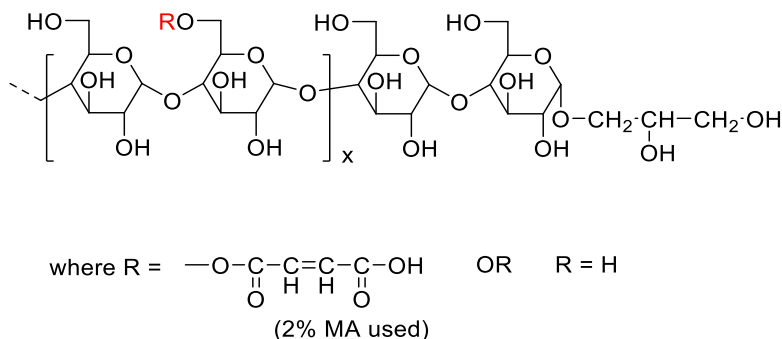


Figure 3.1: Structure of maleated thermoplastic starch

It has been shown that MTPS has a high reactivity towards polyesters[11]. It can undergo transesterification reaction with other polyesters to yield graft copolymers (US patent 7629405). Hence, it can be blended with hydrophobic polymers to reduce its hydrophilic nature and improve mechanical properties. [9]

Glycol modified PET (PETG) is a modification of Polyethylene Terephthalate (PET). PETG is synthesized by replacing a portion of glycol component of PET with a cyclic diol called cyclohexanedimethanol (CHDM). It is a highly hydrophobic polymer with excellent tensile strength and elongation properties. PETG is used in wide range of industrial applications and is one of the important polymers in packaging. The main disadvantage of PETG is in terms of its end of life- it is not biodegradable in aqueous or composting environment. Increasing pollution of aquatic and terrestrial environments by plastics has fueled the research on biobased and biodegradable plastics. Various studies claim that addition of biodegradable polymers or additives like starch, polylactide (PLA), polycaprolactone (PCL) increase the biodegradation of non-biodegradable polymers like polyethylene (PE), PET etc.[12–15]. This hypothesis was tested in this study. Neat PETG itself is not biodegradable. Our hypothesis

was - by incorporating 30% of thermoplastic starch in the blend, the biodegradability of this compatibilized blend will be much higher. The SEM and Soxhlet extraction studies confirmed the presence of a well dispersed MTPS phase in PETG matrix and in-situ formation of a graft copolymer. Aqueous biodegradation studies of these pellets showed that only the MTPS portion of the blend degraded rapidly in water leaving the PETG portion as it is. Addition of starch did not affect the biodegradability of PETG. Mechanical and thermal properties of the blends were also analyzed and compared with neat PETG. This study provides a good example of false and misleading claims made for accelerated biodegradation of non-biodegradable polymers and refutes the many claims of biodegradability of non-biodegradable polymers by the addition of starch and similar additives in the marketplace.

3.3 EXPERIMENTAL

3.3.1 *Materials*

High amylose corn starch was obtained from National Starch (NJ, USA) with equilibrium moisture content of about 12% (w/w). Glycerol was obtained from J.T. Baker (NJ, USA) and was used as received. Maleic anhydride (MA) and 2,5-bis(tert-butyl-2,5-dimethylhexane, tech. 90% (Luperox 101) were obtained from and Sigma-Aldrich (WI, USA). Glycol modified PET (PETG) was purchased from the Eastman Chemical Company (TN, USA) and was used as it is. Figure 3.2 shows the structure of PETG.

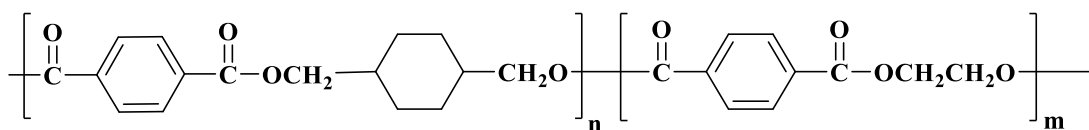


Figure 3.2: Structure of PETG

3.3.2 *Preparation of maleated thermoplastic starch (MTPS)*

MTPS was prepared in a twin screw co-rotating CENTURY ZSK-30 extruder. The screw diameter was 30 mm and transport length was 1260 mm with L/D ratio of 42. Moisture is not preferred in the reactive extrusion experiment because it can interfere with the reactivity of glycerol and can cause foaming of the extrudate. So, the corn starch was dried for 48 hours in oven at temperature of 65°C to reduce its moisture content to 0.1%.

MA (20g) was ground to fine powder using a mortar and pestle and was premixed with dry starch (800g). Luperox (1.1 g) was mixed with glycerol (200g) and the mixture was then pumped into the extruder directly via peristaltic pump. The feeder was calibrated to get the ratio of 80:20 (starch: glycerol). [8]

The temperature profile was set as 70/90/110/120/130/140/150/150/150/140 from the feed port to the die. The screw speed was set at 100 rpm and melt temperature was 150°C.

The vent port was kept open to remove the moisture formed during the reaction. The extrudate coming out of the extruder was air cooled and pelletized simultaneously using Scheer Bay pelletizer as shown in Figure 3.3. The resulting MTPS pellets were dried overnight in oven at 65°C and then stored in vacuum sealed bags before using for any further characterization.

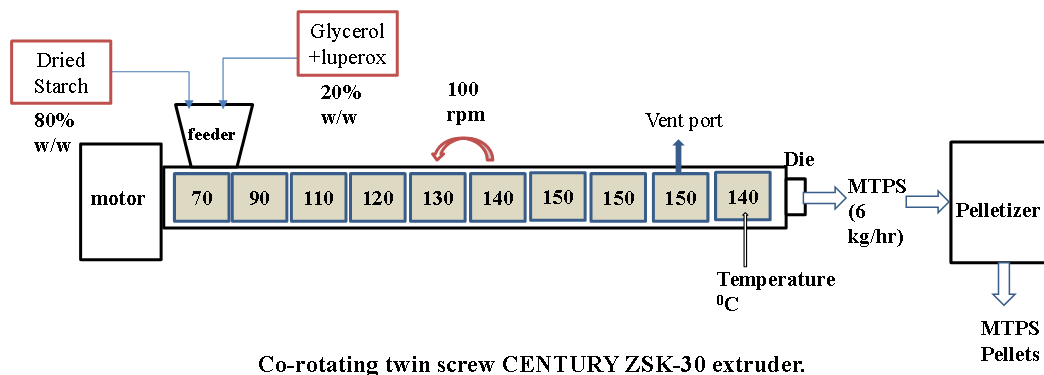


Figure 3.3: Preparation of maleated thermoplastic starch

3.3.3 Preparation of MTPS-PETG graft copolymers

MTPS-PETG graft copolymers were prepared via transesterification reaction mechanism. MTPS with more than 80% grafting was dried for at least 24 hours to remove excess moisture. Similarly, PETG was also dried to remove moisture. The dried MTPS and PETG were mixed in 30:70 w/w ratio and fed through the single screw feeder. The feed rate was maintained at 100 g/min or 6 kg/h for the mixture by calibrating it. The temperature profile was set at 90/110/120/130/140/150/160/160/160/150. The screw speed was set at 100 rpm and melt temperature was about 140°C. The resulting MTPS-PETG was pelletized in line after cooling in water bath. The pellets were dried overnight in an oven at 65°C before storing.

3.4 CHARACTERIZATION AND ANALYSIS

Initial thermal characterization of the raw materials- corn starch, PETG and glycerol was done to determine the degradation and melting temperatures of the raw materials. After preparing the blend in the extruder, the extent of reaction or grafting was measured using soxhlet extraction and was further confirmed using thermogravimetric analysis. FT-IR spectroscopy was used to provide further validation of transesterification reaction. The mechanical properties of the MTPS-PETG graft copolymer were determined and compared with neat PETG properties. Scanning Electron Microscopy (SEM) was used to study the dispersion of MTPS in PETG phase. Aqueous biodegradation of the reactive blend was also studied using ISO 14852.

3.4.1 Soxhlet extractions using acetone and dichloromethane

Selective solubility of glycerol in acetone was used to establish and determine percent covalent grafting of glycerol[8], [10]. The MTPS pellets prepared were ground to a fine powder and about 5 g of sample was put in a pre-dried and pre-weighed cellulose extraction thimble. The thimbles were then inserted in the soxhlet extractor connected to a 500 mL round bottom flask containing around 200–250 mL acetone. The flasks were heated, and the solvent was allowed to reflux. The extraction was continued for 72 h. After the extraction, the thimbles were removed; residue and extract were separated and dried overnight at 70°C. The dried thimble with residue was weighed again and the weight change in the residue was calculated. The reproducibility of the results was confirmed by testing three replicates for each sample. It was expected that the covalently grafted glycerol will not get extracted in acetone and there will be a weight gain in the residue. Percent grafting was calculated from the mass balance as shown in the following equation-

Equation 3.1

$$\% \textit{grafting} = \frac{|W_1 - W_2|}{W_1} \times 100$$

where, W_1 is the weight of glycerol present in the sample originally and W_2 is the glycerol in the extract after 72 h. i.e., free glycerol. Similar Soxhlet analysis was used to determine % grafting of PETG on MTPS backbone. In this the solvent used was Dichloromethane (DCM) which selectively dissolves PETG. The residues and extracts of all the samples were analyzed using TGA in order to confirm the results from Soxhlet analysis.

3.4.2 Thermal analysis

The degradation temperature of samples was obtained by thermogravimetric analysis (TGA). TGA measurements of all the samples were conducted under an inert atmosphere of nitrogen using a TGA Q50 (TA Instruments, New Castle, DE, USA). The general sample weight used was 5–7 mg. The sample was placed in an aluminum pan and was heated to 600 °C at the rate of 10 °C/min. The weight loss (%) of a sample as a function of temperature (°C) was obtained from this analysis. Also, the glass transition temperature of PETG and the blend were obtained by using a differential scanning calorimeter (DSC). The sample was heated to 200 °C in DSC Q20 (TA Instruments, New Castle, DE, USA) with a heating rate of 10 °C/min and held for 5 min to erase thermal history. The sample was then cooled back to 20 °C and heated again to 200 °C with a heating rate of 10 °C/min. The glass transition temperature (T_g) was calculated using TA universal analysis 2000 software. Since PETG is amorphous polymer, further analysis of melting point and crystallinity was not performed.

3.4.3 Tensile testing

The injection molded test bars were prepared using a tabletop DSM 15 cc mini extruder (DSM Research B. V., Sittard-Geleen, The Netherlands) and 3.5 cc mini-injection molder

(DACA Instruments, Santa Barbara, CA, USA). The injection pressure was set as 140 psi and the cylinder and mold temperatures were 210 and 65 °C, respectively. The samples were stored for 2 days at 25 °C in a humidity chamber with RH of 50% before any analysis. Tensile testing was performed using an Instron model 5565-P6021 (Instron, Norwood, MA, USA) with a 5 kN load cell and grip separation speed of 12.5 mm/min as per ASTM D882. Data from five samples of each formulation were averaged and compared with the properties of neat PETG.

3.4.4 Impact Testing

Injection molded test bars required for notched Izod impact testing were also prepared by a DSM 15 cc mini extruder (DSM Research B. V., Sittard-Geleen, The Netherlands) & 3.5 cc mini injection molder (DACA Instruments, Santa Barbara, CA, USA). The injection pressure was set as 140 psi and the cylinder and mold temperatures were 210 and 65°C respectively. The samples were tested with Ray-Ran RR-IMT (Warwickshire, UK) pendulum impact tester as per ASTM D256-10(2018). The samples with a dimension 64 mm* 12.7 mm* 4 mm were notched using a Tinius Olsen Model 22-05-03 Motorized Specimen Notcher (Pennsylvania, USA). The notch marked was 2.54 mm deep and six replicates were used per sample.

3.4.5 Fourier Transform Infrared Spectroscopy (FT-IR)

FT-IR spectra of pure PETG, MTPS and of MTPS-PETG residue after Soxhlet extraction were recorded on Shimadzu IRAffinity-1 spectrometer (Columbia, USA) equipped with MIRacle ATR attachment. The spectra were recorded between the wavelength on 500-4000 cm⁻¹ in absorption mode.

3.4.6 Scanning Electron microscopy

A JOEL 6610 LV scanning electron microscope (JEOL Ltd., Tokyo, Japan) was used to study the dispersion of MTPS in PETG in the pellets. They were treated with 6 N HCl for 12 h to remove the MTPS phase from the samples and air-dried for 12 h in a fume hood. Then they were mounted on aluminum stubs using high vacuum carbon tabs, and coated with gold using a sputter coater and examined using JOEL at 3000× magnification at 10 kV. A set of fractured tensile bars was also examined to look at the fracture morphology of the samples. The bars were immersed in liquid nitrogen for ~2 min and then fractured. Fracture surfaces were mounted on aluminum stubs and examined using JOEL at 3000× magnification at 10 kV.

3.4.7 Aqueous biodegradation

The biodegradability of MTPS-PETG samples was tested in an aqueous environment. All the tests were performed in an aerobic environment at 30 °C. A respirometry mineralization test system for calculating CO₂ evolution was set up based on International Standard ISO 14852. The system comprised blank, positive reference (cellulose) and the test material (MTPS-PETG) for all the runs. All the samples, blanks, and references were run in duplicates. An optimized test medium containing all the nutrients and buffers was prepared according to the ISO standard as explained in section 2.4

3.5 RESULTS AND DISCUSSIONS

3.5.1 *MTPS analysis: Soxhlet extraction*

Soxhlet analysis provided percent covalent grafting of glycerol to the starch backbone. Acetone was used as the extraction solvent. In this, the covalently bonded glycerol is not extracted, and only free, ungrafted glycerol is extracted by acetone. The results are shown in Table 4. The removal of free glycerol by acetone was further confirmed from the results of TGA analysis as shown in Figure 3.4. A decrease in the peak corresponding to glycerol was observed in the residue after Soxhlet extraction whereas the TGA of the extract showed a peak only for glycerol with no MTPS indicating that acetone extracts only free glycerol and no MTPS. Results indicated that 79% of added glycerol was chemically grafted on the starch backbone. Similar results have been observed in the previous studies from our group[10], [11]

Table 3.1: Results for percent grafting of glycerol on MTPS

Sample	1	2	3
Weight (g)	5.009	5.015	5.003
Starch (g)	4.007	4.012	4.002
Glycerol (g)	1.002	1.003	1.001
Extract (g)	0.214	0.221	0.201
Residue (g)	4.794	4.793	4.801
%Grafting	78.58	77.87	79.90
Average Grafting (%)	78.7 ± 0.7		

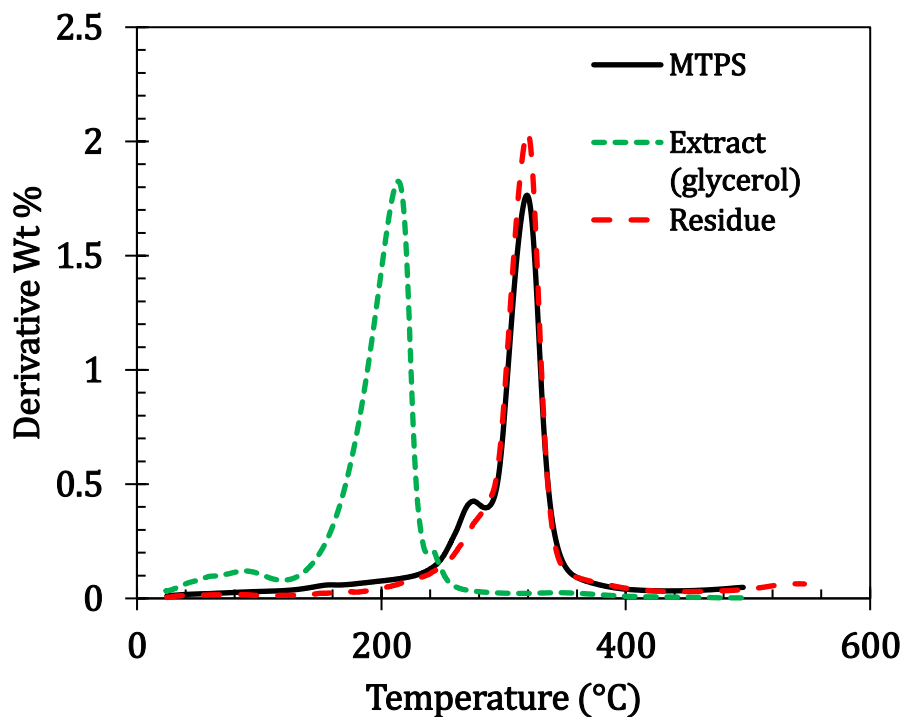


Figure 3.4: DTG curves of MTPS, glycerol and residue showing only MTPS after Soxhlet extraction

3.5.2 PETG-MTPS analysis: Soxhlet extraction

PETG/MTPS (70/30) resins prepared by reactive extrusion were analyzed using Soxhlet extraction and TGA. Figure 3.5 shows the comparative TGA graphs for MTPS, PETG and MTPS-g-PETG reactive blend. It was found that the degradation temperature for the reactive blend was in between that of pure MTPS and PETG. It showed 2 degradation stages. The first one corresponding with MTPS and the second with PETG.

These PETG pellets were analyzed for % grafting using Soxhlet extraction as explained in section 3.4. PETG is soluble in DCM and MTPS is not. Hence, DCM was used for Soxhlet extraction to find the % grafting of PETG on MTPS. To confirm that the grafting reaction has occurred, the residues and extracts of the resin after Soxhlet extraction were compared with a control. The control here was a physical mixture of PETG and MTPS. PETG and MTPS pellets

were mixed in the same ration of 70:30. The mixture was then extracted with DCM for 72 hours. It was found that, entire PETG gets extracted with DCM in 72 hours and none of the MTPS gets dissolved in DCM. Thus, the residue consists of pure MTPS and the extract is pure PETG. These results were confirmed by TGAs of residue and extract. When PETG-g-MTPS extruded resins were extracted with DCM, it was found that some PETG remains in the residue even after 72 hours. Since DCM dissolves only PETG, it was expected that after extraction the extract TGA should show a peak only for PETG and the residue should only show MTPS if no grafting reaction had occurred. However, it was observed that, the residue showed a distinct peak for PETG accounting for 25% of total weight as shown in Figure 3.6. Considering that 70% of PETG was introduced while making the blend, it was concluded from the mass balance that around 33% of added PETG was grafted on the MTPS backbone.

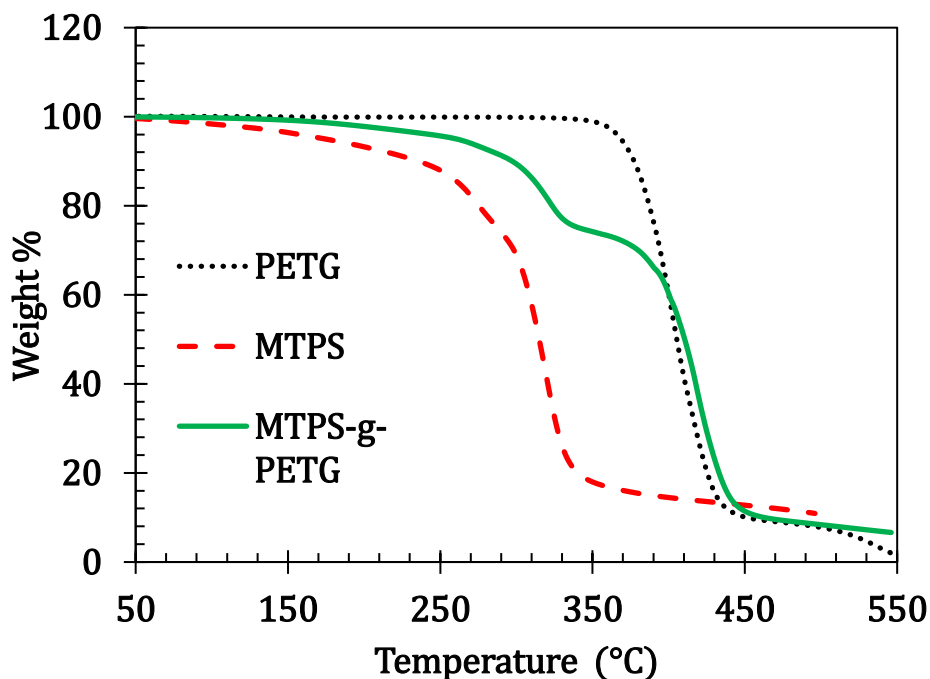


Figure 3.5: TGA graphs for MTPS, PETG and MTPS-g-PETG

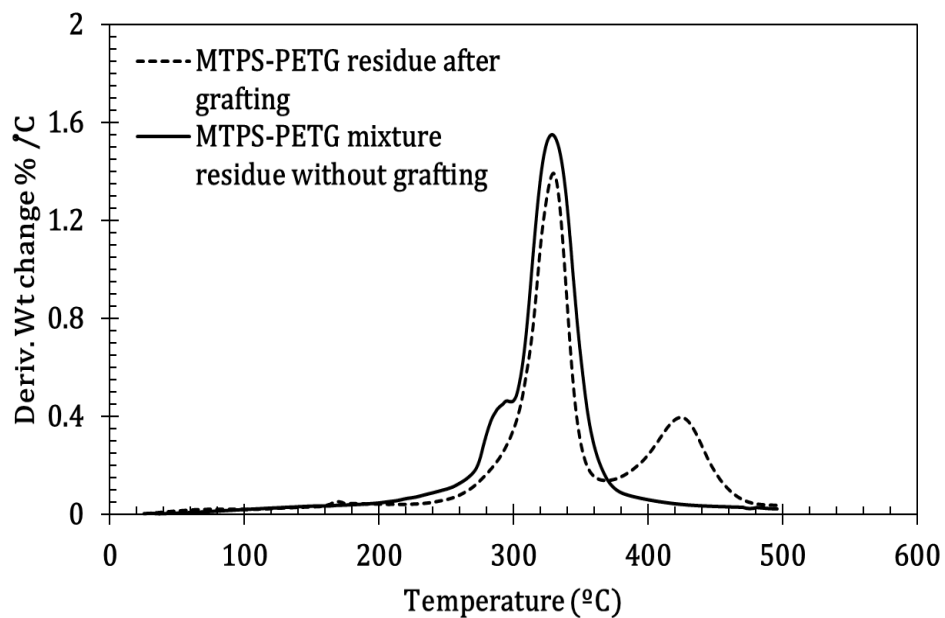


Figure 3.6: DTG curve of residue remaining after Soxhlet extraction

3.5.3 PETG-MTPS analysis: FTIR

To confirm the grafting of PETG on MTPS, FT-IR spectra of PETG, MTPS and residue of MTPS-PETG copolymer were recorded as shown in Figure 3.7 . The MTPS spectra clearly showed presence of broad OH peak between 3100-3600 cm^{-1} . PETG spectrum shows presence of C=O and C-C-O bonds at 1740 cm^{-1} and 1240 cm^{-1} . The MTPS-g-PETG residue showed presence of both MTPS and PETG characteristic peaks. The presence of PETG in the residue was confirmed from the characteristic peaks of the ester linkage at 1741 and 1240 cm^{-1} .

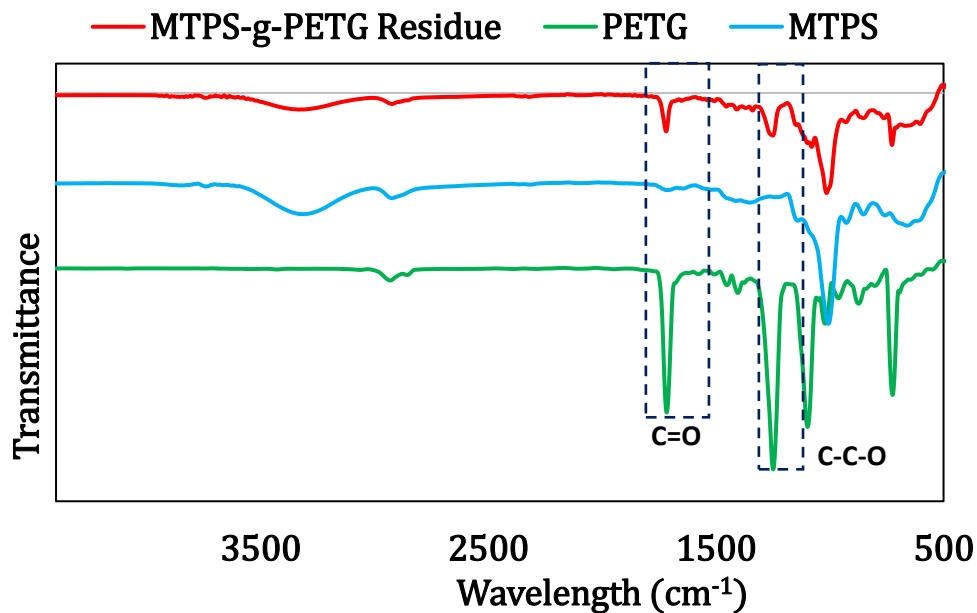


Figure 3.7: Comparative FT-IR spectra of PETG, MTPS and MTPS-PETG residue

3.5.4 PETG-MTPS analysis: Mechanical properties

Tensile properties of PETG and MTPS-g-PETG (30:70) graft copolymer were analyzed on a universal testing machine (UTS). This data was compared to the tensile properties of PETG. The results are as shown in Figure 3.8. It was observed that inclusion of 30% MTPS in PETG caused only a 15% reduction in the tensile stress of the sample whereas the elongation properties decreased by almost 40%. However, the resulting elongation is still significant looking at the brittle nature of MTPS. The resulting blend still has acceptable mechanical properties for many applications. The results of the data are summarized in Table 3.2.

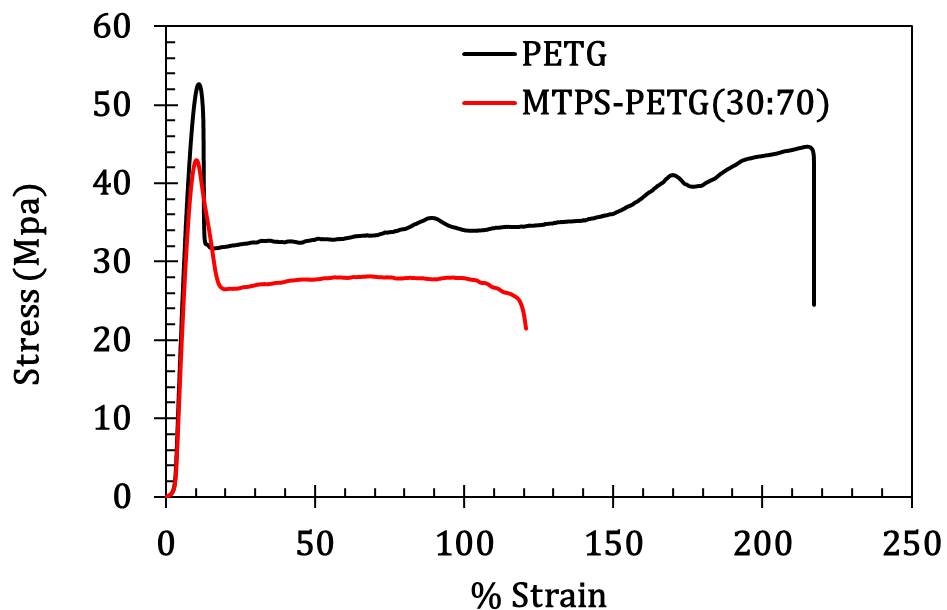


Figure 3.8: The average stress-strain curves of PETG and MTPS-g-PETG

Table 3.2: Tensile properties of PETG and MTPS-g-PETG blend

	Modulus (MPa)	Tensile stress at yield (MPa)	Tensile strain at yield (mm/mm)	Tensile stress at break (MPa)	Elongation at break (%)
PETG	632.7±45.7 ^a	53.8±0.8 ^a	2.2±0.1 ^a	41.9 ±0.8 ^a	215 ± 10.6 ^a
MTPS-g-PETG	483.68 ± 29.3 ^b	44.5 ± 1.2 ^b	1.5 ± 0.1 ^b	22.9± 1.5 ^b	120.7 ± 15.5 ^b

Impact properties of MTPS-g-PETG (30:70) graft copolymer were also analyzed and compared with neat PETG as shown in Figure 3.9. Around 40% reduction in notched Izod impact strength was observed for the MTPS-g-PETG reactive blend. Impact strength testing for neat MTPS could not be performed because of its extremely brittle nature.

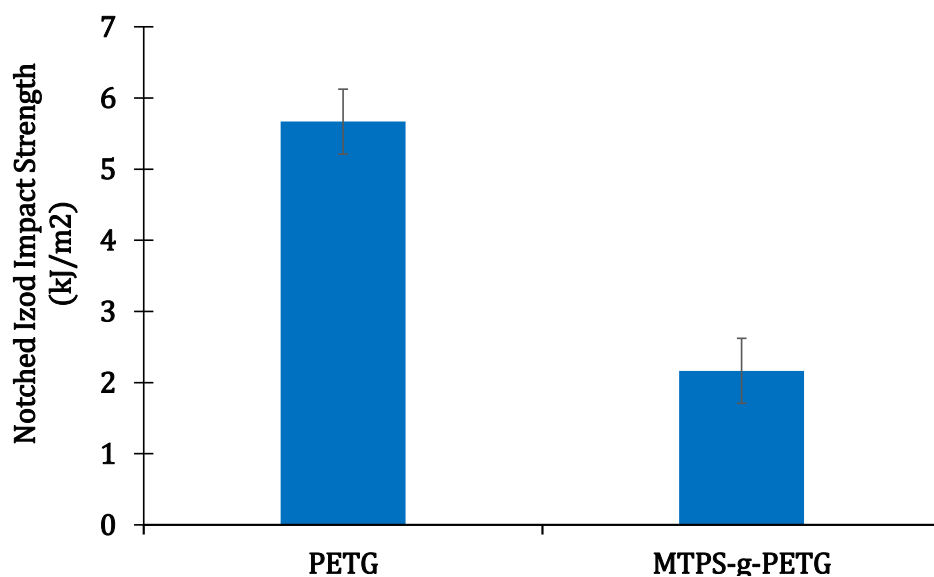


Figure 3.9: Notched Izod impact strength of PETG and MTPS-g-PETG reactive blend

3.5.5 MTPS-PETG analysis: Morphology

Figure 3.10-a shows the morphology of the MTPS-g-PETG blends produced by extrusion after selective removal of the MTPS phase. Cavities represent the spaces occupied by MTPS particles before their selective removal by dissolution in concentrated HCL. The proportion of cavities was close to 30% which correlated with the percentage of MTPS added in the blend. Figure 3.10-a shows micron size distribution of MTPS particles evenly distributed in PETG matrix. It was observed that the particle size for MTPS was between 1-5 μm , which indicated good compatibilization between MTPS and PETG. The reduction in the mechanical properties of the blend as observed in section 3.4.3 might be due to the high amount of MTPS added and the inherent brittle nature of MTPS.

The morphological behavior of neat PETG and the blend was analyzed using SEM images of tensile fracture surfaces. The representative images are as shown in Figure 3.10: b and c. The SEM images of tensile fractured surfaces of PETG showed stretch marks indicating a ductile

fracture whereas for the reactive blend, rougher surface was observed indicating comparatively brittle fracture.

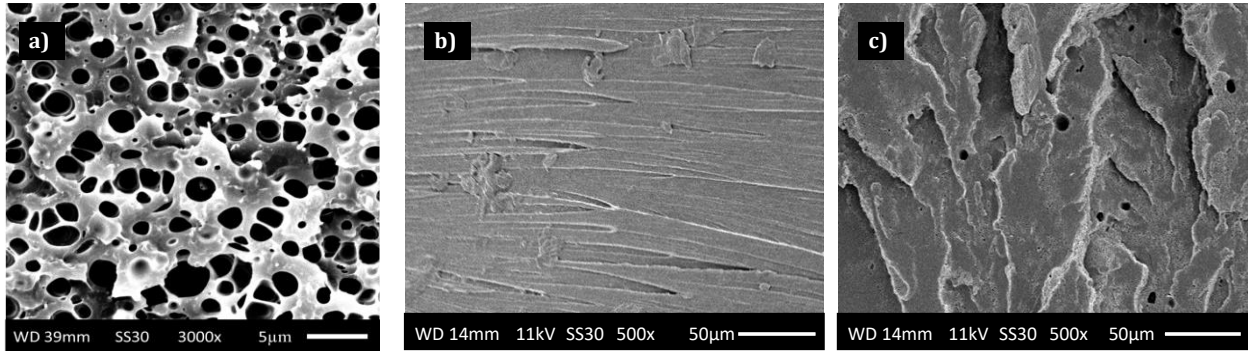


Figure 3.10: SEM images of a) MTPS-PETG blend after leaching of MTPS phase with HCL; b) Tensile fracture surface of PETG c) Tensile fracture surface of MTPS-g-PETG

3.5.6 MTPS-PETG analysis: Biodegradability testing

Figure 3.11 shows the test setup for aqueous biodegradation according to ISO 14852. The system was kept in a dark, temperature-controlled room maintained at 30 °C. The test flasks were agitated throughout the run with the help of magnetic stirrers. Air inlet was passed through NaOH solution to get CO₂-free air. This air was then divided and passed through flowmeters for each bioreactor at a constant flow rate. The CO₂ evolved from the flasks was collected in NaOH solution and titrated with HCl to determine the CO₂ that evolved from the samples and % biodegradation as described in Section 3.4.7.

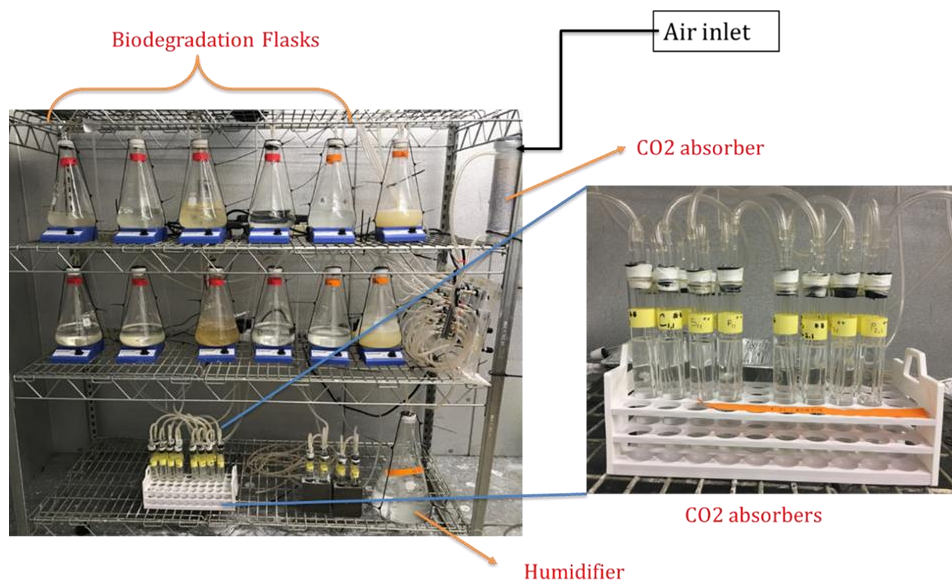
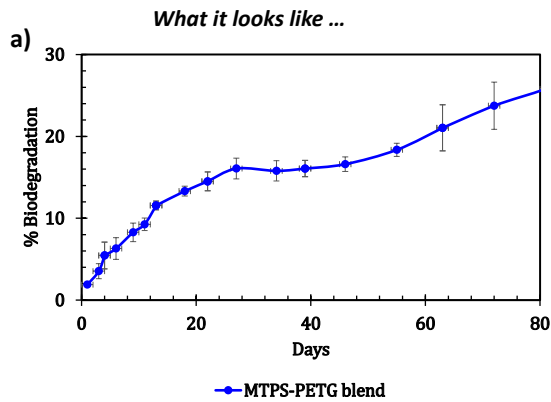


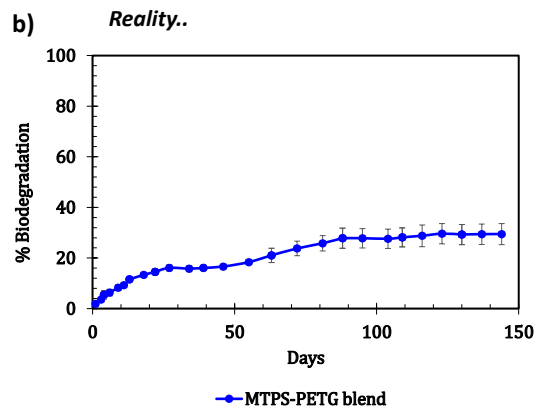
Figure 3.11: Experimental aqueous biodegradation setup

The initial curve obtained for aqueous biodegradation till day 80 is as shown in Figure 3.12-a. It was observed that during the first 80 days, the slope for this curve was linear and increasing. It was continued till the biodegradation reached about 30%. However, once it reached a biodegradation of 30% the biodegradation curve reached a plateau, and no further biodegradation was observed in Figure 3.12-b. This might be due to the fact that this blend contained only 30% of MTPS, which is the component that is readily biodegradable. PETG is not biodegradable in aqueous or composting environments as observed in our another study (data not shown here). Hence, once the MTPS present in the blend was consumed by the microbes, no further biodegradation was observed. From the SEM images it was confirmed that the dispersion of MTPS in PETG was uniform. So PETG was as accessible to the micro-organisms as MTPS.



Increasing biodegradation with linear slope till day 80

We should be able to extrapolate this to 100%??



After reaching 30% biodegradation, the curve becomes flat

*Only the 30% MTPS part biodegraded
No further biodegradation observed after that.*

Figure 3.12: Biodegradation curve for MTPS-PETG for a)Initial 80 days b)Total 150 days

Even then, only MTPS was selectively consumed leaving non-biodegradable PETG. This showed that blending of a biodegradable polymer like starch with a non-biodegradable polymer like PETG does not improve the biodegradability of the PETG. Many studies claim that addition of biodegradable polymers to non-biodegradable polymers like LDPE accelerate the biodegradation of LDPE[15], [18]. However, that is not the case. The increased biodegradation that is observed in these blends is only due to the consumption of the biodegradable polymer. The non-biodegradable part of the blend is still expected to last in the environment for a long time and form microplastics. Thus, we should be aware of the invalid the claims made for accelerated biodegradability of such plastics.

3.6 CONCLUSIONS AND FUTURE STUDY

Maleated thermoplastic starch (MTPS) was successfully prepared by reacting glycerol with corn starch using maleic anhydride as a promoter. It was found that 79% of added glycerol was grafted on the starch during reactive extrusion. Further, this MTPS was melt blended with PETG to undergo transesterification to form in situ MTPS-g-PETG graft copolymers. It was observed that, although addition of starch reduces the strength and percent extension of the copolymer, it is still significant and hence, this polymer can be used for many applications. Currently, the grafting of PETG on MTPS is about 30% which is quite less. Hence, efforts should be done to improve the percent grafting and the effect of that on the properties of the reactive blend should also be studied. SEM analysis of the pellets showed that MTPS was evenly distributed in the PETG matrix. Aqueous biodegradation studies showed that addition of starch did not enhance the biodegradability of PETG. The increase in the biodegradation of the blend was solely due to the biodegradation of MTPS. After consumption of 30% MTPS, the biodegradation did not increase further. This finding refutes many claims of biodegradability of non-biodegradable polymers by the addition of starch and similar additives in the marketplace.

REFERENCES

REFERENCES

- [1] R. Narayan, *Degradable Polymers and Materials: Principles and Practice (2nd Edition)*, vol. 1114. Washington, DC: American Chemical Society, 2012. doi: 10.1021/bk-2012-1114.
- [2] R. Narayan, "Biobased & biodegradable plastics: Rationale, drivers, and technology exemplars," *ACS Symposium Series*, vol. 1114, pp. 13–31, Nov. 2012, doi: 10.1021/bk-2012-1114.ch002.
- [3] K. L. Law and R. Narayan, "Reducing environmental plastic pollution by designing polymer materials for managed end-of-life," *Nature Reviews Materials*, 2021, doi: 10.1038/S41578-021-00382-0.
- [4] J. Muller, C. González-Martínez, and A. Chiralt, "Combination Of Poly(lactic) acid and starch for biodegradable food packaging," *Materials*, vol. 10, no. 8, pp. 1–22, Aug. 2017, doi: 10.3390/ma10080952.
- [5] Dr. R. Humphreys, "Thermoplastic Starch: A Renewable, Biodegradable Bioplastic," *Polymer innovation blog*, 2013. <https://polymerinnovationblog.com/thermoplastic-starch-a-renewable-biodegradable-bioplastic/> (accessed Mar. 02, 2020).
- [6] H. Li and M. A. Huneault, "Comparison of sorbitol and glycerol as plasticizers for thermoplastic starch in TPS/PLA blends," *Journal of Applied Polymer Science*, vol. 119, no. 4, pp. 2439–2448, Feb. 2011, doi: 10.1002/APP.32956.
- [7] A. M. Nafchi, M. Moradpour, M. Saeidi, and A. K. Alias, "Thermoplastic starches: Properties, challenges, and prospects," *Starch/Staerke*, vol. 65, no. 1–2, pp. 61–72, Jan. 2013, doi: 10.1002/star.201200201.
- [8] E. Hablot *et al.*, "Reactive extrusion of glycerylated starch and starch-polyester graft copolymers," *European Polymer Journal*, vol. 49, no. 4, pp. 873–881, Apr. 2013, doi: 10.1016/j.eurpolymj.2012.12.005.
- [9] P. Giri, C. Tambe, R. Narayan, M. Junction, and U. States, "Greener Products : From Laboratory Fundamentals to Commercial Scale," in *Biomass Extrusion and Reaction Technologies: Principles to Practices and Future Potential*, vol. 1304, Washington, DC: American Chemical Society, 2018, pp. 1–23. doi: 10.1021/bk-2018-1304.ch001.
- [10] J. M. Raquez, Y. Nabar, M. Srinivasan, B. Y. Shin, R. Narayan, and P. Dubois, "Maleated thermoplastic starch by reactive extrusion," *Carbohydrate Polymers*, vol. 74, no. 2, pp. 159–169, 2008, doi: 10.1016/j.carbpol.2008.01.027.
- [11] J. M. Raquez, Y. Nabar, R. Narayan, and P. Dubois, "In Situ Compatibilization of Maleated Thermoplastic Starch / Polyester Melt-Blends by Reactive Extrusion," *Polymer Engineering & Science*, vol. 48, no. 9, pp. 1747–1754, Sep. 2008, doi: 10.1002/pen.

- [12] M. R. Amin, B. F. Abu-Sharkh, and M. Al-Harthi, "Effect Of Starch Addition On The Properties Of Low Density Polyethylene For Developing Environmentally Degradable Plastic Bags," *Journal of Chemical Engineering*, vol. 26, pp. 38–40, Mar. 2012, doi: 10.3329/JCE.V26I1.10180.
- [13] I. N. Vikhareva, E. A. Buylova, G. U. Yarmuhametova, G. K. Aminova, and A. K. Mazitova, "An Overview of the Main Trends in the Creation of Biodegradable Polymer Materials," *Journal of Chemistry*, vol. 2021, 2021, doi: 10.1155/2021/5099705.
- [14] K. S. Veethahavya, B. S. Rajath, S. Noobia, and B. M. Kumar, "Biodegradation of Low Density Polyethylene in Aqueous Media," *Procedia Environmental Sciences*, vol. 35, pp. 709–713, 2016, doi: 10.1016/J.PROENV.2016.07.072.
- [15] V. Ocelić Bulatović *et al.*, "Biodegradation of LDPE_TPS blends under controlled composting conditions," *Polymer Bulletin 2022*, pp. 1–27, Apr. 2022, doi: 10.1007/S00289-021-03982-6.
- [16] A. Hoshino *et al.*, "Study of the Aerobic Biodegradability of Plastic Materials under Controlled Compost," in *Biodegradable Polymers and Plastics*, Springer US, 2003, pp. 47–54. doi: 10.1007/978-1-4419-9240-6_3.
- [17] A. Hoshino, H. Sawada, M. Yokota, M. Tsuji, K. Fukuda, and M. Kimura, "Influence of weather conditions and soil properties on degradation of biodegradable plastics in soil," *Soil Science and Plant Nutrition*, vol. 47, no. 1, pp. 35–43, 2001, doi: 10.1080/00380768.2001.10408366.
- [18] M. R. Amin, B. F. Abu-Sharkh, and M. Al-Harthi, "Effect Of Starch Addition On The Properties Of Low Density Polyethylene For Developing Environmentally Degradable Plastic Bags," *Journal of Chemical Engineering*, vol. 26, pp. 38–40, Mar. 2012, doi: 10.3329/JCE.V26I1.10180.

4. EFFECTS OF MODIFIED THERMOPLASTIC STARCH ON CRYSTALLIZATION

KINETICS AND BARRIER PROPERTIES OF PLA

4.1 ABSTRACT

This study reports on using reactive extrusion (REX) modified thermoplastic starch particles as a bio-based and biodegradable nucleating agent to increase the rate of crystallization, percent crystallinity and improve oxygen barrier properties while maintaining the biodegradability of PLA. Reactive blends of maleated thermoplastic starch (MTPS) and PLA were prepared using a ZSK-30 twin-screw extruder; 80% glycerol was grafted on the starch during the preparation of MTPS as determined by soxhlet extraction with acetone. The crystallinity of PLA was found to increase from 7.7% to 28.6% with 5% MTPS. The crystallization temperature of PLA reduced from 113 °C to 103 °C. Avrami analysis of the blends showed that the crystallization rate increased 98-fold and $t_{1/2}$ was reduced drastically from 20 min to <1 min with the addition of 5% MTPS compared to neat PLA. Observation from POM confirmed that the presence of MTPS in the PLA matrix significantly increased the rate of formation and density of spherulites. Oxygen and water vapor permeabilities of the solvent-casted PLA/MTPS films were reduced by 33 and 19% respectively over neat PLA without causing any detrimental impacts on the mechanical properties ($\alpha = 0.05$). The addition of MTPS to PLA did not impact the biodegradation of PLA in an aqueous environment.

Significance: Given the increasing demand for novel, nature compatible materials, this chapter presents a completely biobased and biodegradable nucleating agent with a green end of life option and potential for reduced cost.

4.2 INTRODUCTION

Replacing petro-fossil carbon with bio-based carbon in polymers offers a reduced material carbon footprint and managed end of life [1–3]. The most widely studied and commercial bioplastic is polylactide (PLA) polymer. It is manufactured commercially by NatureWorks LLC, MN, USA (<https://www.natureworksllc.com/>) (Accessed 2nd June 2021) (150 kton plant in Blair, Nebraska), and Total Corbion (<https://www.total-corbion.com/>) (Accessed 22nd September 2021) (a total capacity of 175 kton with plants in Thailand, and France). PLA is 100% bio-based and at its end-of-life recyclable [4] or industrially compostable. However, several property deficiencies in PLA have restricted its use in many packaging applications—primarily a low percentage of crystallinity and slow rate of crystallization. Nucleating agents like talc, nanocrystalline cellulose, hydrazine, PDLA, and other molecules have been used for increasing the crystallization rate and percent crystallinity of neat PLA [5–12].

PLA has mechanical and barrier properties comparable to polystyrene (PS) and thermal properties similar to polyethylene terephthalate (PET). The water vapor permeability of PLA films is low ($1-4 \times 10^{-14}$ kg.m²/s.m.Pa) [13–16] because of its hydrophobic nature. However, the oxygen permeability of PLA is very high as compared to PET, which limits its use in many packaging applications [17–19]. Table 4.1 shows a comparison of the literature values of mechanical, thermal, barrier, and tensile properties of some commonly used polymers in packaging including PLA, Polyethylene terephthalate (PET), Low density polyethylene (LDPE), polystyrene (PS), polypropylene (PP) and starch.

Table 4.1: Summary of physico-mechanical properties of packaging polymers

	PLA	PET	LDPE	PS	PP	Starch	Ref.
Tensile Strength (MPa)	50-80	50-70	10-20	40	44	<6	11, 12
Glass Transition Temperature (°C)	60	70	-130	170	100	-	11
Melting Temperature (°C)	160-170	260	110	160	222	120-150 (T _d)	16, 17
Oxygen permeability (cm ³ ×mm/m ² ×d×atm) *	7.9-52	1.18	98-453	98.5-171	35-377	0.35-2.19	17-19
Water permeability (cm ³ ×cm/cm ² ×s×mmHg (×10 ¹⁰)) *	139-617	130	68	123-600	35	533-3300	4, 13- 15, 19-20

* Values from the literature have been converted to the same units for ease of comparison.

REX offers several advantages over traditional batch and flow reactors (CSTR, PFR) like fast reaction time, enhanced heat and mass transfer, better mixing and does not require any solvents [18]. Starch based films have shown some desirable properties like high barrier to oxygen and CO₂ which is useful in packaging [27,28]. The oxygen permeability of starch films ranges between $0.4\text{--}2.5 \times 10^{-13} \text{ cm}^3/\text{m.s.Pa}$. Because of these advantages, different types of starch are often blended with PLA to reduce its cost and improve properties. However, pure starch and PLA blends are thermodynamically immiscible due to the hydrophobic nature of PLA and the hydrophilic nature of starch. Hence, the resulting system shows reduced strength and ductility compared to neat PLA. Several strategies have been tried to improve the compatibility by modifying either PLA or starch [29–31]. Studies have also shown the effect of starch and thermoplastic starch as a completely bio-based and biodegradable nucleating agent for PLA as opposed to inorganic talc [24]. Sun et al. studied the crystallization kinetics of PLA and starch composites and found that the addition of 1% of starch increased the crystallization rate considerably [25]. Jang et al. studied the thermal properties and morphology of PLA/starch blends using MA as compatibilizer and it was found that MA modified starch was much more compatible with PLA than pure starch [26]. Starch is hydrophilic and highly water sensitive. However, encapsulating the starch within the hydrophobic PLA matrix can mitigate this issue. This is in fact observed in several starch-based blends with various polyesters [35,36]. Multilayer films of starch and PLA have higher oxygen and moisture barrier compared to neat PLA [37–39]. There are no reports on the compatibilized blends of maleated thermoplastic starch and PLA and their effect on the properties like crystallinity, crystallization rate, barrier, thermal, mechanical, and biodegradability.

In this paper, we report on using inexpensive, REX modified thermoplastic starch particles in the PLA matrix to increase the rate of crystallization and percent crystallinity of PLA. The MTPS-filled PLA polymer films were found to improve oxygen and water vapor permeability without any effect on biodegradability. Crystallinity, crystallization kinetics, and barrier properties were studied and compared with neat PLA. Mechanical and thermal properties as well as morphology of the MTPS-filled thermoplastic PLA were also analyzed. This MTPS could be used as bio-based and biodegradable nucleating agent with a responsible end of life option and a replacement for talc of inorganic origin.

4.3 MATERIALS AND METHODS

4.3.1 Materials

High amylose corn starch with an initial moisture content of 12.8% (w/w) was obtained from National Starch (NJ, USA). Glycerol was obtained from J.T. Baker (NJ, USA) and was used as received. 2,5-bis(tert-butyl-2,5-dimethylhexane), 90% (Luperox 101), and Maleic anhydride (MA) were obtained from and Sigma–Aldrich (WI, USA). Ingeo™ biopolymer 3001D, a commercially available semi-crystalline grade of polylactide (PLA) was supplied from NatureWorks LLC (MN, USA). It had a molecular weight M_w of 128,000 Da and polydispersity of 1.52. It was prepared from the polymerization of L-lactide and had a meso content of 9%.

4.3.2 Preparation of and Polylactide (PLA)/MTPS Blends

MTPS was prepared in a co-rotating twin-screw CENTURY ZSK-30 extruder (MI, USA) as explained in chapter 3. Next step was using this MTPS in PLA as additive. Both polylactide and MTPS quickly absorb moisture from the atmosphere. Therefore, they were dried at 55 °C for 12 h before reactive extrusion. Then, MTPS and PLA pellets were mixed in various proportions of 1–10 wt. % in an aluminum tray before feeding. The detailed compositions are listed in the table below (Table 4.2)

Table 4.2: Sample name and composition

Sample	PLA wt. %	MTPS wt. %
PLA	100	-
PLA-1	99	1
PLA-2	98	2
PLA-5	95	5
PLA-10	90	10

The temperature profile used on the extruder going from the feed section to the die is as follows: 150/160/165/170/180/180/175/175/160/155 °C. These temperatures were selected based on the processing temperatures required for semicrystalline PLA. The screw speed and throughput were 100 rpm and 130 g/min. The extrudate was quenched in a water bath and was then pelletized. The resulting pellets were dried overnight in an oven at 50 °C and then stored in vacuum-sealed bags before using for any further characterization.

4.3.3 Soxhlet extraction

Selective solubility of PLA in dichloromethane (DCM) was used to establish and determine percent covalent grafting of PLA[23,24]. About 5 g of sample was put in a pre-dried and pre-weighed cellulose extraction thimble. The thimbles were then inserted in the soxhlet extractor connected to a 500 mL round bottom flask containing around 200–250 mL DCM. The flasks were heated, and the solvent was allowed to reflux. The extraction was continued for 72 h. After the extraction, the thimbles were removed; residue and extract were separated and dried overnight at 70 °C. The dried thimble with residue was weighed again and the weight change in the residue was calculated. The reproducibility of the results was confirmed by testing three replicates for each sample. It was expected that the covalently grafted MTPS will get extracted in DCM and there will be a weight gain in the extract. Percent grafting was calculated from the mass balance as shown in Equation (1).

Equation 4.1

$$\% \textit{grafting} = \frac{|W_1 - W_2|}{W_1} \times 100$$

where, W_1 is the weight of MTPS present in the sample originally and W_2 is the weight of residue in the thimble after 72 h. i.e., free MTPS.

4.3.4 Thermal analysis

The degradation temperature of samples was obtained by thermogravimetric analysis (TGA). TGA measurements of all the samples were conducted under an inert atmosphere of nitrogen using a TGA Q50 (TA Instruments, New Castle, DE, USA). The general sample weight used was 5–7 mg. The sample was placed in an aluminum pan and was heated to 600 °C at the rate of 10 °C/min. The weight loss (%) of a sample as a function of temperature (°C) was obtained from this analysis. Also, the thermal transitions of the samples were obtained by using a differential scanning calorimeter (DSC). The sample was heated to 200 °C in DSC Q20 (TA Instruments, New Castle, DE, USA) with a heating rate of 10 °C/min and held for 5 min to erase thermal history. The sample was then cooled back to 20 °C and heated again to 200 °C with a heating rate of 10 °C/min. The glass transition temperature (T_g), melting temperature (T_m), the crystallinity of samples (% X_c), enthalpy of melting (ΔH_m), and enthalpy of cold crystallization (ΔH_c) were calculated using TA universal analysis 2000 software. The % crystallinity of PLA samples was calculated from the formula given by Bher et al., 2017 [40][41].

Equation 4.2

$$\textit{Crystallinity} (\%) = \frac{\Delta H_m - \Delta H_m}{\Delta H_o(1 - \alpha)} \times 100$$

where, ΔH_m and ΔH_c are enthalpies of melting and crystallization respectively. α is the weight fraction of MTPS in the blends and ΔH_o is the enthalpy of melting for 100% crystalline PLA which was obtained from the literature as 93.1 J/g [29, 33, 41].

4.3.5 Isothermal Crystallization Analysis

To study the isothermal crystallization kinetics, the samples were heated to 200 °C and maintained for 5 min at that temperature to remove any thermal history. Then they were cooled to the desired crystallization temperatures (90, 95, 100, 105 and 110 °C) at a rate of 20 °C/min and held at that temperature till crystallization was complete, then heated again to 200 °C to obtain the melt temperature and final crystallinity after annealing.

4.3.6 Polarized Optical Microscopy (POM)

POM observation was performed on an Olympus BH-2 microscope (Olympus corp., Japan) with crossed-polarizers, equipped with a digital camera system and a Mettler Toledo FP82 (Ohio, USA) hot stage. All the samples were first inserted between two microscope coverslips and squeezed at 200 °C to obtain a thin slice. The films were held at 200 °C for 2 min to achieve thermal equilibrium. This was followed by rapid cooling to the selected crystallization temperature of 105 °C. The polarized optical micrographs during isothermal crystallization were recorded after every 90 s to monitor the formation and growth of crystallites.

4.3.7 Mechanical Properties

The injection molded test bars were prepared using a tabletop DSM 15 cc mini extruder (DSM Research B. V., Sittard-Geleen, The Netherlands) and 3.5 cc mini-injection molder (DACA Instruments, Santa Barbara, CA, USA). The injection pressure was set as 140 psi and the cylinder and mold temperatures were 200 and 65 °C, respectively. The samples were

stored for 2 days at 25 °C in a humidity chamber with RH of 50% before any analysis. Tensile testing was performed using an Instron model 5565-P6021 (Instron, Norwood, MA, USA) with a 5 kN load cell and grip separation speed of 12.5 mm/min as per ASTM D882. Data from five samples of each formulation were averaged and compared with the properties of neat PLA.

4.3.8 Scanning electron microscopy

A JOEL 6610 LV scanning electron microscope (JEOL Ltd., Tokyo, Japan) was used to study the dispersion of MTPS in PLA using the tensile fracture surfaces of all samples. The tensile bars were immersed in liquid nitrogen for ~2 min and then fractured. Fracture surfaces were mounted on aluminum stubs using high vacuum carbon tabs and coated with gold using a sputter coater. A different set of bar specimens were also treated with 6 N HCl for 12 h to remove the MTPS phase from the samples and air-dried for 12 h in a fume hood. Then they were mounted on aluminum stubs as explained before and examined using JOEL at 500× magnification at 10 kV.

4.3.9 Barrier properties

The barrier properties were measured using MOCON instruments (OX-TRAN Model 2/21 and PERMATRAN-W Model 3/33). All the measurements were undertaken at 50% RH for oxygen and 100% for water vapor. Circular films of 3.14 cm² area were used. The thickness of the samples was measured using a micrometer (TMI) and was used to calculate the permeability to oxygen and moisture. Water vapor permeability (*WVP*) is given as:

Equation 4.3

$$WVP = \frac{WVTR}{\Delta P} \times Th$$

Oxygen permeability (OP) was calculated from oxygen transmission rate (OTR) data using Equation (4):

Equation 4.4

$$OP = \frac{OTR}{\Delta P} \times Th$$

where, $WVTR$ is water vapor transmission rate, OTR is oxygen transmission rate, Th (m) was the thickness of the sample and ΔP was the pressure difference between both sides of the sample (Pa) [34].

4.3.10 Aqueous biodegradability Testing

The biodegradability of neat PLA and PLA + 5% MTPS samples was tested in an aqueous environment using ISO 14852 as explained in chapter 2. All the tests were performed in an aerobic environment at 30 °C.

4.4 RESULTS AND DISCUSSION

MTPS and all the PLA/MTPS blends were prepared in a Century ZSK-30 twin screw extruder (MI, USA). MTPS was first characterized to ensure sufficient grafting of glycerol and then it was used for blending with PLA.

4.4.1 Percent Grafting for MTPS-PLA blends

Soxhlet extraction was carried out for the blends of PLA and MTPS as well using DCM as extraction solvent. It was found that the weights of residues and extracts did not change after the extraction. Entire PLA was extracted in the solvent and MTPS remained in the residue. There were no additional peaks in residue or extract TGA which could represent any sign of reaction between PLA and MTPS. Hence, it was concluded that there was no reaction between MTPS and PLA.

4.4.2 Mechanical Testing and Phase Morphology

Figure 4.1 illustrates the modulus, tensile stress, and strain for neat PLA and the various blends. Table 4.3 summarizes all the data of tensile stress at yield, tensile stress at break, modulus, and strain at break with averages and standard deviations. The analysis of the tensile testing of neat PLA samples reveals a characteristic brittle behavior of PLA with tensile strength values of ~82 MPa and elongation at break ~8%. The results indicated that there was no significant change in the modulus, tensile stress, and strain after addition of 1% and 2% MTPS ($p > 0.05$). Only for 5% MTPS containing blends, the modulus increased by 15% indicating they were stiffer than neat PLA whereas tensile stress reduced by 12%. Increasing MTPS content in PLA increased the brittleness of PLA bars. Similar results were observed by Wootthikanokkhan 2012 et al. [45] where the modulus of the samples was found to increase with an increasing per-centage of starch at the expense of elongation and

tensile toughness. For PLA + 10% MTPS, the samples became brittle and broke after loading on the tensile machine. Hence, the readings for modulus, stress, and strain were not recorded. Because of the reduction in mechanical properties, they were not considered for any further analysis. This reduction in mechanical properties could be due to the reduced compatibilization and increased particle size of the MTPS particles in the PLA matrix. This was observed in the SEM images of the samples as explained in Figure 4.2 and Figure 4.3

Table 4.3: Effect of MTPS content on tensile properties of PLA

Materials	Modulus	Tensile Stress at Yield	Tensile Strain at Break	Tensile Stress at Break
	(MPa)	(MPa)	(mm/mm)	(MPa)
PLA neat	1796.45 ± 110.08 ^a	82.10 ± 1.14 ^a	0.077 ± 0.004	73.30 ± 2.74
PLA-1	1825.34 ± 47.76 ^a	80.67 ± 1.60 ^a	0.073 ± 0.005	72.76 ± 2.01
PLA-2	1748.27 ± 44.03 ^a	78.210 ± 0.65 ^a	0.068 ± 0.002	73.63 ± 2.17
PLA-5	2059.88 ± 47.09 ^b	72.38 ± 1.14 ^b	0.066 ± 0.005	67.77 ± 3.97

Different superscript letters within the same column indicate significant differences among formulations ($p < 0.05$)

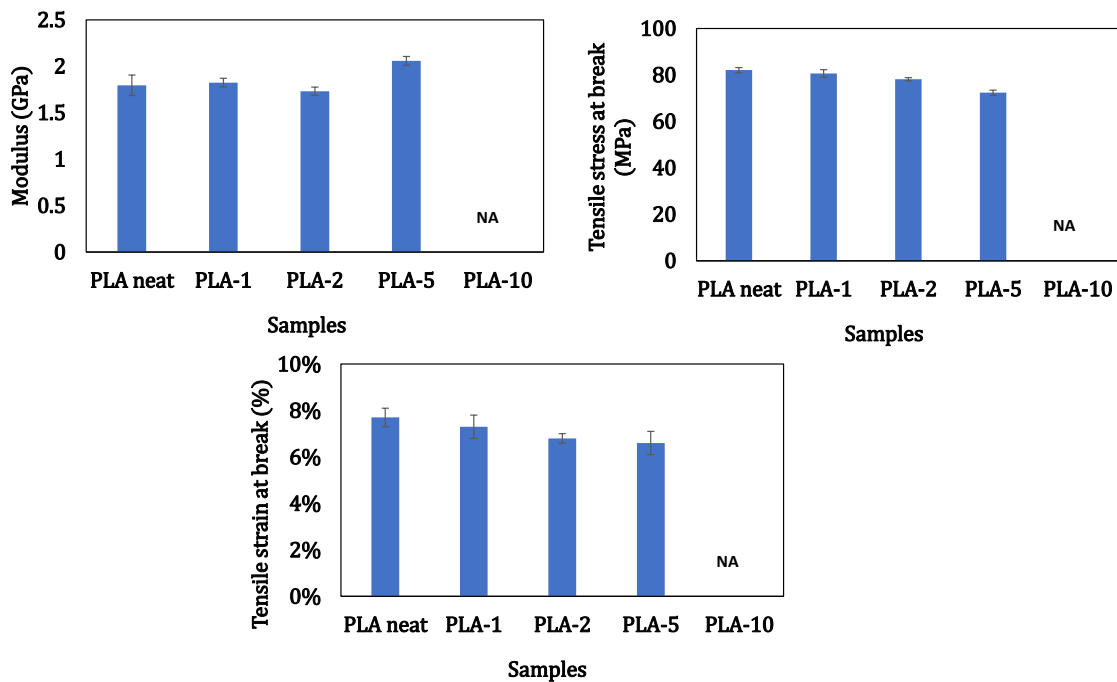


Figure 4.1: Modulus, tensile stress, and tensile strain graphs for PLA and blends

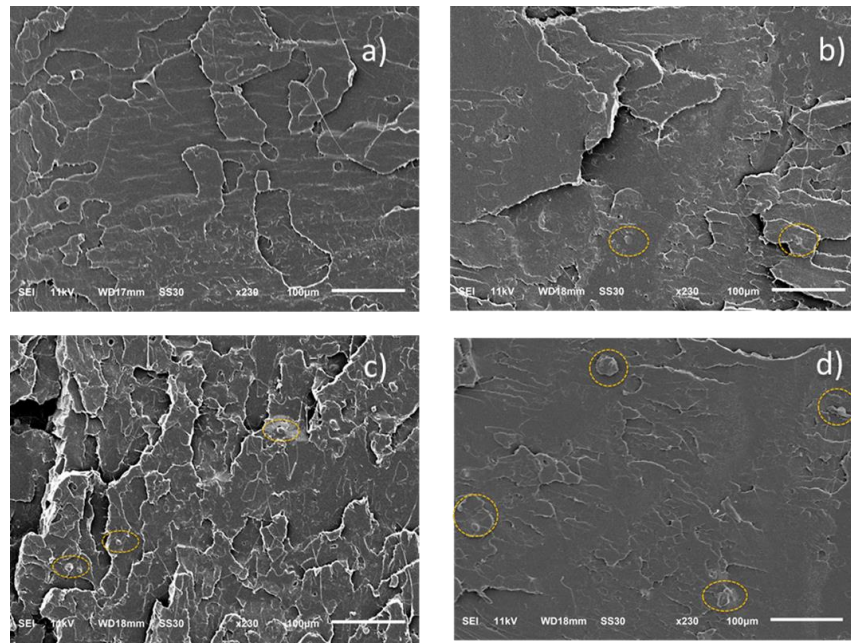


Figure 4.2: Scanning electron microscopy (SEM) images of fractured tensile surfaces of (a) PLA, (b) PLA + 1% MTPS, (c) PLA + 2% MTPS, (d) PLA + 5% MTPS

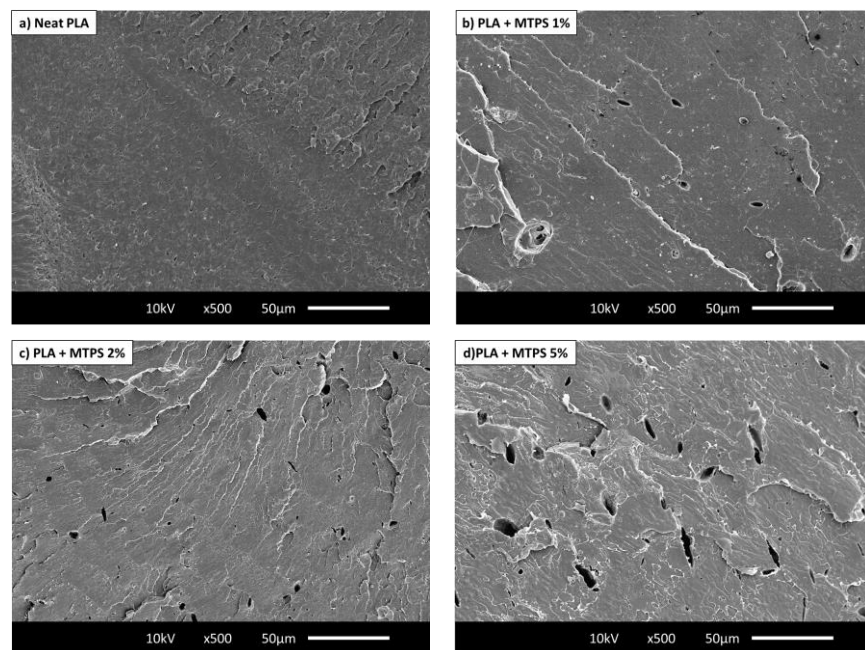


Figure 4.3: SEM images of the blends after selective extraction of MTPS phase (a) PLA, (b) PLA + 1% MTPS, (c) PLA + 2% MTPS, (d) PLA + 5% MTPS

The morphological behavior of neat PLA and the blends was analyzed using SEM images of tensile fracture surfaces. The main results are reported in Figure 4.2. The tensile fracture surface of neat PLA shows a smooth and featureless surface which is an indicator of typical brittle behavior. Figure 4.2-b, c and d show presence of small spherical MTPS particles (shown with dotted yellow circles) with good interfacial adhesion with PLA. They showed a smooth surface and were well wetted by the PLA. The size of MTPS particles seemed to increase with increasing content of MTPS (Figure 4.2-b vs d). However, the number of MTPS particles did not increase much and their effect on thermal properties was also negligible. Figure 4.3 shows the morphology of the PLA matrix and the PLA/MTPS blends produced by extrusion after selective removal of the MTPS phase. Cavities represent the spaces occupied by MTPS particles before their selective removal by dissolution in concentrated HCl. The proportion of cavities was well correlated with the percentage of MTPS added in the particular blend. Figure 4.3-b to d all show micro size distribution of MTPS particles in the PLA matrix. The size of the cavities increased with increase of MTPS content which suggested a reduction in compatibilization of MTPS. The particle size for MTPS increased from 4.1 ± 1.5 μm for 1% MTPS to 9.5 ± 3.5 μm for 5% MTPS blends. An increase in the domain size is indicative of less compatibilization between PLA and MTPS. This could explain the reduction in mechanical properties for 5% and 10% MTPS containing blends. The 1% and 2% MTPS (Figure 4.3-a,b) had smaller size and more spherical particles which indicated greater compatibilization, and hence no reduction in tensile strength was observed compared to neat PLA. These particle sizes of 4–9 μm were much smaller as compared to the 30 μm size observed by Clasen SH et al. (2015) in the PLA-TPS blends without any compatibilizer[35].

4.4.3 Thermal analysis

Thermogravimetric (TGA) and derivative (DTG) graphs of the blends containing 1%, 2%, 5%, and 10% MTPS along with neat PLA are shown in Figure 4.4. With increment in MTPS until 5%, the weight loss in the first part of the curve ($< 200^{\circ}\text{C}$), was almost the same and was found to be less than 0.5% which is a significant feature since it represents the range and possible process temperatures for the blends after production. With 10% MTPS, the weight loss until 200°C increased to 0.7%. Thermal stabilities of the blends were also characterized by the temperatures at which 5% ($T_{5\%}$), 10% ($T_{10\%}$), and peak wt. loss (T_{peak}) occurred. Increasing the percentage of MTPS caused a steady decrease in 5% and 10% wt. loss temperatures. The peak degradation temperatures shifted towards the lower temperature with increase in the percentage of MTPS. The results are summarized in Table 4.4.

Table 4.4: Thermogravimetric analysis (TGA) of PLA and blends

Sample	$T_{5\%}$ ($^{\circ}\text{C}$)	$T_{10\%}$ ($^{\circ}\text{C}$)	T_{peak} ($^{\circ}\text{C}$)
PLA	337.4	347.7	377.5
PLA-1	333.4	342.7	371.9
PLA-2	327.1	336.9	371.0
PLA-5	308.4	320.9	343.3
PLA-10	295.68	310.7	342.6

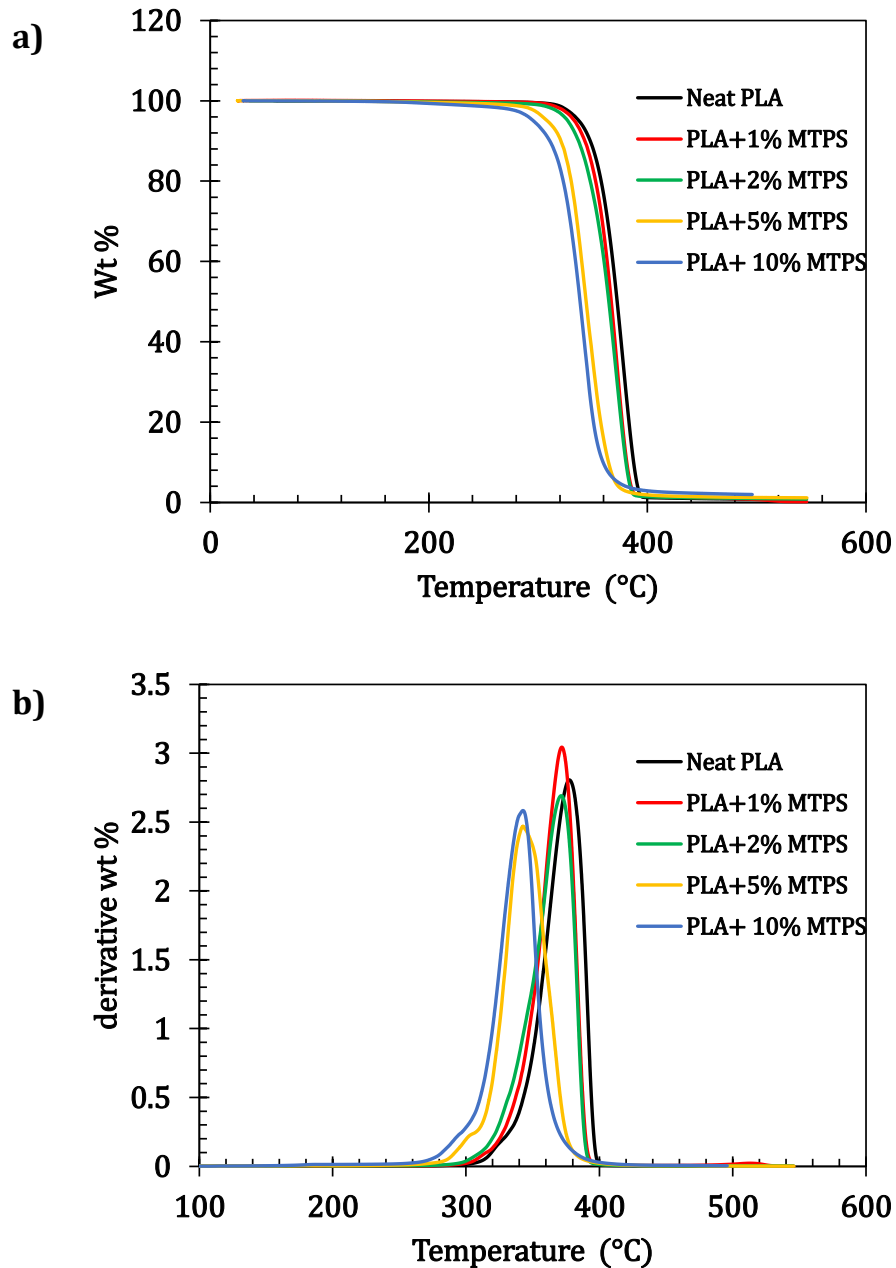


Figure 4.4: a)TGA and b)DTG curves for PLA and PLA/MTPS blends

The glass transition temperature T_g (°C), crystallization temperature T_c (°C), melting temperature T_m (°C), enthalpy of crystallization (J/g), enthalpy of melting (J/g), and crystallinity (%) data of PLA and modified PLA pellets were determined from the DSC analysis and are given in Table 4.5. All the thermal properties were obtained from the second

heating curve (Figure 4.5). Thermal degradation and mechanical properties of PLA with 10% MTPS (explained in Section 4.4.2) were significantly lower as compared to neat PLA. Hence, that sample was not used for further testing of isothermal crystallization, barrier properties, etc. Figure 4.5 shows the second heating curves for PLA and PLA/MTPS blends. T_g was found to decrease negligibly with addition of MTPS to PLA whereas T_c reduced from 113.8 to 103.1 °C. In our opinion, this decrease might be due to the migration of some glycerol from the MTPS phase to the PLA phase. This might lead to the formation of plasticized PLA with lower T_g .

Table 4.5: Thermal transition temperatures and percent crystallinity of modified PLA samples

	T_g (°C)	T_m (°C)	T_c (°C)	ΔH_m (J/g)	ΔH_c (J/g)	% Crystallinity	% Crystallinity After Annealing
PLA neat	63.30	171.50	113.86	40.94	33.74	7.74	43.18
PLA + 1% MTPS	62.30	171.00	111.40	40.72	31.13	10.42	47.28
PLA + 2% MTPS	61.38	170.57	108.46	45.45	32.55	14.15	48.20
PLA + 5% MTPS	59.50	161.40	103.10	45.03	19.71	28.66	50.61

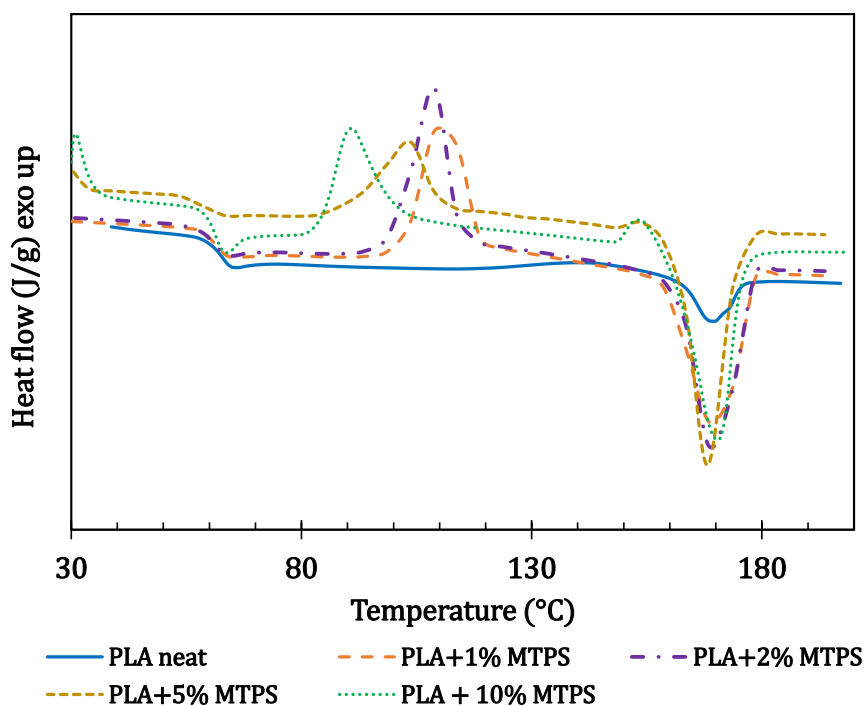


Figure 4.5: Differential scanning calorimetry (DSC) thermograms of PLA and the blends

From DSC of neat PLA, it seemed that there was just a little endothermic peak on the curve of pure PLA and the crystallinity was about 7.74%. After adding MTPS, an exothermic peak appeared on the heating curve. In the course of heating, more crystals were formed and hence the crystallinity of PLA increased with increasing concentration of MTPS suggesting its function as a nucleating agent similar to starch [24]. The final crystallinity of the samples was also calculated after annealing of the samples as explained in the isothermal crystallization analysis. Figure 4.6 shows the melting curves for annealed samples. The final crystallinity of the samples after annealing increased to 50.6% with 5% MTPS compared to 43% for neat PLA.

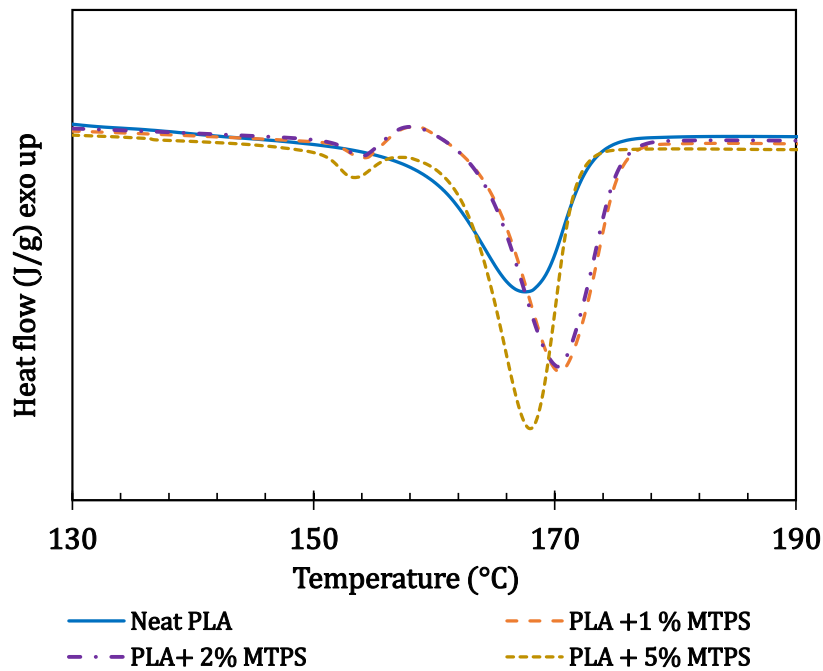


Figure 4.6: Melting curves for PLA blends after annealing

4.4.4 Isothermal Crystallization Kinetics

The isothermal crystallization isotherms of PLA and the blends obtained by cooling the molten polymer to the selected crystallization temperature (T_c) are as shown in Figure 4.7. The shape of the exotherm was dependent on T_c . The time required for crystallization was found to be minimum at 100 °C. Above and below that temperature, the isotherm became flatter, and the time required for complete crystallization increased. A similar effect was observed for the PLA/MTPS blends as well. Fractional crystallinity X_t vs time is the ratio of the area of the endotherm until time t divided by the total area of the endotherm, as shown in Equation (7).

Equation 4.5

$$X(t) = \frac{X_c(t)}{X_c(t_\infty)} = \frac{\int_0^t \frac{dH_c(t)}{dt} dt}{\int_0^\infty \frac{dH_c(t)}{dt} dt}$$

where H_c is the heat flow at time t , and t_∞ is the end time for complete crystallization.

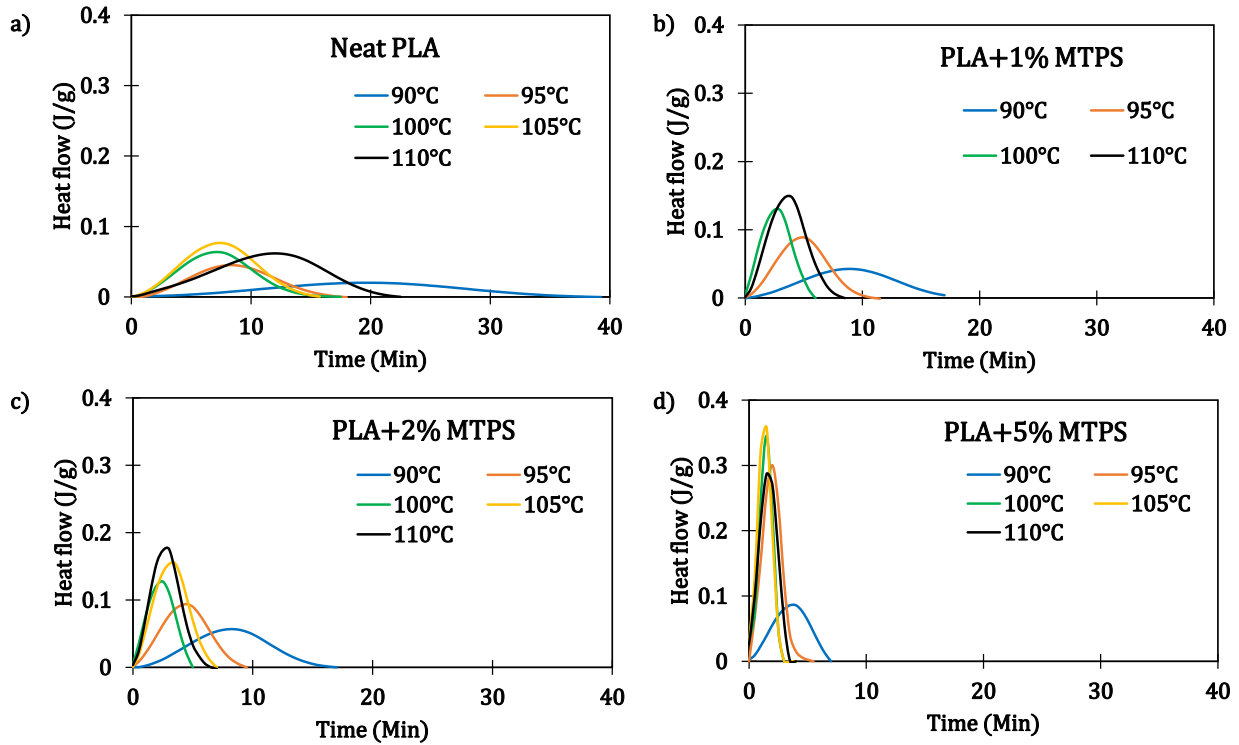


Figure 4.7: DSC melting thermograms of a) PLA and blends (b) PLA+1% MTPS, c) PLA+2% MTPS, d) PLA+5% MTPS) at various temperatures

Typical crystallization isotherms showing the degree of crystallinity $X(t)$ vs time were plotted for PLA and the blends as shown in Figure 4.8. It was observed that the rate of crystallization increased with an increasing amount of MTPS addition and was fastest for neat PLA as well as all the blends for the temperature of 100 °C.

The Avrami Equation (Equation 4.6) was used for studying the isothermal crystallization behavior of PLA and the blends. It is often written in logarithmic form as shown in Equation 4.7.

Equation 4.6

$$X(t) = 1 - \exp(-kt^n)$$

Equation 4.7

$$\ln [-\ln(1 - X(t))] = n \ln t + \ln k$$

where $X(t)$ is the fractional crystallinity at time t , k is the overall kinetic rate constant, and n is the Avrami exponent, which depends on the mechanism of nucleation and the form of crystal growth. The rate constant k contains the nucleation and growth parameters for crystallization. It was observed that the total crystallization time was reduced significantly (<8 min for 5% MTPS) by the addition of MTPS as compared to neat PLA (~20 min at 100 °C). The half time ($t_{1/2}$) was calculated and reported for all the temperatures in Table 4.6. Avrami plots of $\ln[-\ln(1-X(t))]$ versus $\ln(t)$ were plotted to obtain the values of k and n as shown in Figure 4.9. The crystallization rates (k) were much higher for the blends containing MTPS as compared to neat PLA at all temperatures indicating that MTPS increased the crystallization rate of PLA. Also, from Avrami analysis results, two-dimensional crystal growth was observed as n values were around 2 [5]. Thus, it can be concluded that MTPS was acting as a nucleating agent for PLA. The half crystallization time, $t_{1/2}$, the time in which 50% of the total crystallinity is achieved, was calculated using Equation 4.8.

Equation 4.8

$$t_{1/2} = \ln \left(\frac{2}{k} \right)^{1/n}$$

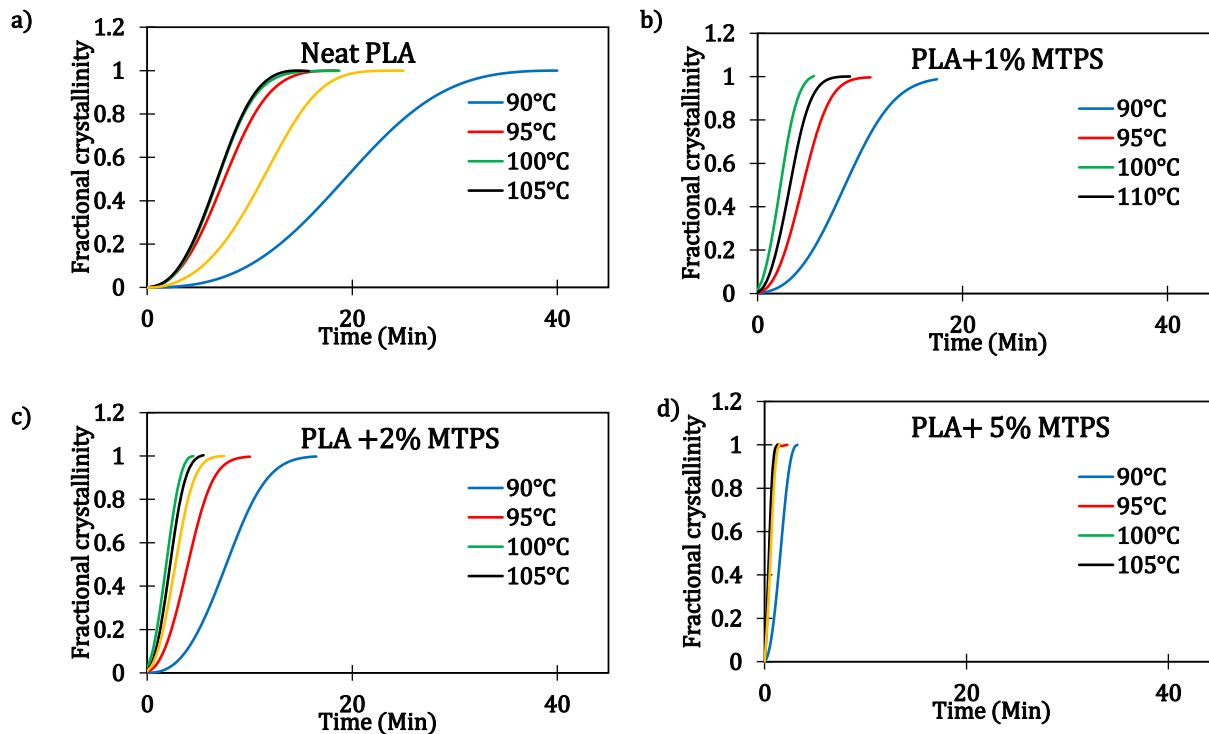


Figure 4.8: Fractional crystallinity vs. time of a) PLA and blends (b) PLA+1%MTPS, c) PLA+2%MTPS, d) PLA+5% MTPS) at various temperatures

Saddle-shaped curves were obtained by plotting T_c vs. $t_{1/2}$ for PLA and its blends with MTPS as shown in Figure 4.10. As the MTPS content increased, $t_{1/2}$ values decreased and the rates for crystallization k were found to increase. The minimum $t_{1/2}$ for neat PLA was observed as 6.83 min at 100 °C and 1.66 and 0.94 min for 2% and 5% of MTPS at 100 °C.

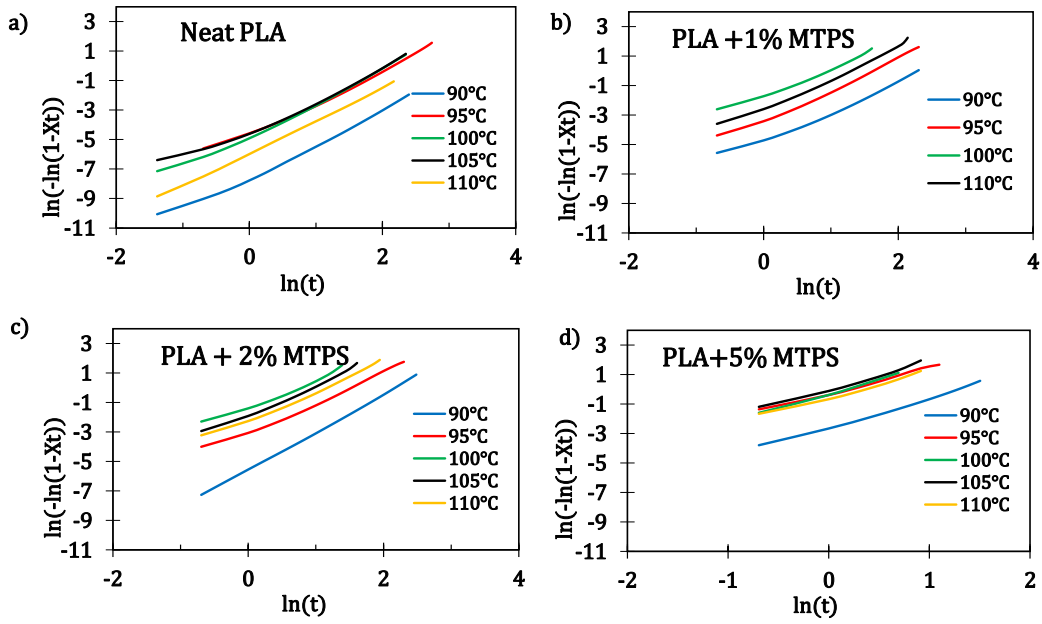


Figure 4.9: Plots of $\ln(-\ln(1-X(t)))$ vs $\ln t$ of a) PLA and blends (b) PLA+1%MTPS, c) PLA+2%MTPS, d) PLA+5% MTPS)at various temperatures

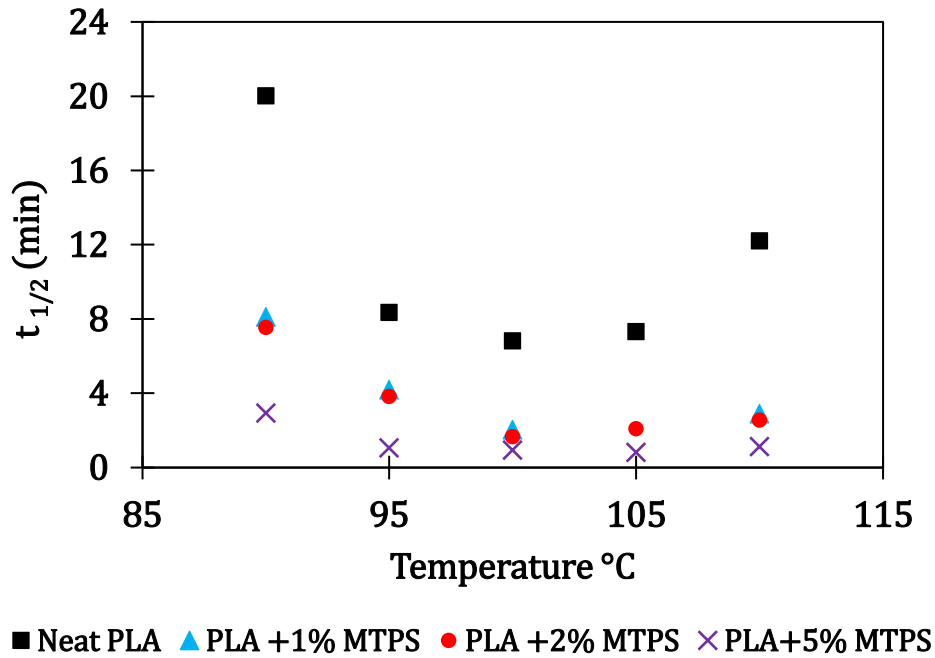


Figure 4.10: Half time for crystallization vs isothermal crystallization temperatures for PLA and blends

The values for $t_{1/2}$ obtained for PLA/MTPS blends were compared with several nucleating agents including starch, talc, CNC, wood flour, polyoxymethylene, etc. [5,7–9,11,12,33,46,47] from the literature. Figure 4.11 shows the comparison for $t_{1/2}$ values of other nucleating agents compared to MTPS. The $t_{1/2}$ values for MTPS were found to be lower compared to all the other nucleating agents except talc. Talc is one of the most effective nucleating agents for PLA. 1–2% of talc is commonly added to decrease the $t_{1/2}$ of PLA to less than one minute [25]. Thus, MTPS, although not as effective as talc, could be a completely bio-based and biodegradable nucleating agent as opposed to talc of inorganic origin.

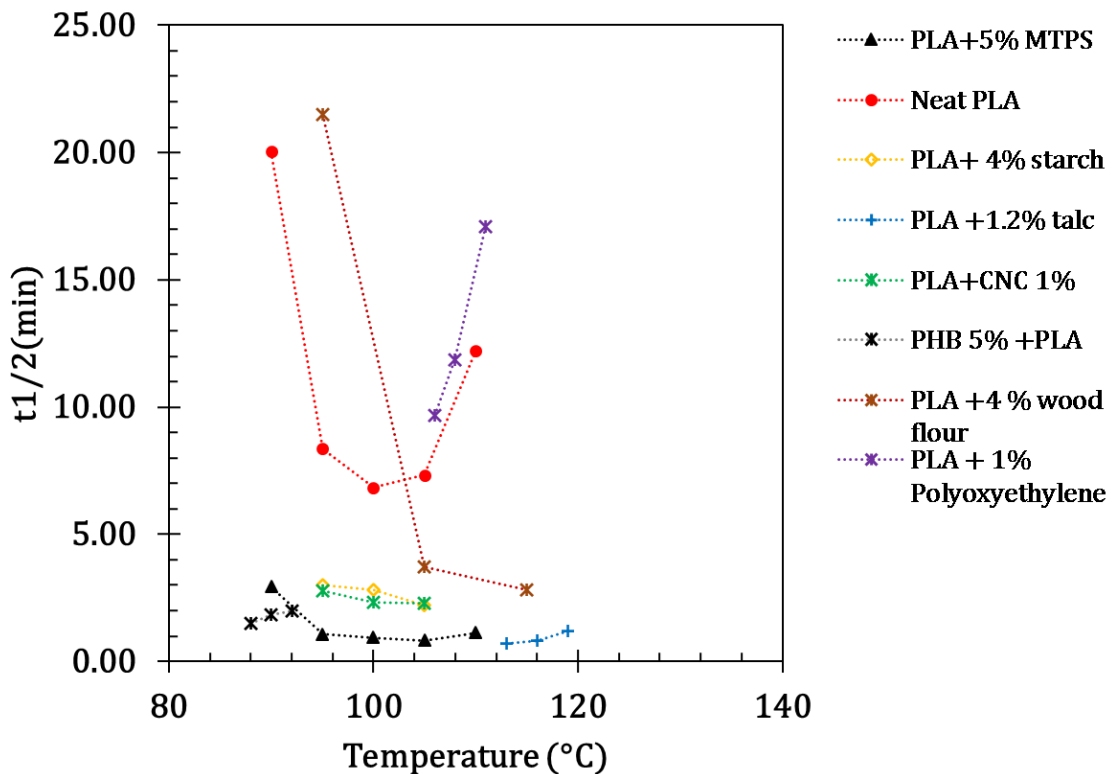


Figure 4.11: Comparing the $t_{1/2}$ values of PLA/MTPS blends with other nucleating agents

The effect of MTPS on crystal morphology and size was studied using polarized optical microscopy. Figure 4.12 shows the morphology of crystals for all the compositions after crystallization at 105°C for 6 min. As expected, neat PLA showed larger size spherulites and

the rate of formation of spherulites was less as compared to other samples. As shown in Figure 4.12-b, neat PLA started forming the spherulites well after holding it at 105°C for 3 minutes, whereas, for all other PLA/MTPS samples we could see a good number of spherulites by that time (Figure 4.12-e, h and k). For PLA+5% MTPS, this was even faster, and the crystals were visible within 90 sec (Figure 4.12- j). This agreed well with the k values obtained by Avrami analysis for the samples which indicated 98-fold faster crystallization for PLA+ 5% MTPS at 100°C. This can be attributed to the nucleation effect of MTPS, which provides much more heterogeneous nuclei, reduces the spherulite size, and speeds up the crystallization process.

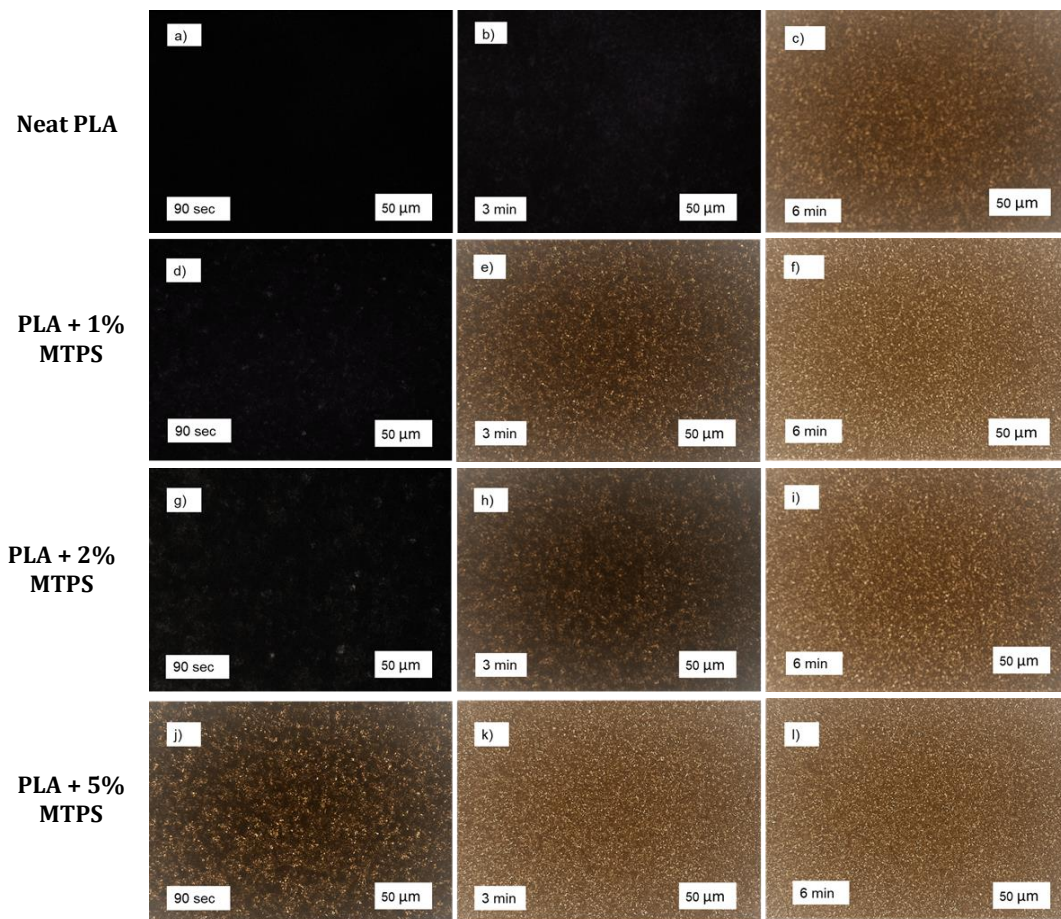


Figure 4.12: Polarized optical microscopy (POM) images of PLA/MTPS blends with MTPS content of 0%: (a-c); 1%: (d-f); 2%: (g-i); 5%: (j-l)

Table 4.6: Crystallization half times and Avrami constants for PLA samples at different temperatures

Sample	Temperature (°C)	t _{1/2} (min)	n	ln k	k
Neat PLA	90	20.03	2.520	-7.919	3.64×10 ⁻⁴
	95	8.36	1.890	-4.380	1.25×10 ⁻²
	100	6.83	2.320	-4.825	8.03×10 ⁻³
	105	7.32	2.420	-5.184	5.61×10 ⁻³
	110	12.21	2.240	-5.972	2.55×10 ⁻³
PLA + 1% MTPS	90	8.12	2.198	-4.969	6.95×10 ⁻³
	95	4.19	2.127	-3.412	3.30×10 ⁻²
	100	2.03	1.797	-1.641	1.94×10 ⁻¹
	110	2.91	2.084	-2.593	7.48×10 ⁻²
PLA + 2% MTPS	90	7.54	2.619	-5.657	3.49×10 ⁻³
	95	3.83	1.964	-3.004	4.96×10 ⁻²
	100	1.66	1.811	-1.289	2.76×10 ⁻¹
	105	2.10	1.946	-1.809	1.64×10 ⁻¹
	110	2.55	1.958	-2.200	1.11×10 ⁻¹
PLA + 5% MTPS	90	2.94	1.960	-2.479	8.38×10 ⁻²
	95	1.06	1.410	-0.447	6.40×10 ⁻¹
	100	0.94	2.010	-0.242	7.85×10 ⁻¹
	105	0.82	1.780	-0.018	9.82×10 ⁻¹
	110	1.12	1.740	-0.566	5.68×10 ⁻¹

4.4.5 Permeability Studies

Starch based films have demonstrated their good oxygen barrier properties in previous studies [13,42,37–39]. Figure 4.13 summarizes the effect of MTPS on WVP and OP of PLA films. A decrease of 33% and 27% in oxygen permeability was observed by adding 5% and 1% MTPS, respectively. This improvement can be attributed to increased crystallinity. Crystalline regions in PLA form the impermeable regions which create a tortuous path for the diffusion for permeants, which leads to lower permeability [48–52]. Also, high oxygen barrier properties of starch might also be helpful in reducing the OP of the films with blends. WVP and OP show a significant reduction for the addition of 1% MTPS, whereas it becomes less significant as the concentration is increased to 2% and 5%. This could also be explained

by the particle size of MTPS observed from the SEM analysis. The 1% MTPS blends had an average particle size of 4.1 ± 1.5 μm whereas, for 5% MTPS, the size was almost double: 9.5 ± 3.5 μm . More small particles could have caused a greater number of tortuous paths leading to reduced permeability. The water vapor permeabilities of the blends did not show any significant increase even after addition of hydrophilic MTPS. This might be due to the morphology of the blend in which the MTPS particles were observed to be surrounded by hydrophobic PLA matrix thus shielding it from water (Figure 4.3 and Figure 4.2).

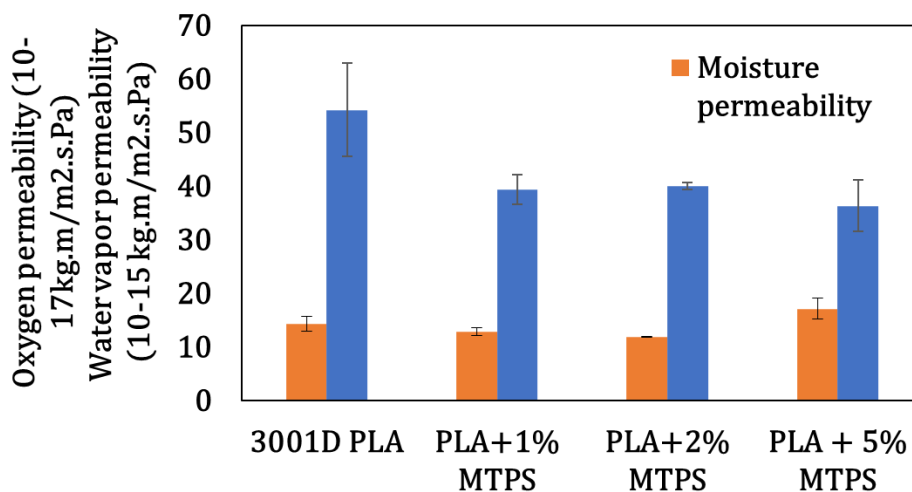


Figure 4.13: Effect of MTPS content on moisture permeability (WVP) and oxygen permeability (OP) of PLA films

4.4.6 Biodegradability Studies

Figure 4.14 shows the test setup for aqueous biodegradation according to ISO 14852. The system was kept in a dark, temperature-controlled room maintained at 30 °C. The test flasks were agitated throughout the run with the help of magnetic stirrers. Air inlet was passed through NaOH solution to get CO₂-free air. This air was then divided and passed through flowmeters for each bioreactor at a constant flow rate. The CO₂ evolved from the flasks was

collected in NaOH solution and titrated with HCl to determine the CO₂ that evolved from the samples and % biodegradation as described in chapter 2.

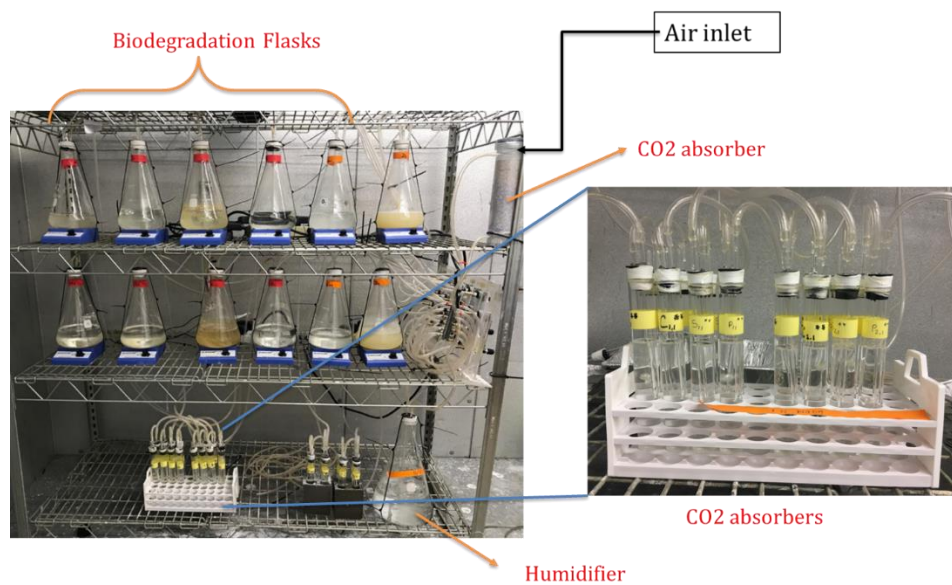


Figure 4.14: Experimental aqueous biodegradation setup

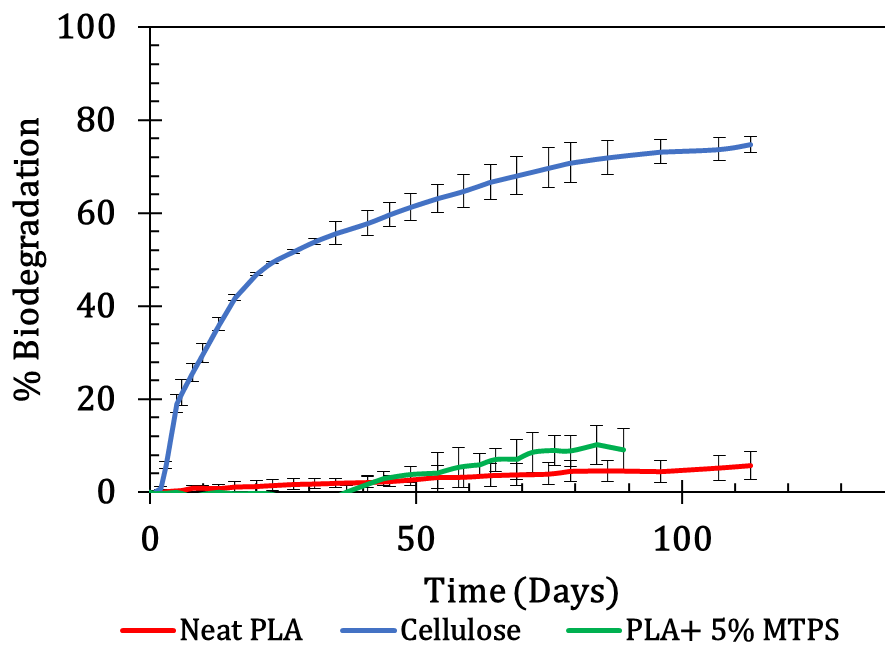


Figure 4.15: Aqueous biodegradation curves for PLA and PLA + 5% MTSP

The average % biodegradation curves for cellulose and PLA and PLA + 5% MTPS at 30 °C are as shown in Figure 4.15. It was observed that neat PLA and PLA + 5% MTPS have almost the same biodegradation curve. Both showed negligible biodegradation in aqueous environment (<10%) at the end of the test. Therefore, it can be concluded though MTPS acted as a nucleating agent and increased the crystallinity and crystallization rate of PLA, it was well embedded in the hydrophobic PLA matrix and hence did not change the biodegradation properties of PLA. Poor biodegradability of PLA was attributable to the temperature at which the aqueous biodegradation test was carried out: 30 °C. The glass transition temperature of PLA is 58 °C. Below this temperature, PLA does not biodegrade easily due to the polymer segments behaving as a glass with little or no mobility of the polymer chains. Hence, no difference could be observed at lower temperature studies. Similar to any chemical reaction the rate of biodegradation depends on temperature and is expected to increase as temperature increases. A higher biodegradation rate is expected in the high temperature composting environment testing which is the ideal environment for PLA biodegradation. PLA reaches 80–90% biodegradation within 60–90 days in composting environment at temperatures of 58 °C as observed in several studies [53–55]. These compatibilized blends with maleic anhydride are also expected to have higher biodegradability as compared to PLA and pure starch blends in the composting environment [34,56]. During composting, the presence of MA might lead to the formation of an acid group due to its reaction with water. That can accelerate the chain scission in PLA resulting in faster biodegradation [47]. Further testing for biodegradation in composting environment needs to be done to validate this hypothesis.

4.5 CONCLUSIONS

Maleated thermoplastic starch (MTPS) was successfully prepared by reacting glycerol with corn starch using maleic anhydride as a promoter. It was found that 79% of added glycerol was grafted on the starch during reactive extrusion. The dual effect of MTPS as a nucleating agent and barrier property enhancer for PLA was studied. MTPS increased the rate of crystallization of PLA significantly (98-fold at 100 °C). A decrease in glass transition and thermal degradation temperature was observed with increasing concentration of MTPS. Percent crystallinity of PLA increased from 7.7% to 28.6% by addition of 5% MTPS whereas total crystallinity of the blends was as high as 50.6% after annealing. SEM images of tensile fractured samples showed good interfacial adhesion and wetting between MTPS and PLA. The 1% MTPS showed the best compatibilization with domain sizes of 4.1 ± 1.5 μm as observed from the SEM images of tensile bars after selective extraction of the MTPS phase. Melt isothermal crystallization kinetics using Avrami analysis showed a drastic reduction in half crystallization time $t_{1/2}$ from 20 min to less than 1 min with addition of 5% MTPS. An increased crystallization rate was also confirmed by POM images of neat PLA and the blends. More number of smaller spherulites were observed with an increasing percentage of MTPS in the blends. MTPS was found to be more effective as compared to many other nucleating agents used for PLA such as starch, CNC, wood flour, polyoxyethylene, etc. Oxygen permeability values of PLA were reduced by 27% by the addition of just 1% MTPS whereas water vapor permeability values remained constant. No significant change in the mechanical properties of the blends was observed as opposed to neat PLA until 5% addition of MTPS by weight. A small decrease in tensile stress and elongation at break was observed after addition of 10% MTPS which could be explained by the brittle nature of MTPS. There was no

significant increase in the aqueous biodegradability of these blends compared to neat PLA, which suggested that the MTPS particles were well embedded in the hydrophobic PLA matrix. It is expected that the presence of starch and MA will enhance the biodegradability of these blends in a composting environment. Further studies need to be undertaken to obtain the actual experimental data supporting this hypothesis. These MTPS/PLA blends have demonstrated improved barrier and crystallization properties and similar mechanical, thermal and biodegradation properties to neat PLA. These blends have a potential for reduced cost due to use of an inexpensive, naturally abundant, completely bio-based, and biodegradable nucleating agent and can find applications in several food contact packaging purposes.

REFERENCES

REFERENCES

- [1] R. Narayan, *Degradable Polymers and Materials: Principles and Practice (2nd Edition)*, vol. 1114. Washington, DC: American Chemical Society, 2012. doi: 10.1021/bk-2012-1114.
- [2] R. Narayan, "Biobased & biodegradable plastics: Rationale, drivers, and technology exemplars," *ACS Symposium Series*, vol. 1114, pp. 13–31, Nov. 2012, doi: 10.1021/bk-2012-1114.ch002.
- [3] K. L. Law and R. Narayan, "Reducing environmental plastic pollution by designing polymer materials for managed end-of-life," *Nature Reviews Materials*, 2021, doi: 10.1038/S41578-021-00382-0.
- [4] R. Narayan, "Opinion Missing the point about biodegradability," *Bioplastics Magazine*, pp. 38–39, 2020.
- [5] M. Nofar, W. Zhu, C. B. Park, and J. Randall, "Crystallization kinetics of linear and long-chain-branched polylactide," *Industrial and Engineering Chemistry Research*, vol. 50, no. 24, pp. 13789–13798, 2011, doi: 10.1021/ie2011966.
- [6] W. Ding, R. K. M. Chu, L. H. Mark, C. B. Park, and M. Sain, "Non-isothermal crystallization behaviors of poly(lactic acid)/cellulose nanofiber composites in the presence of CO₂," *European Polymer Journal*, vol. 71, pp. 231–247, 2015, doi: 10.1016/j.eurpolymj.2015.07.054.
- [7] P. N. Tri, S. Domenek, A. Guinault, and C. Sollogoub, "Crystallization behavior of poly(lactide)/poly(β -hydroxybutyrate)/talc composites," *Journal of Applied Polymer Science*, vol. 129, no. 6, pp. 3355–3365, 2013, doi: 10.1002/app.39056.
- [8] T. Xu, A. Zhang, Y. Zhao, Z. Han, and L. Xue, "Crystallization kinetics and morphology of biodegradable poly(lactic acid) with a hydrazide nucleating agent," *Polymer Testing*, vol. 45, pp. 101–106, 2015, doi: 10.1016/j.polymertesting.2015.05.009.
- [9] J. Cai, M. Liu, L. Wang, K. Yao, S. Li, and H. Xiong, "Isothermal crystallization kinetics of thermoplastic starch/poly(lactic acid) composites," *Carbohydrate Polymers*, vol. 86, no. 2, pp. 941–947, 2011, doi: 10.1016/j.carbpol.2011.05.044.
- [10] D. He, Y. Wang, C. Shao, G. Zheng, Q. Li, and C. Shen, "Effect of phthalimide as an efficient nucleating agent on the crystallization kinetics of poly(lactic acid)," *Polymer Testing*, vol. 32, no. 6, pp. 1088–1093, 2013, doi: 10.1016/j.polymertesting.2013.06.005.
- [11] X. Guo, H. Liu, J. Zhang, and J. Huang, "Effects of polyoxymethylene as a polymeric nucleating agent on the isothermal crystallization and visible transmittance of poly(lactic acid)," *Industrial and Engineering Chemistry Research*, vol. 53, no. 43, pp. 16754–16762, 2014, doi: 10.1021/ie502104y.

- [12] A. Gupta, W. Simmons, G. T. Schueneman, and E. A. Mintz, "Lignin-coated cellulose nanocrystals as promising nucleating agent for poly(lactic acid)," *Journal of Thermal Analysis and Calorimetry*, vol. 126, no. 3, pp. 1243–1251, 2016, doi: 10.1007/s10973-016-5657-6.
- [13] J. Muller, C. González-Martínez, and A. Chiralt, "Combination Of Poly(lactic) acid and starch for biodegradable food packaging," *Materials*, vol. 10, no. 8, pp. 1–22, Aug. 2017, doi: 10.3390/ma10080952.
- [14] S. Mattioli, M. Peltzer, E. Fortunati, I. Armentano, A. Jiménez, and J. M. Kenny, "Structure, gas-barrier properties and overall migration of poly(lactic acid) films coated with hydrogenated amorphous carbon layers," *Carbon N Y*, vol. 63, pp. 274–282, Nov. 2013, doi: 10.1016/j.carbon.2013.06.080.
- [15] J. Bonilla, E. Fortunati, M. Vargas, A. Chiralt, and J. M. Kenny, "Effects of chitosan on the physicochemical and antimicrobial properties of PLA films," *Journal of Food Engineering*, vol. 119, no. 2, pp. 236–243, 2013, doi: 10.1016/j.jfoodeng.2013.05.026.
- [16] J. W. Rhim, S. I. Hong, and C. S. Ha, "Tensile, water vapor barrier and antimicrobial properties of PLA/nanoclay composite films," *LWT - Food Science and Technology*, vol. 42, no. 2, pp. 612–617, Mar. 2009, doi: 10.1016/j.lwt.2008.02.015.
- [17] D. Ferrari, "High Barrier PLA Films For Flexible Packaging," 2007.
- [18] P. Giri, C. Tambe, R. Narayan, M. Junction, and U. States, "Greener Products : From Laboratory Fundamentals to Commercial Scale," in *Biomass Extrusion and Reaction Technologies: Principles to Practices and Future Potential*, vol. 1304, Washington, DC: American Chemical Society, 2018, pp. 1–23. doi: 10.1021/bk-2018-1304.ch001.
- [19] K. M. Dang and R. Yoksan, "Morphological characteristics and barrier properties of thermoplastic starch/chitosan blown film," *Carbohydrate Polymers*, vol. 150, pp. 40–47, Oct. 2016, doi: 10.1016/j.carbpol.2016.04.113.
- [20] R. Ortega-Toro, S. S. Collazo-Bigliardi, A. Chiralt, S. S. Collazo-Bigliardi, and P. Talens, "Thermoplastic starch: improving their barrier properties," *Agronomía Colombiana*, vol. 34, pp. 73–75, 2016, doi: 10.15446/agron.colomb.v34n1supl.57864.
- [21] S. W. Hwang, J. K. Shim, S. Selke, H. Soto-Valdez, M. Rubino, and R. Auras, "Effect of Maleic-Anhydride Grafting on the Physical and Mechanical Properties of Poly(lactic acid)/Starch Blends," *Macromolecular Materials and Engineering*, vol. 298, no. 6, pp. 624–633, Jun. 2013, doi: 10.1002/mame.201200111.
- [22] V. H. Orozco, W. Brostow, W. Chonkaew, and B. L. López, "Preparation and Characterization of Poly(Lactic Acid)-g-Maleic Anhydride + Starch Blends," *Macromolecular Symposia*, vol. 277, no. 1, pp. 69–80, Feb. 2009, doi: 10.1002/masy.200950309.

- [23] J. F. Zhang and X. Sun, "Mechanical properties of poly(lactic acid)/starch composites compatibilized by maleic anhydride," *Biomacromolecules*, vol. 5, no. 4, pp. 1446–1451, Jul. 2004, doi: 10.1021/bm0400022.
- [24] K. S. Kang, S. Il Lee, J. Lee, R. Narayan, and B. Y. Shin, "Effect of biobased and biodegradable nucleating agent on the isothermal crystallization of poly(lactic acid)," *Korean J. Chem. Eng.*, vol. 25, no. 3, pp. 599–608, 2008.
- [25] T. Ke and X. Sun, "Melting behavior and crystallization kinetics of starch and poly(lactic acid) composites," *Journal of Applied Polymer Science*, vol. 89, no. 5, pp. 1203–1210, Aug. 2003, doi: 10.1002/APP.12162.
- [26] W. Y. Jang *et al.*, "Thermal Properties and Morphology of Biodegradable PLA / Starch Compatibilized Blends," *Journal of Industrial and Engineering Chemistry*, vol. 13, no. 3, pp. 457–464, 2007.
- [27] L. Avérous, "Biodegradable multiphase systems based on plasticized starch: A review," *Journal of Macromolecular Science - Polymer Reviews*, vol. 44, no. 3. Taylor & Francis Group, pp. 231–274, Aug. 2004. doi: 10.1081/MC-200029326.
- [28] L. Averous, N. Fauconnier, L. Moro, and C. Fringant, "Blends of thermoplastic starch and polyesteramide: processing and properties," *Journal of Applied Polymer Science*, vol. 76, no. 7, pp. 1117–1128, May 2000, doi:10.1002/(SICI)10974628(20000516)76:7<1117::AID-APP16>3.0.CO;2-W.
- [29] J. Muller, C. González-Martínez, and A. Chiralt, "Poly(lactic) acid (PLA) and starch bilayer films, containing cinnamaldehyde, obtained by compression moulding," *European Polymer Journal*, vol. 95, pp. 56–70, Oct. 2017, doi: 10.1016/j.eurpolymj.2017.07.019.
- [30] R. Ortega-Toro, I. Morey, P. Talens, and A. Chiralt, "Active bilayer films of thermoplastic starch and polycaprolactone obtained by compression molding," *Carbohydrate Polymers*, vol. 127, pp. 282–290, Aug. 2015, doi: 10.1016/j.carbpol.2015.03.080.
- [31] M. L. Sanyang, S. M. Sapuan, M. Jawaid, M. R. Ishak, and J. Sahari, "Development and characterization of sugar palm starch and poly(lactic acid) bilayer films," *Carbohydrate Polymers*, vol. 146, pp. 36–45, Aug. 2016, doi: 10.1016/j.carbpol.2016.03.051.
- [32] J. M. Raquez, Y. Nabar, R. Narayan, and P. Dubois, "In Situ Compatibilization of Maleated Thermoplastic Starch / Polyester Melt-Blends by Reactive Extrusion," *Polymer Engineering & Science*, vol. 48, no. 9, pp. 1747–1754, Sep. 2008, doi: 10.1002/pen.
- [33] E. Hablot *et al.*, "Reactive extrusion of glycerylated starch and starch-polyester graft copolymers," *European Polymer Journal*, vol. 49, no. 4, pp. 873–881, Apr. 2013, doi: 10.1016/j.eurpolymj.2012.12.005.

- [34] R. Turco *et al.*, "Poly (lactic acid)/thermoplastic starch films: Effect of cardoon seed epoxidized oil on their chemophysical, mechanical, and barrier properties," *Coatings*, vol. 9, no. 9, pp. 1–20, 2019, doi: 10.3390/coatings9090574.
- [35] S. H. Clasen, C. M. O. Müller, and A. T. N. Pires, "Maleic Anhydride as a Compatibilizer and Plasticizer in TPS/PLA Blends," *J Braz Chem Soc*, vol. 26, no. 8, pp. 1583–1590, Aug. 2015, doi: 10.5935/0103-5053.20150126.
- [36] W. Wu, G. Wu, and H. Zhang, "Effect of wood flour as nucleating agent on the isothermal crystallization of poly(lactic acid)," *Polymers for Advanced Technologies*, vol. 28, no. 2, pp. 252–260, 2017, doi: 10.1002/pat.3881.
- [37] L. Chang and E. M. Woo, "Crystallization of poly(3-hydroxybutyrate) with stereocomplexed polylactide as biodegradable nucleation agent," *Polymer Engineering and Science*, vol. 52, no. 7, pp. 1413–1419, 2012, doi: 10.1002/pen.23081.
- [38] T. Chen, G. Jiang, G. Li, Z. Wu, and J. Zhang, "Poly(ethylene glycol-co-1,4-cyclohexanedimethanol terephthalate) random copolymers: Effect of copolymer composition and microstructure on the thermal properties and crystallization behavior," *RSC Advances*, vol. 5, no. 74, pp. 60570–60580, Jul. 2015, doi: 10.1039/c5ra09252c.
- [39] E. Fortunati, M. Peltzer, I. Armentano, L. Torre, A. Jiménez, and J. M. Kenny, "Effects of modified cellulose nanocrystals on the barrier and migration properties of PLA nanobiocomposites," *Carbohydrate Polymers*, vol. 90, no. 2, pp. 948–956, Oct. 2012, doi: 10.1016/j.carbpol.2012.06.025.
- [40] M. Hietala, A. P. Mathew, and K. Oksman, "Bionanocomposites of thermoplastic starch and cellulose nanofibers manufactured using twin-screw extrusion," *European Polymer Journal*, vol. 49, no. 4, pp. 950–956, Apr. 2013, doi:10.1016/j.eurpolymj.2012.10.016.
- [41] L. M. Matuana, S. S. Karkhanis, N. M. Stark, and R. C. Sabo, "Cellulose Nanocrystals as Barrier Performance Enhancer of Extrusion-Blown PLA Films for Food Applications," *biotech, biomaterials and biomedical*, 2016.
- [42] S. S. Karkhanis, N. M. Stark, R. C. Sabo, and L. M. Matuana, "Performance of Poly(lactic acid)/ Cellulose Nanocrystal Composite Blown Films Processed by Two Different Compounding Approaches," *Polymer Engineering & Science*, vol. 58, pp. 1965–1974, 2018, doi: 10.1002/pen.24806.
- [43] G. Kale, R. Auras, S. P. Singh, and R. Narayan, "Biodegradability of polylactide bottles in real and simulated composting conditions," *Polymer Testing*, vol. 26, no. 8, pp. 1049–1061, Dec. 2007.

[44] N. K. Kalita, S. M. Bhasney, A. Kalamdhad, and V. Katiyar, "Biodegradable kinetics and behavior of bio-based polyblends under simulated aerobic composting conditions," *Journal of Environmental Management*, vol. 261, p. 110211, May 2020, doi: 10.1016/J.JENVMAN.2020.110211.

[45] N. K. Kalita, A. Sarmah, S. M. Bhasney, A. Kalamdhad, and V. Katiyar, "Demonstrating an ideal compostable plastic using biodegradability kinetics of poly(lactic acid) (PLA) based green biocomposite films under aerobic composting conditions," *Environmental Challenges*, vol. 3, p. 100030, Apr. 2021, doi: 10.1016/J.ENVC.2021.100030.

[46] B. Y. Shin, R. Narayan, S. Il Lee, and T. J. Lee, "Morphology and rheological properties of blends of chemically modified thermoplastic starch and polycaprolactone," *Polymer Engineering & Science*, vol. 48, no. 11, pp. 2126–2133, Nov. 2008, doi: 10.1002/pen.21123.

[47] P. Dubois and R. Narayan, "Biodegradable compositions by reactive processing of aliphatic polyester/polysaccharide blends," *Macromolecular Symposia*, vol. 198, no. 1, pp. 233–244, Aug. 2003, doi: 10.1002/masy.200350820.

5. ANTIMICROBIAL SOLID STARCH-IODINE COMPLEX VIA REACTIVE EXTRUSION AND ITS APPLICATION IN PLA-PBAT BLOWN FILMS

5.1 ABSTRACT

Solid starch-iodine complex was prepared in pellets form using ZSK-30 twin-screw extruder. Thermogravimetric (TGA) and isothermal TGA analysis of the pellets showed that there was no significant loss of iodine due to sublimation during reactive extrusion. The antifungal and antibacterial activity of the solid pellets was analyzed using dip coating on strawberries and Kirby Bauer test. These pellets were further blended with PLA-PBAT film formulations in different percentages to make blown films. Iodine containing blown films showed superior antibacterial activity against *E. coli* compared to PLA control films and the commercial silver antimicrobial containing films. SEM analysis of the films showed a non-uniform dispersion of starch-iodine complex in the film. Tensile strength and elongation at break in machine direction for the starch-iodine containing films was comparable to the control films in machine direction (MD) whereas tear strength was found to be better for the starch-iodine containing films in transverse direction (TD).

5.2 INTRODUCTION

Iodine is a well-known antimicrobial agent, used for more than a century in the pharmaceutical/medical industry[1, 2]. It has a broad spectrum of antimicrobial activity with efficacy against bacteria, mycobacteria, fungi, protozoa and viruses and can be used to treat both acute and chronic wounds. Tincture of iodine is a mixture of iodine and sodium/potassium iodide in water and ethanol and has been widely used in sterilization. Various patents and papers also describe incorporation of iodine into fabrics, polymers, and other materials for the sole purpose of antibacterial and antiviral activity[3–6]. The main disadvantage associated with iodine is its instability. A unique feature of iodine is its ability to bind with various polymeric materials[1]. Recently, a study was shown that povidone-iodine (PVP-I), a widely used antiseptic for skin disinfection, can be used to rapidly and effectively eliminate SARS-CoV-2 at a reduction rate >99.99% with a contact time of 30 s[2]. However, PVP-I is known for its toxicity at higher doses, and it has found limited uses in applications (automotive, packaging, etc.) outside the medical field[7].

As a biobased, biodegradable material, starch is a naturally occurring resource which is biocompatible and safe for humans. Amylose in starch is known to form complexes with iodide polyanions (blue colored complex). Various studies for structures of amylose-iodine complex have shown that amylose exists in the form of a helical spiral with each turn of the helix containing 6 glucose units and the iodine molecules get arranged along the spiral as triiodide ions[8–10]. Cross-linked starch iodine (CSI) has been studied for its antibacterial, antiviral activity[11,12]. Reactive extrusion has allowed mass production of thermoplastic starch (TPS) and maleated thermoplastic starch (MTPS)[13]. This TPS and MTPS is often added to other polymers like PLA, PBAT, PCL to improve their biobased content, certain

performance properties like oxygen barrier or crystallization, biodegradation etc., and to reduce the cost of the blends[14–16]. Iodine can be added during thermoplastic starch production in the extruder to make these thermoplastic starch-iodine complex pellets in solid form which can be used as a vehicle to introduce iodine in an environment, without the usual hazards associated with handling solid iodine. Targeted applications of this product could be - (1) As an additive for film to be applied in active packaging for food-safe packaging, (2) As an additive to make foams or filters to be used in air filtration systems for deactivating airborne viruses, including SARS-CoV-2, and (3) In pellet form as an additive to provide antibacterial, antiviral properties in other plastics and polymers.

In the present study, solid thermoplastic starch-iodine complex was prepared in the form of pellets in ZSK 30 twin screw extruder. These pellets were characterized for iodine content and their antimicrobial activity. Further, this complex was added in various proportions to PLA-PBAT blown films and the morphological, mechanical, thermal, and antibacterial properties of these films were evaluated.

5.3 STARCH IODINE COMPLEX

As explained in the previous chapters, starch is a mixture of amylose and amylopectin. In the Amylose unit all monomers are D-glucose which have α -1,4 linkages. Because of the bond angles and arrangement of these acetal linkages, amylose forms a spiral spring like structure as shown in the Figure 5.1 [17]

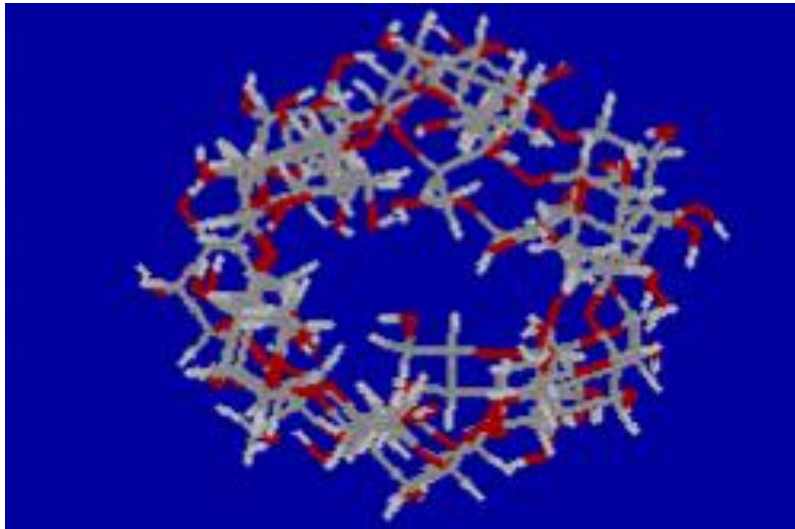
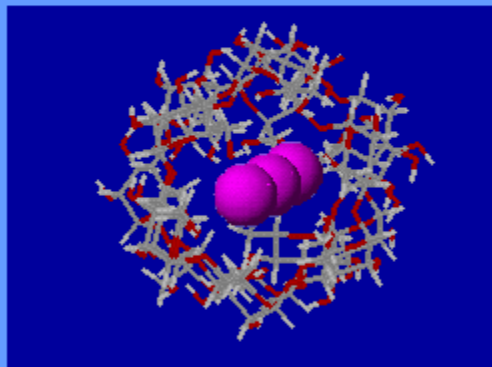


Figure 5.1: Amylose coil structure - due to acetal linkages

Iodine is not very soluble in water. Iodine is dissolved in water in presence of potassium iodide (KI) to form a linear triiodide (I_3^-) complex that is soluble in water. This triiodide molecule then slips up inside the hollow amylose helix. Water molecules interact with iodide to form a charge transfer complex which causes the blue color of the complex as shown in the Figure 5.2.

Starch - Iodine Complex



Iodine slides into starch coil
to give a blue-black color

Figure 5.2: Structure of amylose-iodine complex

5.4 **EXPERIMENTAL SECTION**

5.4.1 Materials

High amylose corn starch with an initial moisture content of 12.8% (w/w) was obtained from National Starch (NJ, USA). Glycerol was obtained from J.T. Baker (NJ, USA) and was used as received. 2,5-bis(tert-butyl-2,5-dimethylhexane), 90% (Luperox 101), and Maleic anhydride (MA) were obtained from and Sigma–Aldrich (WI, USA). Molecular Iodine and Potassium iodide were obtained from Thermo Fisher Scientific (MA, USA). Strawberries were bought from a local grocery store and were washed with distilled water and dried before use. The bacterial strain *E. Coli* (TB0484) was used for bacterial cultivation and antimicrobial activity tests.

5.4.2 Preparation of MTPS-Iodine pellets

The MTPS-iodine pellets were prepared in co-rotating twin-screw CENTURY ZSK-30 extruder (MI, USA) using a process similar to described in Kulkarni;2021[15] . The optimum quantity of iodine and potassium iodide to be added in the high amylose corn starch was calculated as shown in the appendix 1. For 1 kg of total masterbatch, Potassium Iodide 26.9 gm (0.162 mol) was dissolved in 40 ml of water. To this solution, 53.2 g (0.419 mol) of solid Iodine was added with stirring. The result was a black/blue colored solution of iodide anions in water. Pre-dried high amylose corn starch (800g) was mixed with glycerol (200g) to make 1000 gm of starch glycerol mixture. To this mixture, 20 gm of maleic anhydride and 2 gm of Luperox 101 were added. Then the Iodide solution was added to form a deep blue colored powder. This powder was then extruded in a Century ZSK-30 co-rotating twin screw extruder using temperature profile as 60/80/100/110/120/120/130/140/140/130. Other screw speed, feed rate and vent conditions were the same as that used for MTPS [15] The

extrudate coming out of the extruder was air-cooled and pelletized simultaneously using Scheer Bay pelletizer as shown in Figure 5.3.

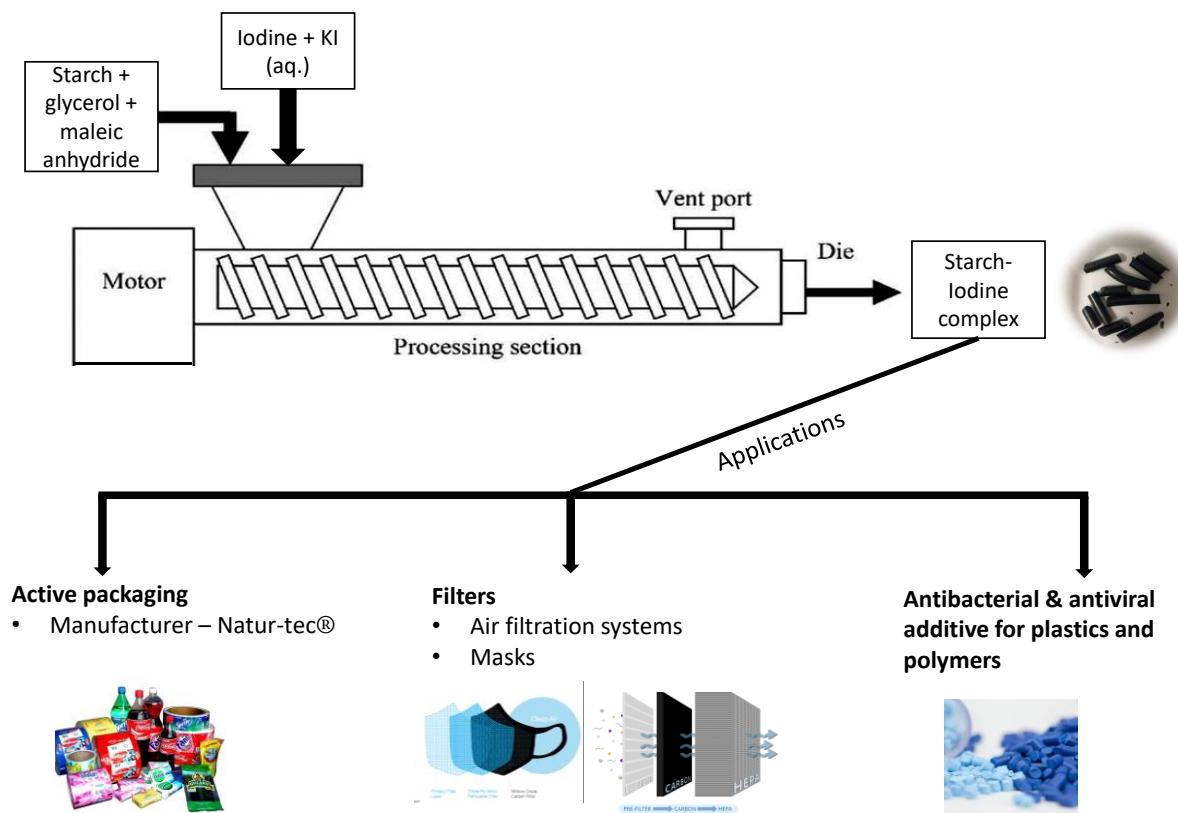


Figure 5.3: Production of MTPS-iodine pellets via reactive extrusion

5.4.3 Preparation of PLA-PBAT-Starch-Iodine films

The MTPS-iodine masterbatch pellets were shipped to Natur-tec® (MN, USA) for production of blown films. The MTPS-iodine pellets were mixed in 10 and 18% by wt. with commercial PLA and PBAT film formulations (detailed formulation not disclosed here) to yield films with 0.7% and 1.3 % iodine in the resulting films. A LabTech LE20-30/C (Thailand) extruder with 20mm diameter screw with L:D of 30:1 and LabTech LF-250 blown film frame (Thailand) with die diameter of 2 inches were used for making these films. The detailed temperature and processing conditions for making the films were as shown in Table 5.1. Three different films with different thickness and iodine content were prepared as shown in the Table 5.2

and their properties were compared with neat PLA blown films and a commercial antimicrobial film supplied by Natur-tec® with silver as the antimicrobial agent.

Table 5.1: Temperature and processing conditions for making blown films

Upper Die Temp (°C)	Lower Die Temp (°C)	Die Adapter Temp (°C)	Zone 3 (°C)	Zone 2 (°C)	Zone 1 (°C)	Screw RPM	Upper Pull Rate (ft/min)	Lower Pull Rate (ft/min)	Motor Amps
170	170	165	160	154	148	100	10	10.5	77

Table 5.2: Sample name and composition

Formulation code	Iodine content	Film thickness
SI1	0.7 %	1 mil (25.4 µm)
SI2	0.7%	2 mil (50.8 µm)
SI3	1.3%	2 mil (50.8 µm)
PLA film	-	1 mil (25.4 µm)
AM film	Silver Antimicrobial present	1 mil (25.4 µm)

5.5 CHARACTERIZATION AND ANALYSIS

5.5.1 *Thermogravimetric analysis (TGA)*

The MTPS-iodine pellets, solid iodine and neat MTPS pellets without any iodine were analyzed using TGA. TGA measurements of all the samples were conducted under an inert atmosphere of nitrogen using a TGA Q50 (TA Instruments, New Castle, DE, USA). The general sample weight used was 5-7 mg. The sample was placed in an aluminum pan and was heated to 600 °C at the rate of 10 °C/min. The weight loss (%) of a sample as a function of temperature (°C) was obtained from this analysis. Then, to determine the Iodine content in MTPS-iodine pellets, isothermal TGAs were also run on neat MTPS and MTPS-iodine samples. Sample was heated to 160 C and maintained at that temperature for 30 mins. Then it was heated further to 550°C. Same was done with the control (neat MTPS) for comparison.

5.5.2 *Antimicrobial Properties: Antifungal test*

As a simple qualitative way for testing the antifungal properties of the synthesized starch-iodine pellets, it was dissolved in water and applied to fresh strawberries as a coating[18]. The solution was prepared by dissolving 1g and 2 g of starch-iodine pellets in water to yield 1% and 2 % solutions. Fresh strawberries were obtained from Meijer grocery store, East Lansing, MI. USA. The strawberries were washed carefully using distilled water and were air dried for 1 hour before use. Then 15 strawberries were selected based on uniform size, color, and absence of any physical or pathological damage. The fruits were evaluated for visual decay and weight loss. Then 5 strawberries each were coated with 1% and 2% solutions of starch-iodine and 5 were kept uncoated. All the strawberries were kept in 75% relative humidity chamber for 11 days and were tested for visual decay, fungal growth, and weight loss immediately after coating (day 0) and at day 2, 4, 6, 8 and 11.

5.5.3 Visual decay and weight loss of strawberries

Photographs of the strawberries were taken every day and were observed for signs of lesion, brown spots, or fungal growth. Weight loss of strawberries was expressed as percentage loss based on initial weight measured after coating[18]. Weight loss was calculated using the equation below:

Equation 5.1

$$\text{Weight loss} = \frac{\text{initial weight} - \text{final weight}}{\text{initial weight}} \times 100$$

5.5.4 Antimicrobial properties

The antimicrobial properties were tested using the disk diffusion assay and direct inoculation assay following Shojaeiarani et. al, 2020[19]. *Escherichia coli* (*E. coli*) strain (TB0484) was streaked on nutrient media from a -80°C freezer stock dissolved in glycerol. One colony was picked and used to inoculate 5 ml nutrient (TSB) broth. The bacteria were left to grow at 37°C for 18 hours.

Antibacterial (Kirby-Bauer Test) test

The disk diffusion test was performed on the synthesized MTPS-iodine pellets with iodine content of 6.7% by weight. 100 ml of the 18-hour broth culture was used to inoculate nutrient media plates, and a single pellet was kept in the middle. These plates were left to grow for 20 hours. Three replicates of plates were used for each pellet type. After 20 hours, zone of inhibition was indicative of the measure of antimicrobial property.

Antimicrobial properties: antibacterial (direct inoculation) test

The direct inoculation test was performed as per “ISO 22196- Measurement of antibacterial activity on plastics surfaces”. PLA control films, silver antimicrobial film (AM Film) and the

PLA films containing different concentrations of iodine were cut in sterile squares of 5 cm X 5 cm. The stomacher bag was cut in 4cm X 4cm, which was used to cover the films. 2 ml of 18-hour grown culture was centrifuged, the pellet was washed with 1XPBS (phosphate buffer saline) suspension buffer, centrifuged once again, and later dissolved in 2ml 1X PBS, 100 µl of which was placed on top of every PLA film in a petri plate, covered with the stomacher bag film and placed in the 37°C incubator for 24 hours. The enumeration of *E. coli* from PLA control films were taken at the time of inoculation and after 24 hours, whereas readings from all the test films were taken after 24 hours. To enumerate *E. coli*, the inoculated film sandwich was dropped with a set of sterile forceps in small sterile Whirlpack bags with 10 ml of 1X PBS buffer, mixed for 2 minutes, diluted at different concentrations, and plated on to nutrient media. Three technical replicates were tested for all the experiments. More than three biological replicates were tested for each film type.

5.5.5 Mechanical Properties

The tensile strength, tear strength and penetration strength of PLA control film supplied by Natur-tec® were compared with the Starch-iodine-PLA film samples SI1, SI2 and SI3. The samples were stored for 24 hours at 25 °C in a humidity chamber with RH of 50% before any analysis. Tensile testing was performed using an Instron model 5544 (Instron, Norwood, MA, USA) with a 100 N load cell and grip separation speed of 20 inch/min as per ASTM D882-10. Data from five samples of each formulation were averaged and compared with the properties of control PLA films. Tear strength test was performed using Thwing-Albert Elmendorf tear tester (NJ, USA) as per ASTM D1922. Five film samples were prepared and tested in the machine direction (MD) and transverse direction (TD) for each group.

5.5.6 Scanning Electron Microscopy

A JOEL 6610 LV scanning electron microscope (JEOL Ltd., Tokyo, Japan) was used to study the dispersion of MTPS-iodine in PLA films using the fracture surfaces of all samples. The films were treated with 6 N HCl for 24 h to remove the MTPS phase from the samples and air-dried for 12 h in a fume hood. Then the films were immersed in liquid nitrogen for ~2 min and then fractured. Fracture surfaces were mounted on aluminum stubs using high vacuum carbon tabs and coated with gold using a sputter coater and examined using JOEL at 500× magnification at 10 kV.

5.6 RESULTS AND DISCUSSION

5.6.1 *Iodine content evaluation*

During the MTPS-iodine pellets preparation, iodine and KI were added to the starch glycerol mixture to give a total iodine content of 6.7 %. However, during extrusion there is a possibility of iodine sublimation at the higher temperatures. Hence, to calculate the final content of iodine retained in the pellets after cooling, thermogravimetric analysis was used. From the derivative thermogravimetric graphs (DTG) of neat MTPS (without iodine), iodine and MTPS-iodine the peak degradation temperatures for each of the compounds were determined (Figure 5.4). It was found that MTPS and MTPS-iodine start degrading above 180-200°C, whereas the complete degradation of iodine is completed by 150°C, with peak degradation temperature at 133°C. Hence, to calculate % iodine present in the MTPS-iodine sample, it was heated to 160°C and maintained at that temperature for 30 mins to ensure all the iodine present in the sample is degraded. Then it was heated further to 550° C. Same was done with the control (neat MTPS) for comparison. This was done in triplicate to get an average iodine percentage. Figure 5.5 shows the isothermal TGA curves for MTPS and MTPS-iodine. For neat MTPS, the average weight loss from 25 to 200°C was 3.52% which might be due to the moisture present. For MTPS-iodine samples, the average weight loss from 25 to 200°C was found to be 10.18%. So, it was concluded that the difference in the weight loss between these two samples corresponded to the amount of iodine present in the MTPS-iodine sample which was calculated as 6.66 %. Thus, the total amount of iodine added during the pellets' preparation (6.7% by weight) and the iodine present in the final pellets after cooling down (6.66% by weight) was similar and no significant iodine loss happened during the extrusion step.

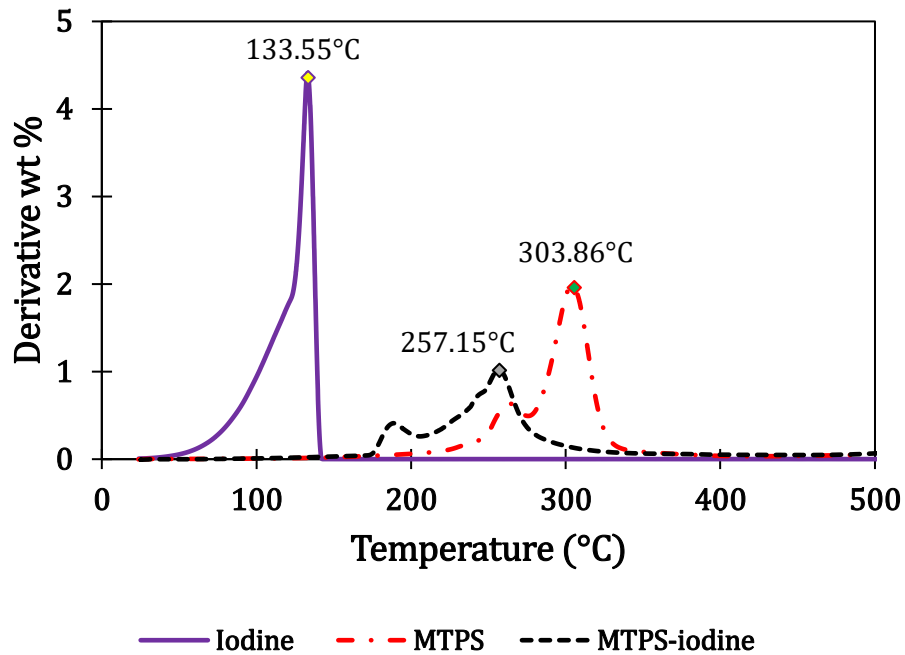


Figure 5.4: DTG curves for MTPS, MTPS-iodine and iodine

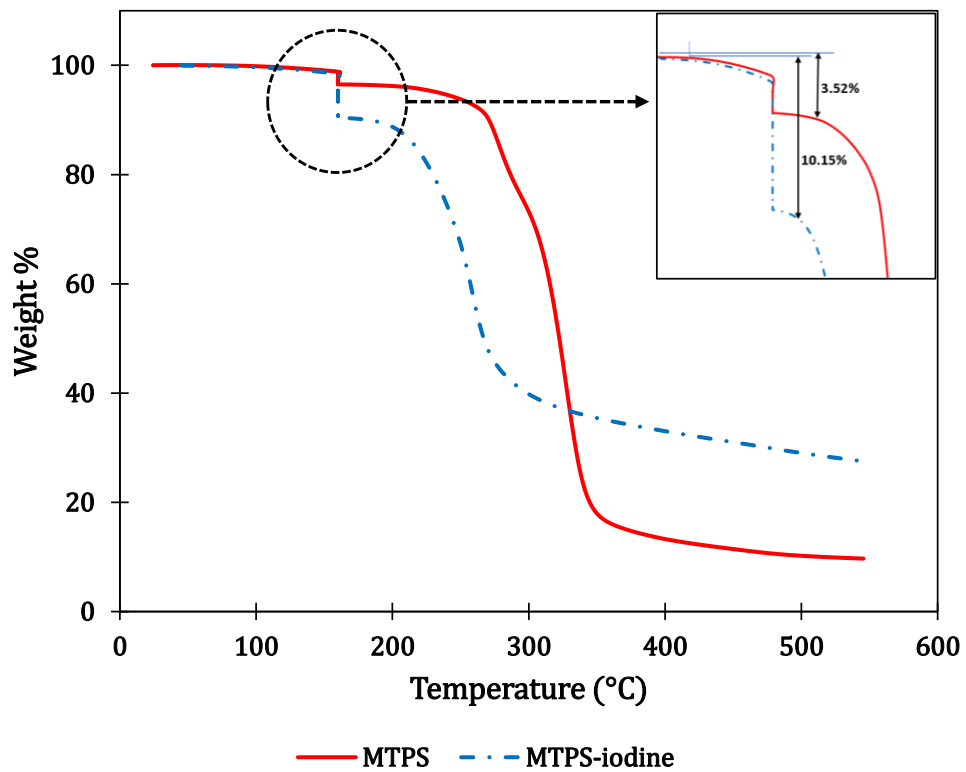


Figure 5.5: Isothermal TGA for MTPS and MTPS-iodine

5.6.2 Antifungal properties: Changes in weight loss and visual decay

To determine the effectiveness of starch-iodine for antifungal properties, weight loss and visual decay of strawberries were observed every other day and were compared to the control (uncoated) samples. Figure 5.6 shows the summary of the procedure followed and the results for this testing. The effect of coating the strawberries with starch-iodine solution on weight loss is shown in the weight loss analysis graph. It was observed that the weight loss increased with increasing storage period for all the treatments. There was no significant difference between the weight loss of control and 1% starch-iodine coated samples. Control and 1% starch-iodine coated samples showed higher weight loss compared to the 2% starch-iodine coated samples. Visual fungal decay started quickly on the control samples on day 4 of the storage. Coated samples started showing visual decay on day 6. For 2% starch-iodine coated samples the visual decay was even less, and it started on day 8 of the storage. Thus, the starch-iodine coating showed great potential in reducing the fungal growth and visual decay for the strawberries for extended time.

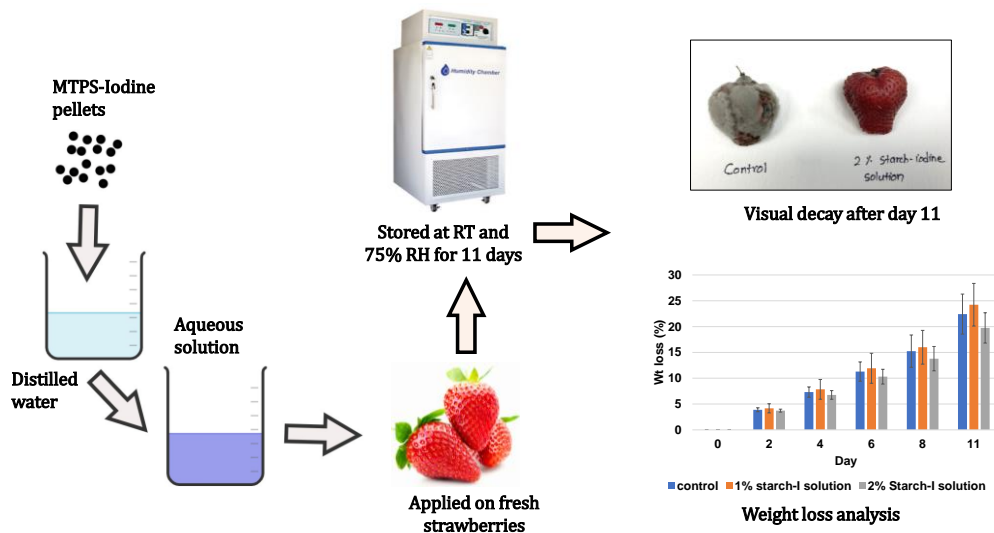


Figure 5.6: Weight loss and visual decay analysis for coated and uncoated strawberries

This was a good preliminary test as a proof-of-concept for establishing the antifungal-antimicrobial properties of the starch-iodine pellets. In case of its use for actual food applications, further detailed studies for checking the compatibility of this formulation with human body, studies on toxicity of iodine, edibility of this coating will all have to be done. Those were not focused on in this project.

5.6.3 Antimicrobial activity studies on the pellets and films

Two separate assays were employed to evaluate the antimicrobial activity of starch-iodine pellets and the blown films. First, a disk diffusion method was used for starch-iodine pellets and films. A clear zone of inhibition was observed in the bacterial lawn around the pellets (Figure 5.7-a). For the films, there was no growth on the surface of the films, no clear zone of inhibition was observed for them (pictures not shown). It could be due to factors such as diffusibility of iodine from the film.

In a separate approach, a slightly modified direct inoculation method “ISO 22196- Measurement of antibacterial activity on plastics surfaces” was used, where *E. coli* cells were directly inoculated on the surface of the films. The bacterial counts were observed on PLA control and test films after the 24 h of inoculation in comparison to the bacterial counts observed on the PLA control films at the time of inoculation (Figure 5.7 b-f). The differences in the average change in log CFU/ml were calculated. Figure 5.8 shows the average results for CFU/ml for all the samples.

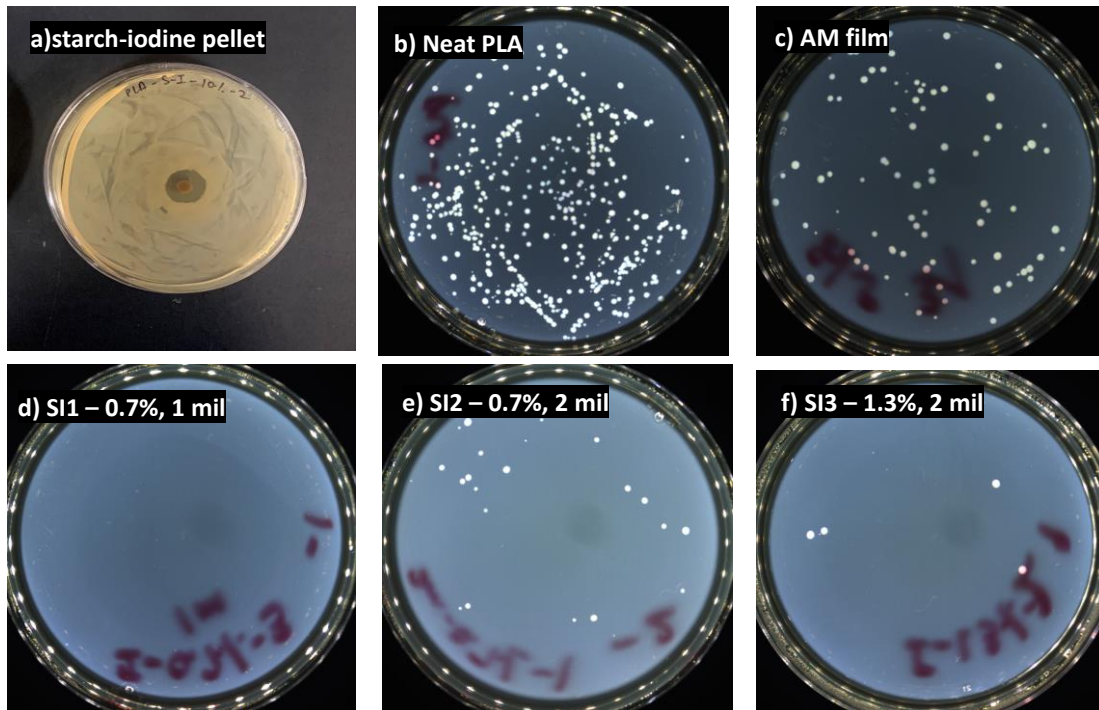


Figure 5.7: Photographs of the petri plates from disk diffusion and direct inoculation test with *E. coli*. a) Kirby Bauer test on starch-iodine pellets showing antibacterial zone of inhibition b)-f) bacterial colonies growth on the petri plates after 24 hours b) control PLA films c) AM: Silver antimicrobial films d) SI1: starch-iodine-PLA films with 0.7% iodine and 1 mil thickness e) SI2: starch-iodine-PLA films with 0.7% iodine and 2 mil thickness f) SI3: starch-iodine-PLA films with 1.3% iodine and 2 mil thickness

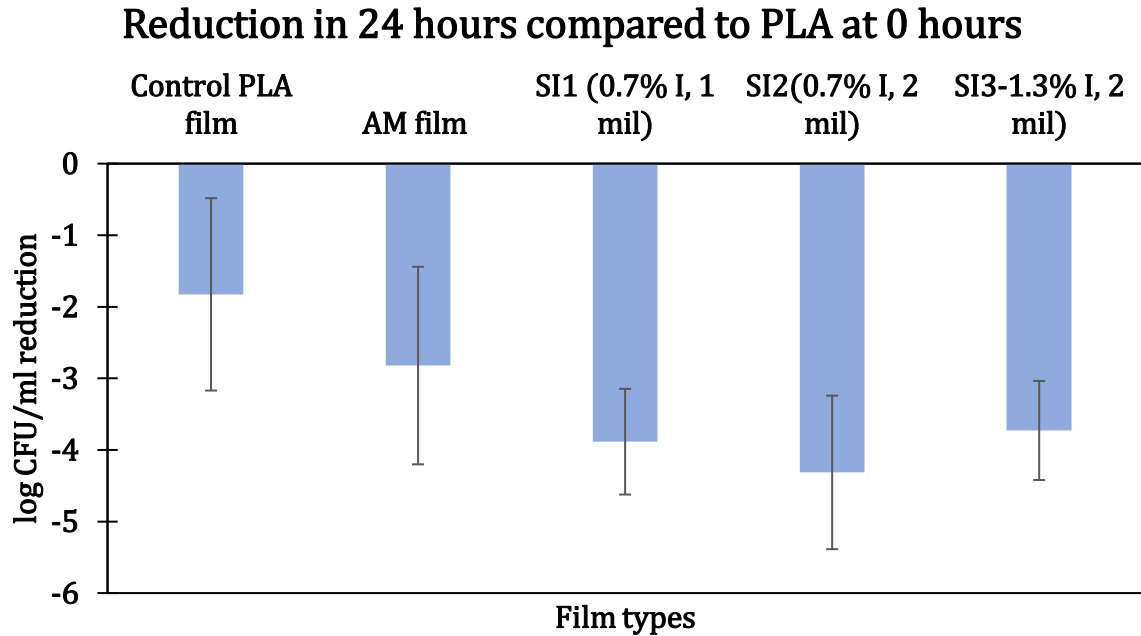


Figure 5.8: Average change in Log CFU/ml of the Escherichia coli (*E. coli*) strains after 24 h incubation on five different PLA film configurations (control PLA;AM film and SI1, SI2 and SI3)

It was observed that survival of *E. coli* was negatively impacted by all the films during incubation compared to the control films. All the iodine containing films (SI1, SI2 and SI3), showed a greater negative impact on survival of *E. coli* compared to the commercial antimicrobial film supplied by Natur-tec® (AM film). It should be noted that, these values represented in the graph are not an actual representation of all the replicates. During these studies, for multiple biological replicates a limit of detection was reached. i.e., no growth of bacteria was observed on any plates for that dilution (for example- Figure 5.7 d and f). Log CFU/ml values for those replicates were not calculated and were not included while plotting the graph. Considering this limit, it was observed that SI3 showed the best performance. The limit of detection was reached for the highest number of replicates for this sample followed by SI1 and SI2.

5.6.4 Mechanical Properties and morphology of the films

Mechanical properties like tensile strength, extension at break and tear strength were measured for the PLA-MTPS films (SI1, SI2 and SI3) and were compared with the control PLA films supplied by Natur-tec®. Tensile strength in machine direction (MD) for SI1 and SI2 was comparable to the control PLA films (Figure 5.9-a). In TD, a significant reduction in the tensile strength and elongation at break was observed (Figure 5.9). This might be due to the fact that the dispersion of MTPS-iodine complex in the PLA-PBAT blends used for blown film was poor. This was also observed in the morphology studies done on the fractured surfaces of the films (Figure 5.10). Two images for the same sample represent different areas on the films fractured surfaces. The cavities represent the MTPS-iodine phase that was leached out with concentrated HCL. It was observed that there were some areas where the MTPS-iodine phase was very concentrated. Large size cavities observed in Figure 5.10 b, e and h represent the agglomeration of MTPS-iodine phase in the films. There were also some areas which had very less concentration of MTPS-iodine (Figure 5.10- c,f and i). This confirmed that the MTPS-iodine was not uniformly distributed in the films. This agglomeration was more pronounced in SI1 and SI2. SI3 samples showed comparatively smaller size of the agglomerates and they were also distributed more uniformly compared to SI1 and SI2. This maybe be the reason why the mechanical properties of SI3 were comparable, or even better in some cases (for example – tear strength in TD) than SI1 and SI2, even though the MTPS-iodine content was almost double in these films. Better distribution of the additives helps in enhancing the mechanical properties of the films. This was also observed visually by looking at the films themselves. As shown in Figure 5.10-a and d, the SI1 and SI2 have visual stripes in the films in some places indicating a poor dispersion

of the additive. For SI3, the run was smoother, and we could not see any visual difference in the dispersion of the additive (Figure 5.10-g). Starch is hydrophilic and polyesters are hydrophobic. So inherently it is difficult to disperse starch or starch-based compounds in PLA or other hydrophobic polyesters. Using modified thermoplastic starch like MTPS improves the compatibility as shown in chapter 3 and 4 [16, 20]. However, it was observed that the dispersion of MTPS-iodine in blown films was not uniform in this case. One way to improve the dispersion could be to make graft polyester of MTPS-iodine with PBAT as studied by Hablot et al. [16] and then blend that with the blown film's formulation.

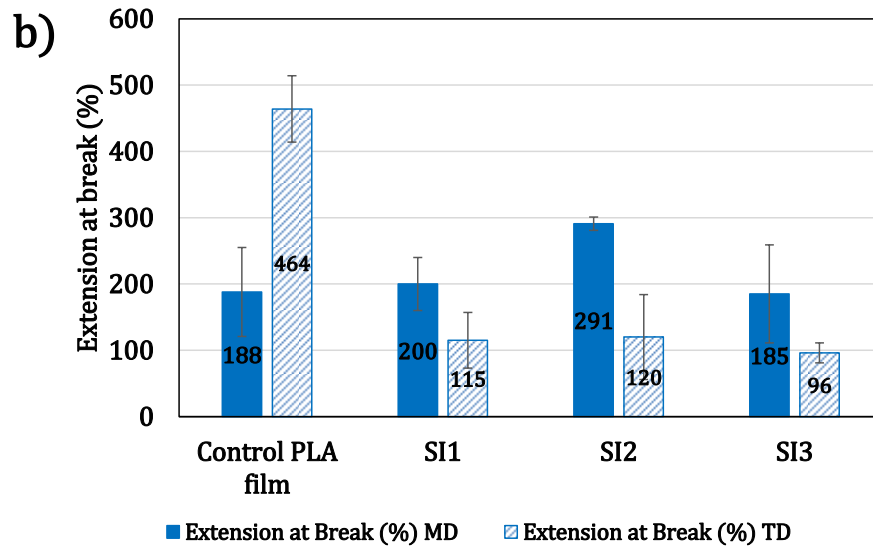
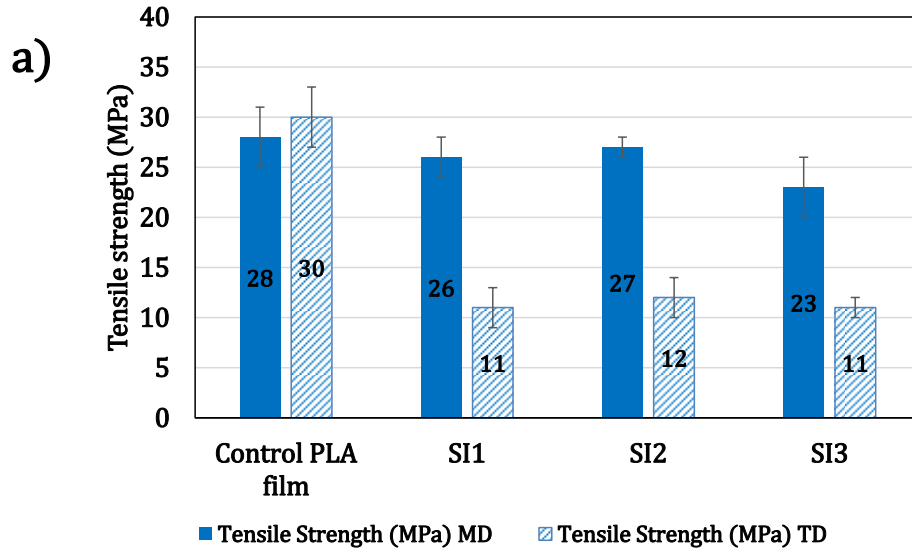


Figure 5.9: Mechanical properties for the different PLA blown film formulations in machine and transverse direction a) tensile strength b) Elongation at break c) Tear strength

Figure 5.9 cont'd

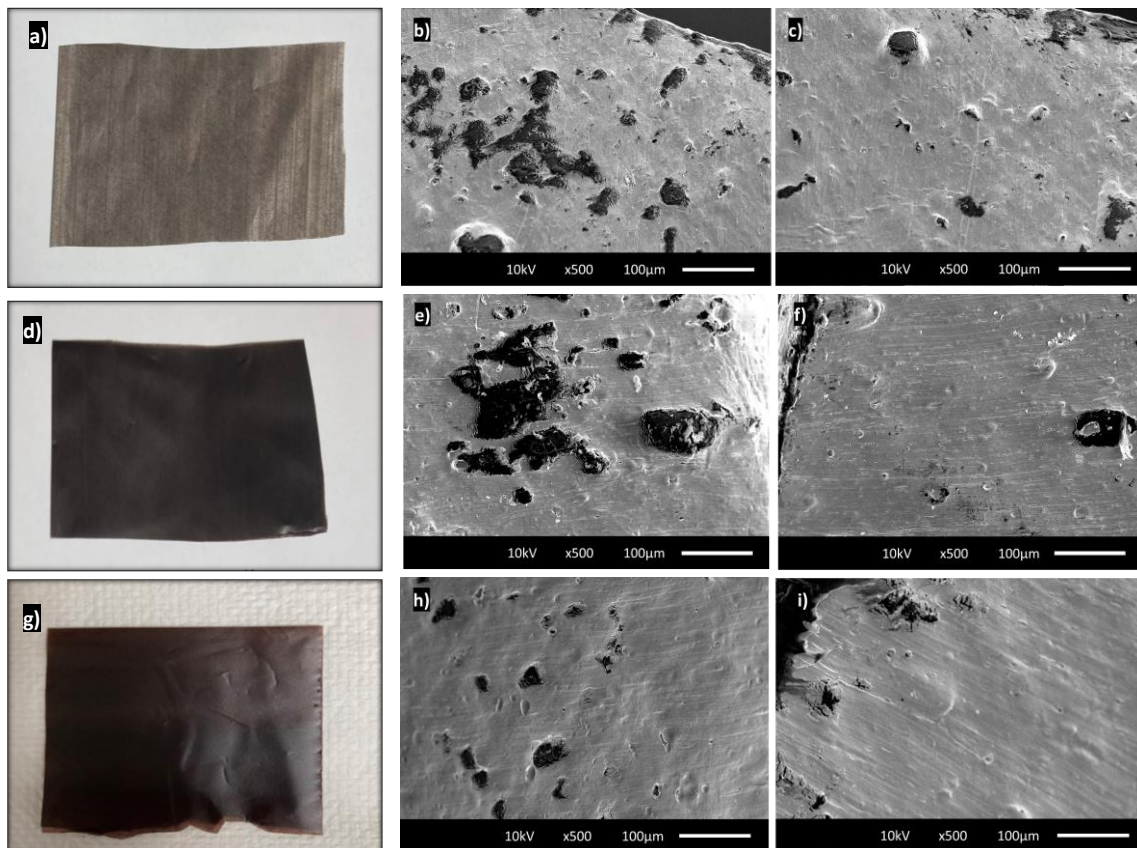
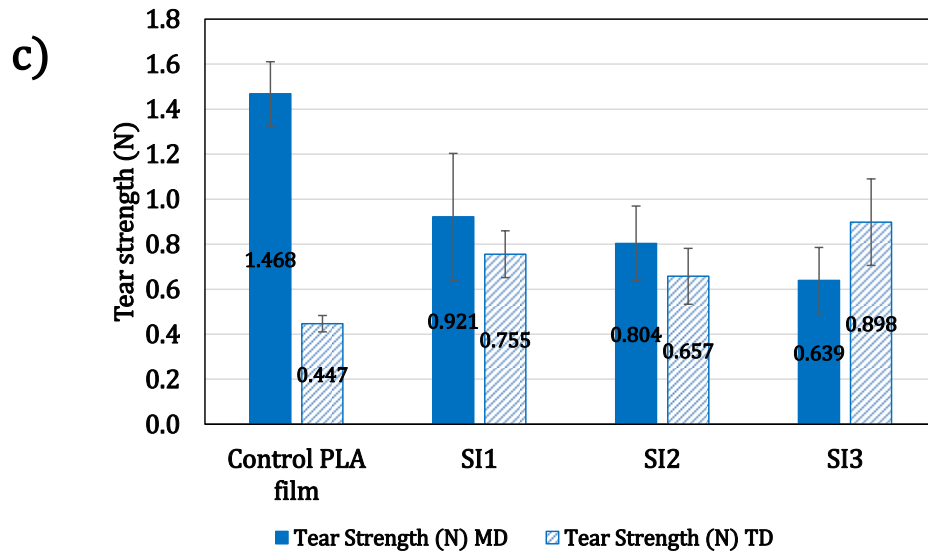


Figure 5.10: Visual and SEM images of the fractured surface of the films after selective extraction of MTPS-iodine phase a), b) and c) : SI1- 0.7% iodine, 1 mil; d), e) and f) : SI2 - 0.7 % iodine, 2 mil; g),h) and i) : 1.3% iodine, 2 mil

5.7 CONCLUSIONS AND FUTURE WORK

Solid MTPS-iodine complex was prepared in a ZSK-30 twin screw extruder. The masterbatch pellets contained 6.7% of iodine by weight. TGA analysis of these pellets confirmed that there was no significant loss of iodine due to sublimation during the reactive extrusion process. This MTPS-iodine complex was dissolved in water and was coated on strawberries to check its antifungal properties. The weight loss studies, and visual decay observations established that these pellets have great potential in reducing the fungal growth and visual decay for the strawberries for extended time. Antibacterial properties for the pellets against *E. Coli* were also analyzed using Kirby Bauer test. The presence of zone of inhibition clearly indicated the antibacterial activity of pellets against *E. Coli*. These pellets were further used as antimicrobial additive to make three PLA-PBAT blown films with two different thicknesses (1 mil and 2 mil) and 2 different iodine concentrations (0.7% and 1.3% by weight). The antimicrobial activity of the films against *E. Coli* was analyzed using ISO 22196 method. Colony forming units were counted and Log CFU/ml reduction values were reported for all the films. It showed that the films with 2 mil thickness and 1.3 % iodine concentration (SI3), were the most effective against *E. coli* followed by the films with 0.7% iodine and 1 mil thickness (SI1) and the films with 0.7% iodine and 2 mil thickness (SI2). In general, all the films containing iodine showed superior antimicrobial activity vs *E. Coli* as compared to the control PLA films and the commercial silver antimicrobial (AM film) containing films. SEM imaging of the fractured surfaces of the films showed poor dispersion of MTPS-iodine complex in the blown films. This also explained the loss of tensile strength and elongation at break in transverse direction for the SI1 and SI2 blown films compared to control PLA films. This might be due to the hydrophilic nature of starch which makes it difficult to blend with

hydrophobic polymers like PLA and PBAT. One way to improve the dispersion might be to make graft copolyesters of MTPS-iodine and PBAT similar to the work done by Hablot et. al., 2013[16] and then use that as an additive in the blown film formulation.

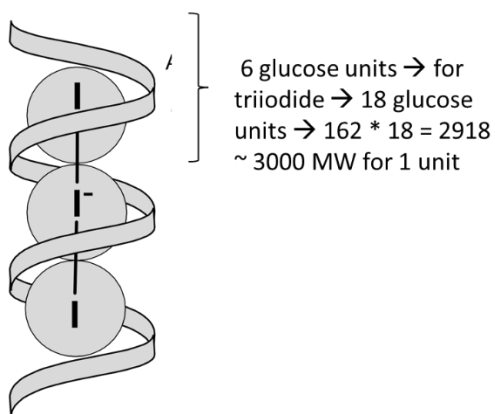
This solid MTPS-iodine complex can be used as an easy and effective way to introduce iodine in an environment, without the usual hazards associated with handling solid iodine. One of the applications of this complex- an additive in the PLA-PBAT blown films was studied in detail in this project. Other applications of this product could be - as an additive to make foams or filters to be used in air filtration systems for deactivating airborne viruses, including SARS-CoV-2, in pellet form as a biobased additive to provide antibacterial, antimicrobial properties in other plastics and polymers. The antibacterial activity of pellets and films against *E. Coli* was studied in this project. Other gram positive and gram negative bacteria as well as antifungal and antiviral studies of these pellets and the products could be useful in establishing the broad spectrum activity of this product and widen the scope for possible applications in many fields.

APPENDIX

APPENDIX

Calculation for iodine loading

Based on several studies done on structure and chemistry of amylose-iodine complex, it has been postulated that amylose in the complex assumes a 6-fold helical conformation and the iodine molecule slips inside the amylose coil. Iodine, by itself is not very soluble in water. Hence KI is added. Together, they form polyiodide ions in the form I_n^- . These facts were used to calculate the total theoretical quantity of iodine that can be added to the high amylose starch used in this project.



According to Baily et.al, 6 glucose units are required for 1 iodine atom.

So, for a tri-iodide ion, 18 glucose units are required

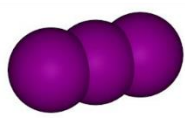
Molecular wt. for 1 anhydro glucose unit à 162 g/mol

Hence for 18 glucose units à $162 * 18 = 2918 \sim 3000$ g/mol

The high amylose starch used in this project has amylose content of 60-70% as given by the supplier.

An average of 65% amylose content was assumed for these calculations.

For making 1 kg of MTPS-iodine batch, the formulation was –



Triiodide I_3^-
Mw = 380.71



Iodine I_2
Mw = 253.8



Iodide I^-
Mw = 126.9

800 g starch + 200 g glycerol + 20g MA + catalyst

out of 800g, 65 % is amylose

$$800 \times 0.65 = 520 \text{ g amylose}$$

1 helix unit containing 1 triiodide ion = 3000 g/mol

$$\text{hence, } \frac{520}{3000} = 0.173 \text{ moles of amylose helix units are present}$$

for 1: 1 ratio of amylose helix unit to triiodide, 0.173 moles of triiodide will be required

This corresponds to a total of 65.74 g of triiodide (43.96 g of iodine, and 21.78 g of iodide).

$$\frac{65.7}{800} = 8.21\% \text{ by wt of starch}$$

Assuming that there will be some loss in handling and processing, 10-12% extra iodine was added in the batch.

REFERENCES

REFERENCES

- [1] S. Moulay, "Molecular iodine/polymer complexes," *Journal of Polymer Engineering*, vol. 33, no. 5, pp. 389–443, 2013, doi: 10.1515/polyeng-2012-0122.
- [2] D. E. Anderson *et al.*, "Povidone-Iodine Demonstrates Rapid In Vitro Virucidal Activity Against SARS-CoV-2, The Virus Causing COVID-19 Disease," *Infectious Diseases and Therapy*, vol. 9, no. 3, p. 669, Sep. 2020, doi: 10.1007/S40121-020-00316-3.
- [3] T. L. Landsman *et al.*, "A shape memory foam composite with enhanced fluid uptake and bactericidal properties as a hemostatic agent," *Acta Biomaterialia*, vol. 47, pp. 91–99, 2017. doi: 10.1016/j.actbio.2016.10.008.
- [4] J. G. Lundin *et al.*, "Iodine binding and release from antimicrobial hemostatic polymer foams," *Reactive and Functional Polymers*, vol. 135, pp. 44–51, 2019. doi: 10.1016/j.reactfunctpolym.2018.12.009.
- [5] E. L. Papadopoulou, P. Valentini, F. Mussino, P. P. Pompa, A. Athanassiou, and I. S. Bayer, "Antibacterial bioelastomers with sustained povidone-iodine release," *Chemical Engineering Journal*, vol. 347, no. April, pp. 19–26, 2018, doi: 10.1016/j.cej.2018.04.091.
- [6] Richard J. Greffian N. AskillConnie C. Lee, "EP1028848A1 - Prepolymer compositions comprising an antimicrobial agent - Google Patents," EP1028848A1, Aug. 23, 2000 Accessed: Apr. 30, 2022. [Online]. Available: <https://patents.google.com/patent/EP1028848A1/en>.
- [7] S.-H. Li, Y. Wang, H.-B. Gao, K. Zhao, Y.-C. Hou, and W. Sun, "Experimental study on the toxicity of povidone-iodine solution in brain tissues of rabbits," *International Journal of Clinical and Experimental Medicine*, vol. 8, no. 9, p. 14863, 2015, Accessed: Mar. 28, 2022. [Online]. Available: [/pmc/articles/PMC4658857](https://pubmed.ncbi.nlm.nih.gov/2658857/).
- [8] W. Saenger, "The Structure of the Blue Starch-Iodine Complex," *Naturwissenschaften*, vol. 71, pp. 31–36, Jan. 1984, Accessed: Mar. 28, 2022. [Online]. Available: <https://link.springer.com/article/10.1007/BF00365977>.
- [9] X. Yu, C. Houtman, and R. H. Atalla, "The complex of amylose and iodine," *Carbohydrate Research*, vol. 292, pp. 129–141, Oct. 1996, doi: 10.1016/S0008-6215(96)91037-X.
- [10] "Starch and Iodine - Chemistry LibreTexts." [https://chem.libretexts.org/Bookshelves/Biological_Chemistry/Supplemental_Modules_\(Biological_Chemistry\)/Carbohydrates/Case_Studies/Starch_and_Iodine](https://chem.libretexts.org/Bookshelves/Biological_Chemistry/Supplemental_Modules_(Biological_Chemistry)/Carbohydrates/Case_Studies/Starch_and_Iodine) (accessed Mar. 28, 2022).

- [11] M. Tran, J. Castro, K. R. O'Brien, C. Pham, T. H. Bird, and P. M. Iovine, "Release Kinetics and Antimicrobial Properties of Iodinated Species Liberated from Physically and Chemically Modified Starch Granules," *Starch/Staerke*, vol. 72, no. 1–2, pp. 1–7, 2020, doi: 10.1002/star.201900134.
- [12] R. Klimaviciute, J. Bendoraitiene, R. Rutkaite, J. Siugzdaite, and A. Zemaitaitis, "Preparation, stability and antimicrobial activity of cationic cross-linked starch-iodine complexes," *Int J Biol Macromol*, vol. 51, no. 5, pp. 800–807, Dec. 2012, doi: 10.1016/j.IJBIOMAC.2012.07.025.
- [13] J. M. Raquez, Y. Nabar, M. Srinivasan, B. Y. Shin, R. Narayan, and P. Dubois, "Maleated thermoplastic starch by reactive extrusion," *Carbohydrate Polymers*, vol. 74, no. 2, pp. 159–169, 2008, doi: 10.1016/j.carbpol.2008.01.027.
- [14] J. M. Raquez, Y. Nabar, R. Narayan, and P. Dubois, "In Situ Compatibilization of Maleated Thermoplastic Starch / Polyester Melt-Blends by Reactive Extrusion," *Polymer Engineering & Science*, vol. 48, no. 9, pp. 1747–1754, Sep. 2008, doi: 10.1002/pen.
- [15] A. Kulkarni and R. Narayan, "Effects of Modified Thermoplastic Starch on Crystallization Kinetics and Barrier Properties of PLA," *Polymers (Basel)*, vol. 13, no. 23, Dec. 2021, doi: 10.3390/POLYM13234125.
- [16] E. Hablot *et al.*, "Reactive extrusion of glycerylated starch and starch-polyester graft copolymers," *European Polymer Journal*, vol. 49, no. 4, pp. 873–881, Apr. 2013, doi: 10.1016/j.eurpolymj.2012.12.005.
- [17] "Starch and Iodine - Chemistry LibreTexts." [https://chem.libretexts.org/Bookshelves/Biological_Chemistry/Supplemental_Modules_\(Biological_Chemistry\)/Carbohydrates/Case_Studies/Starch_and_Iodine](https://chem.libretexts.org/Bookshelves/Biological_Chemistry/Supplemental_Modules_(Biological_Chemistry)/Carbohydrates/Case_Studies/Starch_and_Iodine) (accessed Apr. 25, 2022).
- [18] I. Khan, C. N. Tango, R. Chelliah, and D. H. Oh, "Development of antimicrobial edible coating based on modified chitosan for the improvement of strawberries shelf life," *Food Science and Biotechnology*, vol. 28, no. 4, pp. 1257–1264, 2019, doi: 10.1007/s10068-018-00554-9.
- [19] J. Shojaeiarani, D. S. Bajwa, N. M. Stark, T. M. Bergholz, and A. L. Kraft, "Spin coating method improved the performance characteristics of films obtained from poly(lactic acid) and cellulose nanocrystals," *Sustainable Materials and Technologies*, vol. 26, p. e00212, 2020, doi: 10.1016/j.susmat.2020.e00212.
- [20] J. Wootthikanokkhan *et al.*, "Effect of blending conditions on mechanical, thermal, and rheological properties of plasticized poly(lactic acid)/maleated thermoplastic starch blends," *Journal of Applied Polymer Science*, vol. 124, no. 2, pp. 1012–1019, Apr. 2012, doi: 10.1002/APP.35142.

6. UNDERSTANDING BIODEGRADABILITY OF BIOBASED POLYMERS IN MARINE ENVIRONMENT

6.1 ABSTRACT

The use of biobased and biodegradable polymers instead of carbon-carbon backbone polymers promises to reduce plastics accumulation in natural environment. For most of the polymers, the biodegradation process is highly temperature dependent. We present a novel approach to study the effect of temperature on the biodegradability of cellulose and PHBV in an aqueous environment seeded with a biologically aggressive microbial inoculum. The testing was done at three different temperatures using ISO 14852. We use a global equation derived from reparametrized Arrhenius equation and the kinetic rate law to estimate the time required for 90% removal of polymer from the low temperature ocean environment. The time required for 90% biodegradation of PHBV at 10°C ranged from 6.2-6.9 years whereas it was found to be 1.1-1.2 years for cellulose. This model can be used to estimate the persistence of plastics in ocean in case of their inadvertent leakage. The progress of biodegradation was also monitored for any morphological, structural and chemical modifications to analyze the mechanism for PHBV biodegradation. Surface erosion by SEM and optical imaging, slight decrease of molecular weight by GPC and crystallinity and melting point changes by DSC all suggested the presence of enzymatic surface erosion mechanism for PHBV.

6.2 INTRODUCTION AND BACKGROUND

6.2.1 *Need for lifetime prediction and end of life analysis*

The end-of-life of plastics, particularly packaging and disposable products is raising serious concerns worldwide and driving regulations on plastics waste management in the USA and around the world. Ocean plastics pollution is of particular concern and articles in print and e-media appear daily on the subject. The global plastics pollution statistics indicate plastic pollution of 300 million tons/year out of which only 10% is recycled whereas 4.8-12.7 million tons enter into the ocean every year[1, 2]. "Petroleum-based polymers such as polyethylene, polypropylene, polystyrene, aromatic polyesters, and polyamides with strong C-C or C-heteroatom backbone are considered to be the main sources of environmental pollution with microplastics. In contrast, conventional biodegradable polymers (aliphatic and aliphatic-aromatic polyesters), such as polylactic acid (PLA), polycaprolactone (PCL), lactide-glycolide copolymers, have not attracted the main attention as sources of microplastics. Probable reasons could be the limited use of these polymers and the common misconception that they would degrade under any environmental conditions. However, biodegradable polymers degrade only under certain conditions (temperature, humidity, light, oxygen availability, and microorganisms)."[3] Complete biodegradation of plastics occurs when all of the original polymer is broken down to carbon dioxide, methane and water. All the biodegradation standards including ISO 14852, ASTM D6691, ISO 14851, ASTM D6400 etc. are static, and they generate the data for percent biodegradation data at a single temperature.

However, for most of the polymers this process is temperature dependent. For example, some plastics like PLA labelled as 'biodegradable' biodegrade only in industrial composting

conditions with temperatures of 58°C [4–6]. Some studies have shown upto 97% biodegradation of polymers based on PBAT in marine environment within 1 year [7, 8] However, these studies were done at a temperature of 30°C which hardly represent the temperatures of ocean. In another study by Atsuyoshi Nakayama et al. [9] biodegradation of aliphatic polyesters was studied in seawater at 2 different temperatures, and they found that the rate of biodegradation was almost twice at 27°C as compared to the rate at 10°C. This suggests that the temperature has a very strong impact on the activity of micro-organisms which control the rate of biodegradation. Another study has reported that temperature and rate of biodegradation soil environment follow Arrhenius relationship [10].

To our knowledge, no systematic efforts have been done till now to quantify the effect of temperature on the rate of biodegradation and predict the expected time for which the polymer will linger in the marine environment. The ocean water is divided into 3 parts- the surface layer, then a boundary layer called the thermocline and the deep ocean as shown in Figure 6.1. 90% of total volume of ocean is found below the thermocline in deep ocean. And most of this deep-water temperature is between 0-4°C [11]

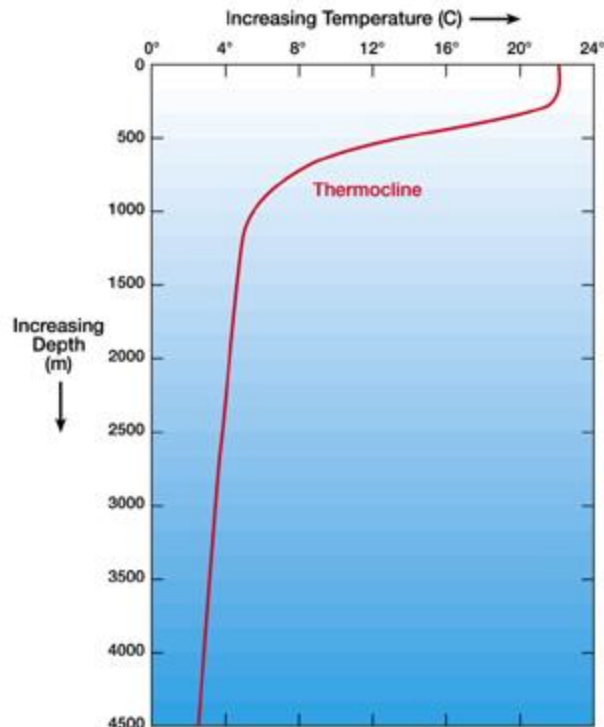


Figure 6.1: Temperature-depth Ocean water profile[11]

Thus, it is expected that the rate of biodegradation at such temperatures will be very low and they will exist in the ocean environment much longer than observed in lab studies done at 30°C. During this time the plastics will impact marine life and habitats. Therefore, unqualified “ocean biodegradability” claims and certifications based on room temperature respirometry analysis is misleading.

This paper provides a method based on kinetic analysis to estimate the time required for 90% removal of the polymer at low temperatures through microbial metabolism.

In this the biodegradation of so-called biodegradable polymers (PHBV) and cellulose was studied in aqueous environment at 3 different temperatures of 10, 30 and 40°C according to ISO 14852. A relation between the rate of biodegradation and temperature was found out using reparametrized Arrhenius equation and using that, the time required for complete biodegradation of PHBV and cellulose at actual sea temperatures i.e., 4°C was calculated. This

simulation-based approach is useful in estimating the potential environmental buildup of the polymer in low temperatures of marine environments. Further, the biodegradation mechanism for PHBV was also investigated. For this purpose, initial properties of the pellets (TGA, DSC, Molecular weight, pellet size and morphology) were characterized and the changes in these properties was monitored over the course of biodegradation. The percent biodegradation values were combined with other indicators like morphological, structural, and chemical modifications induced on the surface of the PHBV to for confirming surface erosion as the mechanism of PHBV biodegradation.

6.3 BIODEGRADATION PROCESS

Lifetime estimation for biodegradable polymers starts with the basic understanding of the biodegradation process, mechanisms of hydrolysis, factors affecting hydrolysis and the methods used for measuring the percent biodegradation.

Complete biodegradation of plastics occurs when all of the original polymer is broken down to carbon dioxide (aerobic biodegradation) and/or methane (anaerobic biodegradation) and water. In general, the biodegradation process is divided into four steps as shown in Figure 6.2 - i) biodeterioration, ii) depolymerization iii) bio assimilation, and iv) mineralization

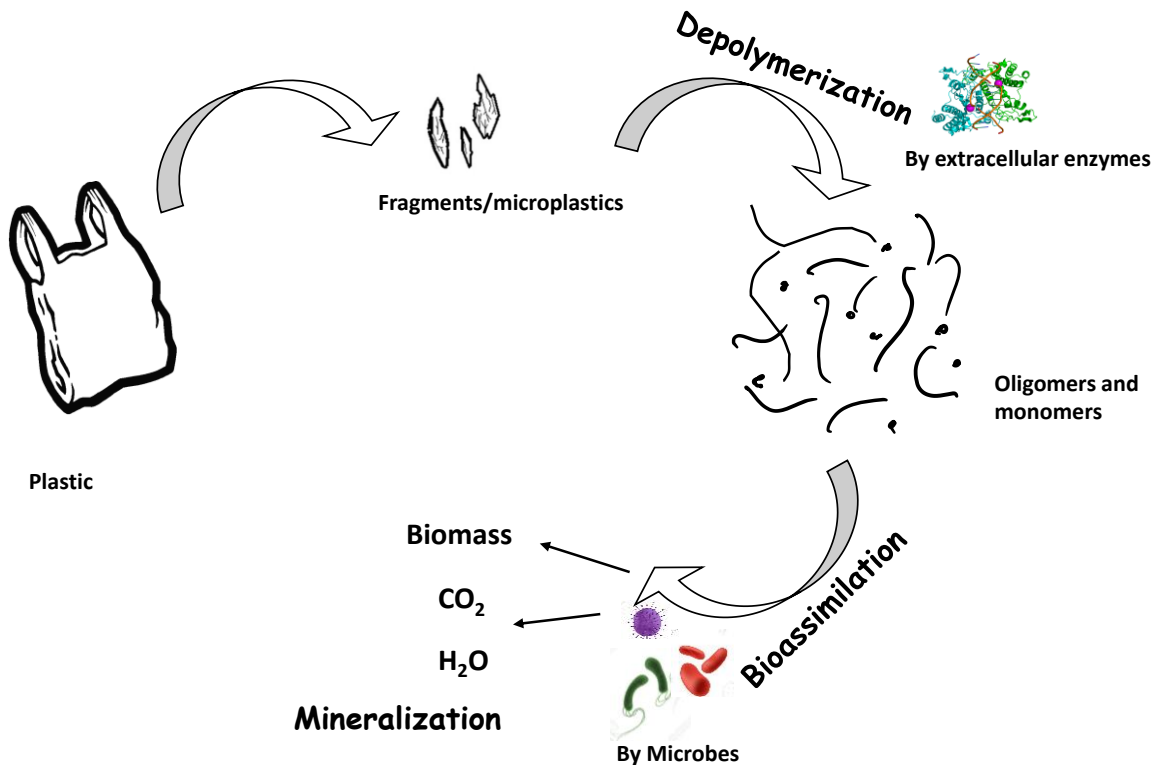


Figure 6.2: The different steps involved in the biodegradation process

Biodeterioration is the formation of a biofilm on the surface of the polymer or plastic. Different microorganisms like bacteria, fungi, protozoa, algae can develop consortia on and/or inside the surface of the material. They can either adhere physically to the surface

with a secreted glue kind of material or can enter inside the surface via chemical deterioration [12, 13]. Formation of biofilm increases the size of pores and promotes formation of cracks on the surface of the material reducing the resistance and durability. Polymer is a very high molecular weight compound and hence unable to enter the cell wall or cytoplasmic membrane of microorganisms. Depolymerization or **biofragmentation** is the process of conversion of high molecular weight polymer to oligomers, dimers and monomers. Then in the step of **assimilation**, microorganisms use this as a substrate for growth and reproduction. Once inside cells, the molecules are oxidized through catabolic pathways like glycolysis, oxidative phosphorylation and electron transport to generate energy in the form of adenosine triphosphate (ATP) and other metabolites of cells [5, 13]. These metabolites are then **mineralized** to CO₂, CH₄, H₂O, N₂ etc. and are released back to the environment. The release of CO₂ or other end products or consumption of O₂ is a measure of complete or ultimate biodegradation which is generally estimated by standardized respirometric methods (ISO 14852, ISO 14855, ASTM 6691, ASTM 6400 etc.) in various environments.

6.4 MECHANISMS OF BIODEGRADATION

Hydrolysis is a process of chemical breakdown of a compound due to reaction with water. In this, the polymer bonds sensitive to water break leading to chain scission and molecular weight reduction. It is a major pathway for chemical degradation of many polymers containing heteroatoms like polyesters, polysaccharides, polyamides and their copolymers[13]. This reaction can either be acid or base catalyzed called chemical hydrolysis or enzyme catalyzed called enzyme hydrolysis. For example- hydrolysis of some polymers like polylactic acid (PLA) or poly(lactic-co-glycolic) acid is accelerated under acidic or basic conditions. For some polymers like PHBV, the rate of chemical hydrolysis is very less as compared to enzyme hydrolysis [14]. In natural environment, enzymes play an important role in hydrolysis. Various microbes secrete different extracellular enzymes which act as catalysts and reduce the activation energy barrier required for polymer hydrolysis. Different enzymes can degrade specific bonds.

Hydrolysis can occur via either surface or bulk erosion mechanism. Laylock et.al has described these erosion mechanisms in detail[12]. **Bulk erosion** occurs when the rate of diffusion of water exceeds the hydrolysis reaction rate. Water enters inside the polymer and the degradation occurs uniformly inside the thickness of the material. Hence, there is a significant reduction in the molecular weight of the polymer before any mass occurs. Bulk erosion is found to be more dominant mechanism in hydrolysis of polyesters like PLA, poly(glycolic acid) (PGA), polycaprolactone (PCL) etc.

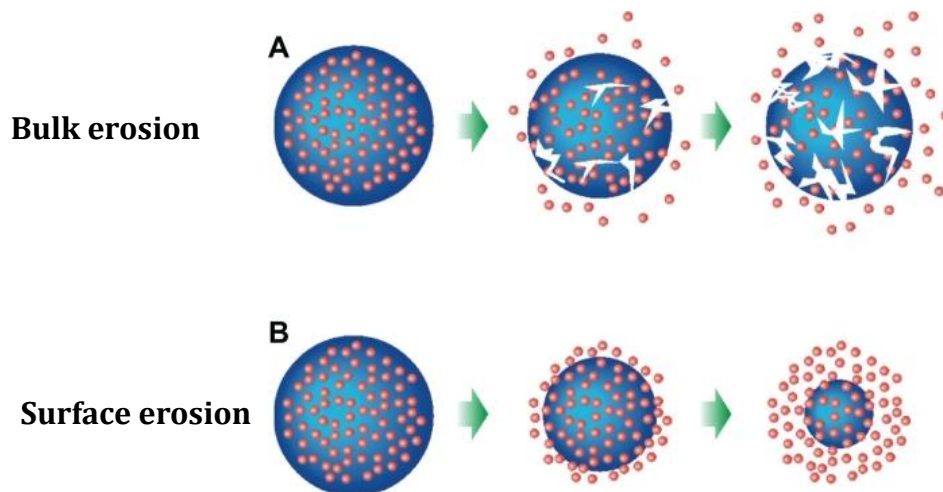


Figure 6.3: Degradation mechanisms for biodegradable polymers A) Bulk erosion, B) Surface erosion[15]

Surface erosion mechanism is generally found to be dominant in enzyme hydrolysis reactions. Enzymes are high molecular weight compounds and hence they cannot penetrate easily to the polymer bulk. **Surface erosion** can also occur when the rate of hydrolysis exceeds the rate of water diffusion in the bulk. This could be due to hydrophobicity, high crystallinity or high glass transition temperature of the polymer. In this, mass is lost from the material surface but the core of the polymer still retains its high the molecular weight [5]. Several studies have shown PHAs as surface degrading polymers [12, 14, 16, 17]. A large number of PHB depolymerases from various bacteria and fungi have been isolated and purified. Enzyme hydrolysis is a heterogenous reaction between water insoluble polymer and water soluble depolymerase enzyme. PHAs are high molecular weight compounds and hence they cannot pass through microbial membranes. Hence, the microbes secrete extracellular enzymes like depolymerase which diffuse out and get adsorbed on the solid surface of the polymer forming enzyme substrate complex. These enzymes catalyze the hydrolysis reaction on the surface and the resulting oligomers diffuse out into the solution. They are then absorbed by the cells for further assimilation and mineralization.

6.5 FACTORS AFFECTING AQUEOUS BIODEGRADATION

Some factors that affect the rate of biodegradation significantly are as follows:

6.5.1 *Shape and surface area*

Rate of biodegradation is expected to increase as the surface area to volume ratio increases. Most of the studies on PHA biodegradation are performed on films (Deroiné et al. 2015a; Doi, Kanesawa, Kunioka, and Saito 1990; Greene 2012; Hoshino et al. 2003; K. ichi Kasuya et al. 1995; Kumagai 1992; Thellen et al. 2008). A few studies used injection molded dogbone samples [23, 24] whereas some studies used polymer pellets or powder as it is [17, 25, 26]. Modelli et al. (1999) studied the biodegradation of PHBV and PCL films and powder in soil and showed that increasing the surface area increases the rate of biodegradation drastically. Powdered samples reached >90% BD very fast compared to the films of the same sample.

6.5.2 *Crystallinity*

Not many studies study crystallinity as a controlling factor for biodegradation. However, it has been generally found that the amorphous regions are first attacked by the enzymes during biodegradation. Hence, the crystallinity values are found to increase with time. Doi et al. 1992b studied the aqueous biodegradation of various PHB films with different crystallinities (53-73 %) using isolated PHB depolymerase from *Alcaligenes faecalis*. They found that the polymer enzymatic erosion was strongly dependent on the crystallinity of PHB films. Weight loss of polymer decreased with increasing crystallinity.

6.5.3 *Static vs dynamic water conditions*

It has been found that biodegradation of plastics varies with the lab or field conditions used during the experiment. Thellen et al. 2008 studied the biodegradation of PHBV under static and dynamic water conditions. PHBV samples were immersed in seawater in lab under static

conditions at temperature of 21°C while for dynamic conditions the samples were incubated in aquarium tanks with continuous flow of water with varying water temperatures according to the season from 12-22°C. Weight loss as a function of time was recorded for both the tests and it was found that the weight loss was less by 40-50% for the dynamic environment. It was argued that the dynamic water flow had lower and constantly changing temperatures. The nutrient supply was also limited as compared to the static water which represents more realistic conditions of marine environment.

6.5.4 Temperature

Temperature has a significant influence on the hydrolytic reactions and hence rate of biodegradation. All the studies which studied the relationship between temperature and biodegradation supported the idea that the rate of biodegradation is higher at higher temperatures. K. ichi Kasuya et al. 1995 studied the kinetics of enzyme hydrolysis as a function of temperature (25-37°) and pH (6.0-8.0)[28, 29]. Rate of enzyme hydrolysis was found to be strongly dependent on increasing temperature. Most of the aqueous biodegradation studies did not use extreme ranges of temperatures. More data for biodegradation at two extremes was taken from soil biodegradation studies. In a study by Nakayama, Yamano, and Kawasaki 2019, biodegradation of aliphatic polyesters was studied in seawater at 2 different temperatures and they found that the rate of biodegradation was almost twice at 27°C as compared to the rate at 10°C[9]. Similar results were observed in a study by Mergaert et al. 1995 where the biodegradation of PHB samples was studied at 15, 28 and 40°C in soil environment. The weight loss was much more rapid at 40°C compared to 15 or 28°C due to increased enzymatic hydrolysis. However, no systematic studies for actual

lifetime prediction of polymers specifically PHBV, at different environmental temperatures were found.

6.6 POLYHYDROXY ALKANOATES (PHAS)

PHAs are bacterial derived polyesters which are largely used for production of bioplastics. More than 150 different monomers in this family can be combined to give various copolyesters with a range of properties [30]. A random copolymer of 3-hydroxybutyrate (HB) and 3-hydroxyvalerate (HV) is produced from bacterial strains like *Ralstonia eutropha* and *Alcaligenes eutrophus* using propionic acid as carbon substrate. This P(2-HB-co-3-HV) also called PHBV has been commercialized by several companies like Enmat, Eureka and Imperial Chemical Industries using fermentation process. The 3-HB unit imparts stiffness whereas 3-HV unit is responsible for the flexibility of the polymer. Thus, PHBV shows a range of physical and thermal properties which depend on the copolymer compositions[27]. PHBV is expected to be degradable in the environment via enzymatic and/or hydrolytic degradation processes [14, 17, 27, 29, 31]. However, a detailed understanding of its estimated lifetime in a specific environment like ocean is required to make informed decisions about their environmental impact. A biodegradable polymer should also mean that it should biodegrade in the natural environment in a reasonable timeframe. ASTM and ISO standards specify that a reasonable time period for biodegradation of plastics should be around 180 days which corresponds to one growing season. It is seen from the biodegradation studies that often harsh (high temperatures, low or high pH) or environmentally unrealistic (isolated microorganisms or pure enzymes, optimum temperature, and other conditions) are used in order to get accelerated biodegradation results. However, these conditions often do not represent the 'real' environmental conditions. For example – A study done at 30°C in aqueous environment has shown 97% biodegradation of polymers based on PBAT in marine environment within one year. Several studies from Deroiné et al. 2014; Doi et al. 1990, 1992; Kumagai, Kanesawa,

and Doi 1992 studied the degradation of PHAs and PHBV in aqueous environment using isolated PHB depolymerase from *Alcaligenes faecalis* and/or at higher temperatures which do not represent actual environmental conditions. The rate of biodegradation under non ideal environmental conditions is expected to be lower and hence, they will exist in the ocean environment much longer than observed in lab studies done at 30°C. Therefore, even if they are termed as “biodegradable polymers” they can contribute to environmental contamination and caution must be taken before making any false and misleading claims of biodegradability.

6.7 EXPERIMENTAL SECTION

6.7.1 *Materials*

Two polymer materials were selected to assess their biodegradation in aqueous environment at various temperatures. Cellulose as a positive reference and polyhydroxybutyrate-co-valerate (PHBV): a bacteria-derived biobased copolymer. PHBV was supplied by TianAn Biologic Materials Co. Ltd., China under the trade name Y100P. The weight average molecular weight (M_w) of the copolymer was 350,000 da. as provided by the manufacturer. The hydroxyvalerate (HV) content was 2% as determined by NMR given in supplementary materials (Appendix 1). Microcrystalline cellulose was obtained from ACROS Organics™ with particle size of less than 90 μm and was used as a positive control material in all biodegradation tests. Same batch of PHBV and cellulose was used for all the tests. All other chemicals used were analytical grade and were purchased from Sigma Aldrich. **Error! Reference source not found.** shows the chemical structures for Cellulose and PHBV

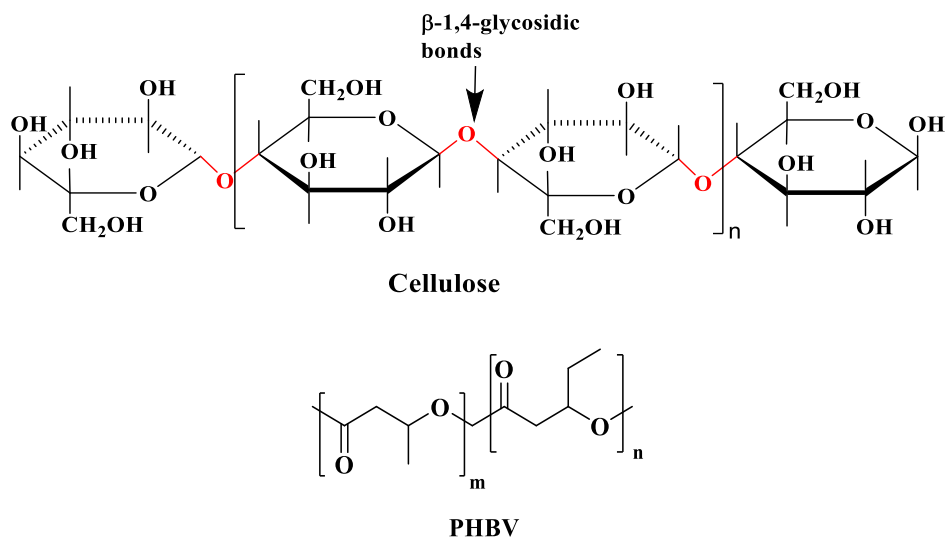


Figure 6.4: Chemical structures of cellulose and PHBV

6.8 MATERIAL PROCESSING AND CHARACTERIZATION

6.8.1 Elemental analysis

The carbon content of test and reference materials determined by elemental analysis using a PerkinElmer 2400 Series II CHNS/O Elemental Analyzer (Shelton, CT, USA) and is shown in Table 6.1, Table 6.2 and Table 6.3. The amount of sample to be added in each flask for the biodegradation test was adjusted according to the carbon % of the polymer so as to get equal number of carbon millimoles for each replicate. The theoretical amount of CO₂ evolved by the total oxidation of test material (ThCO₂) is given by equation Equation 6.1.

Equation 6.1

$$ThCO_2(g) = m \times X \times \frac{44}{12}$$

where m is the mass of the test material added in biodegradation flask. X is the fractional carbon present in the test material, determined from the chemical formula of the polymer or calculated from an elemental analysis; 44 and 12 are the molecular weights of carbon dioxide and carbon, respectively. This ThCO₂ is used to calculate percent biodegradation during biodegradation test. The results are shown in Table 6.1, Table 6.2 and Table 6.3.

Table 6.1: Aqueous biodegradation test setup. Test carried out at 10°C

Test material	Amount of test material added (mg)	% C	Total C in test material (mg)	Theoretical CO ₂ (mmoles)	Inoculum added (ml)
Blank	-		-	-	50
Blank	-		-	-	50
Cellulose	4002	43.58	1744	145.3	50
Cellulose	4003	43.58	1745	145.4	50
PHBV	4001	55.40	2217	184.7	50
PHBV	4005	55.40	2219	184.9	50

Table 6.2: Aqueous biodegradation test setup. Test carried out at 30°C

Test material	Amount of test material added (mg)	% C	Total C in test material (mg)	Theoretical CO ₂ (mmoles)	Inoculum added (ml)
Blank	-		-	-	50
Blank	-		-	-	50
Cellulose	4541.8	43.58	1979.3	164.9	50
Cellulose	4540.9	43.58	1978.9	164.9	50
PHBV	3629.8	55.40	2010.9	167.9	50
PHBV	3635.8	55.40	2014.2	167.8	50

Table 6.3: Aqueous biodegradation test setup. Test carried out at 40°C

Test material	Amount of test material added (mg)	% C	Total C in test material (mg)	Theoretical CO ₂ (mmoles)	Inoculum added (ml)
Blank	-		-	-	50
Blank	-		-	-	50
Cellulose	2626	43.58	1144.4	95.4	50
Cellulose	2602	43.58	1133.9	94.5	50
PHBV	3628	55.40	2009.9	167.6	50
PHBV	3628	55.40	2009.9	167.8	50

6.8.2 Thermal analysis

PHBV and cellulose were characterized for glass transition temperature (T_g), melting temperature (T_m) and degradation temperature as a measure of initial properties. The degradation temperature of samples was obtained by thermogravimetric analysis (TGA) using a TGA Q50 (TA Instruments, USA). A sample (5-10 mg) was heated to 600°C with a heating rate of 10°C /min. The weight loss (%) of a sample as a function of temperature (°C) was obtained from this analysis. Also, the thermal transitions of the samples were obtained by using a differential scanning calorimeter (DSC). The sample was heated to 200°C in DSC

Q20 (TA Instruments, USA) with the heating rate of 10°C/ min to remove any thermal and stress history. The sample was then cooled back to 20°C and heated again to 200°C with the heating rate of 10°C/ min. The samples were used as it is for the biodegradation experiments without any thermal processing. Hence, the transitions appearing on the first heating cycle were recorded for analysis of % crystallinity, T_g , T_m and degradation temperature. The crystallinity of samples was calculated using Equation 6.2. Enthalpy of melting (ΔH_m) and enthalpy of cold crystallization (ΔH_{cc}) was recorded from DSC in W/g. The enthalpy of melting for 100 % crystalline PHBV was obtained as 146 J/g from the literature[32].

Equation 6.2

$$\text{Crystallinity (\%)} = \frac{\Delta H_m - \Delta H_c}{\Delta H_o} \times 100$$

6.8.3 Determination of particle size of pellets

The size of the pellets for PHBV was determined by considering them as cylinders for PHBV. The dimensions of 15-20 pellets were measured using a Keyence VHX-6000 digital microscope. Microcrystalline cellulose was purchased from Thermo Fisher Scientific Inc. in powdered form and was used as it is.

6.8.4 Scanning electron microscopy

A JOEL 6610 LV scanning electron microscope (JEOL Ltd., Tokyo, Japan) was used to study the surface erosion of all the PHBV pellets. The stubs were mounted on the SEM stands using high vacuum carbon tabs and coated with gold using a sputter coater. The stubs were then placed in SEM stands and examined using JOEL at 2000× magnification at 10 kV.

6.8.5 Molecular weight analysis

The PHBV samples dissolved in chloroform at a concentration of 5 mg/ml. PHBV samples needed to be heated to 50 °C and agitated for 1–2 h until complete dissolution could be

achieved. Resulting solutions were then filtered through a Whatman Reziest 30 mm 0.20µ PTFE syringe filter. Molecular weights were measured by GPC (Waters system) at 35 °C using a Agilent PLgel MIXED-C 7.5x300 mm 5 micron HPLC column (PL1110-6500) column and Wyatt Technology TREOS II (LS detector) and Optilab T-rEX (RI detector). HPLC grade chloroform was used as an eluent at a flow rate of 1 ml/min. The number-average (Mn) and weight-average (Mw) molecular weights were calculated using a calibration curve from polystyrene standards using ASTRA 7.3.2 software. The polydispersity index (PDI) was calculated from the following equation

Equation 6.3

$$PDI = \frac{Mn}{Mw}$$

where Mn and Mw are the initial number-average molecular weight and the number-average molecular weight at a given time of biodegradation.

6.8.6 Microbial inoculum

The microbial inoculum used in all the tests was a sample of activated sludge collected from a well operated wastewater treatment plant handling predominantly domestic sewage at East Lansing, MI, USA. The sample was mixed well, kept under aerobic conditions, and was used within 48 hours of collection. metagenomic analysis of the activated sludge was done to map the microbial population present initially in the sludge. it was compared with the seawater population from various locations to check for any similarities. The detailed procedure and results for metagenomic analysis are given in Appendix 3.

6.9 EXPERIMENTAL BIODEGRADATION SETUP

A typical biodegradation curve for percent biodegradation vs time is as shown in Fig. 1a. The basic reaction for aerobic biodegradation of a polymer is:

Equation 6.4



Carbon present in the polymer is first converted to biomass which is then mineralized to CO₂. There are typically 3 different phases involved in the biodegradation reaction - lag phase, activation phase, and plateau phase as shown in the Figure 6.5.

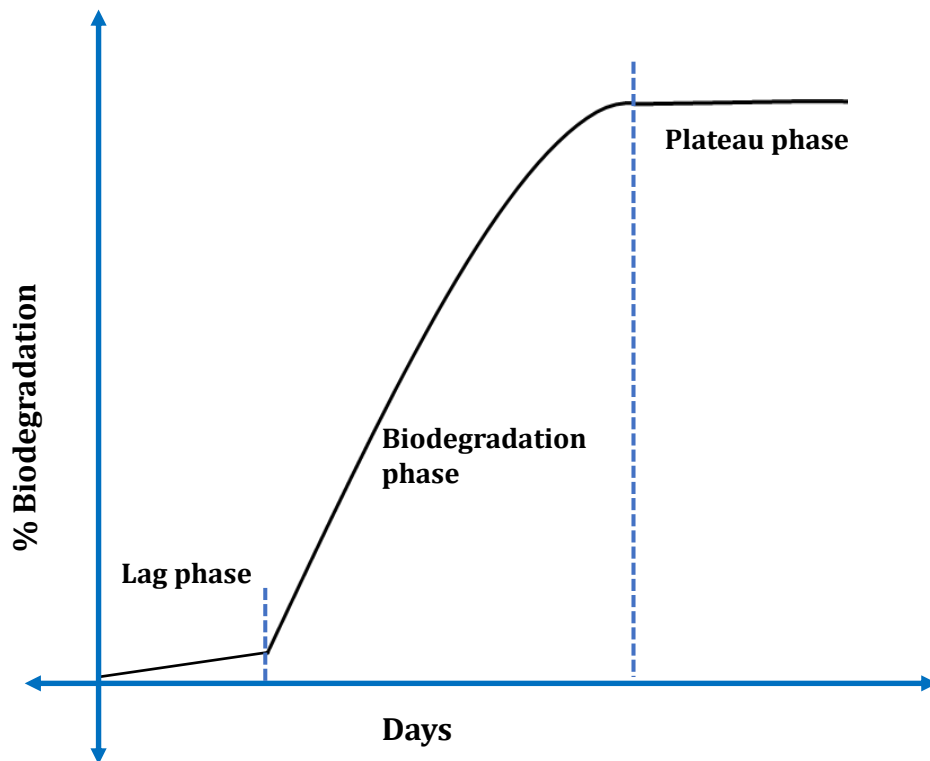
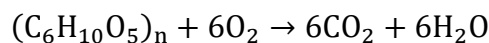


Figure 6.5: A typical biodegradation curve for %biodegradation vs time

Out of those, the activation phase is the phase where majority of the biodegradation takes place. For the two polymers- cellulose and PHBV, considered in this study, these reactions will be -

Equation 6.5



Equation 6.6



Similar to other chemical reactions, the rate of biodegradation can be calculated using either consumption of reactants which in this case is carbon present in the polymer or the oxygen consumed or using the appearance of products which is CO₂ evolution in this case. A reliable method to measure the biomass is still not available. For the assessment of % biodegradation, the mineralization % is commonly used. When the evolved CO₂ is used to calculate the biodegradability, the method is called respirometric method and biodegradation % is given as the ratio between evolved CO₂ and theoretical CO₂ as shown in following equation.

Equation 6.7

$$Biodegradation \% = \frac{C_{Evolved\ as\ CO_2}}{Maximum\ Theoretical\ CO_2\ Polymer} \times 100$$

A respirometric mineralization test system for calculating CO₂ evolution was setup based on International Standard ISO 14852 as shown in Figure 6.6. The system comprised of blank, positive reference (cellulose) and the test material (PHBV) for all the runs. All the samples, blanks and references were run in duplicates. An optimized test medium containing all the nutrients and buffers was prepared according to ISO standard. Table 6.4 gives the detailed composition of the mineral solution prepared for all the tests. Wastewater inoculum was added to all the flasks to obtain the concentration of 5% v/v in the test medium as described in ISO 14852. Then the polymer samples were added to these flasks, and they were subjected to the test conditions as described in Table 6.4.

Table 6.4: Buffer solutions used for aqueous biodegradation

1 L mineral solution	g
Solution A	
KH ₂ PO ₄ (anhydrous)	3.75
Na ₂ HPO ₄ ·2H ₂ O	8.73
NH ₄ Cl	0.2
Solution B	
MgSO ₄ ·7H ₂ O	2.25
Solution C	
CaCl ₂ ·2H ₂ O	3.64
Solution D	
FeCl ₃ ·6H ₂ O	0.025 g
Wastewater inoculum (ml)	50
Distilled water (ml)	Remaining

The system comprised of six flasks in total. Two for blank, two for positive reference cellulose and two for each the PHBV samples. The system was kept in a dark, temperature-controlled room maintained at a temperature specific for that run. The test flasks were agitated throughout the run with the help of magnetic stirrers. Air inlet was passed through NaOH solution to get CO₂ free air. This air was then divided and passed through flowmeters for each bioreactor at a constant flow rate.

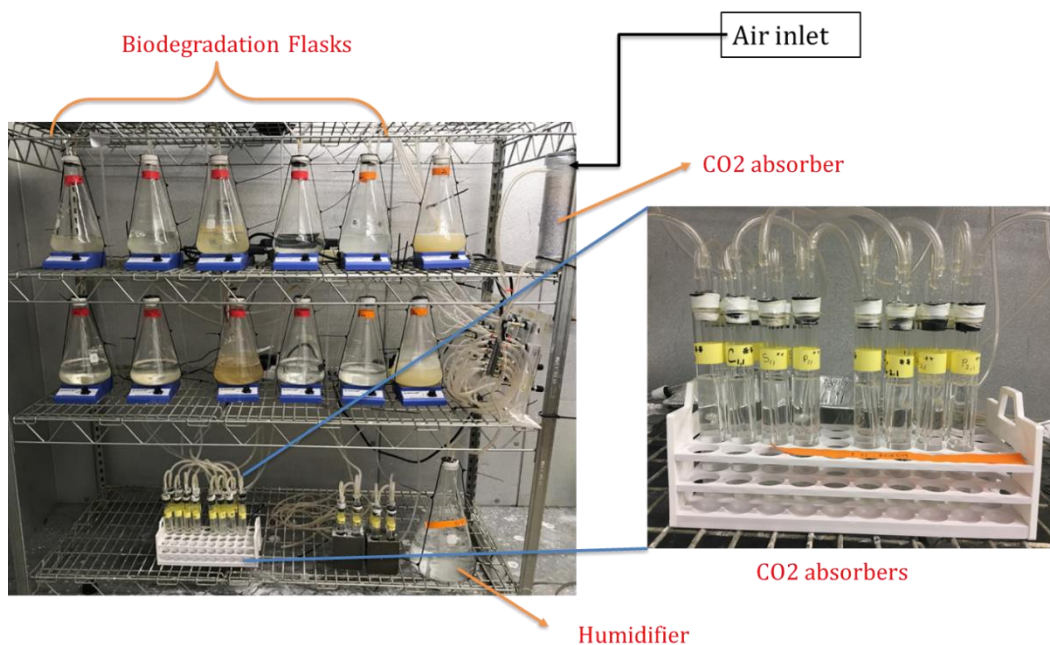
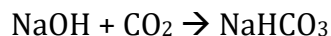


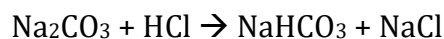
Figure 6.6: Experimental biodegradation setup

A solution of 1N NaOH was used for trapping the CO₂ generated from test flasks. CO₂ trapping is a two-step process as shown below:



1 g of sample was taken from each of the 50mL NaOH trapping solution and titrated with 0.1N standardized hydrochloric acid (HCl) solution to find the amount of CO₂ trapped.[33]

The reactions are as follows:



The titrations were done with the help of autotitrator to get the volumes of HCl, V₁ and V₂ required for reaction 1 and 2 respectively. The amount of HCl consumed can be used to calculate the mmoles of CO₂ evolved using following formula:

Equation 6.8

$$Mmoles\ of\ CO_2 = \frac{(V2 - V1) * N_{HCl} * V_{NaOH}}{Wt\ of\ sample}$$

The percentage biodegradation (% B) was further calculated by the following equation:

Equation 6.9

$$\% B = \frac{\sum(CO_2)_{sample} - \sum(CO_2)_{blank}}{ThCO_2} \times 100$$

$\sum(CO_2)_{sample}$ is the amount of carbon dioxide evolved in test flask between the start of the test and time t ; $\sum(CO_2)_{blank}$ is the amount of carbon dioxide evolved in blank flask between the start of the test and time t ; $ThCO_2$ is the theoretical amount of carbon dioxide evolved by the test material. All the values were expressed as mmoles of CO_2 . The samples were replaced every 2-3 days in the starting phase when the rate of biodegradation was expected to be maximum and weekly or biweekly in the end.[18, 34]

These samples were tested at 3 different temperatures of 10, 30 and 40°C. Table 6.1, Table 6.2, and Table 6.3 show a summary the different tests performed, the materials used in each test and other information like carbon % and theoretical CO_2 evolution expected from each sample. Biodegradation kinetics analysis and other statistical analysis was done using Microsoft excel and Minitab.

6.10 RESULTS AND DISCUSSION

This section first presents results for initial characterization of the test materials and various graphs for percent biodegradation vs time for all the polymers at different temperatures. Using that data kinetics study was done for cellulose and PHBV with the help of Arrhenius equations. Experimental results were compared with several values from the literature and a model was suggested for predicting the rates of biodegradation of Cellulose and PHBV in marine environment. Finally, the mechanism for biodegradation of PHBV was also studied by monitoring various chemical, morphological, and thermal properties of PHBV.

6.10.1 Initial characterization of polymer pellets

Average pellet diameter and height for PHBV was found to be 1.97 ± 0.10 mm and 2.7 ± 0.04 mm and average surface area for the pellets was 23.00 ± 1.48 mm². Microcrystalline cellulose with 60um size was used as positive control. DSC and TGA curves for cellulose and PHBV are shown in Figure 6.7. The thermal degradation temperatures for cellulose and PHBV were found to be 342.1 C and 278 °C respectively. DSC curves show the melting points for cellulose and PHBV at 104.6 and 175.9 °C.

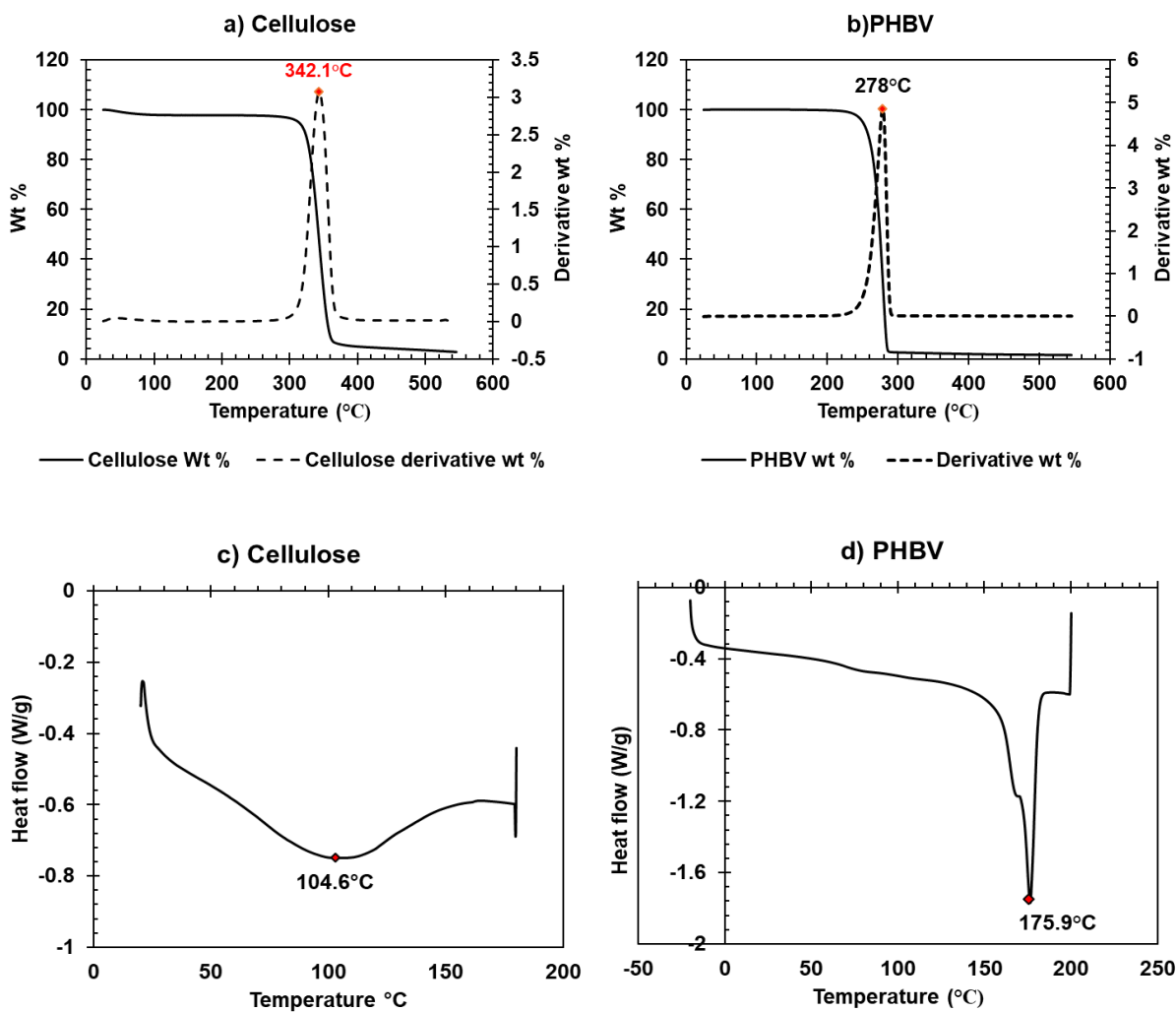


Figure 6.7: TGA and DTG curves for a) cellulose, b) PHBV; DSC curves for c) cellulose d)PHBV

6.10.2 Biodegradation: CO₂ evolution and mineralization

In all tests, the percent biodegradation of cellulose was according to the standard ISO 14852 requirement (i.e. % Biodegradation > 60% at the end of the test). Hence, the inoculum was considered active, and the tests were valid even at the lowest test temperature of 10°C. The values of cumulative mmoles of CO₂ evolved from each sample were divided by the maximum theoretical CO₂ mmoles possible to be generated by the sample to obtain percent biodegradation as shown in Equation 6.9. Theoretical CO₂ was calculated from the elemental analysis of percent carbon present in the polymer. The comparative biodegradation curves for PHBV and cellulose for 3 temperatures are shown in Figure 6.8 and Figure 6.9. It was observed that the rate of biodegradation was strongly dependent on the temperature. It took cellulose almost 200 days to reach 80 % mineralization at 10°C whereas, at 40°C, it was achieved in less than 25 days. Similar results were obtained for PHBV polymer as well. Figure 6.10 shows the normalized graphs for change in concentration of carbon with time for cellulose and PHBV. The experimental percent biodegradation curves were re-plotted in terms of – carbon remaining ($C_{remaining}$) against time (days) by subtracting the $C_{removed}$ from the environment from the initial carbon added to the added in the form of polymer ($C_{initial}$) (Figure 6.10 – a and b). The detailed calculations and the derivation for $C_{remaining}$ is given in Appendix 2.

Biodegradation kinetics study was done to further quantify this dependence of biodegradation rate on temperature.

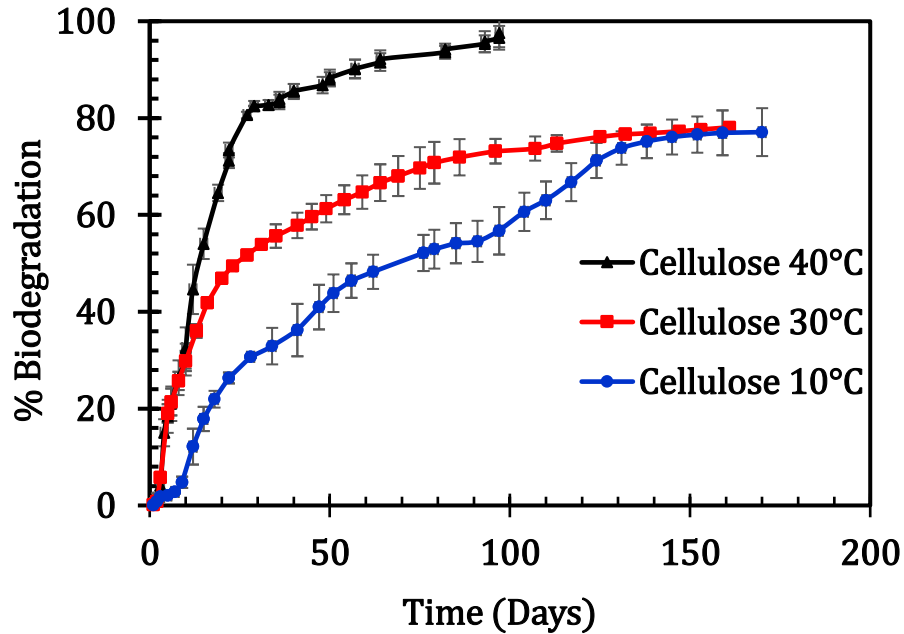


Figure 6.8: Average biodegradation curves of Cellulose tested at different temperature (10, 30, 40°C). Each curve represents average of 2 replicates

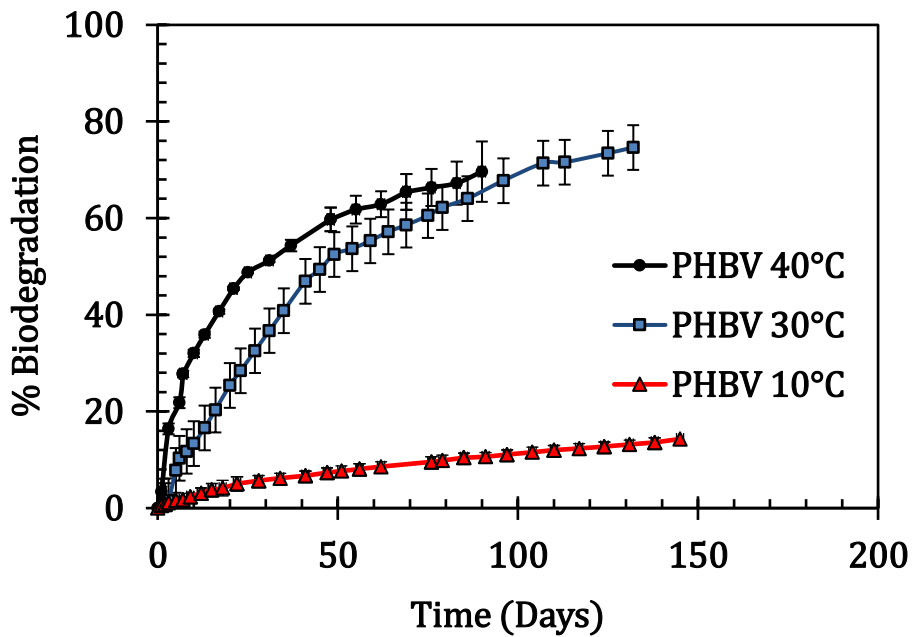


Figure 6.9: Average biodegradation curves of PHBV tested at different temperature (10, 30, 40°C). Each curve represents average of 2 replicates

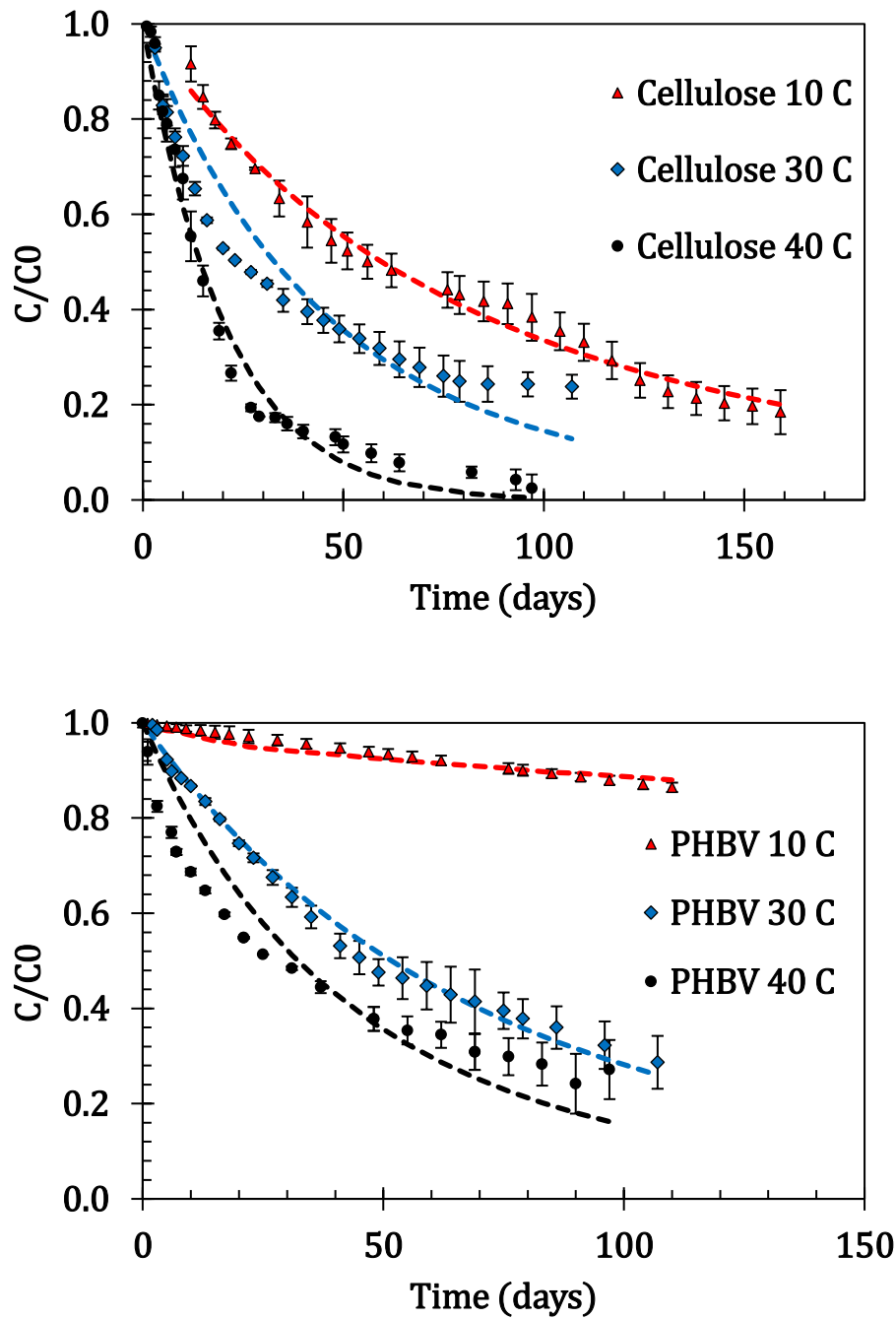


Figure 6.10: C/C_0 as a function of time for aqueous biodegradation of a) Cellulose and b) PHBV at 10, 30 and 40°C. Points represent experimental data whereas dotted lines indicate fitting of 1st order equation

6.10.3 Biodegradation kinetics: Parameter estimation and order of reaction

To calculate the order of the reaction for overall biodegradation reaction of PHBV and cellulose, the general rate law was used.

Equation 6.10

$$\frac{-dC}{dt} = kC^n$$

This nth order kinetic equation can be solved for calculating the order and rate constant of the biodegradation of cellulose and PHBV at various temperatures using either differential method or Non-Linear Least-Squares Analysis

Differential analysis.

Taking natural log of Equation 6.10 on both sides we get

Equation 6.11

$$\ln\left(\frac{-dC}{dt}\right) = \ln k + n \ln C$$

Plot of $\ln(-dC/dt)$ vs $\ln C$ gives order of reaction and rate constant.

Where Slope $\rightarrow n =$ order of reaction

And Intercept $\rightarrow \ln k =$ rate constant

Non-Linear Least-Squares Analysis

Integrating Equation 6.10 gives the rate law equation for n^{th} order reaction as

Equation 6.12

$$C = [C_0^{(1-n)} - (1-n)kt]^{\frac{1}{1-n}}$$

Where - $k \rightarrow$ rate constant, $n \rightarrow$ order of the reaction, $t \rightarrow$ time

$C_0 \rightarrow$ mmoles of carbon added initially in the biodegradation flask

$C \rightarrow$ mmoles of carbon remaining at any time t

Assuming some initial values for k and n, a predicted value for C \rightarrow $C_{predicted}$ can be calculated for each day. Then calculate the root mean square of the errors, i.e., difference between the predicted values and the actual value of C remaining

Minimize that using excel solver to get the optimized values of n and k.

Both these methods were applied to Cellulose and PHBV biodegradation data to calculate and compare the order of reaction, n, and rate constant, k.

Table 6.5 gives the values for order of the biodegradation reaction for cellulose and PHBV at various temperatures calculated using both differential method and RMSE method. The detailed calculations and graphs for each temperature and polymer are given in Appendix .

Table 6.5: Order of reaction for cellulose and PHBV biodegradation

Polymer	Method \rightarrow	Differential method	RMSE	Differential method	RMSE	Differential method	RMSE
	Temperature (°C) \rightarrow	10		30		40	
Cellulose	n	1.045	1.291	1.018	1.14	0.876	0.95
PHBV	n	0.989	1.09	1.038	1.19	1.094	1.234

As expected, the higher the temperature faster the rate of biodegradation. Biodegradation being a microbial reaction, is expected to be sensitive to temperatures. At temperatures higher than 40 or 50°C, it is possible that the rate of reaction might reduce due to inactivation of microbes and denaturation of microbial enzymes resulting in decreased rate of biodegradation. However, for the temperature range considered in this study, no such affect was observed. The order of reaction for both PHBV and cellulose was found to be near one for all the temperatures used in this study. Hence, a first order kinetics equation was used for further analysis.

6.10.4 Biodegradation as a first order reaction

For a first order reaction, the rate law is

Equation 6.13

$$\text{Rate} = -\frac{d[C]}{dt} = k[C]$$

where [C] is the moles of carbon consumed by the micro-organisms to yield CO₂, k is the rate constant and t is the time. [33]

$$\int_{C_0}^C -\frac{d[C]}{dt} = \int_0^t k[C]$$

$$\ln[C] - \ln[C_0] = -kt$$

$$\ln[C] = \ln[C_0] - kt$$

Where [C_t]- moles of carbon remaining at time t and [C₀] is initial moles of carbon present.

Equation 6.14

$$\ln \frac{C_t}{C_0} = -kt \quad \text{or} \quad \ln \frac{C_0}{C_t} = kt \quad \text{or} \quad C_t = C_0 e^{-kt}$$

Where C₀ is initial mmoles of carbon present in added polymer sample calculated from the elemental analysis and C_t is the mmoles of carbon remaining in the sample at any given time t. Millimoles of carbon remaining (C_t) were found by subtracting the mmoles of carbon evolved from the initial mmoles of carbon added in the test (C₀).

6.10.5 Parameter estimation: Arrhenius equation

In this study, the lifetime prediction for PHBV and Cellulose in aqueous environment was done using Arrhenius equation expressed as:

Equation 6.15

$$k = Ae^{-\frac{E}{RT}}$$

Where k is the rate constant for the reaction, A is called the pre-exponential or frequency factor, R is the universal gas constant ($8.314 \text{ J}\cdot\text{mol}^{-1}\cdot\text{K}^{-1}$) and E is the activation energy.

The obtained datasets of temperature vs rate constant were analyzed in 3 different ways to calculate the range for activation energy and pre-exponential factor. First, we applied logarithmic transformation followed by linear regression as commonly followed in the literature. Second method was non-linear regression using reparametrized Arrhenius equation. Reparameterization of Arrhenius equation was done to estimate more accurate range for E_a and avoid the high correlation between E_a and A . This was done by introducing a reference temperature T_{ref} and the corresponding rate constant k_{ref} so that the temperature is centered about the mean value T_{ref} of the temperatures to be studied. The resulting Arrhenius equation is as shown in Equation 6.16

Equation 6.16

$$k = A' \exp - \frac{E_a}{R} \left(\frac{1}{T} - \frac{1}{T_{ref}} \right)$$

These two are 2-step methods in which first we find the rate constants and then the Arrhenius parameters. This 2-step way of analysis is statistically insufficient because too much information is lost on the way. Hence, in the 3rd method, a one-step approach of

incorporating the reparametrized Arrhenius equation in kinetic rate law was used. The rate constant k was replaced by Arrhenius equation in the 1st order kinetic rate law as follows

Equation 6.17

$$\frac{C_t}{C_o} = \exp\left(\left[A' \exp\left(-\frac{E_a}{R} \left(\frac{1}{T} - \frac{1}{T_{ref}} \right) \right) \right] \times -t \right)$$

Thus, we bypass the estimation of rate constants, and we have more data points and more degrees of freedom which yield in more accurate estimation. A schematic for showing the comparison between standard linear regression analysis, reparametrized Arrhenius equation analysis and the one step global equation approach is given in

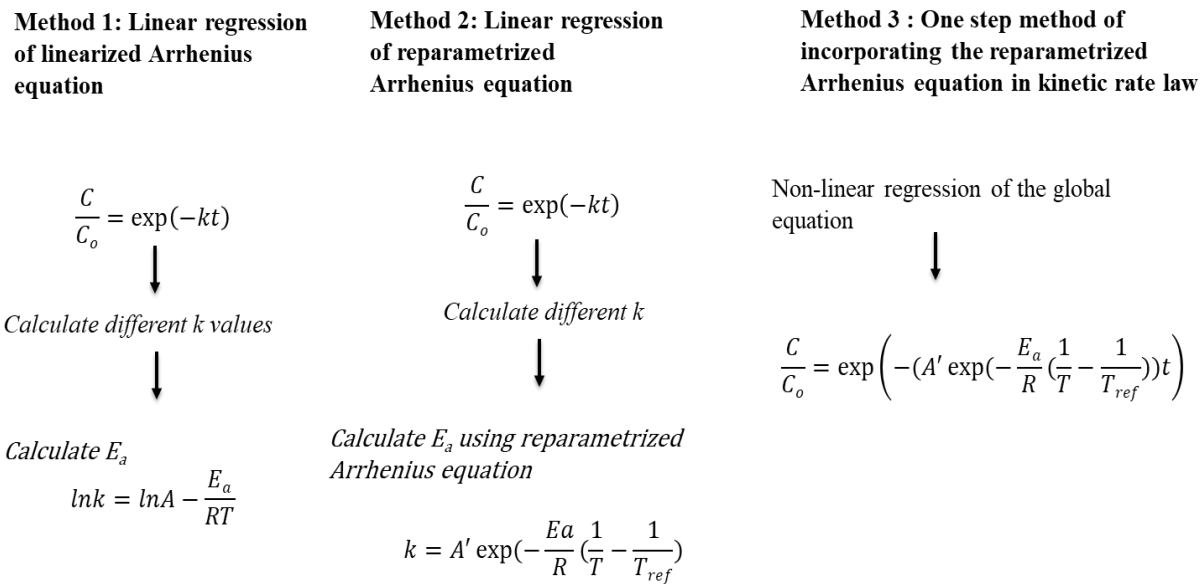


Figure 6.11: Schematic for showing the comparison between standard linear regression analysis, reparametrized Arrhenius equation analysis and the one step global equation approach

The results using these 3 methods of analysis are as shown in Table 6.6. The details for calculating these estimates for are given in Appendix

Table 6.6: Parameter estimates for activation energy and pre-exponential factor using method 1, 2 and 3

<i>Cellulose</i>				
Parameter	Method	Estimate	Standard Deviation	95% CI
<i>ln A</i>	1	7.9	4.64	3.25 - 12.54 (A =25.7 - 268337)
	2	10.79	0.25	10.41 - 11.02
	3	9.53	0.04	9.49 - 9.57
<i>E_a (kJ)</i>	1	29.29	11.53	17.76 - 40.83
	2	36.64	20.36	20.72 - 61.44
	3	33.15	2.82	30.33 - 35.97
<i>PHBV</i>				
Parameter	Method	Estimate	Standard deviation	95% CI
<i>ln A</i>	1	23.41	7.97	15.22 - 31.38
	2	13.69	0.4	13.06 - 14.04
	3	9.9	0.06	9.83 - 9.96
<i>E_a (kJ)</i>	1	70.62	19.79	50.83 - 90.42
	2	45.66	30.35	23.10- 83.80
	3	61.67	4.87	56.51 - 66.26

Note: Method 1, linear regression of Arrhenius equation; method 2, nonlinear regression of reparametrized Arrhenius equation; method 3, one step method of incorporating reparametrized Arrhenius equation in kinetic rate law

The results obtained from the analysis using three different methods clearly showed the difference in the range of estimates. For the first method, the precision obtained was disappointing. Even though the standard errors were not so bad, the 95% confidence intervals (CI) were very large due to small number of degrees of freedom. After reparameterization, the 95% CI for A' was much better than its untransformed counterpart A. This clearly proved the advantage of reparameterization. However, the reparameterization did not improve the estimation ranges for E_a. When one step global equation was used by incorporating the Arrhenius equation in first order reaction rate law

as shown in Equation 6.17, the 95% CI for A' and E_a obtained were much more precise and statistically useful (Table 6.6). It should be noted that the nonlinear regression analysis had difficulties in finding estimates especially when using second method. Only when initial values close to the final values were supplied, a solution was found. This might be due to the limited number of data points (for 3 temperatures in this case) and the strong correlation. Overall, the final parameters and models developed for lifetime predictions of cellulose and PHBV are as shown in Table 6.7. This model is valid for a temperature range between 10 to 40°C. However, an estimate for the time required for biodegradation at temperatures lower than 10°C could also be made by extrapolation of these models. A comparative analysis for the estimated time ranges given by the 3 methods was performed and the results are as shown in Figure 6.12. The model was also extrapolated to find the estimated time range for biodegradation at the ocean temperature of 4°C. A graphical representation illustrating the precision differences between method 1,2 and 3 is shown in Figure 6.12. Details for the calculations are given in appendix 6.

Table 6.7: Final estimated parameter values for the global equation for cellulose and PHBV

Parameters	Cellulose	PHBV
A'	0.023	0.0082
E_a	33.14	61.68
T_{ref}	26.5	26.5
Global equation	$\frac{C_t}{C_o} = \exp \left(-A' \times \exp \left(\left(-\frac{E_a}{R} \right) \times \left(\frac{1}{T} - \frac{1}{T_{ref}} \right) \right) \right) \times t$	

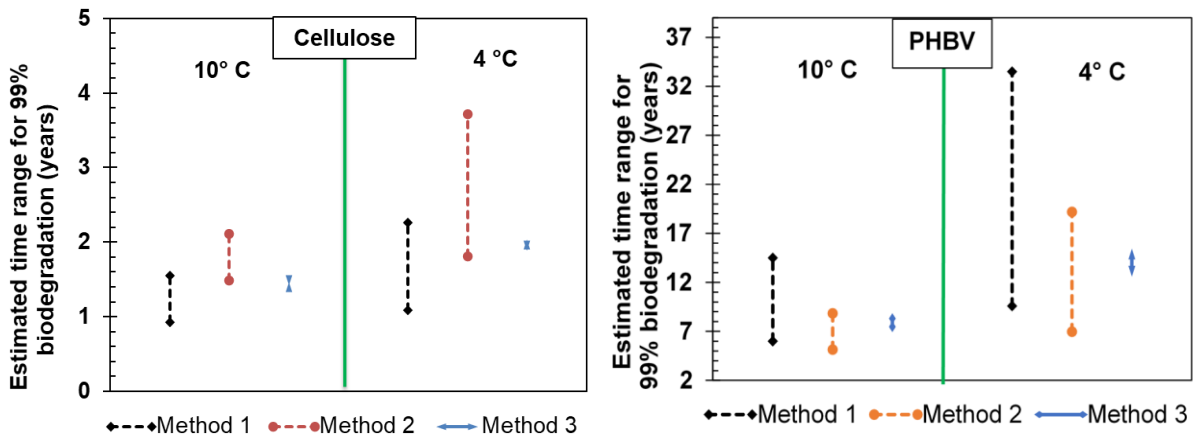


Figure 6.12: Precision differences for biodegradation time estimations for the three methods

The results showed that the time ranges estimated using method 3 were much narrower as compared to method 1 and 2 for all the temperatures. It suggests that even though the polymers like cellulose and PHBV biodegrade readily at 30°C (0.5 -0.6 years for cellulose and 1.2 – 1.5 years for PHBV), they will take much longer time at lower temperature of 10°C (1.4 -1.5 years for cellulose and 7.4 -8.3 years for 99% biodegradation of PHBV). Further, if this model is extrapolated to the actual marine temperature of 4°C, this time will be even higher. Even a readily biodegradable polymer like cellulose is estimated to last for almost 2 years at low ocean temperatures whereas PHBV is estimated to last for 12 -15 years (Figure 6.13). Hence, the standard ASTM or ISO tests for aqueous or marine biodegradation which are carried out at temperatures of 25-30°C might not give an accurate representation of polymer's biodegradability in ocean. A plot of percent carbon remaining as a function of time (years) was plotted from these values of rate constants (Figure 6.13). A straight line was assumed to represent any non-biodegradable polymer. The details for obtaining this graph are given in Appendix .

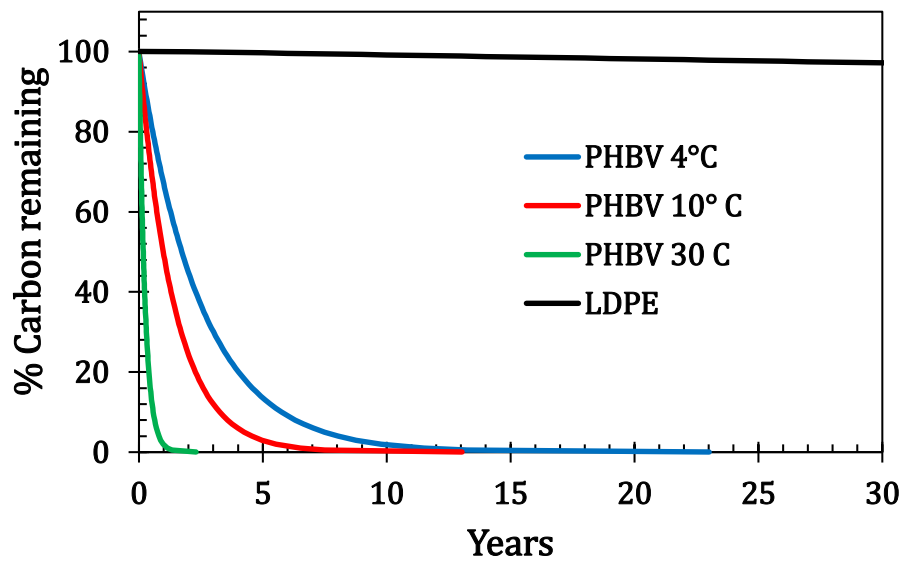
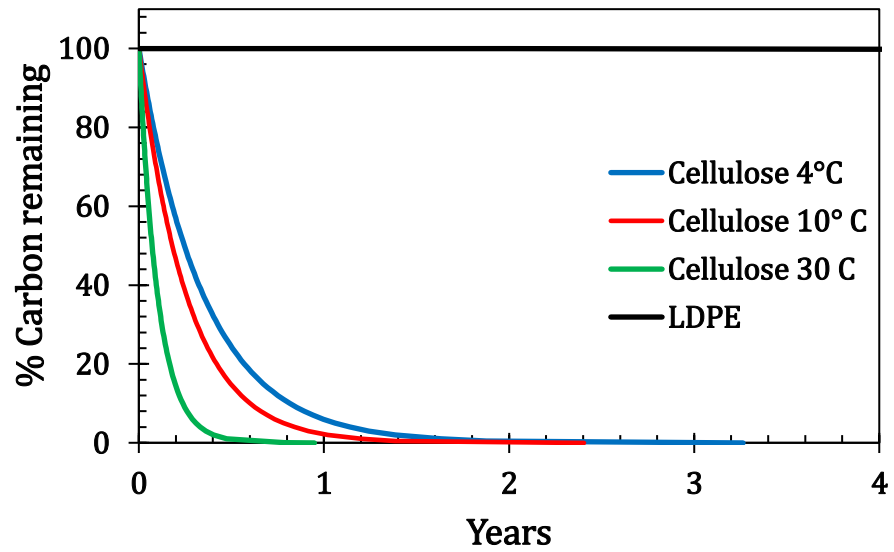


Figure 6.13: percent carbon remaining as a function of time for cellulose and PHBV at 30, 10 and 4 °C

6.10.6 Biodegradation data compilation

To validate the model further, an extensive literature review was done to compare the rates of biodegradation from different studies to our experimental data.

Biodegradation data for aerobic aqueous biodegradation of cellulose and PHBV was identified through a search of peer reviewed literature. Appendix 8 shows a summary for selected articles using several methods for assessing biodegradation of cellulose and PHBV in aqueous environment. The studies using CO₂ evolution or O₂ consumption for determining the % biodegradation were used further to calculate the rate constants for biodegradation. Biodegradation rate was either obtained directly or calculated assuming first order kinetics for each study. Some authors have also used weight loss and other visual inspection techniques for estimating biodegradation. Appendix 8 also provides other relevant information for biodegradation such as the size and shape, molecular weights, time and other characterization methods used. This data was used further for comparison of our experimental data with literature values.

Rate constants for the biodegradation were either used directly as given in the paper or were calculated by digitizing the graphical % biodegradation vs time data using Webplot digitizer and assuming a first order kinetics. Arrhenius graph ($\ln k$ vs $1/T$) as well as temperature vs rate constant graphs were plotted for both PHBV and cellulose and were compared with our experimental data and the predicted data using our model (Figure 6.14). It was observed that the data from literature agrees well with our experimental data. The average activation energy values calculated using the literature rate constants and the values obtained in this study were very similar. For cellulose the activation energy obtained was 33.14 kJ whereas from literature the average activation energy was found to be 35.5 kJ. For

PHBV this difference was even less – calculated 61.68 kJ vs average of 61.98 kJ from literature.

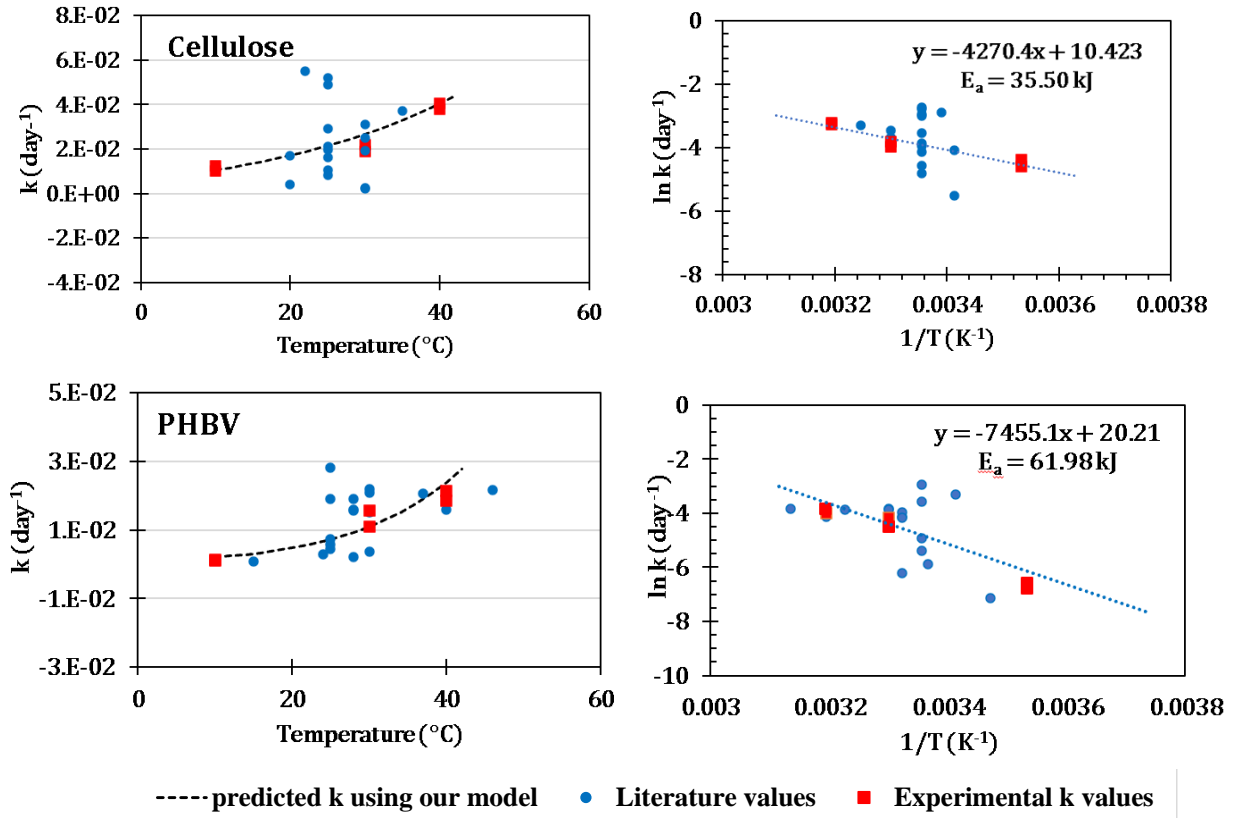


Figure 6.14: Comparing the experimental rate constants to literature values for Cellulose and PHBV

A statistical analysis was done to determine the variation between all the rate constant values obtained from various papers. It was observed that, for a particular temperature, 70% of the obtained rate constant values from various literature lie within ± 1 SD. The type of polymer used, the physical state of the sample (powder, film or injection molded articles), the microbial inoculum used etc. resulted in small variations, but the final rates of biodegradation were similar for most of the cases. Figure 6.15 below represents various datapoints for cellulose and PHBV at 25°C and 30°C and their distance from the mean value. Considering that all these studies were done in various parts of the world, with different samples and different aqueous conditions by different authors, this similarity in the results looks very promising.

a) Cellulose

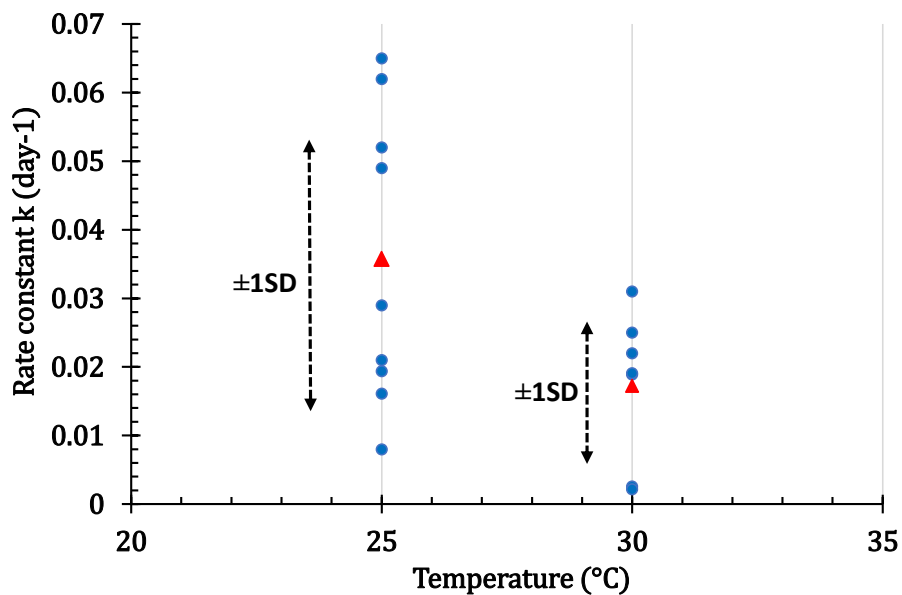
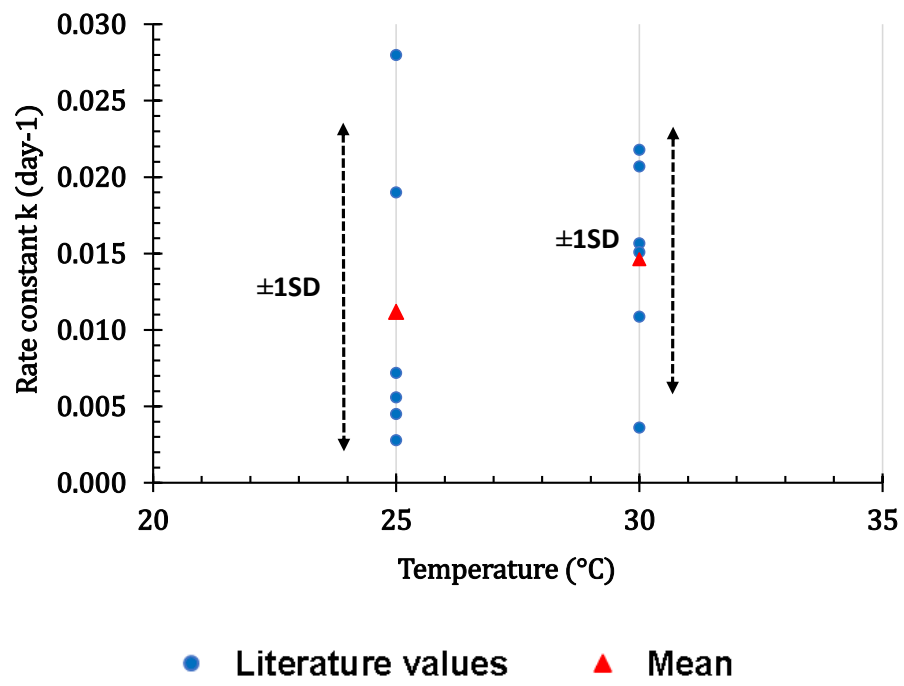


Figure 6.15: Statistical analysis of rate constants for a) cellulose and b) PHBV at 25 and 30 C

Figure 6.15 cont'd

b) PHBV



6.10.7 Accumulation of plastics in ocean

Plastic pollution is a planetary threat affecting nearly all the ecosystems in the world including marine. 8 MT of plastic enters the ocean every year worldwide. United States generates the most solid waste than any country in the world thus contributing to enormous amounts of plastic waste to the environment including oceans [1], [2], [35]. However, all these claims lack a quantitative model that could predict a measurable reduction in ocean plastic accumulation by replacing the petroleum-based plastics by biodegradable plastics. Here, we present a model to evaluate how replacing a certain percentage of non-biodegradable plastics by biodegradable plastic would reduce the plastic accumulation in ocean by 2030. We assume the current benchmark of 8 MT annual ocean plastic pollution and impact of replacing the plastics in that waste by a percentage of biodegradable plastics. The calculations are done by using the rate constant k and E_a obtained for PHBV at temperature of 10°C (0.00161 day⁻¹ and 61.68 kJ respectively). The detailed model and calculations can be found in Appendix 8 Our results show that the plastic accumulated in ocean in 10 years can reduce by 77.5 % (from 80 Mt to 17.95 Mt) if 100% plastics are replaced by bioplastics with biodegradation rate similar to PHBV. Out the plastics accumulated in sea at the end of 10 years, 8 MT addition will be from the year 10. 92% of the plastics remaining would be from year 6-10 whereas there would be hardly any plastic remaining from year 1-6 as shown in the Figure 6.16. The results indicate that replacement of non-biodegradable plastics by 20, 40, 60 and 80% biodegradable plastics will result in 15.5, 31.0, 46.5 and 62.0 % reduction in ocean plastic accumulation respectively. Thus, even though the biodegradable plastics will take longer time to biodegrade in the low

temperature ocean environment, they won't last there for hundreds of years like the non-biodegradable counterparts.

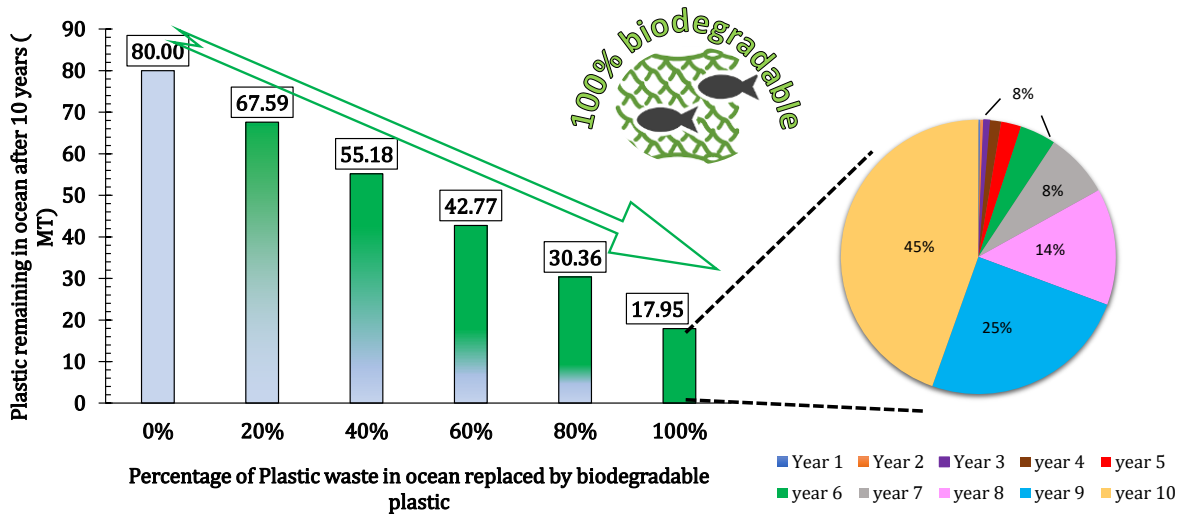


Figure 6.16: Model for plastics accumulation in ocean – impact of replacing a fraction of non-biodegradable plastics with biodegradable plastics

Following formula was derived for estimating the amount of bioplastics accumulated in ocean at any time –

Equation 6.18

$$P_f = W(1 - x) * f + \sum_{n=1}^f W \times x \times \exp[-k(t_f - t_n) \times 365]$$

Where,

P_f = plastic remaining in ocean after 'f' years (MT)

W = amount of plastic leaking in ocean every year in MT (for eg 8MT)

x = fraction of plastic waste replaced by biodegradable plastic (0.2, 0.4, 0.6 etc.)

k = rate constant of the biodegradable plastic at a particular temperature (as determined from kinetics studies for that polymer) in day⁻¹

6.11 MECHANISM OF PHBV BIODEGRADATION

To follow macroscopic modifications occurring on the surface of the PHBV pellets, optical microscopy and SEM images of the pellets were taken at different time intervals. Figure 6.17 shows the optical microscopy and SEM images and the corresponding level of biodegradation at that time obtained from the CO₂ evolution measurements. It was observed that the degradation occurred on from the surface of the pellets and the size of the pellets decreased with time. These pellets became porous with time with formation of eroded structures on the surface. This formation of porous structures could be due to faster degradation of the amorphous phases compared to crystalline phase of PHBV as generally reported in literature about PHBV[36, 17]. This clearly indicated enzymatic surface erosion mechanism.

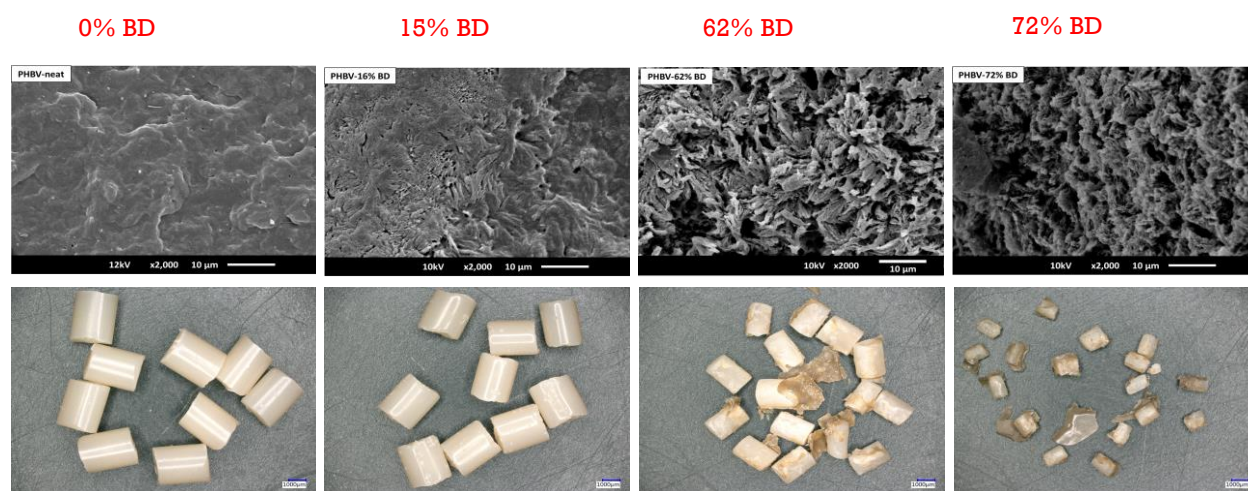


Figure 6.17: PHBV SEM and optical microscopy images at various stages of biodegradation

Changes in the molecular weight of PHBV (M_n and M_w) were also monitored as a function of biodegradation. Table 6.8 shows the M_n, M_w and PDI values for the PHBV samples at various stages of biodegradation.

Table 6.8: Evolution of number-average molecular weight (Mn), weight-average molecular weight (Mw), polydispersity index (Mn/Mw) and melting point (Tm) of PHBV samples during the course of biodegradation

% BD	Mn	Mw	PDI	T_m(°C)
0	2.52E+05	3.73E+05	1.48	176.25
15	1.71E+05	2.44E+05	1.43	175.90
62	1.33E+05	1.81E+05	1.36	172.40

A linear decrease in Mn was observed as % biodegradation increased. 30% loss in Mn was observed after 15 % biodegradation. Afterwards the rate in decrease of molecular weight was reduced. A molecular weight of 133000 was maintained even after 72% biodegradation. Polydispersity index also reduced slightly from 1.48 to 1.36. These results matched with other PHBV degradation studies in the literature [17, 24, 37]. These results suggested that the chain scission via hydrolytic degradation is not the mechanism for PHBV degradation. It is due to enzymatic activity on the surface. The slight change in molecular weight might be due to the loss of oligomers from the film surface which might be small enough to diffuse in the aqueous medium. This loss of small Mn molecules might also be the reason for decrease in PDI[36].

Next step was analysis of the thermal properties of the PHBV pellets. Figure 6.18 shows the DSC and TGA measurements for the PHBV pellets at various stages of biodegradation.

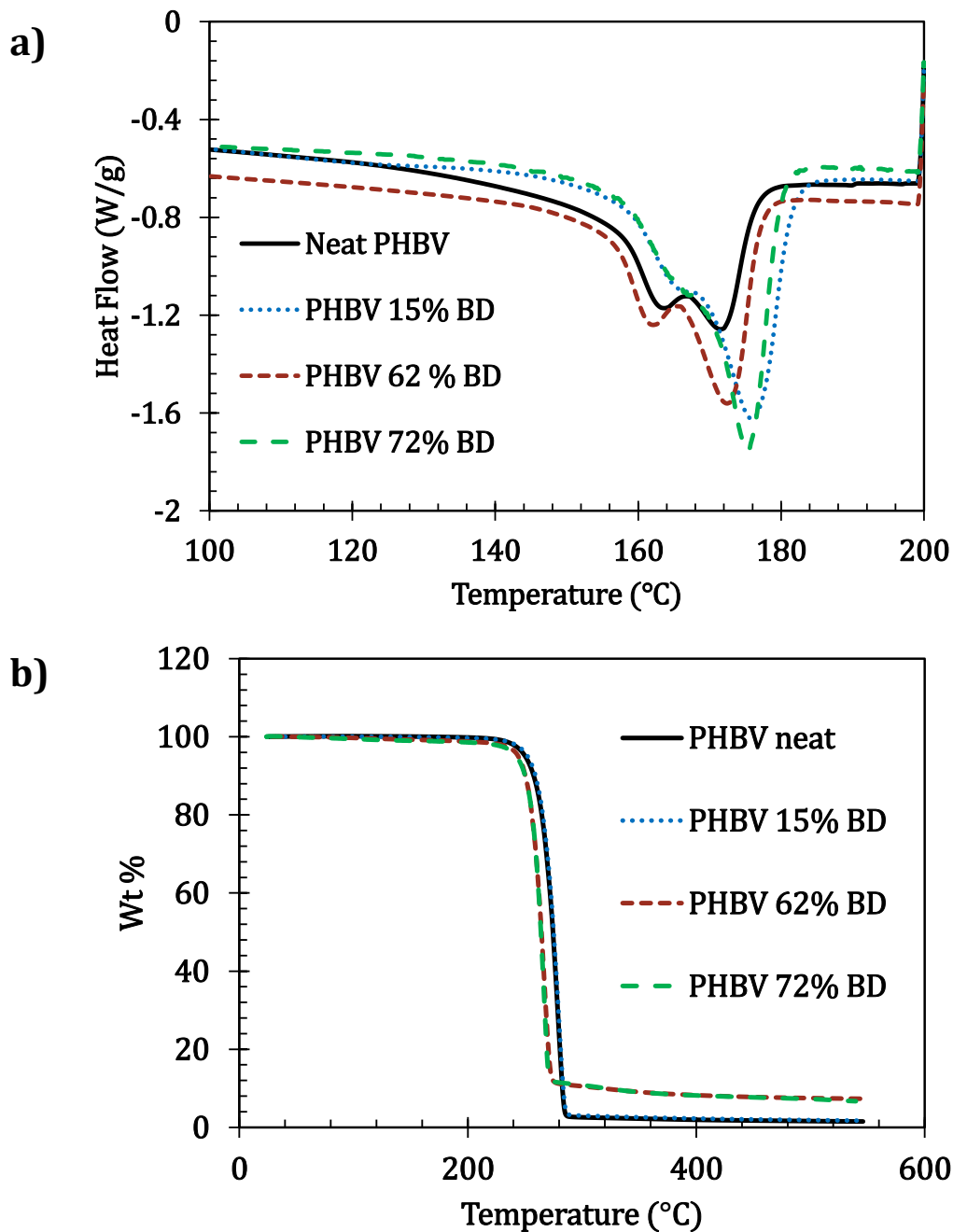


Figure 6.18: a) DSC melting peaks and b) TGA degradation curves of PHBV pellets as a function of biodegradation percentage in laboratory scale aqueous biodegradation

The DSC analysis of PHBV at various stages of biodegradation revealed that the crystallinity remained almost the same till 72% biodegradation. This suggested that both amorphous and crystalline stages are equally biodegraded from the enzymes as observed by Salomez et al. It

was also observed that the PHBV pellets showed presence of two melting peaks evolving conversely over time. the enthalpy of firs peak decreased, and the second melting peak increased with time. This suggests that there was a reorganization of the crystalline phase of the polymers during aqueous biodegradation conditions. There was a gradual decrease observed in melting temperatures for PHBV which was supported by the corresponding reduction in molecular weights as shown in Table 6.8.

6.12 CONCLUSION AND FUTURE WORK

In conclusion, this study was aimed at studying the temperature dependence of biodegradation of the two well-known polymers cellulose and PHBV. All the current ASTM and ISO standards are static approaches and they do not focus on the rate of biodegradation as a function of temperature. Aqueous biodegradation of these polymers was studied under 3 different temperatures of 10, 30 and 40°C according to ISO 14852. The rate of biodegradation was found to increase with increase in temperature following the Arrhenius relationship. Order of the reaction for biodegradation were calculated using the general nth order kinetic equation by differential and RMSE analysis. All the orders of the reactions for both cellulose and PHBV were found to be close to one. Hence, a first order kinetics was used for further analysis. The values for rate constants at different temperatures for cellulose and PHBV, activation energy for the reaction and the pre-exponential factors were calculated using three statistical approaches. It was observed that the logarithmic linearization of Arrhenius equation gave statistically insignificant values for E_a and A with large standard deviations and large confidence intervals. Reparameterization of Arrhenius equation was found to reduce the error in pre-exponential factor, but it did not improve estimation of the activation energy E_a . The third approach of incorporating reparametrized Arrhenius equation in the first order rate law and solving the resulting non-linear global equation in one step gave the most accurate and statistically useful results with narrow confidence intervals.

Based on our model, the activation energies for cellulose and PHBV were calculated to be 33.1 and 61.6 kJ/mol. These values matched very well with the average literature values for activation energies. Further, this model was used to estimate the time required for 90%

removal of the polymer from ocean environments at low temperatures through microbial metabolism. The time required for 90% biodegradation of PHBV at 10°C ranged from 6.2-6.9 years whereas it was found to be 1.1-1.2 years for cellulose. Thus, it was confirmed that the polymers will last for much longer in low temperature ocean environment than in the lab studies done at 30°C. It underlined the need for a new ASTM standard which needs to take temperature effects in account.

Based on these results, a model for plastics accumulation in ocean was also developed. It was calculated that, if 100% of the plastics accumulating in ocean every year were replaced by a biodegradable plastic with a rate of biodegradation similar to PHBV, the accumulation after 10 years would decrease from 80 MT to 17.9 MT of plastics. Moreover, 45% of that plastic will be due to fresh addition of plastic in year 10; less than 8% of the total plastic would be from the first six years. Thus, we could say that, even if these biodegradable plastics leaked into the ocean inadvertently, they will be removed from the environment within a few years. They won't remain in the ocean for hundreds of years like the non-biodegradable counterparts.

The last part of the study was to investigate the mechanism of biodegradation for PHBV. The percent biodegradation values were combined with other indicators like morphological, structural and chemical modifications induced on the surface of the PHBV to confirm surface erosion as the mechanism of PHBV biodegradation. SEM and optical imaging were powerful tools in assessing the erosion and morphological changes in the pellets throughout the course of biodegradation. High molecular weights of the pellets till the end of biodegradation were one more indication pointing towards enzymatic surface erosion

mechanism. Lastly, the changes in the thermal properties of the pellets such as melting points and enthalpies of the melting peaks suggested a recrystallization phenomenon.

It should be noted that all this work was done for two well-known and easily biodegradable polymers- cellulose and PHBV. Both of them have many degraders present in the natural environment. The situation might change for other polymers. More detailed studies might be required for the specific case.

APPENDICES

Appendix 1: NMR analysis of PHBV

The poly(3HB-co-3HV) samples were characterized by proton nuclear magnetic resonance spectroscopy (H^1 NMR). About 10 mg of polymer sample was dissolved in chloroform-d ($CDCl_3$) (99.8%; Cambridge Isotope Laboratories) and recorded using Agilent DDR2 500 MHz spectrophotometer (MSU, Michigan). The conditions were as follows- 45° pulse, 2.04 sec acquisition time, 8012.8 sweep width and 64 scans. The data was processed using MestReNova software.

The characteristic peaks at 0.87 ppm and 1.27 ppm were assigned to the resonance absorption of methyl (CH_3) from hydroxyvalerate (HV) unit and methyl (CH_3) from hydroxybutyrate (HB) unit respectively. (Liu et al 2010). The peaks at 2.47, 2.60 and 5.26 ppm were identified as $-CH_2$ (HV side), $-CH_2$ (HB side) and $-CH$ (for both HB and HV side).

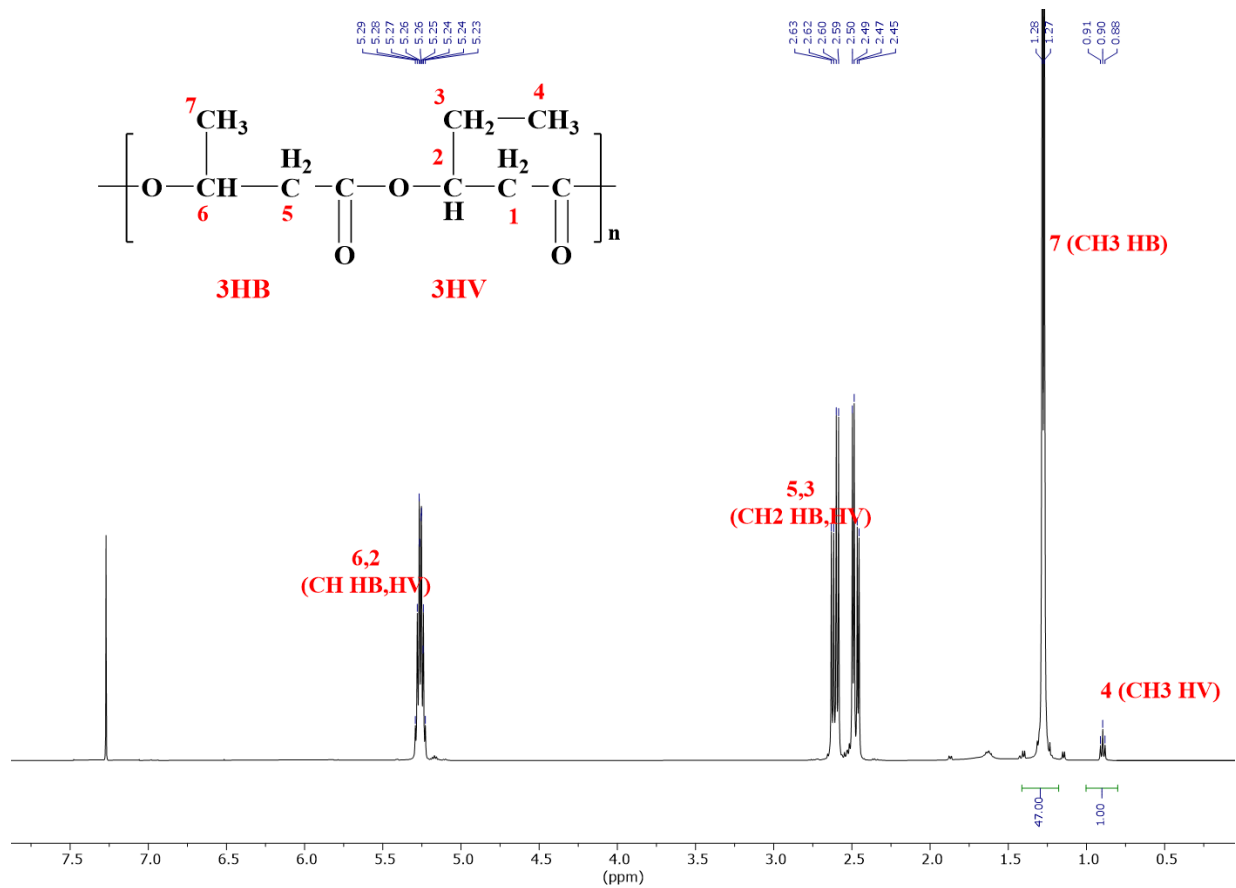


Figure 6.19: NMR curve for PHBV

The characteristic peaks at 0.87 ppm and 1.27 ppm can be used for determining the mole % of HV in poly(3HB-co-3HV) using following equation.

Equation 6.19

$$HV \text{ mol } \% = \frac{\text{Area } (-CH_3)_{HV}}{\text{Area } (-CH_3)_{HV} + \text{Area } (-CH_3)_{HB}}$$

It was found that HV composition is 2 mol %.

Appendix 2: Carbon removal against time curves

Re-plot the experimental percent biodegradation curves in terms of - carbon removal against time (days)

Percent carbon removal or C/C_0 vs time (days)

1 mole of C \rightarrow 1 mole CO_2

Number of moles of CO_2 produced = number of moles of carbon consumed from the sample

$$CO_{2(\text{sample-blank})} = C_{\text{consumed}}$$

$$\text{And } C_{\text{remaining}} = C_{\text{initial}} - C_{\text{consumed}}$$

where C_{initial} can be calculated theoretically from the % C content and the weight of the polymer added at the start of the test. = $CO_{2(\text{theoretical})}$

$$\text{i.e. } C_{\text{remaining}} = C O_{2(\text{Theoretical})} - CO_{2(\text{sample-blank})}$$

Appendix 3: Metagenomic analysis

Activated sludge from east lansing wastewater treatment plant was used as microbial inoculum in all the tests. It was analyzed for the microbial communities present using metagenomic analysis. Illumina sequencing was performed for the 16S rRNA gene region to assess the bacterial community at Research Technology Support Facility (RTSF, Michiagan State University). The sequencing were analyzed using the QIIME2 database to generate taxonomic/phylogenetic data for statistical analysis.

The results were compared with the various seawater microbial communities from literature. Although there are some differences in the quantitative microbial communities in water obtained from different sources, the overall microbial population on family level was more or less the same. Hence, a wastewater sample can be used as an easily obtainable source of inoculum which could be used as a representation for seawater samples.

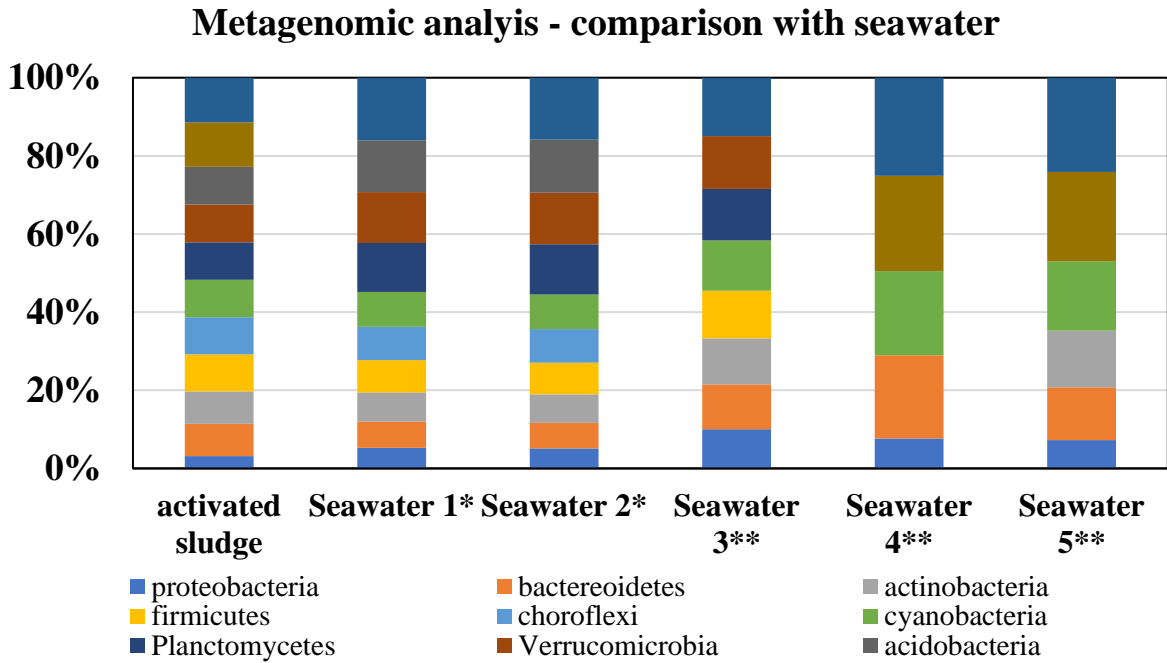


Figure 6.20: Comparing the microbial populations from wastewater and seawaters from various places

* - Rehman, Z. U., Ali, M., Iftikhar, H., & Leiknes, T. (2019), *Water Research (Oxford)*, 149, 263-271.

** - Greer, Charles & Wyglinski et al., (2014). Natural Attenuation Potential for Oil in Ice in the Canadian Arctic Marine Environment

Appendix 4: Order of reaction and rate constant determination using n^{th} order kinetic equation

1. Differential method:

The general rate law equation is

Equation 6.20

$$\frac{-dC}{dt} = kC^n$$

Where, [C] is the moles of carbon consumed by the micro-organisms to yield CO₂, k is the rate constant, n is the order of the reaction and t is the time.

Taking natural log on both sides

Equation 6.21

$$\ln\left(\frac{-dC}{dt}\right) = \ln k + n \ln C$$

If we plot $\ln(-dC/dt)$ vs $\ln C$,

the slope of the line should give n – order of the reaction

And the intercept should give $\ln k$ – rate constant for the reaction

These plots were made for all cellulose samples at 3 different temperatures as follows. It should be noted that only the biodegradation phase of the curves was considered for calculating the rate constants and order of the reaction. Lag phase and the plateau phase of the biodegradation graph was not considered in these calculations.

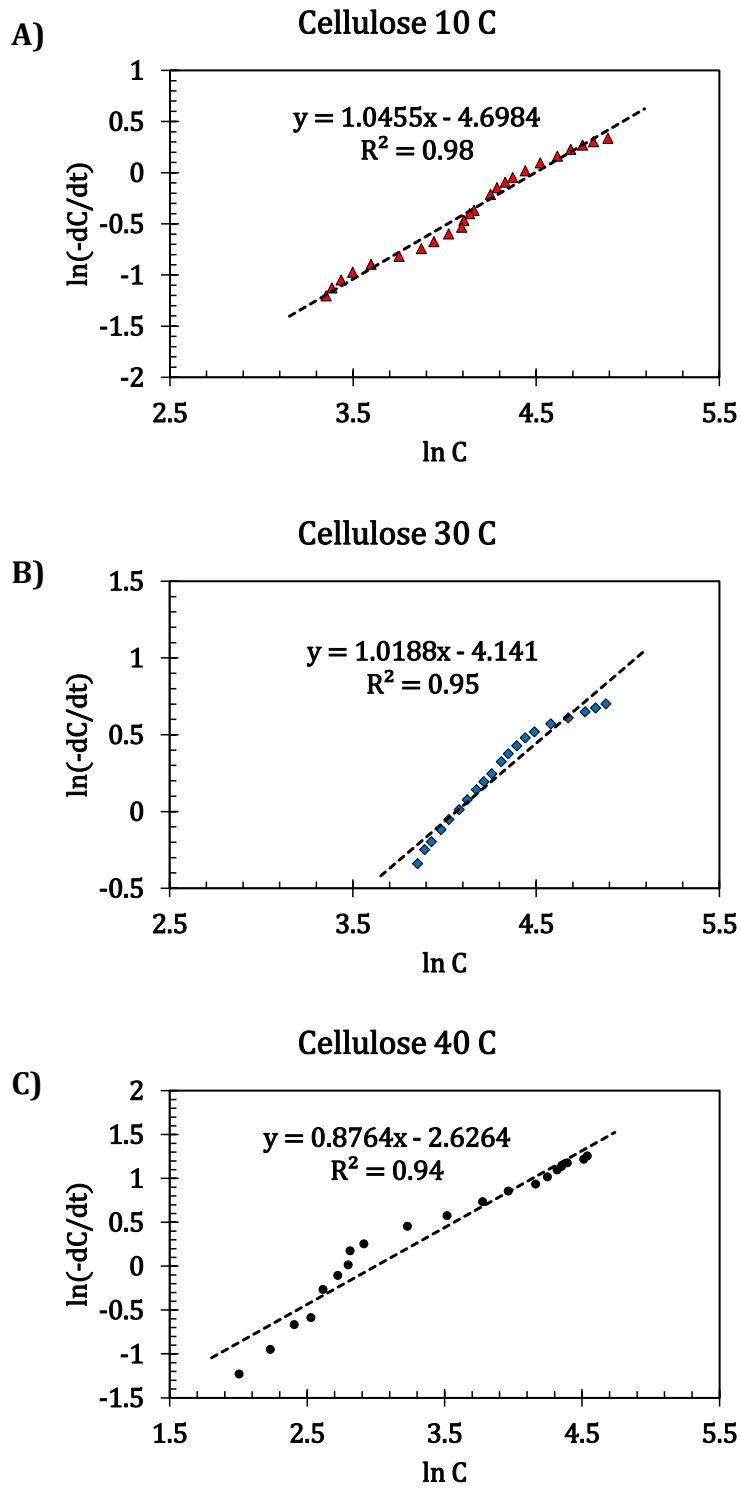


Figure 6.21: $\ln(-dC/dt)$ vs $\ln C$ plot for cellulose at A) 10 C, B) 30 C, C) 40 C

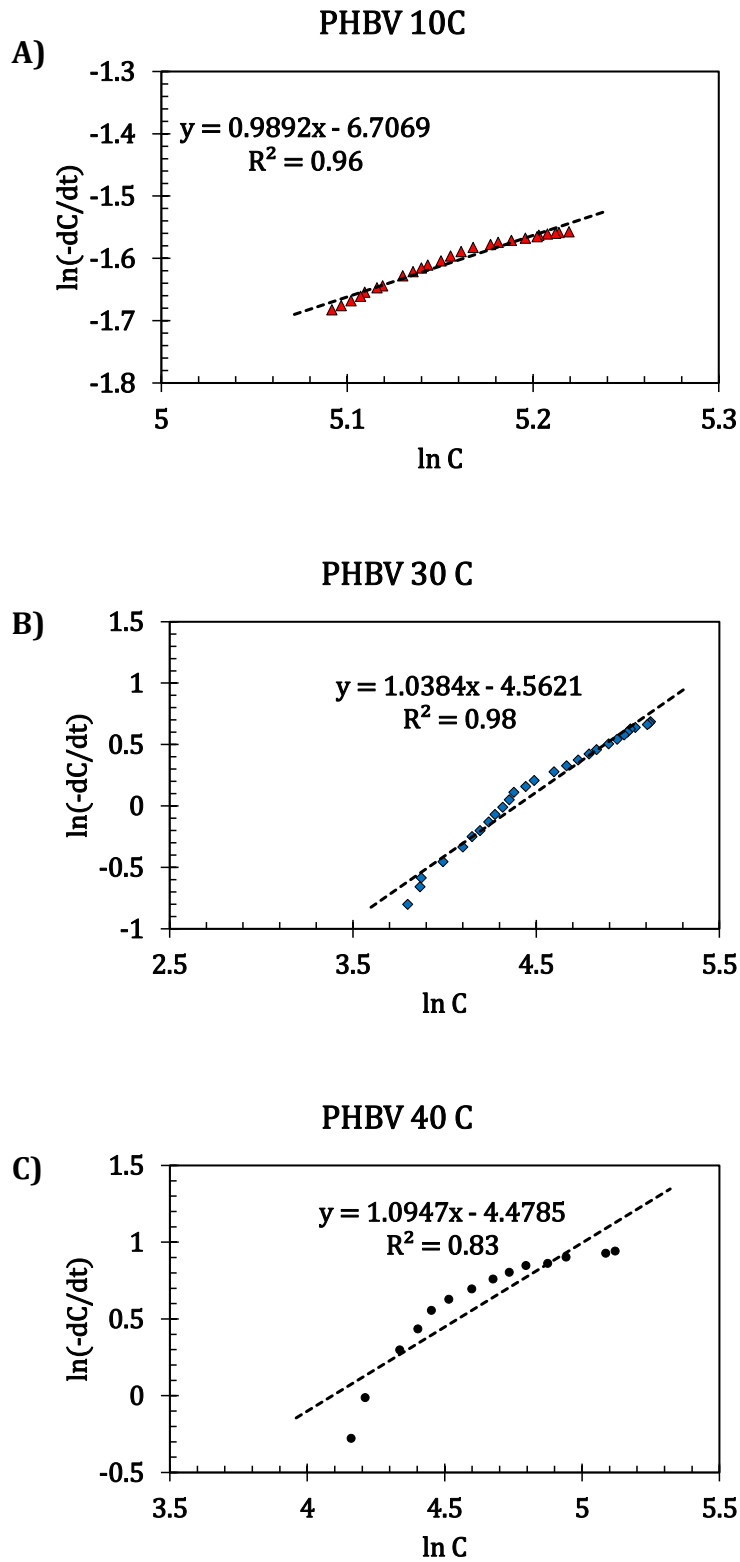


Figure 6.22: $\ln(-dC/dt)$ vs $\ln C$ plots for PHBV at A) 10 C, B) 30 C, C) 40 C

2. RMSE method

The general rate law is -

Equation 6.22

$$\frac{-dC}{dt} = kC^n$$

Integrating gives the rate law equation for nth order reaction as -

Equation 6.23

$$C = [C_0^{(1-n)} - (1-n)kt]^{\frac{1}{1-n}}$$

Where,

C → moles of carbon left at any time t

C₀ → initial moles of carbon added to the biodegradation flask

k → rate constant

n → order of the reaction

Assuming some initial values for k and n, a predicted value for C – C_{predicted} was calculated for each day. Then the root mean square of the errors, i.e. difference between the predicted values and the actual value of C remaining were calculated and was minimized using excel solver to get the optimized values of n and k.

Equation 6.24

$$RMSE_{Errors} = \sqrt{\frac{\sum_{i=1}^n (\hat{y}_i - y_i)^2}{n}}$$

Following graphs show the C_{predicted} vs C_{actual} graphs and the calculated n and k values for cellulose at 3 different temperatures.

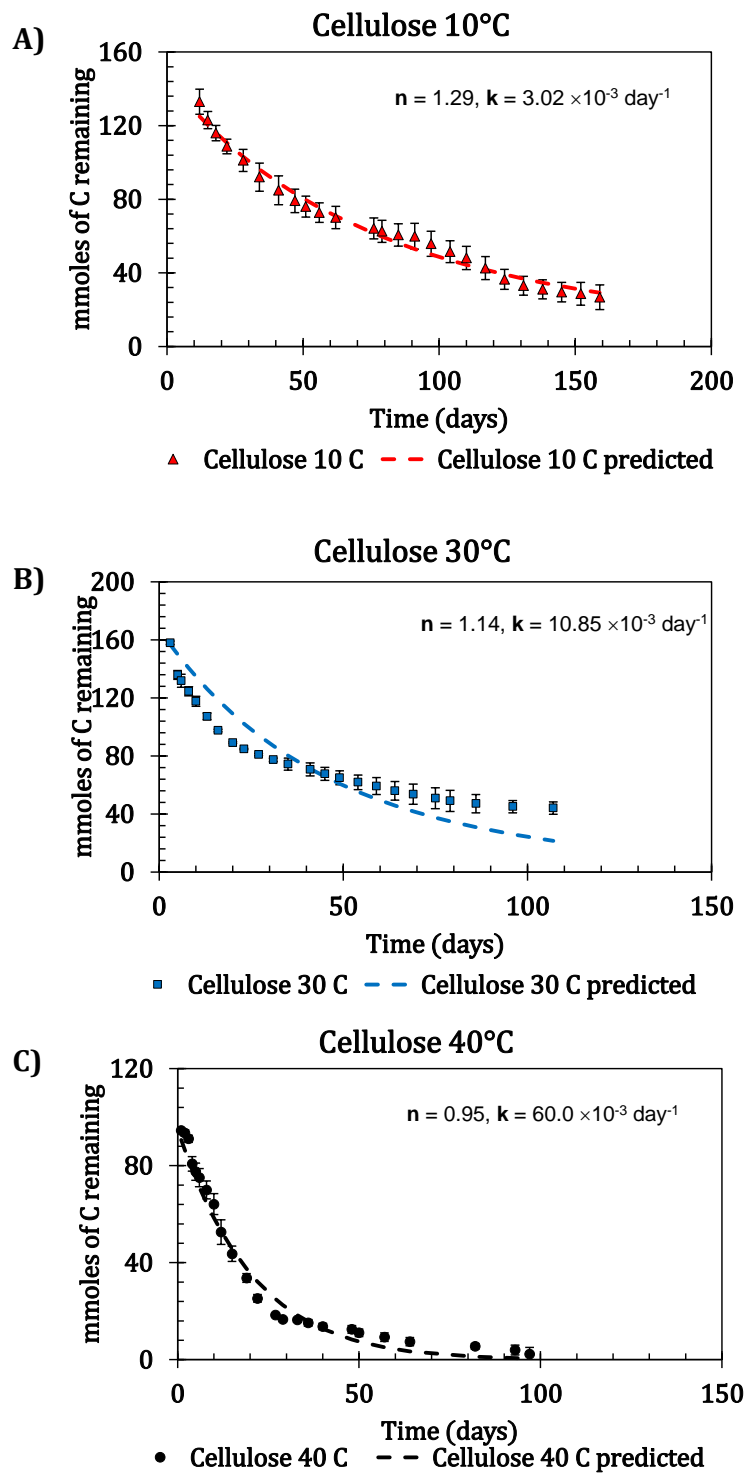


Figure 6.23: mmoles of carbon remaining vs time plots for cellulose at A)10C, B)30C, C) 40 C

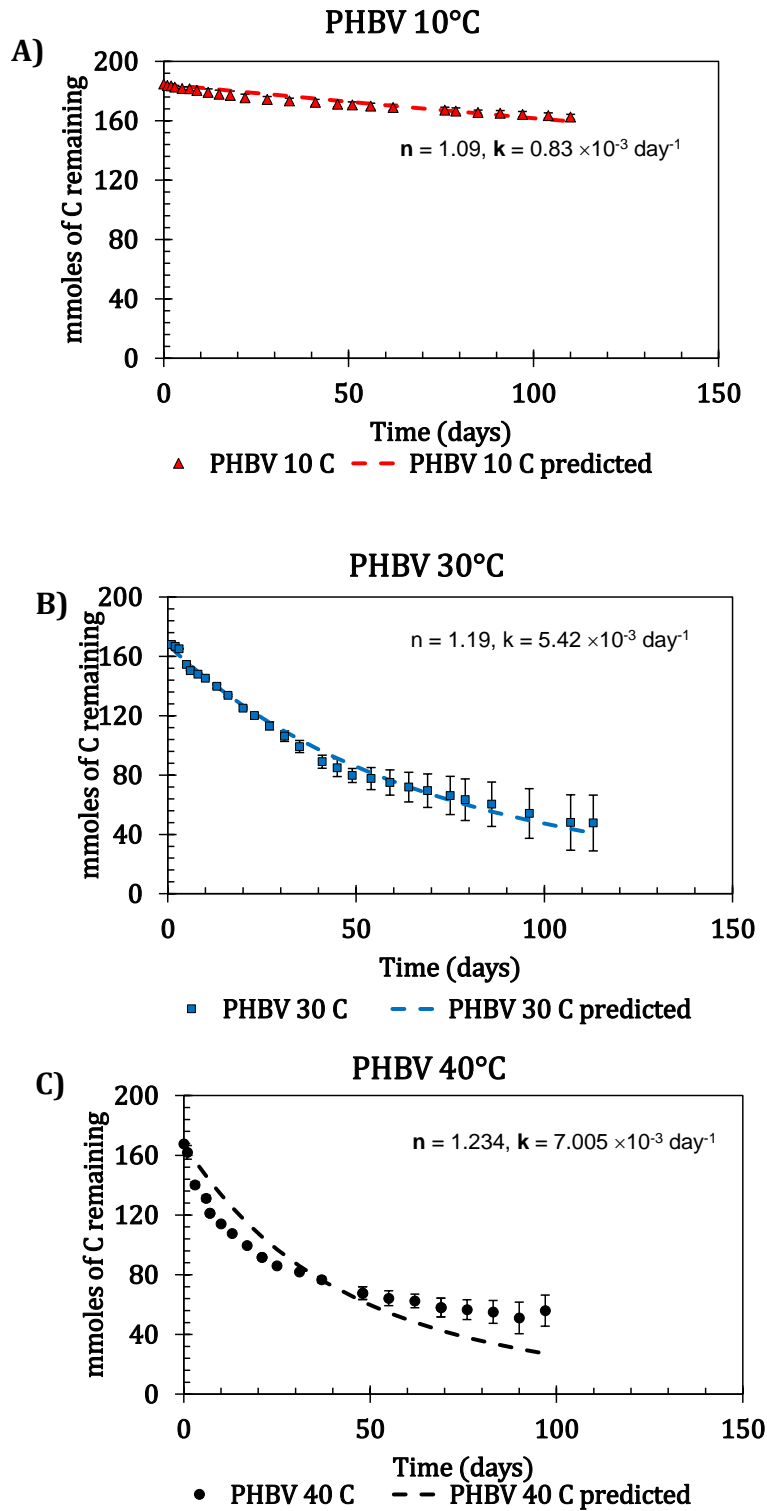


Figure 6.24: Mmoles of carbon remaining vs time plots for PHBV at A)10C, B)30C, C) 40C

Appendix 5: Using global equation for estimating Ea and A' values

Use non-linear regression analysis of the global kinetic rate law equation and plot percent or fraction of polymer carbon removal against time graphically. The reparametrized Arrhenius parameters is put into the rate law equation to generate the global kinetic rate law equation.

Equation 6.25

$$\frac{C}{C_0} = \exp\left(-\left(A' \exp\left(-\frac{Ea}{R}\left(\frac{1}{T} - \frac{1}{T_{ref}}\right)\right)\right)t\right)$$

Use this equation to calculate the values of A' and Ea along with their 95% confidence intervals. (you can use any statistical program like minitab or matlab etc. for getting these values)

Here, C/C₀ values vs time will be obtained from experimental data. You need at least 3 temperature datasets (preferably in replicates) for using this global equation.

T_{ref} is generally taken as average of the testing temperatures.

The method shown here is using Minitab software.

First select the Stat option from main menu bar and go to 'Regression' → 'Nonlinear regression'

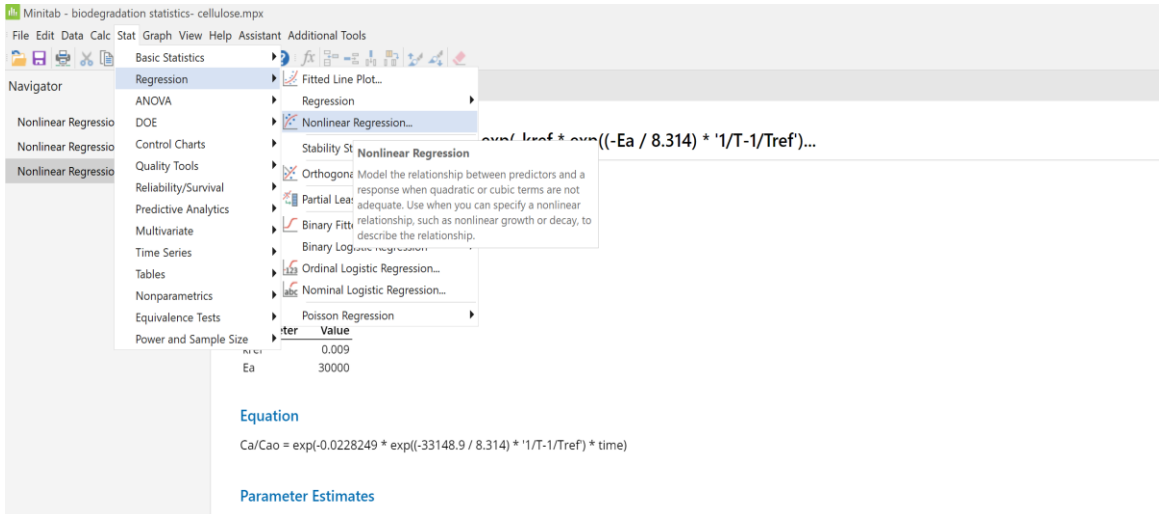


Figure 6.25: minitab methodology for global equation-1

Input the global equation described below in the 'edit directly' dialogue box. Set some initial values for Ea and A' and run the regression.

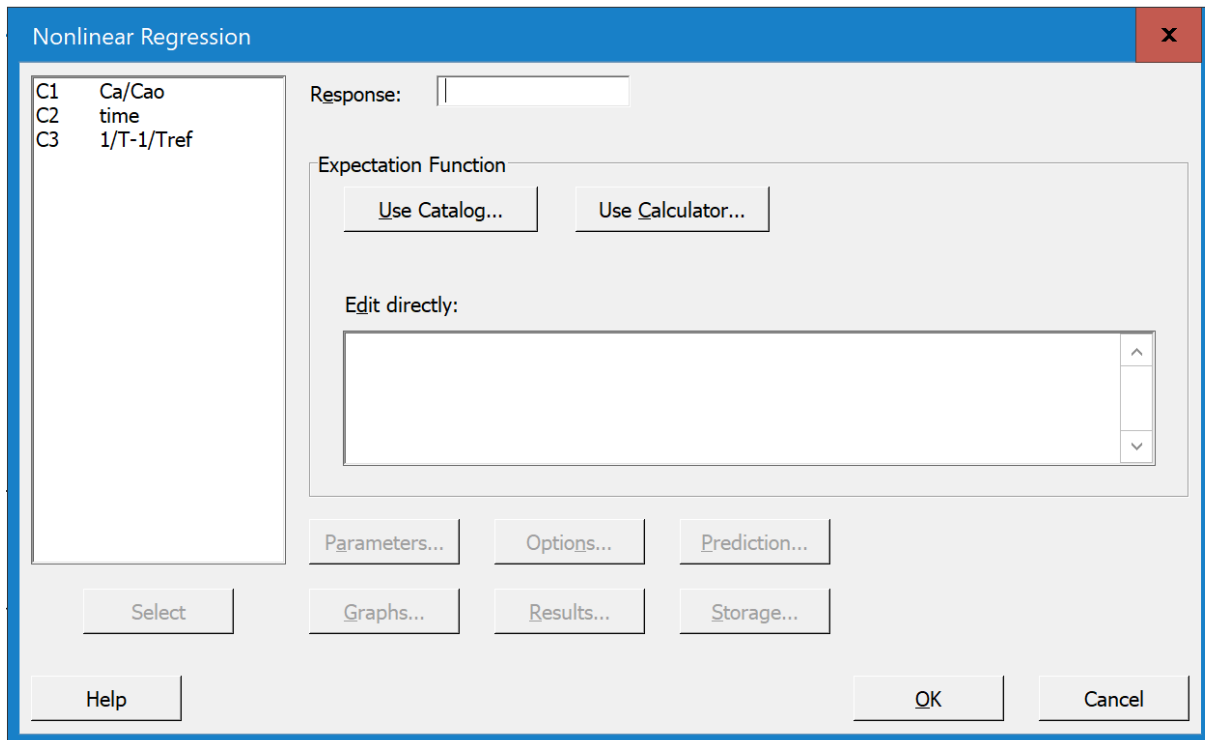


Figure 6.26: minitab methodology for global equation-2

We get the values of the A' (shown as k_{ref} in the picture) and E_a .

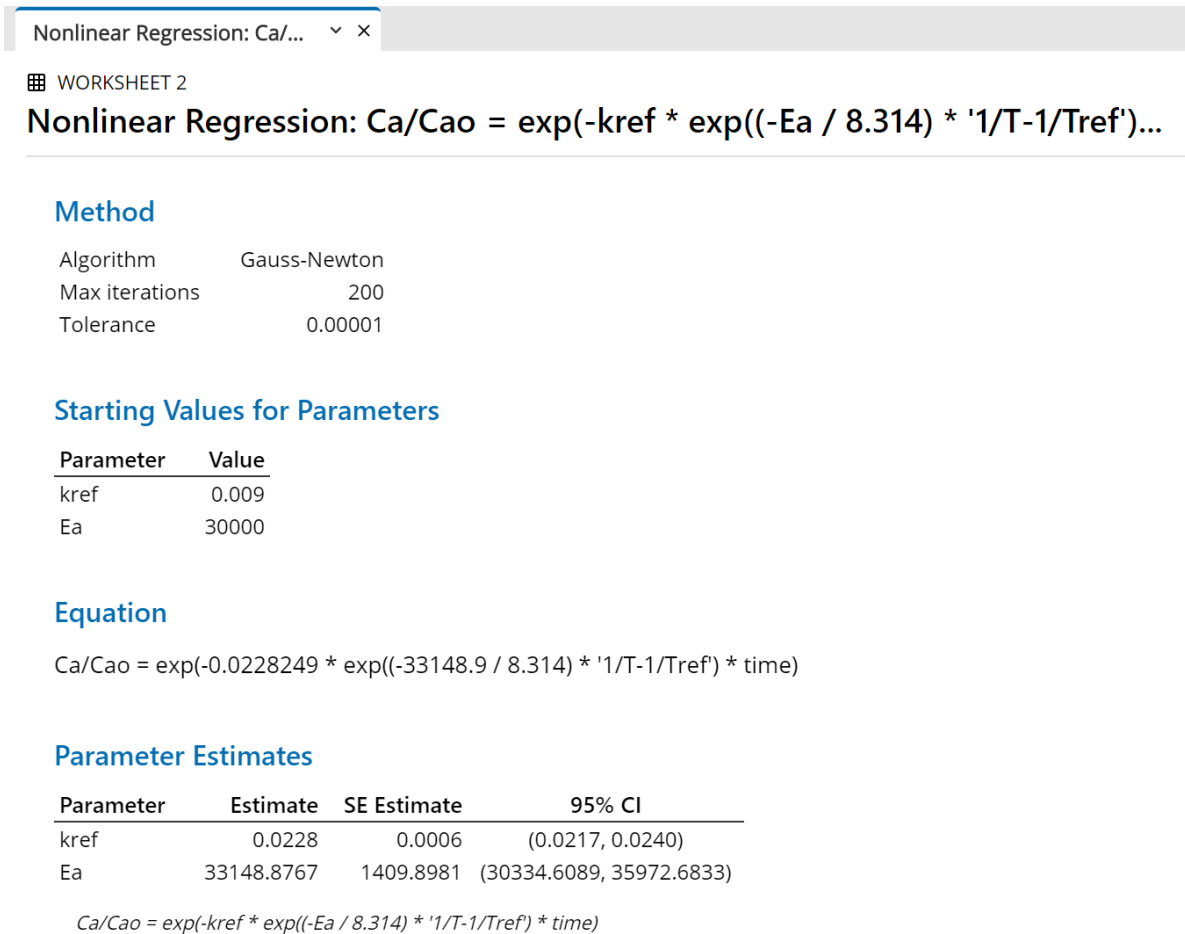


Figure 6.27: minitab methodology for global equation-3

Then you can use these values to calculate the time required for reaching any % biodegradation at any temperature (T) between the studied experimental range using the global equation given above.

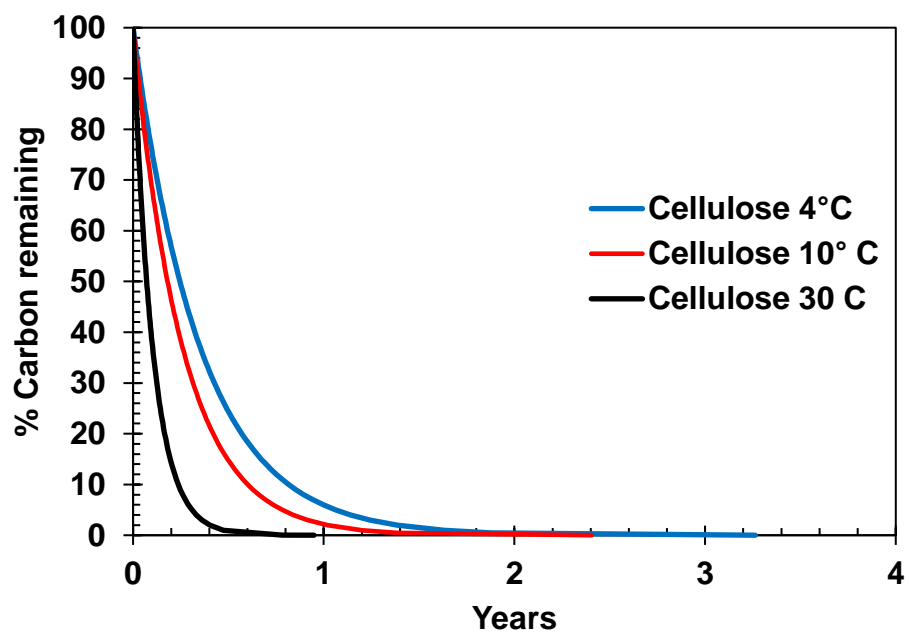


Figure 6.28: Percent carbon remaining vs time graphs (lifetime prediction) for cellulose at various temperatures

Appendix 6: lifetime prediction

Using the values of activation energy and pre-exponential factors obtained from the three methods, time required for 50, 90 and 99 % biodegradation of PHBV and cellulose at temperatures of 10, 30 and 40°C was calculated. An estimation for the time required for biodegradation at 4°C was also made by extrapolation of this model at lower temperatures

Table 6.9: Lifetime estimation for PHBV and cellulose at 30, 10 and 4° C

Polymer					Time range estimation (years)		
	Temperature	Method	k range (10 ⁻³) (day ⁻¹)	E _a range (kJ/mol)	(95% confidence interval)		
					50% Biodegradation	90% Biodegradation	99 % Biodegradation
PHBV	10	1	0.86 -2.1	50.83- 90.42	0.90 -2.19	3.00 -7.28	6.0 -14.5
		2	1.4 -2.4	23.11- 84.07	0.77 - 1.33	2.56 -4.42	5.14 -8.84
		3	1.52 -1.68	56.51 – 66.26	1.12 - 1.25	3.74 -4.15	7.48 - 8.31
	4	1	0.37 -1.32	50.83- 90.42	1.44 - 5.04	4.79 -16.75	9.58 - 33.50
		2	0.66 -1.81	23.11- 84.07	1.04 - 2.87	3.48 - 9.56	6.97 - 19.2
		3	0.81 -1.00	56.51 – 66.26	1.89 -2.32	6.29 - 7.71	12.59 - 15.44
	30	1	8.75- 10.9	50.83- 90.42	0.17 - 0.21	0.58 -0.72	1.15 - 1.44
		2	4.28 -15.0	23.11- 84.07	0.12 - 0.44	0.42 - 1.47	0.84 - 2.95
		3	8.23 -10.0	56.51 – 66.26	0.19 - 0.23	0.63 - 0.76	1.25 - 1.53
Cellulose	10	1	8.13 - 13.7	17.75 - 40.83	0.18 - 0.23	0.46 - 0.78	0.92 - 1.55
		2	5.98 - 8.48	20.71 - 61.44	0.22 - 0.32	0.74 - 1.06	1.49 - 2.11
		3	8.61 - 8.89	30.33 - 33.15	0.21 - 0.22	0.71 - 0.73	1.42 - 1.46
	4	1	5.58 - 11.6	17.75 - 40.83	0.16 - 0.34	0.54 - 1.13	1.09 - 2.26
		2	3.40 - 6.97	20.71 - 61.44	0.27 - 0.56	1.04 - 1.86	1.81 - 3.72
		3	6.19 - 6.72	30.33 - 33.15	0.28 - 0.31	0.94 - 1.02	1.88 - 2.04
	30	1	22.5 - 25.5	17.75 - 40.83	0.07 - 0.08	0.25 - 0.28	0.49 - 0.56
		2	15.1 - 33.5	20.71 - 61.44	0.06 - 0.13	0.19 - 0.42	0.38 - 0.84
		3	20.8 - 23.6	30.33 - 33.15	0.08 - 0.09	0.29 - 0.30	0.53 - 0.57

Appendix 7: Table for obtaining %C remaining vs time graphs

Table 6.10: Percent carbon remaining vs time

% C remaining	Cellulose 10 C	Cellulose 30 C	Cellulose 4 C	PHBV 10 C	PHBV 30 C	PHBV 4 C
100	0.000	0.000	0.000	0.000	0.000	0.000
90	0.028	0.011	0.037	0.149	0.026	0.263
80	0.058	0.023	0.079	0.316	0.056	0.558
70	0.093	0.037	0.126	0.505	0.090	0.891
60	0.133	0.053	0.181	0.724	0.128	1.277
50	0.181	0.071	0.246	0.982	0.174	1.732
40	0.239	0.094	0.325	1.298	0.230	2.290
30	0.314	0.124	0.427	1.705	0.302	3.009
20	0.420	0.166	0.570	2.280	0.404	4.022
10	0.601	0.237	0.816	3.261	0.578	5.755
5	0.782	0.309	1.061	4.243	0.752	7.487
1	1.203	0.474	1.632	6.523	1.156	11.509

Appendix 8: Literature summary

Literature summary for selected articles using several methods for assessing biodegradation of cellulose and PHBV in aqueous environment

Table 6.11: Literature summary

	Referenc e	environme nt	Sampl e	form	size	Mn	Mw	time	Tempe rature (°C)	% Biodegradation
1	Deroine et al., 2014[24]	distilled water	PHBV	solid pelletes	180*10 *4 mm	172600	39880 0	12 mont hs	25, 30, 40, 50	not studied
2	Deroine et al., 2015[17]	marine water (natural)	PHBV (8% HV)	PHBV films	200*12 0 mm* 200 µm		40000 0	180 days	10-20 C	36 % wt loss
3	deroine et al., 2015		PHBV (8% HV)	PHBV powder	-	259000	450,00 0	1 year	25	90%
4	Doi et al., 1990[14]	distilled water (hydrolysis)	PHB , PHBV (HV 45%)	10*10*0. 04 mm	10 mm dia * 0.04- 0.07 mm thick				Hydrol ytic - 55	20% wt loss
		Enzymatic (aqueous)						20 h	Enzym atic - 37	
5	Doi et al., 1992[27]	aqueous	P-3- HBV	films	10*10* 0.04 mm	-	20400 0	19 hr	37	20-25% wt loss

Table 6.10 cont'd

					4.5-6 mg wt		194000			60-70% wt loss
6	Ken-ichi Kasuya," Ko-ichi Takagi et al., 1997[29]	seawater	PHB, PHBV, PHBB	film	10 mg , thickness 0.1 mm	186000	480000	28 days	25	100% wt loss
										80% acc to BOD
7	Yamada, Doi 1995[28]	Enzymatic (aqueous)	PHB			37000-60000		3-4 hr	25-37	
8	Greene et al., 2012[21]	marine	Mirell 2200 PHA	film	1g			6 months	30	38
			Mirel 4100 PHA	film	1g			7 months	30	45
			Micro cellulose	powder	1g			8 months	30	33
9	Ho, Gan et al., 2002[38]	river water	PHA	film	15*15 mm			86 days	28	71% wt loss
10	Lo Wing Hong, Jian Yu[39]	Aqueous	PHBV	discs,	15 mm dia, 0.1 mm thick, 18-23 mg		400000	10-15 days	20, 30, 37	not studied

Table 6.10 cont'd

11	Lotto et al., 2004[25]	soil	PHBV	powder			150000		24, 46	
12	Mergaert et al., 1992[40]	soil	PHBV	injection molded dog bone pieces				200 days	15, 28 and 40	
13	Sashiwa, Nakayama; 2018[26]	seawater	PBHH	pellets	30 mg	280000	550000	28 days	28	30%
14	Thellen et al., 2008[22]	seawater	PHBV	films				100 days	30	80-85 %
15	Tsuji, Suzuyoshi; 2002[41]	static seawater	PHB	films	3*30*50 um and 18*30*25 um	765000	1530000	70 days	25	
17	Wang, Laydon et al; 2018[42]	seawater	PHBH (7.1% hexanoate)	sheet	5*5*1 mm	446203		148-195 days	Ambient temp (20 -25 C)	PHBV sheet - 55.3+_38.3
				flakes		50670				PHBV flakes - 88.6
18	Volova et al.; 2011[37]	seawater (south china sea)	PHB	film disc	73 mg, 30 mm dia, 0.1mm thick			160 days	28-30	40-42 % for both PHB and PHBV disc

Table 6.10 cont'd

			PHBV (11 mol % HV)	molded solids	300 mg, 10 mm dia, 5 mm thick					38% for PHB and 13 % for PHBV for molded solids
19	Nanthini Sridewi, Kesaven Bhubalan, Kumar Sudesh; 2006[43]	Mangrove environment	PHB	film	1cm * 1cm	600000		56 days	30	~ 70%
			PHBV			680000				similar for all 3
			PHBH			460000				
20	Doi, Kanesawa, Tanahashi; 1992[31]	Seawater	P-3-HB-co-3HV	solvent casted and melt extruded films	50-150 um (5*10 cm in size)			variable	variable from 13 to 26	not given
			P-3-HB-co-4HV		2.05-2.10 mm					
21	Shang, Logan, et al; 2011[44]	Distilled water and enzyme hydrolysis	PHBV (9.5 % HV)	films	0.2 mm thick, 2cm ² area	-	-	50 days	37	20% for without enzyme in 50 days, ~ 70% with lipase enzyme

Table 6.10 cont'd

22	Greene J, 2018[45]	Ocean water	PHA	bag	-	-	-	180 days	30	ASTM 6691
23	Wang et al., 2018[42]	seawater	cellulose	powder				150 days	25	90%
24	Greene et al., 2012[46]	marine	Microcellulose	powder	1g			8 months	30	33
25	Iggui, Moigne et al., 2015	Aqueous	Microcrystalline cellulose					28 days	20	85%
26	Vorgelegt von Jan P. Eubeler	Aqueous	Cellulose	powder				300 days	25	>90%
27	U. Pagga et al.; 2001	aqueous	Mater Bi starch blend					50-60 days	25	betn 60-92 %
28	Fa, Wang et al.; 2015	Aqueous	filter paper					60 days	25	85%
29	V. Mezzanotte, M. Tosin et al.; 2004	Aqueous	Cellulose					150 days	RT (assume 25)	average 83%

Table 6.10 cont'd

30	Puccini, Sandra et al.; 2017[47]	Aqueous	filter paper					365 days	20	78%
31	Thellen et al.; 2008	Seawater	cellulose	Powder				100 days	30	90%
32	CiCLO additive technology; 2020	Seawater	Cellulose					498 days	25	78 -80 %
33	Tosin M, Weber M, et. al., 2012[48]	Seawater	Filter paper		-	-	-	250 days	RT (Assume 25)	78%
34	Greene J., 2018[45]	Seawater	Cellulose	Powder	-	-	-	180 Days	30	50%

Appendix 9: Method 1 calculations

Method 1

For a first order reaction, the rate law is

$$\mathbf{Rate} = -\frac{d[C]}{dt} = k[C]$$

where [C] is the moles of carbon consumed by the micro-organisms to yield CO₂, k is the rate constant and t is the time. [33]

$$\int_{C_0}^C -\frac{d[C]}{dt} = \int_0^t k[C]$$

$$\ln[C] - \ln[C_0] = -kt$$

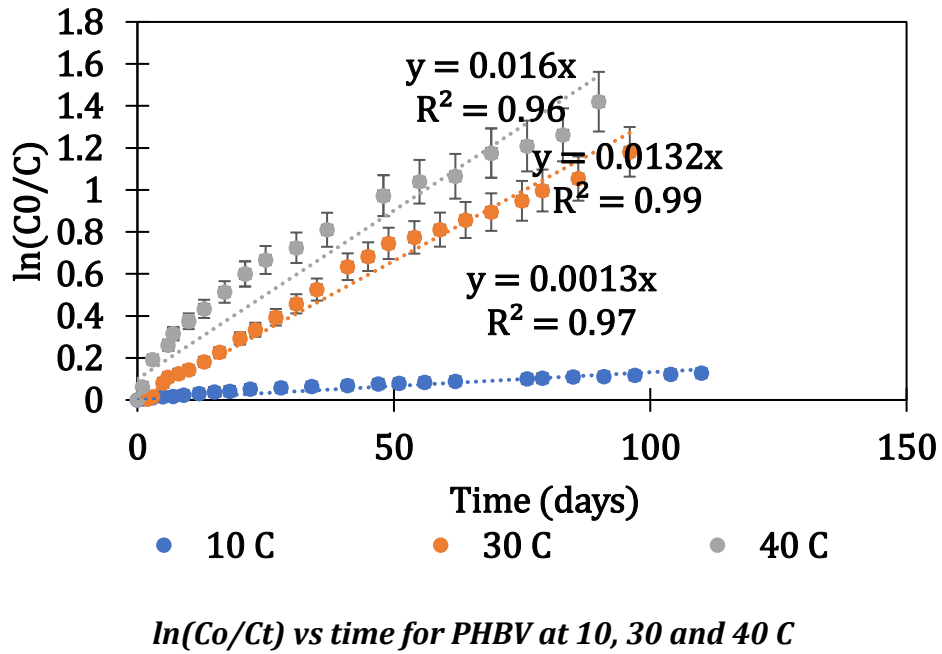
$$\ln[C] = \ln[C_0] - kt$$

Where [C_t]- moles of carbon remaining at time t and [C₀] is initial moles of carbon present.

$$\ln \frac{C_t}{C_0} = -kt \quad \text{or} \quad \ln \frac{C_0}{C_t} = kt$$

Millimoles of carbon remaining (C_t) were found by subtracting the mmoles of carbon evolved from the initial mmoles of carbon added in the test (C₀). A plot of ln[C₀/C_t] vs t was made for the PHBV and cellulose samples at different temperatures .

A)



B)

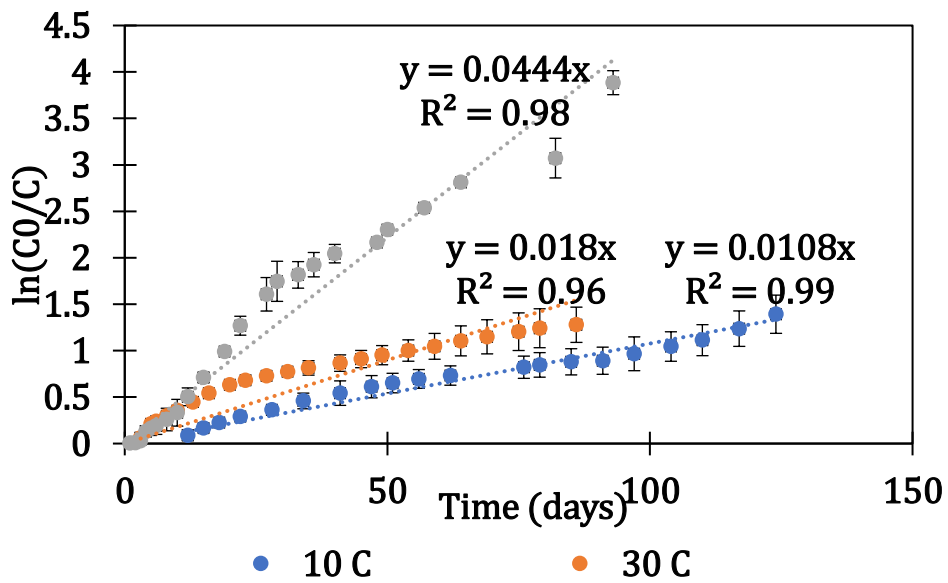


Figure 6.29: $\ln(Co/Ct)$ vs time for PHBV and cellulose at 10, 30 and 40°C

The natural log of rate constants at various temperatures were plotted against reciprocal of temperature to obtain Arrhenius plot.

The biodegradation rate values are reported as positive values. However, in reality, they should be considered as negative, as they are rates of consumption.

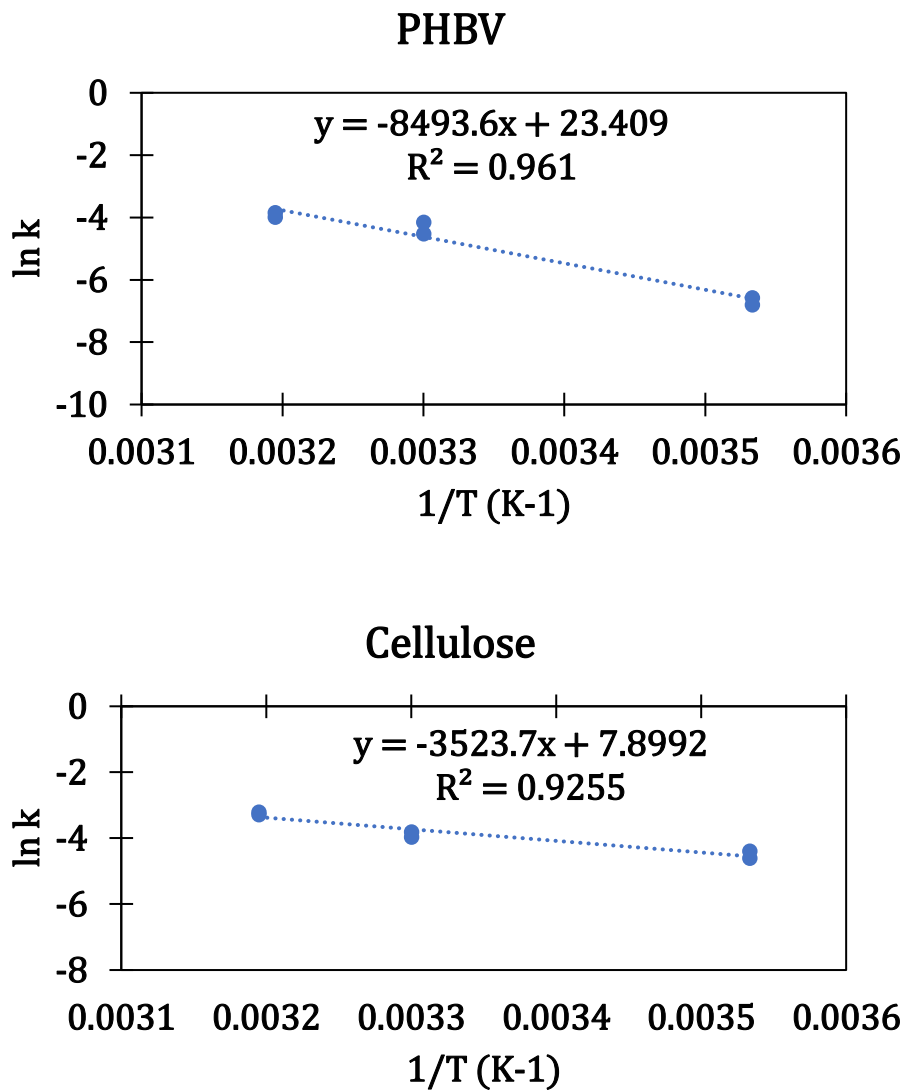


Figure 6.30: Arrhenius plots for PHBV and cellulose

Where k is the rate constant; T is the temperature in K; E is the activation energy and R is the ideal-gas constant (8.314 J/K.mol). The energies of activation were calculated as 70.6 kJ/mol and 29.29 kJ/mol respectively.

Appendix 10: Ocean plastic accumulation model

Table 6.12: Ocean plastics accumulation model

Assume	
if it is BD	PHBV
Temperature	10 C
rate constant	0.00161 day ⁻¹

100 % replaced by biodegradable plastic like PHBV		Plastic remaining from										
Year	amount of plastic added every year (MT)	Year 1	year 2	Year 3	Year 4	Year 5	Year 6	Year 7	Year 8	Year 9	Year 10	
1	8	8										
2	8	4.445	8.000									
3	8	2.470	4.445	8.000								
4	8	1.372	2.470	4.445	8.000							
5	8	0.762	1.372	2.470	4.445	8.000						
6	8	0.424	0.762	1.372	2.470	4.445	8.000					
7	8	0.235	0.424	0.762	1.372	2.470	4.445	8.000				
8	8	0.131	0.235	0.424	0.762	1.372	2.470	4.445	8.000			
9	8	0.073	0.131	0.235	0.424	0.762	1.372	2.470	4.445	8.000		
10	8	0.040	0.073	0.131	0.235	0.424	0.762	1.372	2.470	4.445	8	
											Total plastic remaining after 10 years	
											17.95258455	

REFERENCES

REFERENCES

- [1] K. L. Law and R. Narayan, "Reducing environmental plastic pollution by designing polymer materials for managed end-of-life," *Nature Reviews Materials*, 2021, doi: 10.1038/S41578-021-00382-0.
- [2] J. R. Jambeck *et al.*, "Plastic waste inputs from land into the ocean," *Science (1979)*, vol. 347, no. 6223, pp. 768–771, Feb. 2015, doi: 10.1126/science.1260352.
- [3] A. R. Bagheri, C. Laforsch, A. Greiner, and S. Agarwal, "Fate of So-Called Biodegradable Polymers in Seawater and Freshwater," *Global Challenges*, vol. 1, no. 4, p. 1700048, Jul. 2017, doi: 10.1002/gch2.201700048.
- [4] G. Kale, R. Auras, S. P. Singh, and R. Narayan, "Biodegradability of polylactide bottles in real and simulated composting conditions," *Polymer Testing*, vol. 26, no. 8, pp. 1049–1061, Dec. 2007.
- [5] T. P. Haider, C. Völker, J. Kramm, K. Landfester, and F. R. Wurm, "Plastics of the Future? The Impact of Biodegradable Polymers on the Environment and on Society," *Angewandte Chemie - International Edition*, vol. 58, no. 1, pp. 50–62, Jan. 2019, doi: 10.1002/anie.201805766.
- [6] T. Kijchavengkul, G. Kale, and R. Auras, "Degradation of biodegradable polymers in real and simulated composting conditions," in *ACS Symposium Series*, Jan. 2009, vol. 1004, pp. 31–40. doi: 10.1021/bk-2009-1004.ch003.
- [7] J. Bergman, "Temperature of Ocean Water," *Windows to the universe*, 2011. <https://www.windows2universe.org/?page=/earth/Water/temp.html> (accessed Feb. 29, 2020).
- [8] "Materials: Marine Biodegradable Bioplastic Compound," *Plastics Technology*, 2018. <https://www.ptonline.com/products/materials-marine-biodegradable-bioplastic-compound> (accessed Feb. 29, 2020).
- [9] A. Nakayama, N. Yamano, and N. Kawasaki, "Biodegradation in seawater of aliphatic polyesters," *Polymer Degradation and Stability*, vol. 166, pp. 290–299, Aug. 2019, doi: 10.1016/j.polymdegradstab.2019.06.006.
- [10] A. Pischedda, M. Tosin, and F. Degli-Innocenti, "Biodegradation of plastics in soil: The effect of temperature," *Polymer Degradation and Stability*, vol. 170, p. 109017, Dec. 2019, doi: 10.1016/j.polymdegradstab.2019.109017.
- [11] "Deep Ocean Temperatures," *Environmental news network*, 2010. <https://www.enn.com/articles/41816-deep-ocean-temperatures> (accessed Apr. 23, 2022).

- [12] B. Laycock *et al.*, "Lifetime prediction of biodegradable polymers," *Progress in Polymer Science*, vol. 71, pp. 144–189, Aug. 2017, doi: 10.1016/j.progpolymsci.2017.02.004.
- [13] N. Lucas, C. Bienaime, C. Belloy, M. Queneudec, F. Silvestre, and J. E. Nava-Saucedo, "Polymer biodegradation: Mechanisms and estimation techniques - A review," *Chemosphere*, vol. 73, no. 4, pp. 429–442, Sep. 2008, doi: 10.1016/j.chemosphere.2008.06.064.
- [14] Y. Doi, Y. Kanesawa, M. Kunioka, M.-K. Yokohama, J. T. Saito, and T. Saito, "Biodegradation of Microbial Copolyesters: Poly(3-hydroxybutyrate-co-3-hydroxyvalerate) and Poly(3-hydroxybutyrate-co-4-hydroxybutyrate)," *Macromolecules*, vol. 23, no. 1, pp. 26–31, 1990, doi: 10.1021/ma00203a006.
- [15] R. Dinarvand, N. Sepehri, S. Manoochehri, H. Rouhani, and F. Atyabi, "Polylactide-co-glycolide nanoparticles for controlled delivery of anticancer agents," *Int J Nanomedicine*, vol. 6, pp. 877–895, 2011, doi: 10.2147/IJN.S18905.
- [16] P. Guérin, E. Renard, and V. Langlois, "Degradation of Natural and Artificial Poly[(R)-3-hydroxyalkanoate]s: From Biodegradation to Hydrolysis," in *Plastics from Bacteria: Natural Functions and Applications*, Springer, 2010, pp. 283–315. doi: 10.1007/978-3-642-03287_5_12.
- [17] M. Deroiné, G. César, A. le Duigou, P. Davies, and S. Bruzard, "Natural Degradation and Biodegradation of Poly(3-Hydroxybutyrate-co-3-Hydroxyvalerate) in Liquid and Solid Marine Environments," *Journal of Polymers and the Environment*, vol. 23, no. 4, pp. 493–505, Jul. 2015, doi: 10.1007/s10924-015-0736-5.
- [18] A. Hoshino *et al.*, "Study of the Aerobic Biodegradability of Plastic Materials under Controlled Compost," in *Biodegradable Polymers and Plastics*, Springer US, 2003, pp. 47–54. doi: 10.1007/978-1-4419-9240-6_3.
- [19] K. ichi Kasuya, Y. Inoue, K. Yamada, and Y. Doi, "Kinetics of surface hydrolysis of poly[(R)-3-hydroxybutyrate] film by PHB depolymerase from *Alcaligenes faecalis* T1," *Polymer Degradation and Stability*, vol. 48, no. 1, pp. 167–174, 1995, doi: 10.1016/0141-3910(95)00026-1.
- [20] Y. Kumagai, "films," vol. 57, pp. 53–57, 1992.
- [21] M. Environment and J. Greene, "PLA and PHA Biodegradation in the Marine Environment," 2012. [Online]. Available: www.calrecycle.ca.gov/Publications.
- [22] C. Thellen, M. Coyne, D. Froio, M. Auerbach, C. Wirsen, and J. A. Ratto, "A processing, characterization and marine biodegradation study of melt-extruded polyhydroxyalkanoate (PHA) films," *Journal of Polymers and the Environment*, vol. 16, no. 1, pp. 1–11, 2008, doi: 10.1007/s10924-008-0079-6.

- [23] J. Mergaert, A. Wouters, C. Anderson, and J. Swings, "In situ biodegradation of poly(3-hydroxybutyrate) and poly(3-hydroxybutyrate-co-3-hydroxyvalerate) in natural waters," *Canadian Journal of Microbiology*, vol. 41, no. SUPPL. 1, pp. 154–159, 1995, doi: 10.1139/m95-182.
- [24] M. Deroiné *et al.*, "Accelerated ageing and lifetime prediction of poly(3-hydroxybutyrate-co-3-hydroxyvalerate) in distilled water," *Polymer Testing*, vol. 39, pp. 70–78, 2014, doi: 10.1016/j.polymertesting.2014.07.018.
- [25] N. T. Lotto, M. R. Calil, C. G. F. Guedes, and D. S. Rosa, "The effect of temperature on the biodegradation test," *Materials Science and Engineering C*, vol. 24, no. 5, pp. 659–662, Nov. 2004, doi: 10.1016/j.msec.2004.08.009.
- [26] H. Sashiwa, R. Fukuda, T. Okura, S. Sato, and A. Nakayama, "Microbial degradation behavior in seawater of polyester blends containing poly(3-hydroxybutyrate-co-3-hydroxyhexanoate) (PHBHHx)," *Marine Drugs*, vol. 16, no. 1, pp. 1–11, 2018, doi: 10.3390/md16010034.
- [27] Y. Doi, Y. Kanesawa, N. Tanahashi, and Y. Kumagai, "Biodegradation of microbial polyesters in the marine environment," *Polymer Degradation and Stability*, vol. 36, no. 2, pp. 173–177, 1992, doi: 10.1016/0141-3910(92)90154-W.
- [28] K.-I. Ichi Kasuya, Y. Inoue, K. Yamada, and Y. Doi, "Kinetics of surface hydrolysis of poly[(R)-3-hydroxybutyrate] film by PHB depolymerase from *Alcaligenes faecalis* T1," *Polymer Degradation and Stability*, vol. 48, no. 1, pp. 167–174, 1995, doi: 10.1016/0141-3910(95)00026-I.
- [29] K.-I. I. Kasuya *et al.*, "Biodegradabilities of various aliphatic polyesters in natural waters," *Polymer Degradation and Stability*, vol. 59, no. 1–3, pp. 327–332, 1998, doi: 10.1016/s0141-3910(97)00155-9.
- [30] K. Sudesh, H. Abe, and Y. Doi, "Synthesis, structure and properties of polyhydroxyalkanoates: Biological polyesters," *Progress in Polymer Science (Oxford)*, vol. 25, no. 10, pp. 1503–1555, 2000, doi: 10.1016/S0079-6700(00)00035-6.
- [31] Y. Kumagai, Y. Kanesawa, and Y. Doi, "Enzymatic degradation of microbial poly(3-hydroxybutyrate) films," *Die Makromolekulare Chemie*, vol. 193, no. 1, pp. 53–57, 1992, doi: 10.1002/macp.1992.021930105.
- [32] R. Mara, S. Moreira Thiré, L. Cardoso Arruda, and S. Barreto, "Morphology and Thermal Properties of Poly(3-hydroxybutyrate-co-3-hydroxyvalerate)/Attapulгите Nanocomposites," 2011, doi: 10.1590/S1516-14392011005000046.
- [33] S. R. K. Chalasani, "Efficient green synthetic routes to biobased polyurethane from soymeal," Michigan State University, 2014.
- [34] A. Hoshino, H. Sawada, M. Yokota, M. Tsuji, K. Fukuda, and M. Kimura, "Influence of

weather conditions and soil properties on degradation of biodegradable plastics in soil," *Soil Science and Plant Nutrition*, vol. 47, no. 1, pp. 35–43, 2001, doi: 10.1080/00380768.2001.10408366.

[35] K. L. Law, N. Starr, T. R. Siegler, J. R. Jambeck, N. J. Mallos, and G. H. Leonard, "The United States' contribution of plastic waste to land and ocean," *Science Advances*, vol. 6, no. 44, pp. 1–7, 2020, doi: 10.1126/sciadv.abd0288.

[36] M. Salomez *et al.*, "A comparative study of degradation mechanisms of PHBV and PBSA under laboratory-scale composting conditions," *Polymer Degradation and Stability*, vol. 167, pp. 102–113, Sep. 2019, doi: 10.1016/J.POLYMDEGRADSTAB.2019.06.025.

[37] T. G. Volova, A. N. Boyandin, M. I. Gladyshev, I. I. Gitelson, and S. v. Prudnikova, "Biodegradation of Polyhydroxyalkanoates in Natural Water Environments," *Journal of Siberian Federal University. Biology*, vol. 8, no. 2, pp. 168–186, Jun. 2015, doi: 10.17516/1997-1389-2015-8-2-168-186.

[38] Y. H. Ho, S. N. Gan, and I. K. P. Tan, "Biodegradation of a medium-chain-length polyhydroxyalkanoate in tropical river water," *Applied Biochemistry and Biotechnology - Part A Enzyme Engineering and Biotechnology*, vol. 102–103, pp. 337–347, 2002, doi: 10.1385/ABAB:102-103:1-6:337.

[39] L. W. Hong and J. Yu, "Environmental factors and kinetics of microbial degradation of poly(3-hydroxybutyrate-co-3-hydroxyvalerate) in an aqueous medium," *Journal of Applied Polymer Science*, vol. 87, no. 2, pp. 205–213, Jan. 2003, doi: 10.1002/app.11354.

[40] J. Mergaert, C. Anderson, A. Wouters, J. Swings, and K. Kersters, "Biodegradation of polyhydroxyalkanoates," *FEMS Microbiology Letters*, vol. 103, no. 2–4, pp. 317–321, Dec. 1992, doi: 10.1016/0378-1097(92)90325-1.

[41] H. Tsuji and K. Suzuyoshi, "Environmental degradation of biodegradable polyesters and poly(L-lactide) films in controlled static seawater," *Polymer Degradation and Stability*, vol. 75, no. 2, pp. 347–355, 2002.

[42] S. Wang *et al.*, "Biodegradation of Poly(3-hydroxybutyrate-co-3-hydroxyhexanoate) Plastic under Anaerobic Sludge and Aerobic Seawater Conditions: Gas Evolution and Microbial Diversity," *Environmental Science and Technology*, vol. 52, no. 10, pp. 5700–5709, May 2018, doi: 10.1021/acs.est.7b06688.

[43] N. Sridewi, K. Bhubalan, and K. Sudesh, "Degradation of commercially important polyhydroxyalkanoates in tropical mangrove ecosystem," *Polymer Degradation and Stability*, vol. 91, no. 12, pp. 2931–2940, 2006, doi: 10.1016/j.polymdegradstab.2006.08.027.

[44] L. Shang, Q. Fei, Y. H. Zhang, X. Z. Wang, D. di Fan, and H. N. Chang, "Thermal Properties and Biodegradability Studies of Poly(3-hydroxybutyrate-co-3-hydroxyvalerate)," *Journal of Polymers and the Environment*, vol. 20, no. 1, pp. 23–28,

2012, doi: 10.1007/s10924-011-0362-9.

[45] J. Greene, "Biodegradation of biodegradable and compostable plastics under industrial compost, marine, and anaerobic digestion," *Annual Technical Conference - ANTEC, Conference Proceedings*, vol. 2018-May, no. 1, pp. 13–18, 2018.

[46] M. Environment and J. Greene, "PLA and PHA Biodegradation in the," 2012, [Online]. Available: www.calrecycle.ca.gov/Publications.

[47] M. Puccini, E. Stefanelli, M. Seggiani, E. Balestri, and S. Vitolo, "Biodegradability of polyethylene/hydrolyzed collagen blends in terrestrial and marine environmental conditions," *Journal of Renewable Materials*, vol. 5, no. 1, pp. 117–123, 2017, doi: 10.7569/JRM.2017.634138.

[48] M. Tosin, M. Weber, M. Siotto, C. Lott, and F. D. Innocenti, "Laboratory test methods to determine the degradation of plastics in marine environmental conditions," *Frontiers in Microbiology*, vol. 3, no. JUN, pp. 1–9, 2012, doi: 10.3389/fmicb.2012.00225.